Variant Surface Glycoprotein Synthesis and Cell Cycle Progression in *Trypanosoma brucei*

Nadina Wand

A thesis submitted for the degree of

Doctor of Philosophy

to the Department of Biochemistry, University of Oxford

Somerville College

2011

Thesis abstract

The unicellular eukaryote *Trypanosoma brucei* causes African Sleeping sickness and multiplies extracellularly in the bloodstream of the infected host. The parasite evades antibody-mediated lysis by switching its Variant Surface Glycoprotein (VSG) coat. Blocking VSG synthesis results in an abrupt growth inhibition and a precise pre-cytokinesis cell cycle arrest, with an accumulation of cells with two nuclei and two kinetoplasts. Additionally, induction of *VSG* RNAi triggers a global block in translation, which is not due to a general decrease in transcript levels. The mechanism behind this translation arrest was investigated. It was observed that it correlated with a decrease in polysomes, indicating that translation was blocked at the level of initiation. It was also shown that the *VSG* RNAi-triggered growth inhibition was reversible, which suggests that this is not a lethal phenotype.

The *VSG221* RNAi-induced growth arrest could be alleviated if a second different *VSG* (*VSG117*), which was not recognised by the *VSG221* RNAi, was expressed immediately downstream of the promoter of the active *VSG221* Expression site. Further, it was possible to delete the telomeric *VSG221* in these VSG double-expressors, leaving the cells completely reliant on the second complementing *VSG117* gene. VSG117 expressed from a promoter-adjacent position in the active Expression site was shown to form a functional surface coat that protected the parasites from complement-mediated lysis *in vitro*.

Transiently transfecting cells with anti-*VSG221* morpholino oligonucleotides allowed us to specifically block translation of *VSG221* mRNA without degrading it. This resulted in a pre-cytokinesis cell cycle arrest similar to that induced by *VSG221* RNAi. This indicates that the *VSG* RNAi-triggered growth inhibition was due to a lack of VSG protein or its synthesis rather than the ablation of the abundant *VSG* mRNA. In addition, it was shown that blocking VSG synthesis reduced the rate of surface VSG internalisation in cells that were stalled precytokinesis, but had no effect on other endocytic markers. These experiments give us further insight into the importance of the protective VSG coat for pathogenicity in *T. brucei*.

Statement of Authentication

The work presented in this thesis is, to the best of my knowledge and belief, original except as acknowledged in the text. I hereby declare that I have not submitted this material, either in whole or in part, for a degree at this or any other institution.

Nadina Wand

2011

Table of Contents

Thesis abstract ii
Statement of Authentication iii
Table of contents iv
Acknowledgements vi
Abbreviations vii

Chapter 1 – Introduction 1

DPhil objectives 32

Chapter 2 – Materials and Methods 33

Materials 34
Methods 41

Chapter 3 – Blocking VSG synthesis triggers a growth arrest and a global block in translation 54

Introduction 55
Results 55
Conclusions 73

Chapter 4 – Expression of high levels of a second *VSG* that is not recognised by the *VSG221* RNAi can rescue the cells from *VSG221* RNAi-induced growth arrest 79

Introduction 80
Results 80
Conclusions 101

Chapter 5 – VSG expressed from a non-telomeric location can form a protective surface coat 108

Introduction 109

Results 110
Conclusions 134

Chapter 6 – The cell cycle arrest mediated by blocking VSG synthesis is not a direct consequence of decreased *VSG* transcript levels 139

Introduction 140
Results 140
Conclusions 159

Chapter 7 – Clearance of VSG from the surface of *Trypanosoma brucei* is impeded after the induction of *VSG* RNAi 163

Introduction 164
Results 164
Conclusions 181

Chapter 8 – Conclusions and future perspectives 186

Chapter 9 – References 196

Appendix I 216

Appendix II 230

Acknowledgements

I would like to thank my supervisor Dr Gloria Rudenko for giving me the opportunity to delve into the exciting world of trypanosomes in her laboratory and for providing constant supervision and guidance during the course of this study. I am also grateful to Prof Martin Noble and Prof Mark Sansom for their advice and support.

I thank Dr Mark Carrington for allowing me to perform the polysome experiments in his laboratory and Dr Susanne Kramer in the Carrington laboratory for her generous help and advice. I would like to thank Keith Gull for allowing me to use his laboratory equipment. I am grateful to all the members of the Gull laboratory, particularly Bill Wickstead, Susan Vaughan and Eva Gluenz for their kind help with microscopy and Helen Banks for her generous assistance.

Thank you to all past and present members of the group, particularly Viola Denninger, Tara Stanne, Megan Povelones, Mani Shankar Narayanan, Manish Kushwaha, Andrew Voak and Alexander Fullbrook for their friendship, constant support, and advice.

I would like to thank my family and especially my parents who I blame for my passion for science and my brother who always knows how to make me laugh. I would like to thank Nicholas Wand who has been with me every step of the way through writing this thesis. Finally, thank you to Matthew Wand, my wonderful husband, for teaching me how to work with radiation, for providing useful suggestions for my thesis and for helping me get through the tough times.

This research was funded by the Wellcome Trust, and I was supported by the BBSRC and the Biochemical Society.

Abbreviations

BES	Bloodstream Expression site
bp	basepair
BSA	Bovine serum albumin
CR1	Complement receptor 1
DAPI	4, 6-diamidino-2-phenylinidole
DNA	Deoxyribonucleic acid
dsRNA	double-stranded RNA
EDTA	Ethylenediamine tetraacetic acid
eGFP	enhanced Green fluorescent protein
EGTA	Ethylene glycol tetraacetic acid
ES	Expression site
ESAG	Expression site associated gene
ESB	Expression site body
FITC	Fluorescein isothiocyanate
FP	Flagellar pocket
g	gram
GPI	Glycosylphosphatidylinositol
HEPES	4-(2-hydroxyethyl)-1-piperazineethanesulfonic acid
ISG	Invariant Surface Glycoprotein
kbp	kilobasepair
kDa	kilodalton
M	Molar
m	milli
µ	micro
Mb	Megabases
mRNA	messenger RNA
n	nano
p	pico
PBS	Phosphate Buffered Saline
PCR	Polymerase chain reaction
pNAL	poly-N-acetyllactosamine

RNA	Ribonucleic acid
RNAi	RNA interference
rRNA	ribosomal RNA
SDS	Sodium dodecyl sulphate
SDS PAGE	Sodium dodecyl sulfate polyacrylamide gel electrophoresis
SRA	Serum resistance associated
TetO	Tetracycline operator
UTR	Untranslated region
VSG	Variant Surface Glycoprotein

Chapter 1

Introduction

1.1. *Trypanosoma brucei* morphology and phylogeny

African trypanosomiasis is one of 17 neglected tropical diseases recognised by the World Health Organisation (WHO) (World Health Organisation 2008). The disease is vector-borne and is caused by the unicellular eukaryote *Trypanosoma brucei*, from the class Kinetoplastida, a group of single-cell flagellated protozoa (Figure 1.1). The class name originates from the kinetoplast, which is located at the posterior end of the cell at the base of the flagellum, and contains the DNA of the single mitochondrion (Figure 1.1). The order Trypanosomatida consists of many exclusively parasitic genera, such as *Leishmania* and *Trypanosoma* that are responsible for a number of economically important diseases. For example, species belonging to genus *Leishmania* are the causative agent of leishmaniasis, whereas *Trypanosoma cruzi* is responsible for Chagas disease. It is estimated that trypanosomatids are an ancient, early divergent monophyletic lineage that evolved about 500 million years ago, long before the appearance of their modern insect and mammalian hosts (Fernandes et al. 1993; Hamilton et al. 2004; Wright et al. 1999; Lambrecht 2011).

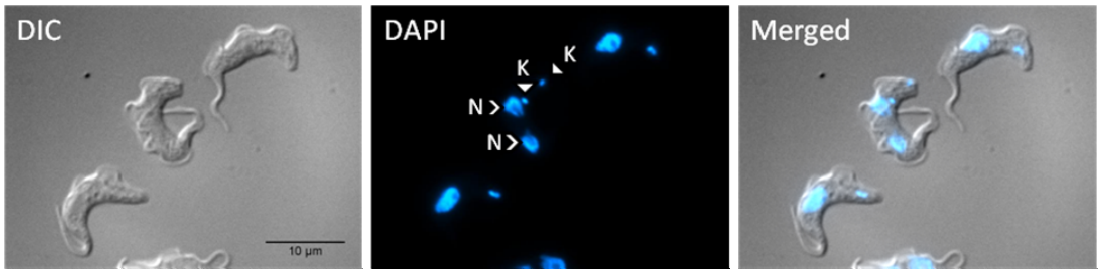


Figure 1.1: Bloodstream form *Trypanosoma brucei*. The nucleus (N) and the kinetoplasts (K), which are equivalent to mitochondrial DNA have been stained with DAPI (blue), as shown in the fluorescent image panel.

Trypanosoma brucei is transmitted between mammalian hosts by tsetse flies of the *Glossina* genus and undergoes complex life cycle differentiations that enable it to survive in the insect gut and the mammalian bloodstream. The geographic distribution of sleeping sickness is limited by the favourable habitat for the insect vector, which coincides roughly with the area between the Sahara and the Kalahari deserts (Figure 1.2) (M. P. Barrett et al. 2003). 60 million people in 36 African countries are estimated to be at risk from the disease [8,9]. Three sub-species can be indentified in the *T. brucei* species, *Trypanosoma brucei brucei*, *Trypanosoma brucei gambiense* and *Trypanosoma brucei rhodesiense*. *Trypanosoma brucei brucei* causes animal African trypanosomiasis, also known as "nagana", whereas *Trypanosoma brucei gambiense* and *Trypanosoma brucei rhodesiense* are the causative agents of human African trypanosomiasis.

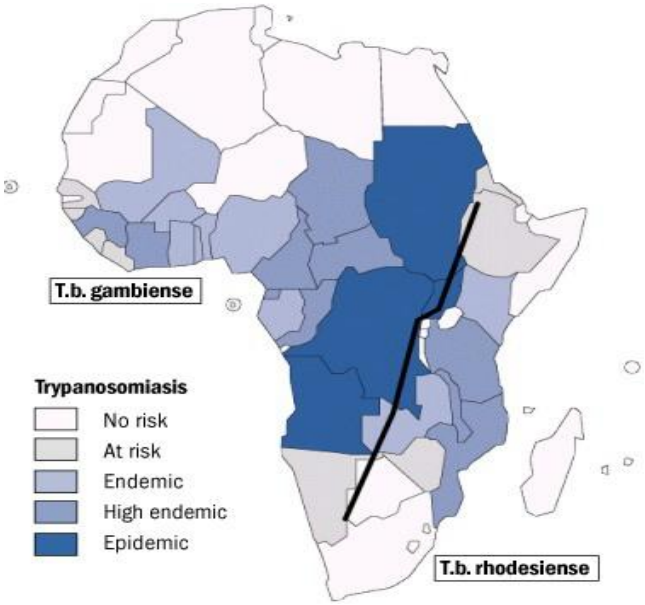


Figure 1.2: Geographical distribution of human African trypanosomiasis (WHO 1999)**.**

1.2. Disease, diagnosis and treatment

In humans the disease can manifest in two forms, which depends on the parasite causing the infection. *Trypanosoma brucei gambiense* (*T. b. gambiense*) is found in west and central Africa, where the primary host is humans. This parasite causes a chronic parasitemia and is responsible for over 95% of reported cases of sleeping sickness (M. P. Barrett et al. 2003). Often symptoms of the disease caused by this organism manifest themselves only at the advanced stage of the infection and the disease can take years to develop. *Trypanosoma brucei rhodesiense* (*T. b. rhodesiense*) is distributed mainly in southern and eastern Africa, where the primary reservoir is considered to be game animals and livestock (M. P. Barrett et al. 2003). This sub-species of the parasite causes a more acute infection and much more rapidly progressing disease symptoms with the first signs of infection emerging within just months or weeks and quick invasion of the central nervous system.

The early stages of the trypanosimiasis in humans is characterised by relapsing fever, which coincides with an increase in the number of parasites found in the blood of the infected host (Figure 1.3) (World Health Organisation 1998; Stich et al. 2002; Reto Brun et al. 2010). Later in the infection, the parasite crosses the blood-brain barrier and infects the central nervous system. This secondary neurological stage of the disease manifests itself with behavioural changes and disturbance of the sleeping cycles, which leads to the name “sleeping sickness” (World Health Organisation 1998). If left untreated, African trypanosomiasis is invariably fatal. *T. b. rhodesiense* versus *T. b. gambiense* are morphologically and immunologically indistinguishable and identification of the type of infection is crucial for the diagnosis of the human trypanosomiasis, as it determines the course of treatment.

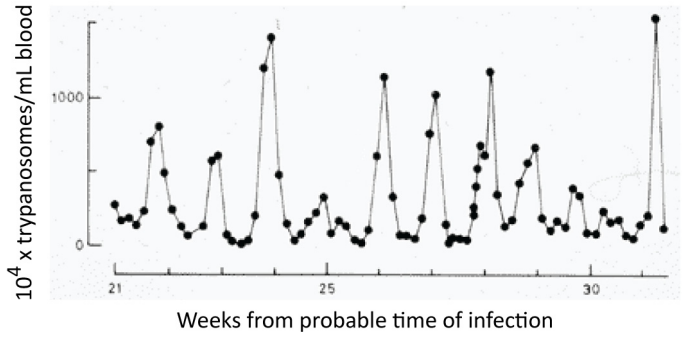


Figure 1.3: Relapsing parasitemia of *T. brucei* in the bloodstream of an infected host. The graph of periodic fluctuation in the number of parasites has been adapted from (R. Ross & Thomson 1910).

Serological tests are employed in the detection of *T. b. gambiense* parasites (Magnus et al. 1978). Trypanosomes multiply extracellularly in the bloodstream of the infected host and are constantly exposed to the challenge of the immune system. Parasites are covered by a dense coat of highly immunogenic Variant Surface Glycoprotein (VSG), and the host continuously mounts a specific antibody response against the predominant VSG population (Borst 2002; Barry & McCulloch 2001). The concentrations of IgG and IgM antibodies against *T. b. gambiense* VSG are high in the blood of a patient and can be detected using the immunodominant antigens (Lejon et al. 2003; Lejon et al. 1998). There is no serological screening test available for *T. b. rhodesiense* infection and diagnosis relies on the clinical features, history of exposure and examination of blood smears (Woodruff et al. 1973; Gear & G. B. Miller 1986; Jelinek et al. 2002; Duggan & M. P. Hutchinson 1966).

Treatment of African trypanosomiasis is dependent on the stage of the disease. Melarsoprol, an arsenic based drug, still remains the most widely used second-stage treatment, but it may have many side effects, such as acute

encephalopathy, that can be fatal in 4 to 12% of patients (Stich et al. 2002). In recent years new effort has been mounted for drug discovery against African trypanosomiasis with the search of drug candidates at the Drug Discovery Unit for Tropical Diseases at the University of Dundee, Scotland (Frearson et al. 2010).

1.3. Life cycle

Trypanosomes have to survive in two vastly different environments, the tsetse fly gut and the mammalian bloodstream, and therefore undergo extensive morphological and metabolic transformations that allow them to adapt to the different environments (Figure 1.4). Infection begins when a tsetse fly takes a blood meal and injects metacyclic non-proliferative form trypanosomes into the bloodstream of a mammal. These bloodstream form parasites express Variant Surface Glycoprotein (VSG) that provides protection from the host immune system (E. Pays et al. 2004; McCulloch 2004; Matthews 2005). In the mammalian host these metacyclic trypanosomes remain extracellular and differentiate into long slender proliferative bloodstream form trypomastigotes (Figure 1.4). At high cell densities, some of the long slender bloodstream form parasites differentiate into the short stumpy form, which is pre-adapted for differentiation into the procyclic form of the parasite that is able to survive in the gut of the fly (Figure 1.4) (Matthews et al. 2004). Short stumpy form trypanosomes also express Variant Surface Glycoprotein (VSG) on their cell surface, but this coat is quickly shed in the mid-gut of the tsetse fly and replaced with another surface protein called procyclin (Roditi & Liniger 2002; Roditi et al. 1989). Procyclic cells eventually migrate to the salivary glands of

the fly and differentiate into metacyclic form trypanosomes that are able to infect a mammalian host and repeat the life cycle (Figure 1.4) (Matthews 2005).

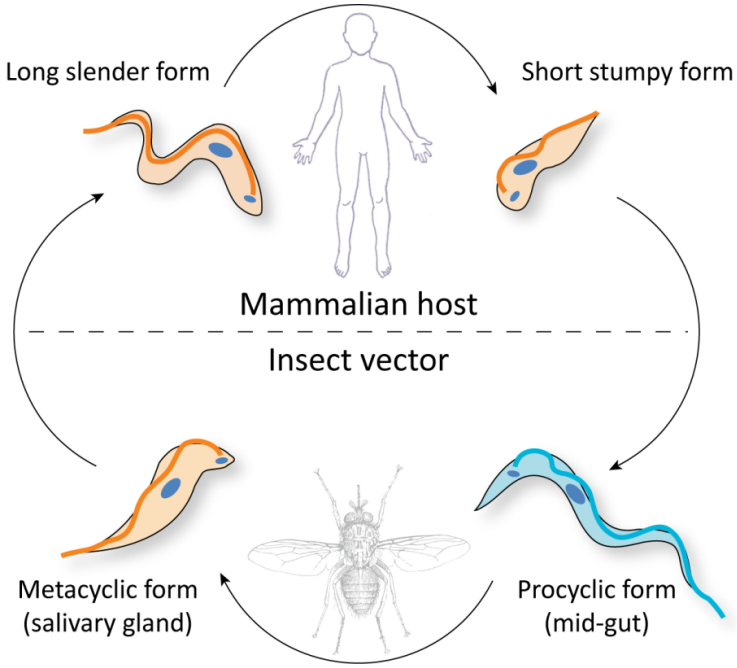


Figure 1.4: Life cycle of *Trypanosoma brucei*. The two major bloodstream forms of the parasite are the long slender and the short stumpy form, which both express a VSG coat (orange) on their cell surface. In the insect host the trypanosomes differente into procyclic form cells, which express procyclin (blue) on their cell surface. Procyclic cells can differentiate into metacyclic trypanosomes, which express a VSG coat (orange) in preparation for infecting a mammalian host.

1.4. Cell cycle

Trypanosoma brucei has a polarised cell body with a single flagellum, which exits the cell at a unique invagination of the plasma membrane, called the flagellar pocket. There are a number of single-copy internal organelles, including the lysosome, nucleus, Golgi apparatus and the single mitochondrion, which harbours the kinetoplast.

T. brucei divides through binary fission (Figure 1.5). The kinetoplast divides and segregates before mitosis takes place, resulting in a cell that contains one nucleus and two kinetoplasts (Figure 1.5) (Sherwin & Gull 1989; D. R. Robinson & Gull 1991; McKean 2003; Acosta-Serrano et al. 2006; Woodward & Gull 1990). Following the nuclear S phase and during the G2 phase of the cell cycle, basal bodies separate and guide the segregation of the kinetoplasts and Golgi (D. R. Robinson & Gull 1991). The mitosis of the replicated nucleus then takes place without chromosome condensation or the breakdown of the nuclear envelope (Ersfeld & Gull 1997; Galanti et al. 1998; Ogbadoyi et al. 2000; Ersfeld et al. 1999). Finally, the cell cycle completes with cytokinesis, which occurs with the formation of a cleavage furrow along the longitudinal axis of the cell, beginning at the anterior end, and passing between the two flagella to separate the daughter cells.

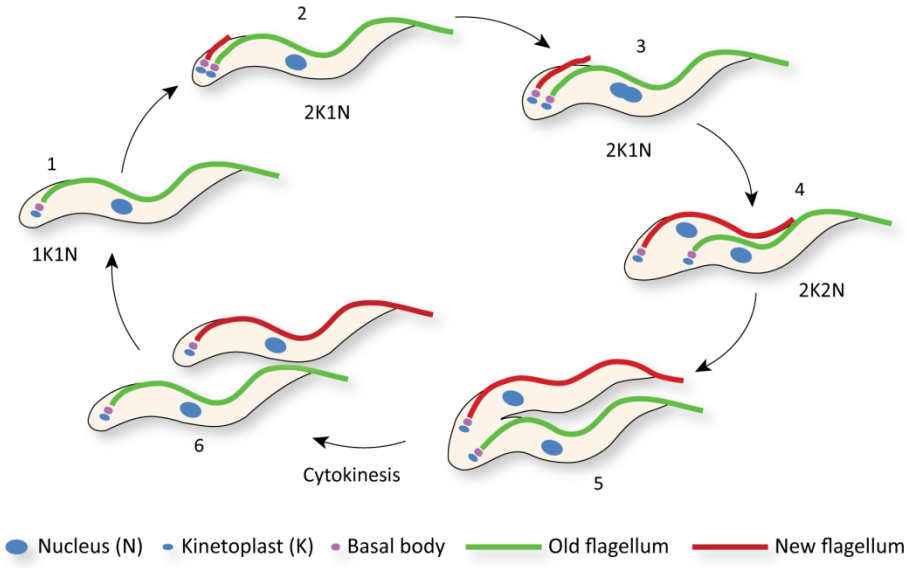


Figure 1.5: *Trypanosoma brucei* bloodstream form cell cycle. 1. The parasite has a single kinetoplast (K), nucleus (N) (1K1N) and flagellum, attached to the cell body. **2.** As the cell cycle progresses, the new flagellum grows guided by the old flagellum, and the basal bodies along with the attached kinetoplasts divide and segregate, resulting in a 2K1N cell. **3.** Nuclear DNA replication has

completed and mitosis is initiated **4.** Nuclear mitosis completes, giving rise to 2K2N cells. **5.** Cleavage furrow forms between the two flagella, initiating cytokinesis. **6.** The two daughter cells separate and complete the cell cycle.

The *T. brucei* cell cycle can be visualised by staining the nuclear and kinetoplast DNA with the fluorescent DNA stain DAPI (Siegel et al. 2008). Abnormal K/N configurations such as 0K1N, 1K0N (zoid), 1K2N or cells with multiple nuclei and kinetoplasts may arise, if the cell cycle is disrupted in some way (Hammarton et al. 2007; Kumar & C. C. Wang 2005; Helms et al. 2006; Rothberg et al. 2006). For example, in procyclic form trypanosomes ablation of the mitotic cyclin CYC6 by RNAi prevents progression of mitosis but not cytokinesis, which causes an accumulation of cells with a 4C nuclear DNA content and 1K0N cells, also known as "zoids" (Hammarton et al. 2003). Interestingly, RNAi-mediated knock-down of CYC6 in bloodstream form cells does not have the same effect, as both mitosis and cytokinesis are inhibited but not kinetoplast replication, resulting in multi-kinetoplastic and multi-flagellated cells (Z. Li & C. C. Wang 2003; Hammarton et al. 2003). Thus, the different life cycle stages may have many differences in their cell cycle check points.

1.5. *T. brucei* genome and genetic manipulations

The haploid genome of *T. brucei* is about 35 Mb and is predicted to contain around 10,000 genes (Berriman et al. 2005; Aslett et al. 2010). Remarkably, about 10% genes are pseudogenes and mostly code defective *VSG* sequences (Berriman et

al. 2005). The genome of *T. brucei* is sub-divided into three different classes of chromosomes. There are 11 megabase chromosome pairs that range between 1.1 Mb and 5.4 Mb (Melville et al. 1998; Melville et al. 2000; Berriman et al. 2005). The intermediate chromosomes range between 200 and 900 kbp and are of variable ploidy (Van der Ploeg, D. C. Schwartz, Cantor, et al. 1984; Bessat & Ersfeld 2009). Finally, there are up to several hundred minichromosomes in each cell, which are approximately 50-150 kbp (Van der Ploeg, D. C. Schwartz, Cantor, et al. 1984; Gottesdiener et al. 1990). Minichromosomes consist of a repetitive palindromic core of 177 bp repeats with telomeric VSGs (Wickstead et al. 2004). The megabase chromosomes carry most active housekeeping genes, but there are some Expression sites containing *VSG* genes on the intermediate chromosomes (Van der Ploeg, Cornelissen, Michels, et al. 1984). The genome of *T. brucei* is segmentally aneuploid with haploid *VSG*-contaning transcription units and *VSG* basic copy arrays at the telomeres of the megabase chromosomes (Melville et al. 1999; El-Sayed et al. 2000; Callejas et al. 2006; Berriman et al. 2005). Most trypanosome genes are organised in constitutively transcribed polycistronic transcription units and they do not appear to be linked in any way other than genomic location (C. E. Clayton 2002; Liang et al. 2003).

Both bloodstream and procyclic form parasites can readily be genetically manipulated by DNA transformation, creating stable transgenic cell lines (McCulloch et al. 2004). Tetracycline inducible RNAi is an extremely useful tool for studying gene function in *T. brucei* (Fire et al. 1998; Ngo et al. 1998; Wirtz & C. E. Clayton 1995; Wirtz et al. 1999). High levels of expression can be achieved by employing T7 promoters that are transcribed by exogenous T7 polymerase. The

regulation of these promoters is possible through using a prokaryotic tetracycline repressor system (Wirtz & C. E. Clayton 1995; Wirtz et al. 1999). The system relies on the ability of the tetracycline repressor protein to bind to tet operator sequences that are inserted downstream of a target promoter thus preventing its transcription. Once tetracycline, which is non-toxic to *T. brucei*, is added to the cell culture medium, it binds to the tet repressor protein and causes its release from the operator sequence, allowing for the transcription of the target gene or sequence to take place. Both 427 bloodstream (90-13) and procyclic (29-13) form trypanosome cell lines that constitutively express T7 RNA polymerase and the tetracycline repressor have been developed as important background cell lines for numerous RNAi studies, but also for transgenic gene expression (Wirtz et al. 1999)

1.6. Regulation of gene expression

In *T. brucei* most genes are organised in long arrays that are constitutively transcribed into polycistronic RNA precursors (C. E. Clayton 2002; Liang et al. 2003). Unlike bacterial operons, where genes from the same or linked pathways are expressed simultaneously, the trypanosome polycistrons are not functionally organised and merely share the same genomic location (Berriman et al. 2005; El-Sayed et al. 2005). Although there is evidence for global downregulation of transcription in *T. brucei* differentiating from bloodstream form into procyclic form parasites, there appears to be no general regulation of RNA polymerase II transcription. Therefore the regulation of gene expression in *T. brucei* occurs at post-transcriptional level through the mRNA processing, stability and translation, protein

modification and turnover. Most notable example of this rule are the developmentally regulated and transcribed by RNA polymerase I genes encoding the major surface proteins – the procyclin of the procyclic stage and the VSG in the bloodstream form stage of the parasite.

Individual mRNAs are cleaved off a polycistronic precursor by means of a *trans*-splicing reaction at the 5' end and polyadenylation at the 3' end. *Trans*-splicing is a process that involves the addition of a 39 nucleotide capped leader RNA, also known as the "spliced leader" RNA onto the 5′ end of the maturing mRNAs (Perry et al. 1987; Freistadt et al. 1988; Bangs et al. 1992). Simultaneously and in a process linked to the *trans*-splicing reaction, the 3' end of the mRNA is polyadenylated (Ullu et al. 1993).

Translation initiation in *T. brucei* appears to be regulated differently to that in other model organisms, presumably due to the highly modified cap-4 structure at the 5′ ends of all trypanosomatid mRNAs. In higher eukaryotes the mRNA 5' cap is bound by the eIF4E cap-binding protein, together with the scaffolding protein eIF4G and the helicase eIF4A. The genome of *T. brucei* encodes four eIF4E homologues (TbEIF4E1 through 4) and the precise functions of these are still unclear. TbEIF4E1 and 2 have been found to be both cytoplasmic and nuclear, whereas TbEIF4E2 and 4 localise exclusively to the cytoplasm and are the only ones to interact with eIF4G (Freire et al. 2010). The two eIF4A helicases identified in the *T. brucei* genome also appear to have distinct functions, with TbEIF4AI involved in translation, whereas TbEIF4AIII may be a component of the exon junction complex (Dhalia et al. 2006).

The 5' and 3' untranslated regions (UTRs) on the mRNA can also confer regulation of translation, as well as RNA stability. In *T. brucei* the 3' UTR has been shown to be involved in the stage-specific expression and high stability of the procyclin and *VSG* mRNAs (Furger et al. 1997; Hotz et al. 1997; Berberof et al. 1995). Conserved elements in the UTRs are presumably targeted by protein factors that act as *trans*-regulators of protein expression (Walrad et al. 2009).

1.7. Antigenic Variation

The extracellular bloodstream form parasite is covered by a dense coat of Variant Surface Glycoprotein (VSG) that can be switched, resulting in antigenic variation (Horn & Barry 2005; Barry & McCulloch 2001; G. A. M. Cross 2002; E. Pays et al. 2001; Borst 2002). It is estimated that there are about 5 million homodimers of VSG on the parasite cell surface (Figure 1.6A) (Auffret & M. J. Turner 1981). VSGs are attached to the cell surface by means of a glycosylphosphatidylinositol (GPI) anchor, which is linked to the C-terminus of each VSG (Ferguson et al. 1986). It appears that VSGs shield invariant surface proteins from recognition by the host immune system. VSGs are highly immunogenic and the host quickly mounts a specific antibody response against the predominant VSG in the trypanosome population (G. A. M. Cross 1975; E. Pays et al. 2004). This results in lysis of cells carrying the recognised variant. However, some of the parasites have already switched to a new VSG that is not recognized by the host. These trypanosomes evade detection and can form the next wave of infection (Figure 1.6B).

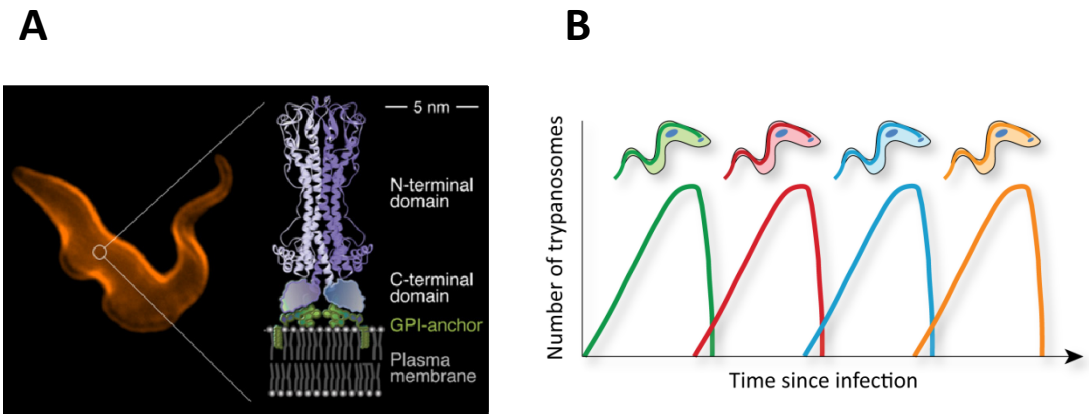


Figure 1.6: Variant Surface Glycoprotein coat of *Trypanosoma brucei* is varied during the course of an infection.

A. The trypanosome cell surface is covered by a dense coat of Variant Surface Glycoprotein (VSG) homodimers. Bloodstream form *T. brucei* has been stained for surface VSG221 (MI Tat 1.2) using anti-VSG221 polyclonal antibody. The model of a complete VSG homodimer is shown as adapted from (Engstler et al. 2007).

B. Progression of infection with peaks of parasitemia. Each wave of parasitemia contains a dominant population of trypanosomes expressing a different VSG variant on its surface.

The sequencing of the *T. brucei* genome revealed a vast reservoir of fully functional *VSG* genes and pseudogenes (Figure 1.7) (Berriman et al. 2005). The parasite has over a thousand antigenically distinct *VSG* sequences, which allow it to maintain a chronic infection lasting for years (Marcello & Barry 2007; Marcello et al. 2007). *VSG* genes are located in several genomic locations – the telomere-associated Expression Sites (ES), the telomeres of minichromosomes and at sub-telomeric arrays (*VSG* Basic Copy genes) (Figure 1.7). However, only one of these *VSGs* is expressed at any given time from one telomeric Bloodstream Expression site (BES) (Figure 1.7).

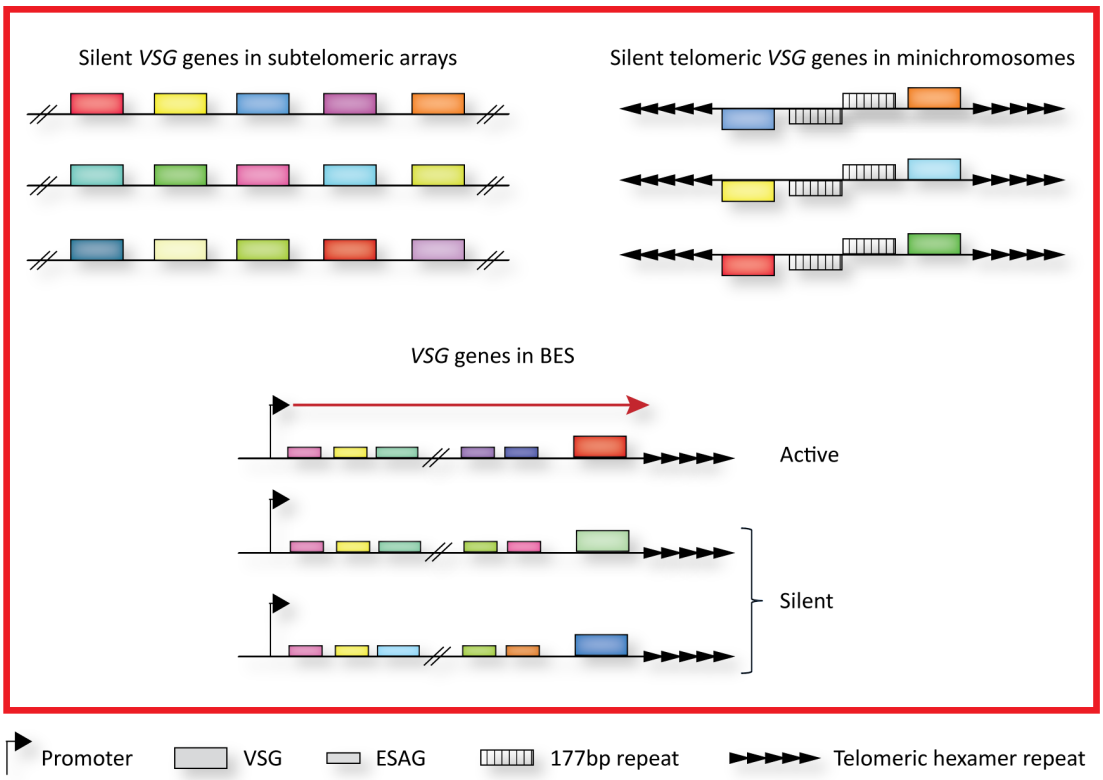


Figure 1.7: Schematic representation of the different genomic locations of *VSG* genes in *Trypanosoma brucei*. Most VSGs are present in tandem arrays at the sub-telomeres. *VSG* genes are also found at the telomeres of the transcriptionally silent minichromosomes. The active *VSG*, however, is always located at the telomere end of a *VSG* Bloodstream Expression site (BES).

The parasite can switch to a new *VSG* by either turning off an active Expression site and turning on a previously silent one (Hughes et al. 2007; Yang et al. 2009; L. M. Figueiredo et al. 2008; Stanne & Rudenko 2010; L. M. Figueiredo & G. A. M. Cross 2009; Q.-ping Wang et al. 2010). Alternatively, homologous recombination of VSGs is the most common strategy (Figure 1.8) (Barry & McCulloch 2001; G. A. M. Cross 2002). DNA re-arrangement events are facilitated by 70 bp repeats and homologous sequences in the Expression site that allow recombination of partial or full copy *VSGs* into the active Expression site (Figure

1.8). More than 90% of all *VSG* sequences in the genome contain one or more imperfect 70 bp repeats upstream of the *VSG*, which are often used as a site for recombination initiation (Shah et al. 1987). Additionally, the *VSG* hinge region sequence, C-terminal domain or 3' non-coding region are highly conserved and can be used as a short sequence of homology and enable recombination (E. Pays et al. 1985; Bernards et al. 1981; Matthyssens et al. 1981; Barry et al. 2005).

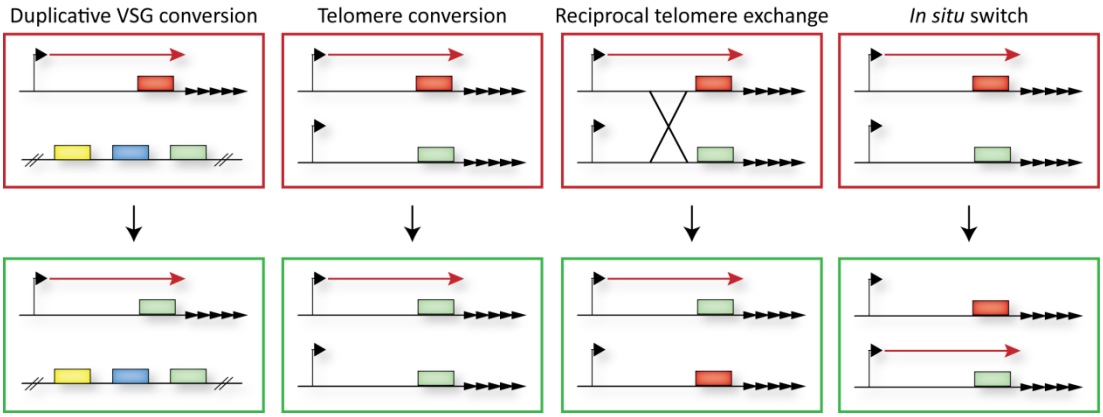


Figure 1.8: Mechanisms of VSG switching in *Trypanosoma brucei* (G. A. M. Cross 1996)**.** Silent *VSG* genes from sub-telomeric arrays can be inserted into the active *VSG* Expression site by homologous recombination. A *VSG* gene located in a silent ES can be activated by telomere cross-over or by duplicative recombination with the active ES. *In situ* switch involves the transcriptional silencing of the active ES and activation of a previously silent one. *VSG* genes are represented by coloured boxes, promoters are indicated with black flags and telomeres are shown with black arrowheads. The red and green box outlines represent the active *VSG*.

The typical BES is a polycistronic transcription unit of approximately 45–60 kbp (Figure 1.9). The relatively simple promoter of the BES is usually preceded by a 10–40 kbp region of 50 bp simple sequence repeats. In addition to the telomeric *VSG* gene, the BES contains Expression Site Associated Genes or *ESAGs*. Imperfect 70 bp

repeats are positioned immediately upstream of the *VSG* gene (Figure 1.9). The *VSG* gene in the ES is invariably at the 3' end of the BES, immediately upstream of the telomere repeats. It is estimated that there are about 15 BESs in each *T. brucei* strain (Hertz-Fowler et al. 2008).



Figure 1.9: Schematic representation of the *T. brucei VSG221* Expression site. The BES promoter is preceded by a region of 50 bp repeats. The Expression site contains additionally Expression Site Associated Genes (E), which are indicated with numbers. The telomeric *VSG* gene is separated from the rest of the polycistronic transcription unit by a stretch of imperfect 70 bp repeats.

The VSG protein comprises 10% of the total protein in the cell, but there is only one copy of the active *VSG* gene. Thus, the parasite faces the challenge of expressing very high levels of one protein from a single copy gene (Overath & Engstler 2004). One of the strategies the cell employs involves the localization of the active ES to a specialised location in the nucleus known as the Expression Site Body (ESB). It is thought that the ESB is a place of concentrated transcription factors and RNA processing machinery that ensure high levels of transcription of the active ES. It is interesting to note that the Expression site is transcribed by RNA polymerase I, rather than RNA polymerase II, as is the case for other protein coding genes in

eukaryotes (Günzl et al. 2003). Therefore, in *T. brucei* RNA polymerase I is used to transcribe not only the *rDNA* genes, but also the active *VSG*.

1.8. Variant Surface Glycoprotein

The VSG protein is approximately 400 to 500 amino acids and its sequence is highly divergent. The VSG contains a large N-terminal domain of around 340 to 400 residues, which has a unique structure without recognisable homologues outside of kinetoplastids. The C-terminal domain is smaller (40 to 80 residues) and shows some sequence conservation between different VSGs (about 40%) but the N-terminus has very little sequence homology (about 20%) (O. C. Hutchinson et al. 2003; Carrington et al. 1991). The tertiary structure of two VSGs have been solved and they have been shown to assume a remarkably similar fold, also known as the VSG fold (Figure 1.10) (Carrington et al. 1991; G. A. M. Cross 1975; Chattopadhyay et al. 2005; N. G. Jones et al. 2008). There are three N-terminal VSG domain types recognised based on the number of conserved cysteine residues that they contain (type A, B or C). The C-terminal domains are classified into one of six groups (1 to 6), also based on cysteine residue numbers and pattern (Carrington et al. 1991). There appears to be no restriction on the combinations of types of N-terminal and C-terminal domains that can occur within different VSGs (O. C. Hutchinson et al. 2003). However, certain types of *VSG* domain combinations appear to be overrepresented in the trypanosome genome, which suggests that not all domain combinations are equally successful. Some might have been selected for, presumably because *VSG* gene recombination might be preferentially taking place within the segment encoding the hinge region

between the two domains of the *VSG*, rather than within the *VSG* domains themselves (E. Pays et al. 1985).

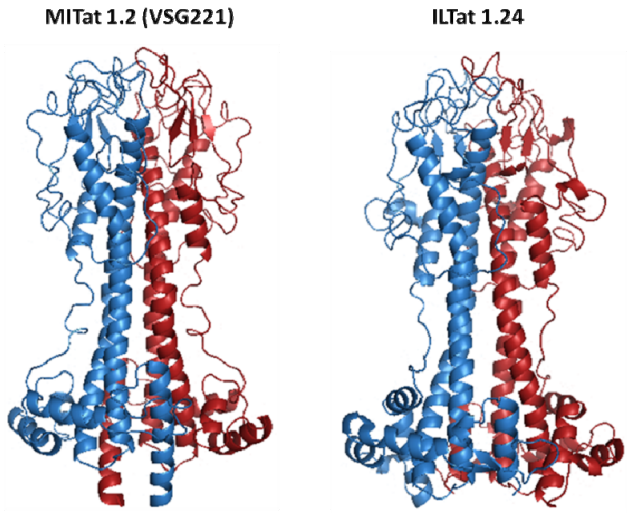


Figure 1.10: The homodimers of the N-terminal domains of VSG variants MI Tat 1.2 (VSG221) and IL Tat 1.24 (M. L. Blum et al. 1993)**.** These models are of the only two VSGs whose structure has been solved. There is significant sequence variation between these two VSGs, but they assume remarkably similar tertiary structure, known as the "VSG fold". Both VSG221 (MITat 1.2) and ILTat 1.24 contain type A N-terminal domains.

The N-terminal domain consists of two α-helices that are connected by unstructured loops which normally comprise the antibody epitope (E. N. Miller, Allan & M. J. Turner 1984b; E. N. Miller, Allan & M. J. Turner 1984a; Masterson et al. 1988). The two α-helices form a 10 nm coiled coil structure whose long axis is orientated perpendicular to the cell membrane of the parasite (M. L. Blum et al. 1993). Interestingly, the tertiary structure of VSG proteins appears to be conserved between VSGs and other proteins that are hypothesized to be related to VSG such as the transferrin receptor encoded by the *ESAG6* and *7* genes (Carrington & Boothroyd

1996; Bussler et al. 1998; M. L. Blum et al. 1993; Mehlert et al. 2002; Campillo & Carrington 2003; Salmon et al. 1997). It has been shown that mutations of the VSG amino acid sequence, such as the insertion of epitope tags into various regions of VSG, result in reduction of expression levels (J. Wang et al. 2003). Therefore, there is evidence for a quality control system operating to prevent the expression of non-functional VSGs on the cell surface.

The structures of the type 1 (from ILTat 1.24) and type 2 (from MITat 1.2 or VSG221) C-terminal domain has also been solved, but the complete VSG structure has not been presented yet (Figure 1.11) (Chattopadhyay et al. 2005; N. G. Jones et al. 2008). Thus, the nature of the interaction between the C-terminal and N-terminal domains of the VSG remains unclear and it is not known if the two domains have co-evolved facilitating particular domain combinations. It appears that the C-terminal domain is hidden from recognition by the immune system, presumably because it is near the surface membrane (Schwede et al. 2011). Therefore, the C-terminal domain is not believed to participate in antigenic variation, which would explain its higher degree of sequence conservation compared to the N-terminal domain.

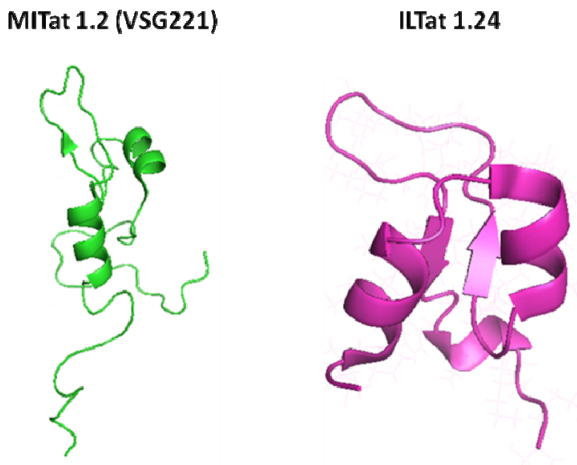


Figure 1.11: The C-terminal domains of VSG variants MI Tat 1.2 (VSG221) and IL Tat 1.24 (Chattopadhyay et al. 2005; N. G. Jones et al. 2008)**.** MI Tat 1.2 has a type 2 C-terminal domain, whereas the C-terminal domain of IL Tat 1.24 is type 1.

1.9. The VSG surface coat and cell membrane architecture

For the extracellular parasite *T. brucei* its cell surface molecules represent an important interface for the interaction of the protozoon with the host immune system. VSG molecules are presented as a dense monolayer of homodimers on the cell surface and on the flagellum (Auffret & M. J. Turner 1981). The VSG proteins are attached to the cell surface by means of glycosylphosphatidylinositol (GPI) anchors. These GPI anchors on this abundant cell surface protein presumably allow a high density of packing on the plasma membrane without the imposition of steric constraints (Figure 1.12). In addition, the lateral diffusion of a GPI-anchored molecule on the trypanosome surface is slightly faster than that of type I transmembrane surface proteins (Engstler et al. 2004). VSGs are often decorated by N-linked chains of oligosaccharides of variable length that might be important in facilitating the dense packing of these molecules on the trypanosome cell surface (Figure 1.12) (Mehlert et al. 2002). The VSG coat is approximately 15 nm thick and recent structural studies on the conserved VSG C-terminal domain indicate that it lies within 5 nm of the plasma membrane, where it cannot be accessed by host immunoglobulins (Chattopadhyay et al. 2005; Schwede et al. 2011).

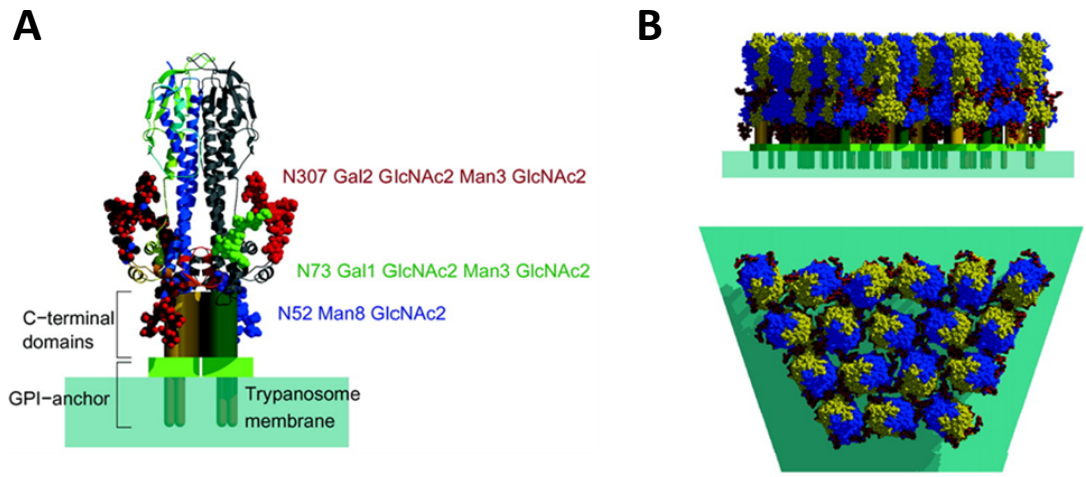


Figure 1.12: Variant Surface Glycoprotein of *Trypanosoma brucei* is a GPI-anchored homodimer that forms a dense monolayer coat on the cell surface of the parasite.

A. Molecular model of MITat 1.5 with attached N-linked oligosaccharides (Mehlert et al. 2002).

B. The modelled VSG surface coat with N-linked oligosaccharides filling in the spaces between individual VSG homodimers viewed from the side and from above (Mehlert et al. 2002).

In addition to the highly abundant VSG, there are other surface proteins presented on the cell membrane of bloodstream form *Trypanosoma brucei*. For example, the Invariant Surface Glycoprotein (ISG) family, which includes ISG65 and ISG75 (with a respective molecular weight of 65 and 75 kDa), are type I transmembrane proteins and are distributed among VSG molecules throughout the cell surface (Ziegelbauer et al. 1992; Ziegelbauer & Overath 1992; D. G. Jackson et al. 1993). The ISG proteins are significantly less abundant than the VSGs, with individual ISG molecules copy numbers estimated to be about 50 to 70 thousand per cell (Ziegelbauer & Overath 1992; D. G. Jackson et al. 1993). The ISGs are thought to be structurally related to the VSG protein family and have a small cytoplasmic

domain and an extracellular domain that is similar in size to VSG (Carrington & Boothroyd 1996). It has previously been thought that the VSG coat completely shields the ISG proteins from recognition by the immune system, but these static views of the surface coat have now been challenged by the observation that antibodies can bind to ISG65 on live trypanosomes (W.-L. Chung et al. 2004).

Most other *T. brucei* surface proteins are localised to a specialised flask-shaped invagination of the plasma membrane, known as the flagellar pocket (FP), where these relatively sequestered proteins are protected from recognition by the host immune system (Figure 1.13). These molecules include surface receptors, such as the *ESAG6/7*-encoded transferrin receptor heterodimers that are also GPI-anchored. In addition there are type I transmembrane proteins encoded by the *ESAG4* gene family containing an extracellular domain of 70–80 kDa and a cytoplasmic adenylate cyclase domain (Steverding et al. 1994; Steverding et al. 1995; Paindavoine et al. 1992). The mechanism for specific localization of different proteins to the FP membrane in unclear. However, it appears that retention in the flagellar pocket may be a subject to saturation, as the overexpression of the transferrin receptor results in its escape to the outer cell surface membrane (Mussmann et al. 2004).

1.10.Endocytosis and endomembrane transport system

The flagellar pocket membrane is continuous with the membrane on the flagellum and cell surface and is the only site of exocytosis and endocytosis in *T. brucei* (Figure 1.13) (Overath et al. 1997; Grünfelder et al. 2002; Gull 2003) The subpellicular microtubule corset lies underneath the plasma membrane and its dense

network restricts membrane exchange with the cell surface to the flagellar pocket. *T. brucei* has a highly polarised cell organisation and this also applies to its endomembrane system. The endocytic network is located between the nucleus and the kinetoplast. The cells contain a single large lysosome which is found close to the nucleus. The endoplasmic reticulum forms an exception to this highly organised network, as it stretches throughout the cell body (Overath & Engstler 2004). The rate of membrane turnover in the flagellar pocket is extremely high, and is, in fact, the highest rate reported to date. Trypanosomes are capable of turning over their entire cell membrane 2.6 times faster than macrophages (Thilo 1985). The whole surface VSG coat is estimated to be recycled through the flagellar pocket in about 12.5 min, which is also the time necessary for fluid-phase endocytosis to occur (Engstler et al. 2004). This rate is remarkable, considering that the surface of the flagellar pocket membrane is only about 5% of the total cell membrane (Overath & Engstler 2004). It is possible that this high rate of endocytosis is a non-specific method employed by the trypanosomes to prevent flagellar pocket-specific proteins escaping onto the pellicular cell membrane.

The rapid turnover of the VSG coat could be important for virulence, because it is one of the protective mechanisms employed by the parasite against attack by the immune system. It has been observed that anti-VSG antibodies bound to the surface VSG coat of living trypanosomes in *in vitro* cultures are rapidly internalized and degraded, whereas the VSG molecules are recycled back to the cell surface (Barry 1979; O'Beirne et al. 1998). Thus, the parasites can clear surface-bound antibodies to withstand the increasing titre of anti-VSG immunoglobulins. At a certain threshold antibody concentration, however, the cells are overwhelmed and killed. Rates of

endocytosis are even higher in stumpy form *T. brucei*, which are a non-proliferative form of the parasite (Figure 1.4) (Acosta-Serrano et al. 2006). This internalization of VSG immune complexes serves to "clean" the surface coat, providing the parasite with some protection from antibody-mediated lysis (Balber et al. 1979; McLintock et al. 1993). Interestingly, VSG and the transferrin receptor, which are both GPI-anchored, are recycled back to the cell surface, suggesting that this might be the default pathway for GPI-attached surface molecules (Kabiri & Steverding 2000). This observation has been confirmed by the expression of GPI-attached GFP that was also actively recycled back to the cell surface (W.-L. Chung et al. 2004; K. J. Schwartz et al. 2005; Engstler & Boshart 2004).

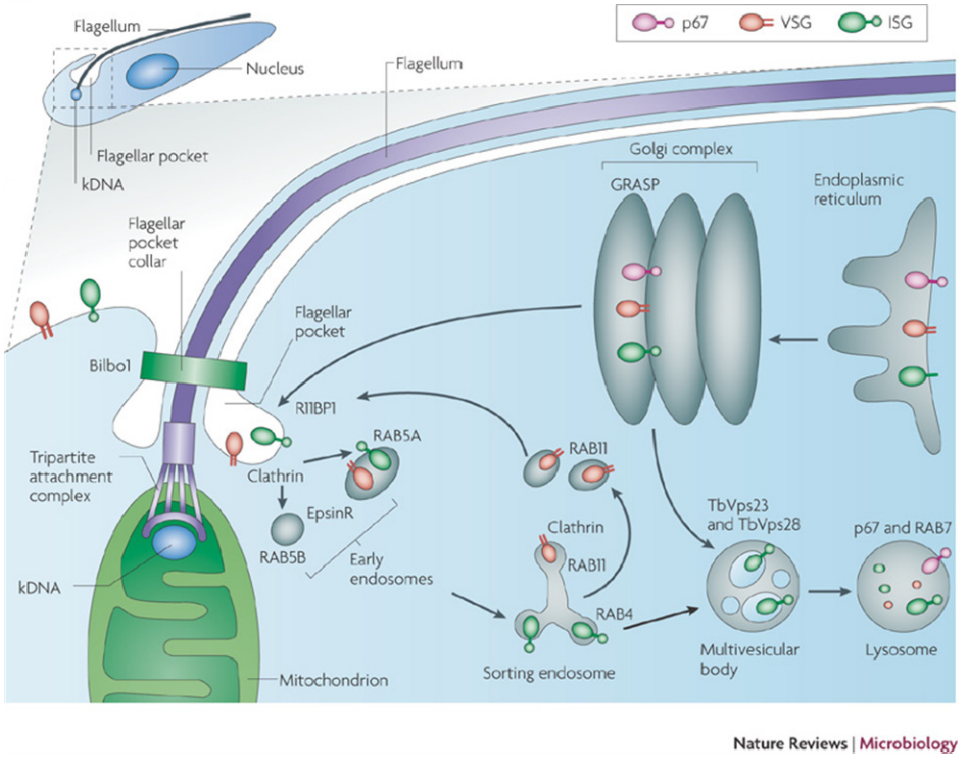


Figure 1.13: The endocytic network of bloodstream form *T. brucei* (M. C. Field & Carrington 2009)**.** The schematic shows the flagellum emerging from the flagellar pocket and extending to the anterior part of the cell. The expanded section shows the endocytic and recycling pathways with arrows indicating the trafficking of internal membranes and the markers defining the different

compartments. The traffic routes of three different surface proteins are shown (p67, ISG – proteins with transmembrane domains and VSG – a GPI-anchored protein).

Endocytosis in mammalian cells can occur through one of the following four mechanisms: clathrin-based endocytosis, calveolae-mediated internalisation, clathrin- and calveolae-independent endocytosis and macropinocytosis. Endocytosis in *T. brucei*, including VSG internalisation, occurs exclusively in a clathrin-mediated fashion, as knock-down of clathrin by inducing RNAi results in a very characteristic, "big-eye" phenotype (Allen et al. 2003). Blocking synthesis of the clathrin heavy chain causes inhibition of endocytosis, but not exocytosis, which leads to a large increase in the size of the flagellar pocket and the "big-eye" appearance of the parasites (Allen et al. 2003).

Clathrin-coated pits bud off the cell membrane lining the flagellar pocket and the lumenal surface of these invaginations appears to be covered with the dense VSG coat covering the rest of the cell membrane (Grünfelder et al. 2003). These vesicles rapidly lose their clathrin lattice and are also known as early endosomes (Figure 1.14). In bloodstream form *T. brucei* there appears to be further differentiation of the early endosomes into subpopulations co-localising with either Rab5A or Rab5B small GTPases. This discrimination seems to exist in response to the need for sorting of endosomal cargo. Thus, Rab5A has been found to be responsible for VSG, anti-VSG antibodies and transferrin receptor uptake, while depletion of Rab5B causes a block in distribution of poly-*N*-acetyllactosamine-containing glycoproteins, as well as endocytosis (Pal et al. 2002; Pal et al. 2003). Early endosomes are the early branch point for sorting of cargo, as it can be delivered to recycling endosomes or late

endosomes. Late endosomes can be identified by the presence of RAB7 and they appear close to the lysosome (Chavrier et al. 1990; Denny et al. 2002).

Bloodstream form *T. brucei* cells contain one giant, flat and highly-branched recycling endosome (Benz et al. 2010). Early endosomes with their cargo fuse with the recycling endosome and it is mainly here that ligands are uncoupled from their receptors and are directed together with endocytosed fluid phase cargo into small clathrin coated vesicles (Engstler et al. 2004). These clathrin-coated vesicles do not contain any VSG molecules or transferrin receptors and their two potential fusion targets are either the late endosomes or the lysosome. By such negative mechanism of exclusion, GPI-anchored proteins are retained in the recycling endosome of the parasite. Later, small disk-shaped vesicles bud off the recycling endosome where VSG is found in concentrated amounts and these vesicles, also known as exocytic carriers, fuse with the flagellar pocket membrane (Grünfelder et al. 2003). The small GTPase Rab11 is an established marker of both the recycling endosome and the exocytic carriers (Figure 1.14) (Grünfelder et al. 2003).

It is interesting to note that although both VSG and transferrin receptor are GPI-anchored to the cell membrane, the recycling of VSG is about 10 times faster than that of the transferrin receptor (Kabiri & Steverding 2000). This poses a question as to how the cells differentiate one GPI-anchored protein from another. In order for the transferrin receptor to liberate its cargo transferrin, an acidic environment is required, which is found in late endosomes. However, it appears that only small proportion of the internalised membrane reaches late endosomes and the preferential route is early and recycling endosomes. For this reason only a small amount of the endocytosed transferrin receptor reaches late endosomes and the bulk

of it is recycled back to the flagellar pocket (Kabiri & Steverding 2000). Endocytosed VSG, however, is conspicuously absent from late endosomes and is instead preferentially and rapidly returned back to the cell surface. It is possible that the number of GPI anchors per protein influences the fate of the protein in the endomembrane system (Triggs & Bangs 2003; K. J. Schwartz et al. 2005; K. J. Schwartz & Bangs 2007). For example, each VSG monomer is GPI-anchored and as the complete VSG is a homodimer, this results in two GPI anchors per native VSG. In contrast, the transferrin receptor is a heterodimer of the products of ESAG6 and ESAG7, but only ESAG6 is GPI-anchored, providing a single GPI attachment to the cell surface per functional protein. Thus, the VSG dimer with its two attachment points is extremely stable with a half-life of about 36 hours and is excluded from the lysosome (Bülow et al. 1989; Seyfang et al. 1990). The transferrin receptor, with a half-life of approximately 1.5 hours, is gradually directed to the lysosome, although it is mainly recycled back to the flagellar membrane (Mussmann et al. 2004; K. J. Schwartz et al. 2005; K. J. Schwartz & Bangs 2007). However, the precise mechanism behind the exclusion of GPI-anchored proteins from late endosomes remains to be elucidated.

It is important to note that there are marked differences in endocytosis rates between the different life cycle stages of *Trypanosoma brucei*. As previously mentioned, the rate of endocytosis increases 3-4 fold as the proliferative slender bloodstream form of the parasite differentiates into the short stumpy stage, pre-adapted for ingestion by the insect vector (Acosta-Serrano et al. 2006). The differences in rates of endocytosis between bloodstream and procyclic form *T. brucei* are even more dramatic, and are estimated to be between 10 to 100 fold, depending

on the particular trypanosome strain (Langreth & Balber 1975; Pal et al. 2002; Engstler et al. 2005). These differences are probably related to the role of endocytosis in immune system evasion of the bloodstream form of the parasite and are reflected in the different roles of the various endosomal marker GTPases in the two life cycle stages. For example, the bloodstream form Rab4 that localises to an early endocytic compartment, is primarily involved in fluid phase endocytosed cargo degradative trafficking to the lysosome and appears to have a minimal role in receptor-mediated endocytosis or recycling (B. S. Hall et al. 2004). In the procyclic form cells, however, Rab4 functions not only in fluid phase cargo transport, but is also involved in recycling and cell surface expression of procyclin, the major surface protein in this life cycle stage (B. S. Hall et al. 2005).

1.11.VSG movement on the parasite cell surface

The high rate of clathrin-mediated endocytosis in the flagellar pocket ensures the rapid internalisation of surface-bound anti-VSG antibodies (Barry 1979; O'Beirne et al. 1998; Pal et al. 2003). As these are removed from the VSG within the cell, before the VSG is returned back to the cell surface, this results in cleaning of the VSG coat (Balber et al. 1979). The VSG coat is densely packed on the parasite cell surface, but individual VSG homodimers can diffuse laterally by random Brownian motion with a diffusion coefficient of 1 x 10^{-10} cm^2/s (Bülow et al. 1988). This random diffusion is too slow to explain the rapid turnover of the VSG surface coat that ensures immune evasion at low anti-VSG antibody titres. Transmembrane proteins are translocated through their interaction with the microtubule lattice

underlying the cell membrane and intermediate proteins. However, VSGs are GPI anchored and therefore lack unique cytosolic domains that could mediate their unidirectional movement. This problem appears to be resolved by the motility of the parasite, which is essential for viability (Broadhead et al. 2006). Trypanosome motility is enabled by the flagellum, which alternately undergoes right-handed and left-handed helical rotations that propagate from tip to base, propelling the cell forward (Rodriguez et al. 2009). In this manner the flagellum tip leads at the anterior end of the cell, whereas the flagellar pocket, where the flagellum emerges out of the cell membrane, is at the posterior end of the cell.

It has been demonstrated that trypanosome forward movement drives the surface molecules towards the flagellar pocket at the posterior end due to the hydrodynamic flow forces that these molecules experience on the cell surface (Figure 1.14) (Engstler et al. 2007; Dean & Matthews 2007). The mammalian bloodstream is a highly viscous environment and when an antibody binds to a VSG molecule it acts like a "sail" for a particular VSG on the parasite surface (Figure 1.14A) (Engstler et al. 2007). The fluid pressure on the trypanosome cell surface due to the movement of the cell through the bloodstream pushes the VSG-antibody complex unidirectionally towards the flagellar pocket where it can be endocytosed. The VSG-antibody complex is transported through the endocytic system, where the antibody is stripped off the VSG and degraded, whereas the VSG is returned to the cell surface.

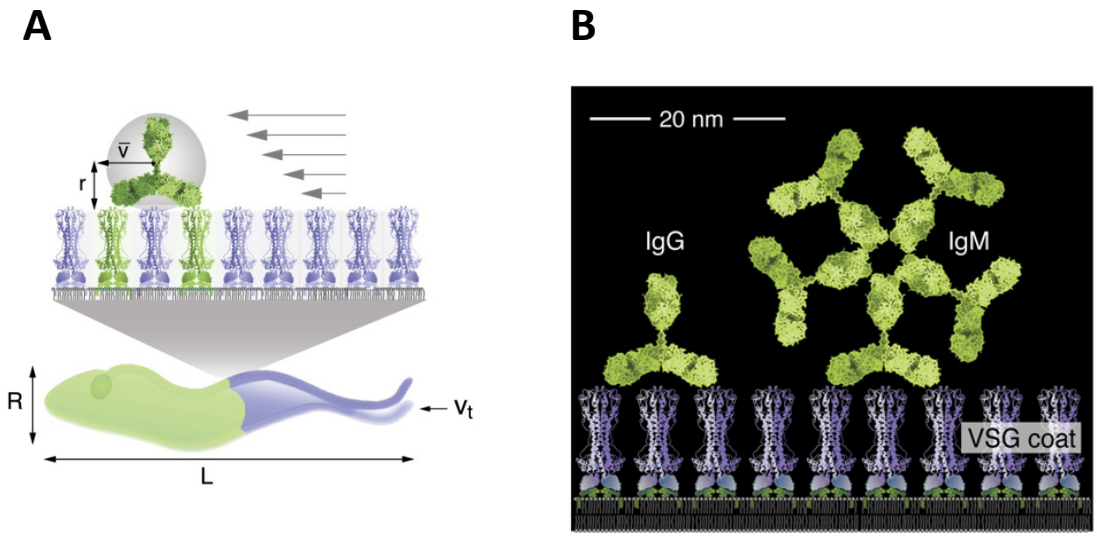


Figure 1.14: Hydrodynamic flow forces are responsible for the drag experienced by antibody-VSG complexes on the cell surface (Engstler et al. 2007)**.**

A. The forward movement of the parasite generates fluid pressure on the cell surface that pushes the VSG-immunoglobulin complexes towards the posterior flagellar pocket more rapidly than VSG molecules not coupled to antibodies.

B. The IgM type of antibodies that are associated with trypanosome infection are even more efficiently internalised than IgG due to their larger size.

The size of the VSG-bound antibody plays an important role in the "sail" hypothesis of VSG-antibody complex sorting on the cell surface, as the larger the size of the antibody, the greater the fluid pressure it will experience and the faster the complex will be pushed towards the flagellar pocket (Figure 1.14B) (Engstler et al. 2007; Dean & Matthews 2007). Therefore, utilising hydrodynamic flow to drive the movement of immune complexes along the trypanosome cell surface could be another evolutionary adaptation of the parasites to aid immune evasion.

1.12.DPhil objectives

My DPhil project can be summarised in the following 4 aims directed to study the cell biology of the Variant Surface Glycoprotein of *T. brucei*:

1. Investigate the cell cycle arrest triggered by the induction of *VSG* RNAi in *T. brucei* in an attempt to elucidate the signalling cascade causing the observed pre-cytokinesis cell cycle arrest.

2. Study the mechanisms through which *T. brucei* senses the intracellular levels of VSG, and investigate the biological relevance of the *VSG* RNAi-triggered phenotype.

3. Identify the specific mechanisms that mediate the parasite clearance from the bloodstream of infected mice after induction of *VSG* RNAi by studying the properties of the VSG coat.

4. Determine the importance of the genomic localisation of the active VSG at the telomere end of the Expression site for adequate levels of *VSG* expression and the protectiveness of the VSG coat.

Chapter 2

Materials and Methods

2.1. Materials

2.1.1. *Trypanosoma brucei* strains

The *T. brucei* strains used in this study are outlined in Table 2.1, Table 2.2 and Table 2.3. The VSG expressed, either VSG221 (MITat 1.2), or VSG117 (MITat 1.5), is indicated. The appropriate drug resistance genes for each cell line are detailed – neomycin (G418), hygromycin (Hygro), blasticidin (Blast), phleomycin (Phleo) or puromycin (Puro).

2.1.1.1. Wild-type strains

Table 2.1: Wild-type bloodstream (BF) and procyclic form (PF) *Trypanosoma brucei* strains used in this study.

Strain	Life cycle stage	VSG expressed	Drug resistance marker	Reference
90-13 427	BF	VSG221	G418; Hygro	(Wirtz et al. 1999)
"Single marker" 427	BF	VSG221	G418	(Wirtz et al. 1999)
29-13	PF	-	G418; Hygro	(Wirtz et al. 1999)

2.1.1.2. Transgenic strains

Transgenic *T. brucei* cell lines used were either generated during the course of this study or were previously described (Table 2.2 and Table 2.3). All of the *T. brucei* cell lines generated in this thesis were bloodstream form.

Table 2.2: Previously described transgenic bloodstream form *Trypanosoma brucei* strains used in this study.

Strain	Parental strain	VSG expressed	Drug resistance markers	Integrated constructs	Selection markers in active ES	Reference
221VB1.1	90-13 427	VSG221	G418 Hygro Blast Phleo	MC^{177}VSG221 RNAi pHNES221Blast	Blast	(Sheader et al. 2005)
221VG1.1	90-13 427	VSG221	G418 Hygro Phleo Puro	MC^{177}VSG221 RNAi 221GP1	Puro	(Sheader et al. 2005)
P221	"Single marker" 427	VSG221	G418 Blast Phleo	MC^{177}VSG221 RNAi pHNES221Blast1.6	Blast	Rudenko laboratory

Table 2.3: Bloodstream form *Trypanosoma brucei* strains generated during this study.

Strain	Parental strain	Active VSG expressed	Drug resistance marker	Integrated constructs	Selection markers in active ES	Reference
221VP117	221VB1.1	VSG221 VSG117	G418 Hygro Phleo Puro	MC^{177}VSG221 RNAi p221-purVSG117UTR	Puro	(T. K. Smith et al. 2009)
221/117mc	P221	VSG221 VSG117	G418 Hygro Blast Phleo	MC^{177}VSG221 RNAi pHNES221Blast1.6 pGad9 177bp –tet op 117 VSG UTR	Blast	Rudenko laboratory
221Tub117	P221	VSG221 VSG117	G418 Hygro Blast Phleo	MC^{177}VSG221 RNAi pHNES221Blast1.6 pGad8-tubulin117VSGUTR	Blast	Rudenko laboratory
V221	"Single marker" 427	VSG221	G418 Blast	pHNES221Blast1.6	Blast	Rudenko laboratory

V221/117	"Single marker" 427	VSG221 VSG117	G418 Puro	p221-purVSG117UTR	Puro	Rudenko laboratory
V117Δ221	V221/117	VSG117	G418 Puro Blast	p221-purVSG117UTR pBS_VSG221KOblast	Puro Blast	Rudenko laboratory
B221/117	90-13 427	VSG221 VSG117	G418 Hygro Puro	p221-purVSG117UTR	Puro	Rudenko laboratory
B221/117 RNAi	B221/117	VSG221 VSG117	G418 Hygro Puro Phleo	p221-purVSG117UTR p2T7 177 Phleo VSG117 RNAi	Puro	Rudenko laboratory
BΔ221/117 RNAi	B221/117 RNAi	VSG117	G418 Hygro Puro Phleo Blast	p221-purVSG117UTR p2T7 177 Phleo VSG117 RNAi pBS_VSG221KOblast	Puro Blast	Rudenko laboratory

2.1.2. Plasmids and constructs

DNA constructs were generated using standard molecular biology techniques (Table 2.4). Constructs were verified by PCR analysis, restriction endonuclease digestions and sequence analysis.

Table 2.4: Plasmids and constructs used in this project.

Construct	Parent	Description	Reference
MC^{177}VSG221 RNAi	p2T7Ti-177 (Wickstead et al. 2004)	A 803-bp *VSG221* target fragment (GenBank accession no. X56762, positions 122–925) was inserted between opposing T7 promoters of p2T7Ti-177 construct.	(Sheader et al. 2005)
pHNES221Blast1.6	pHNES221	A blasticidin resistance gene (399 bp) was inserted between *VSG221* Expression site promoter-proximal targeting sequences targeting it 216 bp downstream of the	Rudenko laboratory

		transcription start site.	
221GP1	pHNES221	An enhanced *GFP* and a puromycin resistance genes were inserted between *VSG221* Expression site promoter-proximal targeting sequences targeting them 216 bp downstream of the transcription start site.	(Sheader et al. 2004)
p221-purVSG117UTR	pHNES221	*VSG117* and a puromycin resistance gene were inserted between *VSG221* Expression site promoter-proximal targeting sequences targeting them 216 bp downstream of the transcription start site.	(T. K. Smith et al. 2009)
pGad9 177bp –tet op 117 VSG UTR	pGad-9-177bp 117VSG UTR	*VSG117* gene was inserted into pGad9 construct, which targets the 177 bp repeats (Wickstead et al. 2003). The tetracycline operator sequence was deleted from the construct enabling constitutive expression of the *VSG117* gene.	Rudenko laboratory
pGad8-tubulin117VSGUTR	pGad8 (Wickstead et al. 2003)	*VSG117* gene was inserted the pGad8 construct with integrates into the αβ-tubulin array (Wickstead et al. 2003).	Rudenko laboratory
pBS_VSG221KOblast	pBS_VSG221KOupdn	A blasticidin resistance gene was inserted between *VSG221* processing splice signal at the 5'-end and *VSG221* polyadenylation sequences at its 3'-end, which were also used as targeting fragments for the construct.	Rudenko laboratory
p2T7 177 Phleo VSG117 RNAi	p2T7Ti-177 (Wickstead et al. 2004)	A 816-bp *VSG117* target fragment (GenBank accession no. X01387, positions 60–875) was inserted between the opposing T7 promoters of the p2T7Ti-177 construct.	Rudenko laboratory

2.1.3. Antibodies

A list of primary and secondary antibodies used during this study, detailing the organism origin, as well as the respective dilutions in western blots and immunofluorescence analysis where appropriate (Table 2.5 and Table 2.6).

Table 2.5: Primary antibodies used for western blotting and immunofluorescence analysis.

Primary antibody	Organism	Origin	Dilution in western blots	Dilution in immunofluorescence
anti-VSG221 (western analysis)	rabbit	A gift from Piet Borst	1:10 000	-
anti-VSG221 (IF analysis)	rabbit	A gift from Jay Bangs	-	1:1000
anti-VSG117	rabbit	G. Rudenko	1:10 000	1:1000
anti-eIF2α	rabbit	A gift from Mark Carrington	1:10 000	-
anti-eIF4A1	rabbit	A gift from Mark Carrington	1:8 000	-
anti-eIF4E1	rabbit	A gift from Mark Carrington	1:100	-
anti-eIF4E2	rabbit	A gift from Mark Carrington	1:100	-
anti-eIF4E3	rabbit	A gift from Mark Carrington	1:5000	-
anti-eIF4E4	rabbit	A gift from Mark Carrington	1:100	-
anti-EP	mouse	CEDARLANE® Laboratories Limited	1:2000	-
anti-BiP	rabbit	A gift from Jay Bangs	1:10 000	-
anti-VSG VO2	rabbit	A gift from Piet Borst	1:1000	-
anti-VSG 1.8	rabbit	A gift from Piet Borst	1:5000	-
anti-ISG65	rabbit	A gift from Mark Carrington	1:1000	-
anti-ISG75	rabbit	A gift from Mark Carrington	1:5000	-
anti-TDP 1	rabbit	A gift from Klaus Ersfeld	1:10 000	-

Table 2.6: Secondary antibodies used for western blotting and immunofluorescence analysis.

Secondary antibody	Organism	Origin	Dilution in western blots	Dilution in immunofluorescence
anti-rabbit IgG horseradish peroxidase	donkey	Abcam	1:5 000	-
anti-mouse IgG horseradish peroxidase	donkey	Abcam	1:5 000	-
Alexa Fluor® 488 anti-rabbit IgG (H+L)	goat	Invitrogen	-	1:10 000
Alexa Fluor® 594 anti-rabbit IgG (H+L)	goat	Invitrogen	-	1: 10 000
IRDye 680LT anti-Rabbit IgG (H + L)	goat	LI-COR Biosciences	1:10 000	-

2.1.4. Frequently used media and buffers

All media and buffers were prepared in molecular biology grade distilled water (Table 2.7). The appropriate method of sterilization (autoclaving at 125°C for 15 min or filtering) has been indicated (Table 2.7).

Table 2.7: Recipes of media and buffers used during this study.

Medium or buffer	Recipe
HMI-9 medium	Recipe in (H. Hirumi & K. Hirumi 1989). HMI-9 was complemented with 10% (v/v) heat-inactivated Foetal Calf Serum (Gibco) and 10% (v/v) Serum Plus (SAFC Biosciences). Appropriate drugs were added to maintain selection on the relevant constructs.
SDM-79 medium	Recipe in (R Brun & Schönenberger 1979). SDM-79 was complemented with

	10% (v/v) heat-inactivated Foetal Calf Serum (Gibco) and 5 mg/L haemin. Appropriate drugs were added to maintain selection.
Cytomix	10 mM K_2HPO_4/KH_2PO_4 pH 7.6; 2 mM EGTA; 120 mM KCl; 150 μM $CaCl_2$; 25 mM HEPES; 5 mM $MgCl_2$; 0.5% (w/v) glucose; 1 mM hypoxanthine; 100 μg/ml BSA. pH 7.6; filter-sterilised
Protein lysis buffer	50 mM HEPES (pH 7.5); 1 mM EGTA; 1.5 mM $MgCl_2$; 10% (v/v) glycerol, 1% (v/v) Triton X-100; one mini complete protease inhibitor cocktail tablet (Roche Diagnostics) per 10 mL of mixture; Filter-sterilised.
4 x Protein loading buffer	250 mM Tris-HCl pH 6.8; 8% (w/v) SDS; 40% (v/v) Glycerol; 0.01% (w/v) Bromophenol Blue
1 x SDS PAGE buffer	25 mM Tris; 250 mM Glycine; 0.05% (w/v) SDS
1 x Protein transfer buffer	20% methanol; 47.9 mM Tris; 38.6 mM glycine; 1.28 mM SDS
Western stripping buffer	100 mM 2-mercaptoethanol; 2% (w/v) SDS; 62.5mM Tris-HCl pH6.7
Coomassie staining solution	0.1% Coomassie brilliant blue R-250, 10% (v/v) acetic acid; 50% (v/v) methanol
Coomassie destaining solution	10% (v/v) acetic acid; 50% (v/v) methanol
Polysome buffer	120 mM KCl; 2 mM $MgCl_2$; 20 mM Tris, pH 7.5; 1 mM DTT; Filter-sterilised
1 x TE buffer	10 mM Tris pH 7.5, 1 mM EDTA; Sterilised by autoclaving.
1 x TDB	5 mM KCl; 80 mM NaCl; 1 mM $MgSO_4$; 20 mM Na_2HPO_4; 2 mM NaH_2PO_4; 20 mM glucose; pH 7.4; Sterilised by autoclaving prior to addition of glucose. Filtered-sterilised after addition of glucose
1 x PBS	1 mM KH_2PO; 10 mM Na_2HPO_4; 137 mM NaCl; 2.7 mM KCl; pH 7.4; Sterilised by autoclaving.
1 x PSG	60 mM Na_2HPO_4; 3 mM NaH_2PO_4; 4.4 mM NaCl; 56 mM glucose; Sterilised by autoclaving prior to addition of glucose. Filtered-sterilised after addition of glucose
1 x TNB	100 mM Tris pH 7.5; 150 mM NaCl; 0.5% (w/v) BSA
Hybridisation mix	50 mM NaPi pH 7.4; 900 mM NaCl; 5× Denhardt solution; 10% (w/v) dextran sulphate; 5 mM EDTA pH 8.0; 0.1% (w/v) SDS; 40% (v/v) formamide; 0.05 mg/mL salmon sperm DNA

2.2. Methods

2.2.1. *Trypanosoma brucei* culturing conditions

Bloodstream form *Trypanosoma brucei* strains were cultured in HMI-9 medium at 37°C (Table 2.7) and 5% CO_2. Parasites were maintained under 7-10 x 10^5 cells/mL density. The medium was supplemented with appropriate drugs as required (Table 2.1, Table 2.2, Table 2.3 and Table 2.8). Procyclic form *Trypanosoma brucei* strains were cultured in SDM-79 medium at 27°C (Table 2.7). The cell density was maintained between 1 x 10^6 and 1 x 10^7 cells/mL. The medium was supplemented with the appropriate drugs to maintain selection on the respective cell lines (Table 2.1 and Table 2.8).

Table 2.8: Concentrations of antibiotics used in maintainance of bloodstream and procyclic form *Trypanosoma brucei* cell lines.

Antibiotic	Final concentration in medium [µg/mL]	
	Bloodstream form	Procyclic form
Neomycin (G418)	2	20
Hygromycin	5	25
Blasticidin	5	20
Phleomycin	2.5	2.5
Puromycin	0.2	1 or 0.5

T. brucei cell density was routinely determined using a Neubauer counting chamber. For growth analysis bloodstream form parasites had a starting density of 1

x 10^5 cells/mL in 1.5 mL per well aliquots on a 24 well plate and cell densities were determined twice per day.

For cumulative growth analysis bloodstream form parasites were plated out at a starting density of 1 x 10^5 cells/mL in 1.5 mL per well aliquots of a 24 well plate and were diluted to the initial cell density once they reached approximately 1 x 10^6 cells/mL to maintain a continuously growing cell population. Cells densities were determined twice per day and plotted using the product of the cell density and the dilution factor.

To harvest parasites for general procedures, bloodstream form *T. brucei* was grown to mid logarithmic stage of between 7-10 x 10^5 cells/mL and procyclic form *T. brucei* was grown to a cell density of between 8-12 x 10^6 cells/mL. Parasites were harvested by centrifugation at 1300 rcf for 10 min at room temperature and washed with either PSG (bloodstream form) or PBS (procyclic form) (Table 2.7).

2.2.2. Transfection of bloodstream form *Trypanosoma brucei*

2.2.2.1. Stable transfection of construct DNA

T. brucei was grown to a mid logarithmic stage of between 7-10 x 10^5 cells/mL. Parasites were harvested by centrifugation at 500 rcf for 10 min at room temperature, and resuspended in 100 µL of Amaxa Human T-cell Nucleofector solution (Lonza). Cells were transferred into an electroporation cuvette and 10 µg of linearised construct DNA in a maximum volume of 10 µL was added. Parasites were electroporated using programme X-001 on an Amaxa Nucleofector® II (Lonza). Transfected cells were transferred into 30 mL HMI-9 containing the appropriate

parental cell line drugs, and x 10 and x 100 dilutions were prepared (Table 2.8). Each dilution was distributed in 1 mL aliquots per well into 24-well plates and incubated at 37°C for at least 8 hours. HMI-9 medium containing the parental drugs at normal concentration and the selective drug at double the normal concentration was prepared (Table 2.8) and 1 mL aliquots were added to each well of the 24-well plates. Individual clones were observed 5-6 days post transfection.

2.2.2.2. Transient transfection of morpholino oligonucleotides

HNI (221+) *Trypanosoma brucei* was grown to a mid logarithmic stage of between 7-10 x 10^5 cells/mL. Parasites were harvested by centrifugation at 500 rcf for 10 min at room temperature, and resuspended at 20 million cells/500 µL of cytomix (Table 2.7). Cells were transferred into an electroporation cuvette, and appropriate volume of 1 mM stock solution of morpholino oligonucleotides (Gene Tools) was added (Table 2.9). Parasites were electroprated at 1500 V using a BTX Electro Square Porator, ECM 830 (VWR Int.), and then transferred into 30 mL HMI-9. The cells were subsequently incubated at 37°C for 12 hours, and the phenotype was analysed.

Table 2.9: Concentrations of morpholino oligonucleotides used for the transient transfection of HNI (221+) *T. brucei* cell line.

Morpholino oligonucelotide	Transfection concentration [µM]	Volume [µL]
Anti-VSG221	12.8	32
Mismatching anti-VSG221	12.8	32
Anti-α-tubulin	3.2	8
Mismatching anti-α-tubulin	3.2	8

2.2.3. Nucleic acids manipulations

2.2.3.1. PCR amplification and general DNA cloning procedures

Trypanosoma brucei oligonucleotides primers (Europhins MWG) were designed according to the published *T. brucei* 927 strain genome sequence (Berriman et al. 2005; R. Young et al. 2008). PCR was performed using standard methods in a Thermal cycler PTC-0200 DNA Engine PTC200/96 (Genetic Research Instrumentation Ltd.). The primer sequences used for the linking PCRs are outlined in Table 2.10.

Table 2.10: Sequences of primers used for PCR analysis to establish linkage of sequences.

Amplicon	Primer sequences (5' → 3')
Blasticidin to *ESAG7* in active *VSG221* ES	BSR_24s: gaatccaccctcattgaaagag ESAG6/7_574as: gcagaaaagcttgcaactcc
VSG221 internal	VSG221_46s: ctagcccaagttcttccaattc VSG221-558as: gctgtatcggcgacaactgcag
Blasticidin internal	BSR1s: atggccaagcctttgtctc BSR138as: gacaccagtgaagatgcggc
Blasticidin to sequences upstream of telomeric VSG position in the active *VSG221* ES	VSG221up 56166s: ggggaaatacagtctgtgaagc BSR138_as: gacaccagtgaagatgcggc
Blasticidin to sequences downstream of telomeric VSG position in the active *VSG221* ES	BSR_321s: agtgaaggacagtgatggacagcc VSG221dn 58851as: aaatccaggatagaggtgtgag

Real-time PCR analysis was carried out in triplicate for each reaction in 20 µL total reaction volume with 19 µL of qPCR reaction mix (containing Brilliant II SYBR QPCR Low ROX Master Mix (Stratagene) and 0.5 µM of sense and anti-sense primers, each) and 1 µL template DNA. Reactions were carried out using a

7500 Real-Time PCR System (ABI applied biosystems). All PCR primers and conditions were first optimized to produce a single amplicon of the correct size (Table 2.11).

Table 2.11: Sequences of primers used for the real-time PCR analysis.

Amplicon	Primer sequences (5' → 3')
VSG221	VSG221_46s: ctagcccaagttcttccaattc VSG221_207as: cctcattttctggattttgctc
VSG221-associated *VSG221* 3'UTR	VSG221_966s_qPC: gcctcagaaatacaaacaga VSG3'UTR_1486as: aaaagttttcaagtagcagg
eGFP	eGFP_184s: gtgaccaccctgacctac eGFP_324as: cttgtagttgccgtcgtc
eGFP-associated *VSG221* 3'UTR	eGFP_442s_qPCR: agccacaacgtctatatc VSG3'UTR_1486as: aaaagttttcaagtagcagg
α-Tubulin	alphaTub 56s: cctgctgggaattgttctg alphaTub 169as: cagtctcagagaagaaggtgttg
Actin	Actin_1031s: gttccatcctctcatcacta Actin_1091as: tcgtattcactcttcgttatc

DNA cloning was performed using standard methods (Sambrook & Russell 2001). Purified plasmid vector DNA was treated with shrimp alkaline phosphatase (SAP) (Roche) to reduce vector re-ligation according to manufacturer's procedure. Insert DNA was ligated to SAP-treated vector DNA at appropriate proportions in a volume not exceeding 20 µL using 1 U of T4 DNA ligase (Roche) and 2 µL of 10 x Ligase Buffer (Roche) according to the manufacturer's instructions. DH5α competent cells (F$^-$ϕ80d*lac*ZΔM15 Δ(*lac*ZYA -*arg*F) U169 *rec*A1 *end*A1 *hsd*R17(rK-, mK+) *pho*A *sup*E44 λ-*thi*-1 *gyr*A96 *rel*A1) (Stratagene) were used for plasmid DNA transformations. For small-scale plasmid DNA isolation QIAprep Spin

Miniprep Kit (Qiagen) was used following the protocol outlined by the manufacturer. For large-scale plasmid DNA isolation QIAGEN Plasmid Midi Kit (Qiagen) was used following the manufacturer's instructions.

2.2.3.2. Isolation and analysis of nucleic acids from *Trypanosoma brucei*

Parasites were harvested by centrifugation and genomic DNA was isolated using the DNeasy Blood & Tissue Kit (Qiagen) according to the manufacturer's protocol. Total RNA was isolated from parasites using the RNeasy Mini Kit (Qiagen) as specified by the manufacturer. Before use for quantitative PCR analysis, total RNA was first DNase treated using the TURBO DNA-free kit (Ambion) following the manufacturer's instructions. 1 mg RNA per sample was subsequently used as a template for cDNA synthesis using oligo-dTs and the Omniscript RT kit (Qiagen) according the manufacturer's specifications.

For Southern blot analysis *T. brucei* genomic DNA (2 µg per sample) was digested using the appropriate restriction enzymes (New England BioLabs) and resolved on 0.6% agarose gels with 1 x TBE buffer. The gel was depurinated (0.25 N HCl for 15 min), denatured (0.5 M NaOH/ 1.5 M NaCl for 30 min) and neutralised (1 M Tris-HCl pH 7.4/1.5 M NaCl for 45 min). DNA was blotted onto Hybond™-XL membrane (GE Healthcare) using standard protocols.

For northern blot analysis total isolated RNA (1-1.5 µg per sample) was mixed with 10 mM MOPS, pH 7.0; 1 mM NaOAc; 0.5 mM EDTA 50% (v/v) formamide; 17.5% (v/v) formaldehyde; 60 µg/mL ethidium bromide and denatured for 15 min at 65°C. 10 x RNA loading dye was added and RNA was resolved on 1.5% formaldehyde-agarose gel in 1 x MOPS buffer (Table 2.7). RNA gel was then

washed 2 x 10 min in deionised water and 2 x 15 min in 20 x SSC. RNA was transferred onto Hybond™-XL membrane (GE Healthcare) using standard protocols.

Blots were pre-incubated in hybridization solution at 42°C in a hybridisation Incubator Techne HB-1DE (Fisher Scientific) for at least 1 hour (Table 2.7). Blots were hybridised overnight with random primed probes that had been radiolabeled with [^{32}P]-dCTP using Amersham Ready-To-Go DNA labelling Beads (-dCTP) (GE Healthcare) following the instructions of the manufacturer. The probes were PCR amplified from the 90-13 *T. brucei* genome using the appropriate primers (Table 2.12). Membranes were washed in 3 x SSC at 42°C for 10 min, 3 x SSC/0.1% SDS at 65°C for 15 min, 0.3 x SSC/0.1% SDS at 65°C for 15 min and 0.1 x SSC/0.1% SDS at 65°C for 45 min. The blots were imaged with a Personal Molecular Imager FX (Bio-Rad).

Table 2.12: Sequences of primers used for the amplification of the DNA probes used in this study.

Probe	Primer sequences (5' → 3')
VSG221	800 bp *VSG221* target fragment (accession number X56762, positions 122-925), sub-cloned from a *T. brucei* HNI genomic DNA clone (Sheader et al. 2005)
VSG117	VSG117 RNAi 65s: tatcactgctttacgccatcac VSG117 RNAi 853as: caagatatgaaggcagacccag
β-Tubulin	BTub_111s: gggtgactctgacctg BTub_810as: cttcatgatgggcttc
Actin	Actin 361s: acgcagattatgtttg Actin 970as: gcaatcttgcaccgt
TDP1	TDP 151s: gcggctatagatgacattgttg TDP 756as: ggagaggaaggtctacgaggag
PFR2	PFR2 761s: gcatcattgggcaaac PFR2 1450as: cacattcaactggag

NUP1	Nup1 65s:gcttctcacatgcccaatattt Nup1 676as: tatttgccttgtgaatttacgg
ESAG3	ESAG3-2s: tgaaatttggtacctcgagagc ESAG3-501as:gtgttatgcccctcagttgg
ESAG5	ESAG5_61s: gttgtatcatcggctctggca ESAG5_565as: aagggaaatcaaaggtgcctaa
ESAG6/7	ESAG6/7_88s: accgccgctaataaagtgtg ESAG6/7_574as: gcagaaaagcttgcaactcc
eGFP	eGFP_7s: agcaagggcgaggagctgtt eGFP-705as: ggatcactctcggcatggac
ISWI	1190 bp *TbISWI* target fragment (accession number Tb927.2.1810, positions 4–1194 of the *TbISWI* open reading frame) (Hughes et al. 2007)
Blasticidin	BSR1s: atggccaagcctttgtctc BSR138as: gacaccagtgaagatgcggc
VSG Ψ	221Pseudo_422s: caagcattaccagagaagt 221Pseudo-948as: ctagtcatttgattccgctacc

2.2.4. Protein manipulations

Total protein was isolated from parasites by suspension in cold protein lysis buffer at a concentration of $1x10^5$ cells/mL (Table 2.7). Lysates were incubated on a rotating wheel at 4°C for 20 minutes.

Before SDS-PAGE, protein loading buffer and 50 mM DTT were added to the protein lysates, and samples were denatured at 100°C for 10 minutes (Table 2.7). Protein lysates were resolved on polyacrylamide gels using 5% stacking gel and 10% separating gel in a Mini-PROTEAN gel apparatus (Bio-Rad) in 1 x SDS PAGE buffer (Table 2.7).

SDS polyacrylamide gels were stained in Coomassie solution for 1 hour at room temperature before de-staining (Table 2.7). The gels were dried using the DryEase Mini-Gel Drying system (Invitrogen) following manufacturer's instructions.

Proteins were blotted from an SDS polyacrylamide gel onto Hybond-P membrane (GE Healthcare) using wet electrophoresis transfer in a Mini Trans-Blot Cell (Bio-Rad) with 1 x Protein transfer buffer (Table 2.7). Blots were blocked in 1 x PBS with 5% milk solution overnight at 4°C or for 1 hour at room temperature and then washed 2 x 5 min in 1 x PBS with 0.1% TWEEN. Proteins were detected with primary and secondary antibodies in 1 x PBS with the addition of 0.1% TWEEN and 2% milk (Table 2.5 and Table 2.6). Blots were washed after each antibody incubation for 3 x 15 min in 1 x PBS with 0.1% TWEEN. Detection was performed using Western Lightning Detection Kit (Perkin Elmer) and a Fluor-S MAX imager (Bio-Rad) or ChemiDoc XRS+ imager (Bio-Rad). Western blots were stripped of bound antibodies by incubating in western blots stripping buffer at 50°C for 30 min, followed by 2 x 10 min washes in 1 x PBS with 0.1% TWEEN.

Western blots for imaging using the LI-COR infrared detection system were probed following essentially the same procedure except that blots were blocked and incubated with antibodies in Odyssey Blocking Buffer (LI-COR). In addition the secondary antibody used was the IRDye 680LT anti-Rabbit IgG (H + L) (LI-COR) and proteins were visualized on an Odyssey IR-Scanner (LI-COR).

2.2.5. Microscopic analysis of *T. brucei*

For general DAPI staining procedure, parasites were harvested by centrifugation at 500 rcf for 10 min, washed with PSG and fixed in a final concentration of 2% paraformaldehyde. The cells were allowed to settle on glass slides for 30 min at room temperature and subsequently mounted with VECTASHIELD Mounting Medium with DAPI (Vector Labs).

Immunofluorescence analysis was performed with slides prepared as above, only with incubation with rabbit antibodies raised against the N-termini of VSG221 or VSG117, followed by incubation with secondary anti-rabbit antibody coupled to Alexa 594 or Alexa 488 (Molecular Probes). All antibodies were re-suspended in 1 x PNB at appropriate concentrations (Table 2.5, Table 2.6 and Table 2.7). Parasites were then mounted VECTASHIELD Mounting Medium with DAPI (Vector Labs).

Microscopic analysis was performed on an Axioplan 2 (Zeiss) microscope or Axio Imager M2 (Zeiss) microscope. Images were captured with a Cool Snap HQ (Roper Scientific) camera or an AxioCam MRc (Zeiss) camera. Images were analysed using METAMORPH 6.20 (Universal Imaging) or Axiovision 4.8 (Zeiss) imaging software and ImageJ software (National Institute of Health).

2.2.6. Polysome analysis

Polysome analysis on 221VG1.1 *T. brucei* cell line was peformed essentially as previously reported (Djikeng et al. 2003; Kramer et al. 2008). 400 mL cultures of parasites were grown to a density of approximately 7.5 x 10^5 cells/mL. *VSG221* RNAi was induced by incubating the cells with 1 µg/mL tetracycline for 24 hours. Pactamycin-treated parasites were incubated with 200 ng/mL Pactamycin (gift of Pfizer) for 20 min at 37°C, and cycloheximide-treated trypanosomes were incubated with 50 µg/mL cycloheximide (Sigma) for 10 min prior to the start of polysome purification procedure. Cells were harvested by centrifugation at 4°C and washed with HMI-9 without serum (containing either pactamycin or cycloheximide where appropriate). Parasites were subsequently resuspended in polysome buffer (containing either cycloheximide or pactamycin where appropriate) (Table 2.7). Cells

were lysed using n-octylglycoside, loaded on 10%-50% sucrose gradients and centrifuged for 2 hours at 36 000 rpm (221830 rcf) at 4ºC in a Beckman ultracentrifuge using a SW41 rotor. Gradients were harvested using a peristaltic pump and analysed with an absorbance reader at 254 nm.

2.2.7. Analysis of the cell biology of the *VSG* RNAi arrest

221VB1.1 *T. brucei* was cultured to a density of approximately 3 x 10^5 cells/mL. Parasites were incubated in the presence of 300 pg/mL doxycycline for 12 hous. Cells were harvested by centrifugation at 1300 rcf, washed with 20 mL drug-free HMI-9 and resuspended in HMI-9 with the addition of the appropriate drugs but without doxycycline. Total RNA was isolated at 0, 4, 8, 24, 32 and 56 hours after the removal of doxycycline and analysed using northern blot analysis according the previously described procedure and probed for *VSG221* transcript (Chapter 2.2.4.5).

In order to measure the cell volume, the 221VP117 *T. brucei* and 221VB1.1 *T. brucei* cell lines were cultured to a concentration of 8 – 10 x 10^5 cells/mL. 50 x dilutions from each culture were prepared in CASY® ton dilution liquid and the cell sizes were determined on a Casy® I Cell analyzer, model TT (Schärfe System GmbH).

2.2.8. Propidium iodide flow cytometry

Parasites were harvested by centrifugation and fixed in 2% paraformaldehyde for 2 hours at room temperature, permeabilised with 10% Triton X-100 and then washed again. Cells were subsequently resuspended in 1 x PBS containing 10 µg/mL

RNase A and 10 µg/mL propidium iodide (Sigma) and incubated at 37°C for 45 min. Propidium iodide staining of the cells was monitored by flow cytometry in the FL2 channel of a Beckman FACSCalibur and analysed using CellQuest software (BD Biosciences).

2.2.9. Analysis of endocytosis

To analyse endocytosis of surface immunostained VSG221, 221VB1.1 and 90-13 TDP C1 *T. brucei* cell lines were cultured to an approximate density of 7 x 10^5 cells/mL. *VSG221* or *TDP 1* RNAi was induced for 0, 8 or 12 hours. Cells were harvested by centrifugation at 500 rcf at 4°C and washed twice with cold 1 x TDB (Table 2.7). Rabbit anti-VSG221 antibody was added to the parasite suspensions and cells were incubated for 1 hour at 4ºC (Table 2.5). Endocytosis of surface immunostained VSG proteins was allowed to occur by incubating the parasites for 0, 2, 4, 8 or 16 min at 37ºC. The cells were subsequenty fixed with 2% paraformaldehyde and the residual rabbit anti-VSG221 antibody on the cell surface was detected by adding goat anti-rabbit Alexa 488-coupled secondary antibody (Table 2.6). For microscopic analysis the parasites were stained with the DNA stain DAPI. For propidium iodide staining and flow cytometry analysis the cells were treated as previously described.

To analyse fluid phase and receptor-mediated endocytosis, 221VB1.1 and 90-13 TDP C1 *T. brucei* cell lines were cultured to an approximate density of 7 x 10^5 cells/mL. *VSG221* or *TDP 1* RNAi was induced for 0, 8 or 24 hours. Cells were harvested by centrifugation at 500 rcf at 4°C and washed twice with cold 1 x TDB (Table 2.7). Parasites were subsequently incubated with either 5 µg/mL Fluorescein

labeled Lycopersicon Esculentum (Tomato) Lectin (Vector Labs) (marker for receptor-mediated endocytosis) or 5 μg/mL Alexa Fluor 488 conjugate of albumin from bovine serum (BSA) (Invitrogen) (marker for fluid-phase endocytosis) for 30 min at 4°C. Endocytosis was allowed to occur by incubating the parasites for a specified length of time at 37 ºC. The cells were then fixed with 2% paraformaldehyde and either analysed microscopically after staining with DAPI or by propidium iodide flow cytometry.

2.2.10. Complement lysis assay

Cells were harvested by centrifugation and re-suspended at a concentration of $1x10^7$ cells/mL in Barbitone complement fixation test diluent (Oxoid Ltd, Fisher) prepared according to the manufacturer's instructions. For the bloodstream form *T. brucei* the buffer was additionally supplemented with 1% glucose. The complement used for this experiment was guinea pig complement (Rockland Immunochemicals), which was added to an end volume of 5% (v/v) for all of the cell lines tested, and to 3.5% for the procyclic form *T. brucei* controls. In addition, procyclic form *T. brucei* was incubated with 5% guinea pig complement and 5μg/mL Complement receptor 1 (CR1) inhibitor (gift from Paul Morgan) to prevent complement-mediated lysis of the cells. This served as an additional control to show the specificity of the complement-mediated lysis. The cells were incubated at 37°C and cell densities were determined every 12 minutes.

Chapter 3

Blocking VSG synthesis triggers a growth arrest and a global block in translation

3.1. Introduction

Blocking VSG synthesis by induction of *VSG* RNAi results in rapid growth arrest in trypanosomes *in vitro*, which is characterised by a precise block in the cell cycle prior to cytokinesis (Sheader et al. 2005). This chapter aims to understand the cell biology and signalling mechanisms operating behind the *VSG* RNAi-induced cell cycle arrest and investigate the biological relevance of this phenotype.

3.2. Results

3.2.1. Induction of *VSG* RNAi inhibits the growth of *T. brucei* and causes a precise pre-cytokinesis cell cycle arrest

A *T. brucei* cell line, capable of expressing *VSG221* RNAi in the presence of tetracycline, had been generated (Sheader et al. 2005). In the 221VB1.1 cell line, a derivative of the *T. brucei* 90-13 bloodstream form cell line, a construct containing a *VSG221* fragment was integrated into 177 bp repeats under the control of opposing tetracycline-inducible T7 promoters (Figure 3.1A) (Sheader et al. 2005; Wirtz et al. 1999). Degradation of *VSG221* mRNA could be triggered by adding tetracycline to the cell medium (Figure 3.1B).

VSG is of paramount importance for the survival of trypanosomes in the hostile bloodstream environment of the infected host. However, blocking VSG synthesis is also detrimental to their growth *in vitro* in the absence of immune selection pressure (Figure 3.1C) (Sheader et al. 2005). Induction of *VSG221* RNAi resulted in rapid disappearance of the *VSG221* transcript and a growth arrest within one cell division (Figure 3.1B and C).

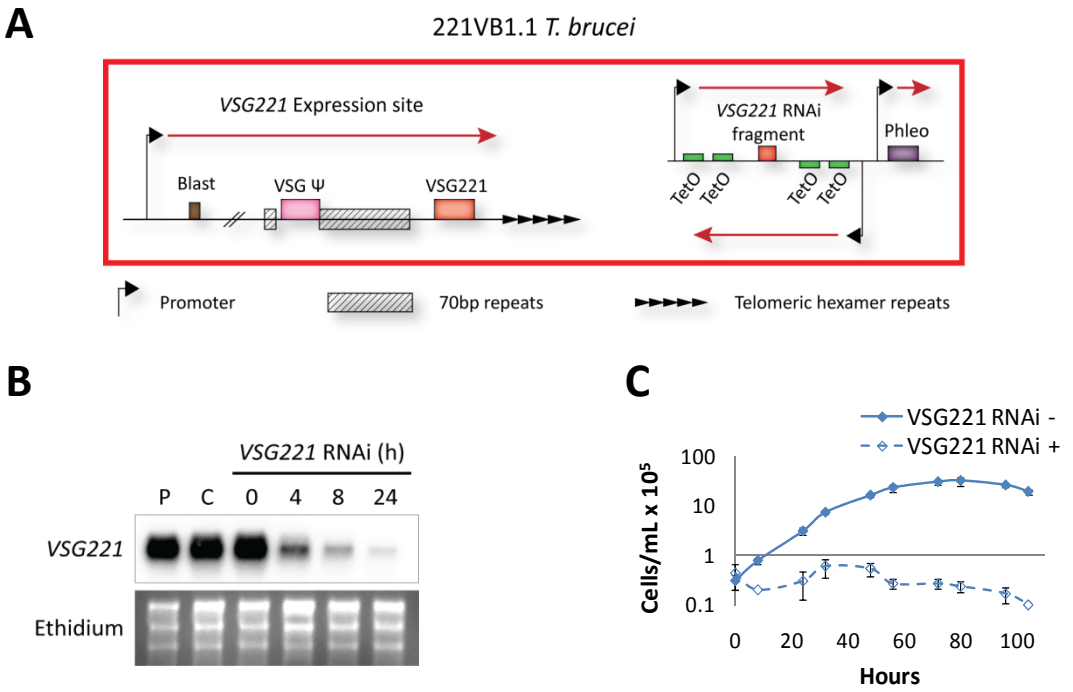


Figure 3.1: Induction of *VSG221* RNAi triggers a rapid growth arrest.

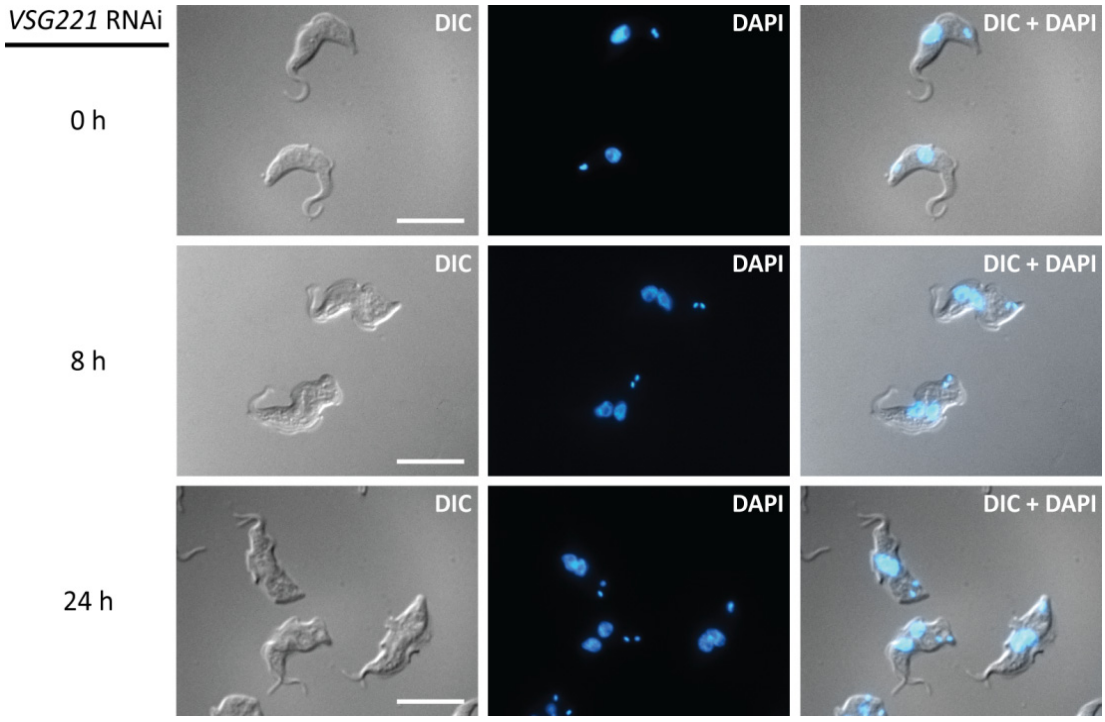
A. A schematic of the transgenic 221VB1.1 *T. brucei* cell line where *VSG221* RNAi can be induced. A blasticidin resistance gene (Blast) was inserted immediately downstream of the promoter in the active *VSG221* Expression site, allowing selection for a homogeneous population expressing only *VSG221*. The construct enabling *VSG221* RNAi was integrated into the cells under phleomycin (Phleo) drug selection. *VSG221* RNAi was induced through the bi-directional transcription of the *VSG221* fragment from T7 promoters under the control of tetracycline operators (TetO).

B. Rapid degradation of *VSG221* transcript after induction of *VSG221* RNAi. Levels of *VSG221* transcript after induction of *VSG221* RNAi in 221VB1.1 *T. brucei* for the times specified in hours were compared to those in the parental 90-13 *T. brucei* (P) and inunduced 221VB1.1 *T. brucei* (C). Ethidium stain of the gel is shown for loading comparison.

C. Induction of *VSG221* RNAi triggers an immediate growth arrest. The 221VB1.1 *T. brucei* was incubated in the presence of 1 µg/mL of tetracycline to induce *VSG221* RNAi for the time indicated in hours. The average cell density from triplicate counts is represented in cells per mL x 10^5 and the standard deviation is shown as error bars.

VSG synthesis appeared to be monitored as part of an essential cell cycle check point for *T. brucei*, because blocking it through induction of *VSG* RNAi prevented the cells from re-initiating S-phase and resulted in accumulation of cells with two nuclei and two kinetoplasts (2K2N) for up to 96 hours post induction (Figure 3.2). After the induction of *VSG* RNAi over 60% of the cells were in the 2K2N configuration. This was an unusual cell cycle arrest phenotype for *T. brucei*, because most other reported cell cycle arrest phenotypes have resulted in the production of "monster" cells containing multiple nuclei and kinetoplasts, indicating lack of coordination between cytokinesis and organelle replication. The minor increase of multinucleated and multikinetoplast cells to about 8% of the total population after blocking VSG synthesis, indicated that most of the stalled parasites had not undegone successive rounds of S-phase and mitosis.

A



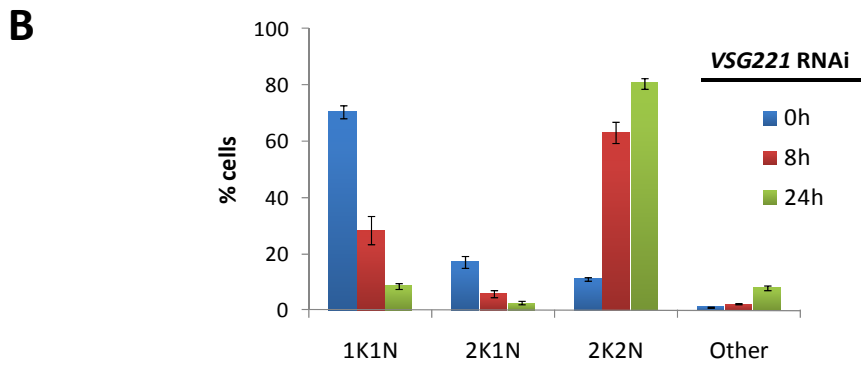


Figure 3.2: Induction of *VSG* RNAi triggers a precise pre-cytokinesis cell cycle block.

A. 221VB1.1 *T. brucei* after induction of *VSG221* RNAi for 8 h and 24 h were analysed by microscopy and compared to uninduced 221VB1.1 *T. brucei* (0 h). The parasites were stained with DAPI (blue) for DNA content. The scale bar represents 10 μm.

B. Quantification of the different cell cycle stages present in the parasite population after induction of *VSG221* RNAi for the times indicated in hours. The average values from three independent experiments are shown with standard deviation represented as error bars. For each cell population counted n>300.

The cells which were arrested pre-cytokinesis after the induction of *VSG* RNAi had a very distinct phenotype, with two kinetoplasts and two nuclei close together (Figure 3.2) (Sheader et al. 2005). The stalled phenotype appeared to represent a very transient stage that occurs naturally in the cell cycle, but is rarely observed in a wild-type population (Sheader et al. 2005; Tyler et al. 2001). The signalling mechanisms connecting VSG synthesis to progression through the cell cycle are not known. Therefore, we further investigated the cell biology behind this unusual cell cycle arrest.

3.2.2. Blocking VSG synthesis by induction of *VSG* RNAi triggers a global translation arrest

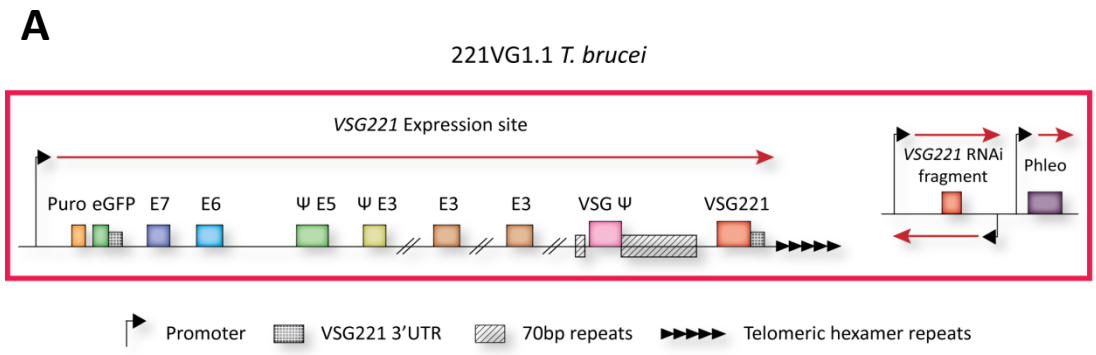
While studying the phenotype triggered by the induction of *VSG* RNAi, we observed a drastic block in total cell protein synthesis. This occurred in a time dependent manner, so that 24 hours after the induction of *VSG* RNAi, global translation in these cells was reduced to 1-2% of original levels (T. K. Smith et al. 2009). Although VSG is the most abundant protein in trypanosomes, comprising 10% total cellular protein, such a dramatic decrease in levels of translation could not be accounted for simply through the loss of VSG protein synthesis. As the incorporation of [^{35}S]-methionine into total protein declined over time, there was a concomitant decrease in its uptake (T. K. Smith et al. 2009). This translation block was not due to a restriction in amino acid uptake. The intracellular levels of 17 different amino acids were measured, most of them appeared to remain largely unchanged with the exception of serine and glutamine, which were reduced to 33% and 22% of normal wild-type levels, respectively (T. K. Smith et al. 2009).

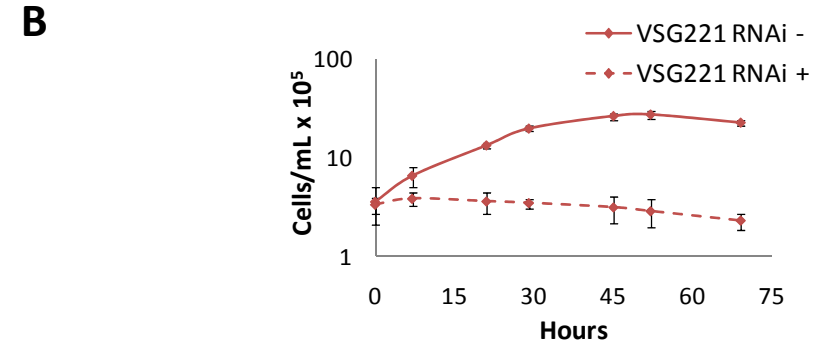
Even though protein synthesis was observed to decrease over time, a more detailed analysis of the total cellular proteome using a 2D-DIGE method did not reveal any significant difference between wild-type cells and cells where *VSG* RNAi had been induced for 24 h (T. K. Smith et al. 2009). The 2D-DIGE analysis investigated changes in the most abundant 1486 proteins in these cells. However it is possible that changes in other less abundant proteins might have been missed due to the relative lack of sensitivity of this technique.

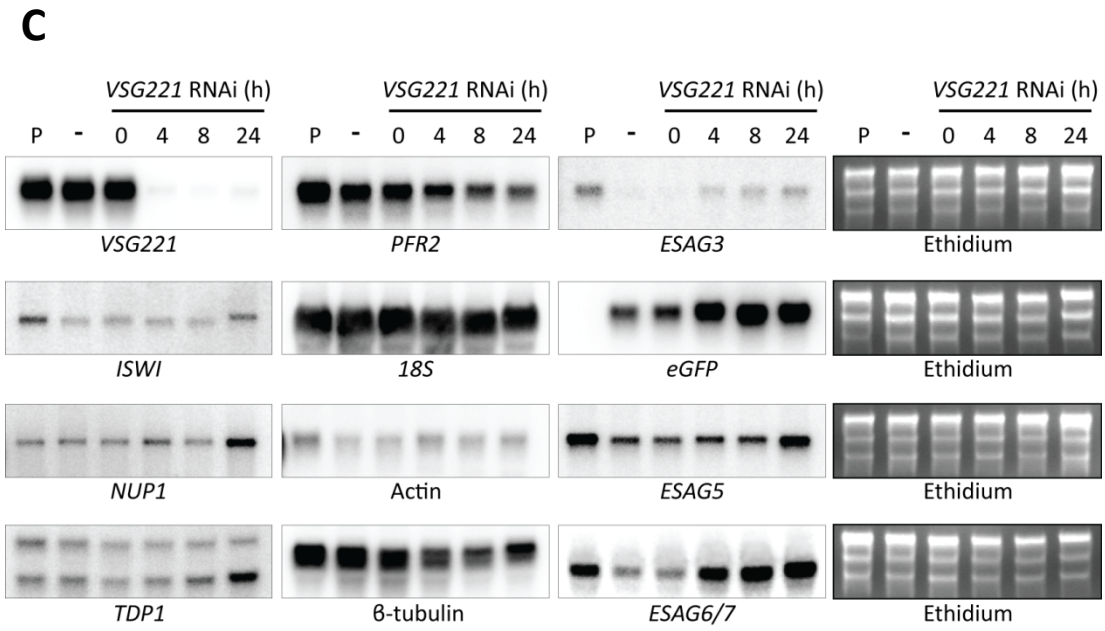
3.2.2.1. The global translation arrest observed after the induction of *VSG* RNAi is not caused by a decrease in levels of transcripts

One explanation for the reduction in the levels of translation in the cells where *VSG* RNAi had been induced, could be that there was a decrease in the total levels of transcripts. Therefore, the levels of a number of housekeeping transcripts were determined after the induction of *VSG* RNAi for various lengths of time (Figure 3.3). The selected transcripts encompassed a wide range of genes with different functions including genes encoding structural proteins and transcription factors (Figure 3.3C).

The 221VG1.1 *T. brucei* is a comparable cell line to 221VB1.1 *T. brucei* that is also capable of performing *VSG221* RNAi. The 221VG1.1 *T. brucei* line is based on the parental 90-13 *T. brucei* line which has been genetically modified to express *eGFP* and a puromycin drug resistance marker immediately downstream of the promoter of the active *VSG221* Expression site (Figure 3.3A) (Wirtz et al. 1999; Sheader et al. 2005). In addition, the 221VG1.1 *T. brucei* has been transfected with a *VSG221* RNAi construct under phleomycin drug selection inserted into the 177 bp repeats (Figure 3.3A). Growth analysis of the 221VG1.1*T. brucei* showed that cell division is rapidly inhibited after induction of *VSG221* RNAi in these cells, which was analogous to the observed growth arrest in 221VB1.1 *T. brucei* (Figure 3.1C and Figure 3.3B).


A
221VG1.1 T. brucei
VSG221 Expression site
Puro eGFP
E7
E6
Ψ E5
Ψ E3
E3
E3
VSG Ψ
VSG221
VSG221 RNAi fragment
Phleo
Promoter
VSG221 3'UTR
70bp repeats
Telomeric hexamer repeats


B
VSG221 RNAi -
VSG221 RNAi +
Cells/mL x 10^5
100
10
1
0
15
30
45
60
75
Hours


C
VSG221 RNAi (h)
P - 0 4 8 24
VSG221
PFR2
ESAG3
Ethidium
ISWI
18S
eGFP
Ethidium
NUP1
Actin
ESAG5
Ethidium
TDP1
ß-tubulin
ESAG6/7
Ethidium

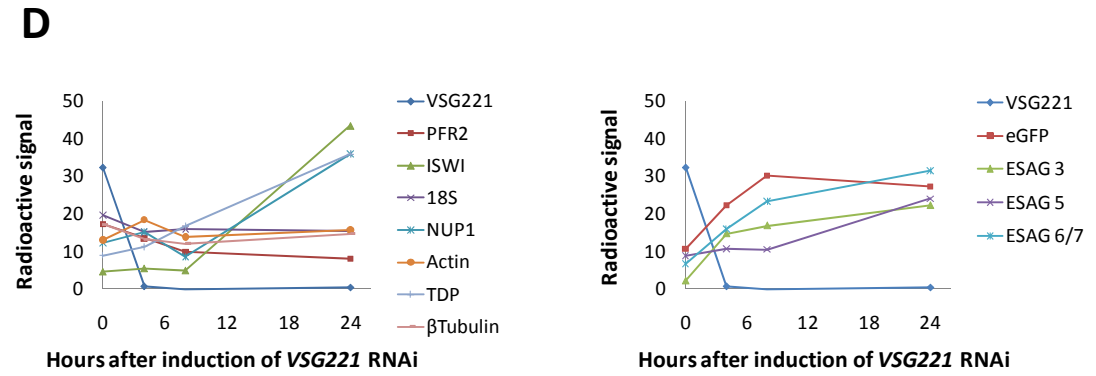

D
Radioactive signal
50
40
30
20
10
0
0
6
12
18
24
Hours after induction of VSG221 RNAi
VSG221
PFR2
ISWI
18S
NUP1
Actin
TDP
βTubulin
Radioactive signal
Hours after induction of VSG221 RNAi
VSG221
eGFP
ESAG 3
ESAG 5
ESAG 6/7

Figure 3.3: Determination of the transcript levels of various genes after induction of *VSG221* RNAi.

A. Schematic of the transgenic 221VG1.1*T. brucei* cell line where *VSG221* RNAi can be induced.

B. Induction of *VSG221* RNAi triggered a rapid growth arrest in the 221VG1.1*T. brucei* cell line. The 221VG1.1*T. brucei* line was incubated in the presence of 1 μg/mL of tetracycline to induce *VSG221* RNAi for the duration of time indicated in hours. The average cell density from triplicate counts is represented in cells per mL x 10^5 and the standard deviation is shown as error bars.

C. *VSG221* RNAi was induced in 221VG1.1*T. brucei* for the times specified in hours (h) and the levels of various of housekeeping gene transcripts were determined by northern blotting. Transcript levels were compared to those from the parental 90-13 *T. brucei* (P) and the Control (-) (uninduced 221VG1.1*T. brucei*) cell lines. The blots were probed for *VSG221*, *ISWI*, *NUP1*, *TDP1*, *PFR2*, *18S* ribosomal RNA, actin, β-tubulin, *ESAG3*, *eGFP*, *ESAG5* and *ESAG6/7* transcripts.

D. Quantification of the transcript levels as determined by northern blot analysis. The first graph represents quantification of various housekeeping gene transcripts. The second graph shows quantification of transcripts originating from the *VSG* Expression site. Radioactive signal was quantified using BioRad Quantity One software and expressed as arbitrary units of radioactivity.

The quantification of the selected range of transcripts after induction of *VSG221* RNAi revealed that although *VSG221* mRNA had virtually disappeared within 4 hours of addition of tetracycline, no global reduction in any of the other transcripts that could explain the total block in translation was observed. The levels of mRNAs for actin remained unchanged, whereas the transcripts for *TDP1* and *ISWI*, which encode transcription factors, increased 4-fold and 10-fold, respectively (Figure 3.3C and D) (Hughes et al. 2007; Erondu & Donelson 1992; T. K. Smith et al. 2009). No significant change could be detected in the amounts of 18S and *NUP1*

mRNA, which encodes a protein that is a component of the nuclear lamina (Figure 3.3C and D) (Rout & M. C. Field 2001; T. K. Smith et al. 2009). There was, however, approximately 50% reduction in the levels of *PFR2* transcript, encoding a paraflagellar rod protein, and a 15% decrease in β-tubulin transcripts, both of which code for structural proteins (Figure 3.3C and D) (Broadhead et al. 2006). It was possible that the stalled cells employed a feedback mechanism resulting in a reduction in the levels of transcripts necessary for growth and cell division. However, these reductions in transcript levels were not low enough to explain the total arrest in protein synthesis.

The levels of *ESAG3*, *ESAG5*, *ESAG6/7* and *eGFP* were also determined. These genes were all present in the active *VSG221* Expression site (Figure 3.3A). All of these mRNAs were found to increase after induction of *VSG221* RNAi. The *eGFP* gene was only present in the active *VSG221* Expression site, where it had been inserted immediately downstream of the promoter (Figure 3.3A). A 3-fold increase in the *eGFP* transcript was observed after blocking VSG synthesis (Figure 3.3C and D). *ESAG3*, *ESAG5* and *ESAG6/7* genes, however, were present in both the active *VSG221* ES, as well as the silent ESs. The levels of *ESAG3*, *ESAG5* and *ESAG6/7* transcripts also increased 10-fold, 3-fold and 5-fold, respectively, after the induction of *VSG221* RNAi (Figure 3.3and D). It was not possible to distinguish between levels of *ESAG6* and *ESAG7* transcripts with the probe fragment that was used, due to similar sequences.

It, therefore, appeared that although the growth of the cells was stalled and the translation levels were decreased to barely detectable levels after the induction of *VSG* RNAi, transcription in these cells continued at a high level (T. K. Smith et al. 2009). The global translation arrest was not a consequence of inhibited transcription

as levels of the transcripts tested remained high after 24 hours of blocking VSG synthesis.

3.2.2.2. The global translation arrest triggered after blocking VSG synthesis operates at the level of translation initiation rather than translation elongation

The global reduction in protein synthesis observed after induction of *VSG* RNAi was therefore likely to be due to an inhibition of translation itself. In order to identify if the observed global translation block occured at the level of translation initiation or elongation, the polysomal profile of cells where *VSG* RNAi was induced for 24 hours was analysed (Figure 3.4). In normal metabolising cells the ribosomal profile shows ribosomes as free ribosomal subunits, free assembled ribosomes and translating assembled ribosomes associated with cellular mRNAs, also known as polysomes.

The polysomal profile of the cells where *VSG* RNAi was induced was compared with the profiles from parasites treated with either cyclohexamide or pactamycin. Both of these drugs interfere with protein synthesis, but their mechanisms of action are different. This allows differentiation between a block in translation initiation versus translation elongation. Cycloheximide inhibits protein biosynthesis by interfering with the translocation step where the tRNAs and the mRNA are moved relative to the ribosome (Baliga et al. 1969). Thus, cycloheximide blocks translation elongation and incubation with this drug generates a profile which shows stabilisation of the ribosomes with the mRNAs forming polysomes and a decrease in free ribosomes in the 80S peak (Figure 3.4A) (Baliga et al. 1969). In contrast, pactamycin prevents the binding of the initiator tRNA to the initiator

complex but allows the completion of translation (Brodersen et al. 2000). Therefore, pactamycin causes a block in translation initiation and generates a polysomal profile where the ribosomes are present mainly as free ribosomal subunits and free assembled ribosomes, but few are associated with the mRNAs to form polysomes (Figure 3.4B) (Brodersen et al. 2000).

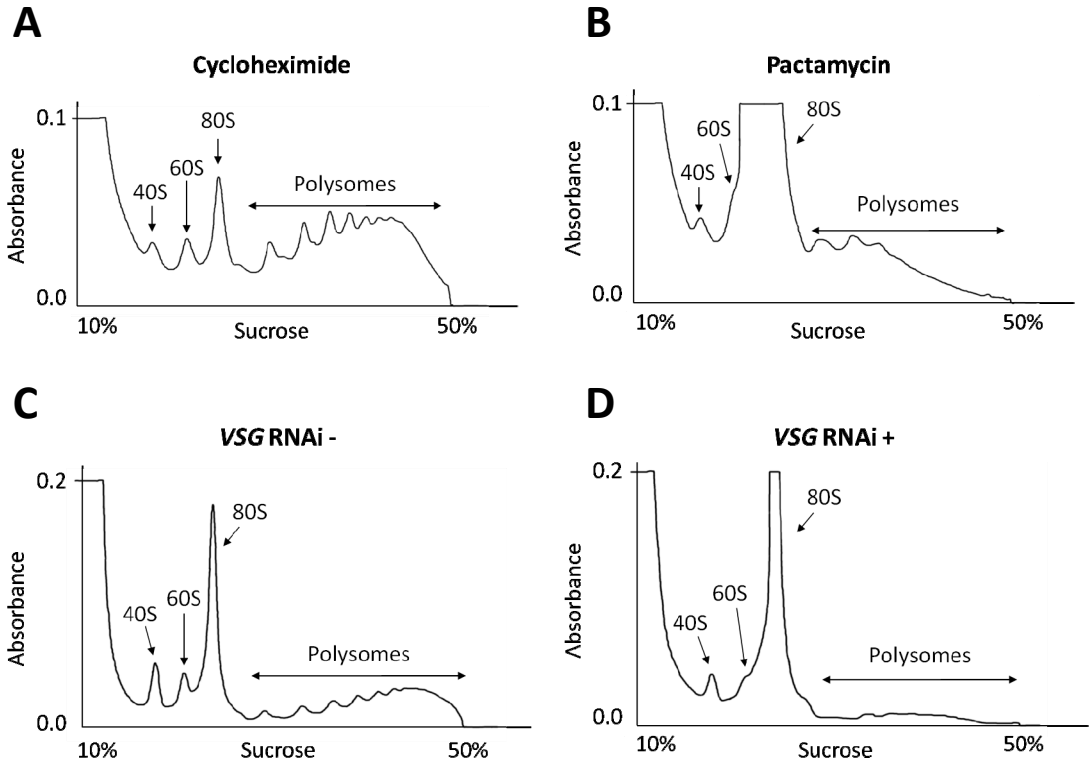


Figure 3.4: Induction of *VSG221* RNAi results in a disruption of translation initiation. Absorbance profiles at 254 nm of 221VG1.1 *T. brucei* cell lysates resolved on sucrose gradients. The relevant ribosomal subunits are indicated with arrows. The polysome analysis has been performed in triplicates and a representative ribosomal profile for each condition is shown.

A. 221VG1.1 *T. brucei* were treated for 10 min with 50 µg/mL Cycloheximide (inhibitor of translation elongation).

B. 221VG1.1 *T. brucei* were treated for 25 min with 200 ng/mL Pactamycin (inhibitor of translation initiation).

C. 221VG1.1 *T. brucei* in which no *VSG221* RNAi has been induced (*VSG221* RNAi -).

D. 221VG1.1 *T. brucei* in which *VSG221* RNAi has been induced for 24 hours (*VSG221* RNAi +).

The ribosomal profile of uninduced cells shows ribosomes both as free subunits, as well as assembled polysomes (Figure 3.4C). In contrast, in the cells where *VSG221* RNAi has been induced for 24 hours, there was a depletion of polysomes and a larger proportion of free ribosomes (Figure 3.4D). This polysome profile in the induced cells closely resembled the one generated by an incubation with pactamycin. Therefore the total translation block observed after induction of *VSG* RNAi appeared to operate at the level of translation initiation, rather than translation elongation.

3.2.3. Levels of various translation initiation factors remain unchanged after blocking VSG synthesis

Various *T. brucei* translation factors were analysed in an attempt to identify the signalling mechanism operating behind the inhibition of translation initiation (Figure 3.5). One of the major translation initiation factors in eukaryotes is eIF4E (eukaryotic initiation factor 4E). This protein binds the m^7Gcap of the mRNA and is often involved in translation control (von der Haar et al. 2004; Culjkovic et al. 2007; Sonenberg 2008; Goodfellow & Roberts 2008). *T. brucei* has four eIF4E homologues. eIF4E1 and eIF4E2 localise both to the nucleus and the cytoplasm and do not appear to be directly involved in translation, whereas eIF4E3 and eIF4E4 are only found in the cytoplasm and may be required for translation. (Freire et al. 2010)

No obvious changes in the levels of any of these proteins could be detected up to 24 hours after induction of *VSG* RNAi (Figure 3.5). eIF4A is another translation factor that is known to be involved in cap-dependent translation initiation (Gebauer & Hentze 2004). However, no significant change was observed in the levels of the *T. brucei* eIF4A1 protein after induction of *VSG* RNAi, (Figure 3.5). eIF2α is also an important eukaryotic translation initiation factor. Levels of this protein also remained constant after the induction of *VSG* RNAi (Figure 3.5).

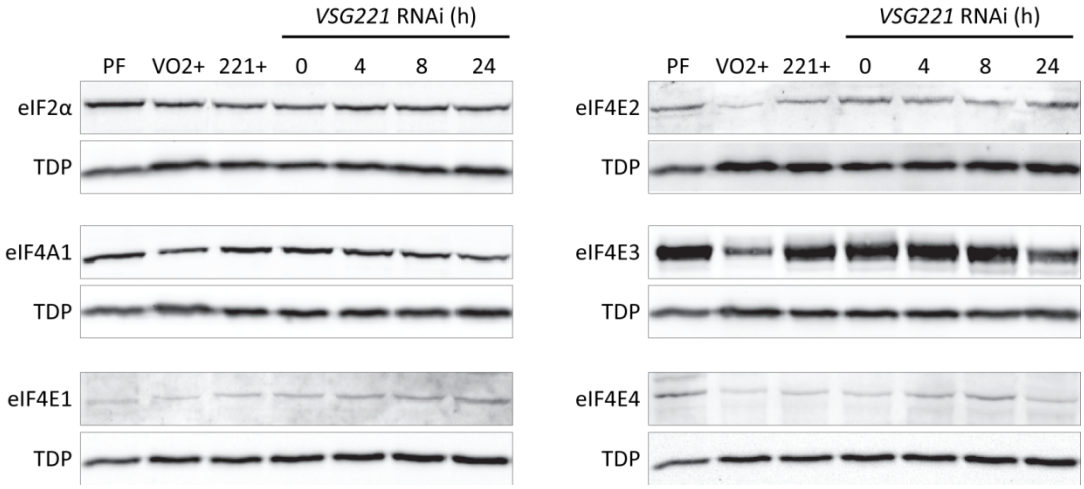


Figure 3.5: Determination of levels of expression of *T. brucei* translation factors after induction of *VSG221* RNAi. *VSG221* RNAi was induced in the 221VG1.1*T. brucei* cell line and protein lysates were collected at times specified in hours. The levels of eIF2α, eIF4A1, eIF4E1, eIF4E2, eIF4E3 and eIF4E4 were determined in the 221VG1.1*T. brucei* after induction of *VSG221* RNAi and compared with uninduced 221VG1.1*T. brucei* (0h), procyclic 29-13 *T. brucei* cell line (PF) and cells expressing either VSGVO2 (VO2+) or VSG221 (221+). The blots were additionally probed for TDP1 as a loading control.

It is, however, possible that the inhibition of translation initiation was a consequence of phosphorylation of one or more translation initiation factors rather than a change in the levels of expression. Studies undertaken to determine potential

changes in the phosphorylation of eIF2α did not reveal any obvious changes after 24 hours of induction of *VSG* RNAi. (Narayanan, M. and Rudenko, G., unpublished results) This does not exclude that the translation initiation factors, including eIF2α, could have undergone some kind of modification that has remained undetected by the currently available methods.

3.2.4. The *VSG* RNAi-triggered growth arrest is reversible

It had been observed that the cells where *VSG* RNAi was induced stalled within one cell division, but the parasites persisted in the culture for days after blocking VSG synthesis (Figure 3.1C and Figure 3.3B). As dramatic and extreme as the phenotype was, it was not immediately lethal. This posed the question of the potential role of such a stalled state in a wild-type population of parasites that might need to respond to fluctuating intracellular levels of VSG protein. It was possible that the *VSG* RNAi-induced growth arrest was similar to a quiescent state that could be potentially reversed.

In order to investigate whether the *VSG* RNAi-triggered growth inhibition was reversible, the minimum effective concentration of the inducer had to be determined. This knowledge would facilitate the experimental design allowing its removal from the medium after a set length of time. Tetracycline is conventionally used for inducible systems in trypanosomes, but it is not readily water soluble and is dissolved in 70% ethanol. Doxycycline is a water-soluble tetracycline analogue. Therefore, to ensure reproducible depletion of the inducer from the culture medium, the use of doxycycline was deemed more appropriate for these experiments.

The minimum effective concentrations of both tetracycline and doxycycline necessary for complete induction of a growth arrest were determined (Figure 3.6). The standard amount of tetracycline used for the induction of RNAi is 1 µg/mL. However, as evident from the tetracycline dilution series, significantly smaller amounts, 1-2 ng/mL, were sufficient to induce *VSG* RNAi-triggered growth arrest (Figure 3.6A). Doxycycline was even more efficient than tetracycline, presumably due to its better solubility in the aqueous culture medium, with levels as low as 50-100 pg/mL causing an observable growth inhibition (Figure 3.6B). For the investigation of the reversibility of *VSG* RNAi-induced phenotype, 300 pg/mL of doxycycline was selected as the minimum effective concentration that caused a clearly identifiable growth arrest.

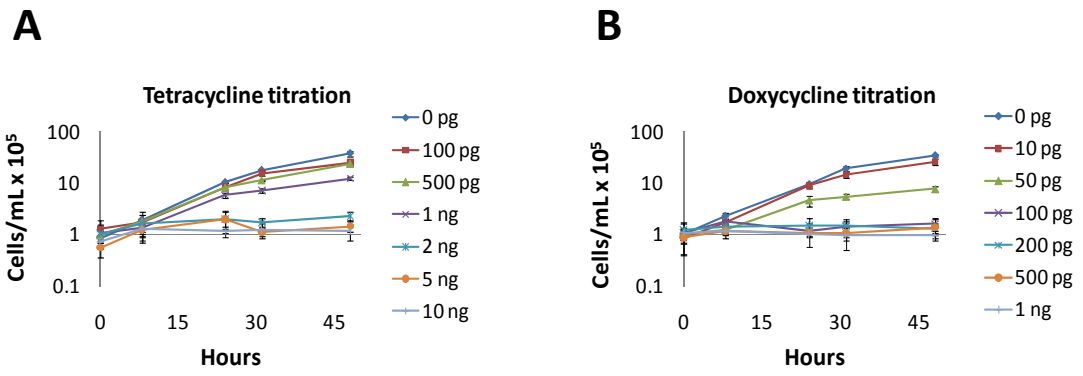


Figure 3.6: Determination of the minimum effective concentration of tetracycline or doxycycline required to trigger *VSG* RNAi-mediated growth inhibition. The 221VB1.1 *T. brucei* was incubated in the presence of the specified concentrations of either tetracycline (**A**) of doxycycline (**B**) for the time indicated in hours. The average cell density from triplicate counts is represented in cells per mL x 10^5 and the standard deviation is shown as error bars.

VSG221 RNAi was induced in *221VB1.1 T. brucei* using 300 pg/mL of doxycycline for 12 hours. Subsequently, the arrested cells were washed and re-

suspended in fresh culture medium not containing any inducer and allowed to recover and resume growth (Figure 3.7A). *VSG221* mRNA analysis of these recovering cells revealed a gradual increase in the *VSG221* transcript that correlated with the resumed growth of the cells (Figure 3.7B). Initially, the cells experienced a growth lag that lasted approximately 24 hours, after which exponential growth resumed. This lag period was presumably due to the necessity of the cells to synthesise sufficient amounts of *VSG* transcript to allow production of VSG protein, enabling the cells to undergo division. Approximately 56 hours after the removal of doxycycline, the cells appeared to have recovered wild-type levels of *VSG*221 transcript (Figure 3.7B).

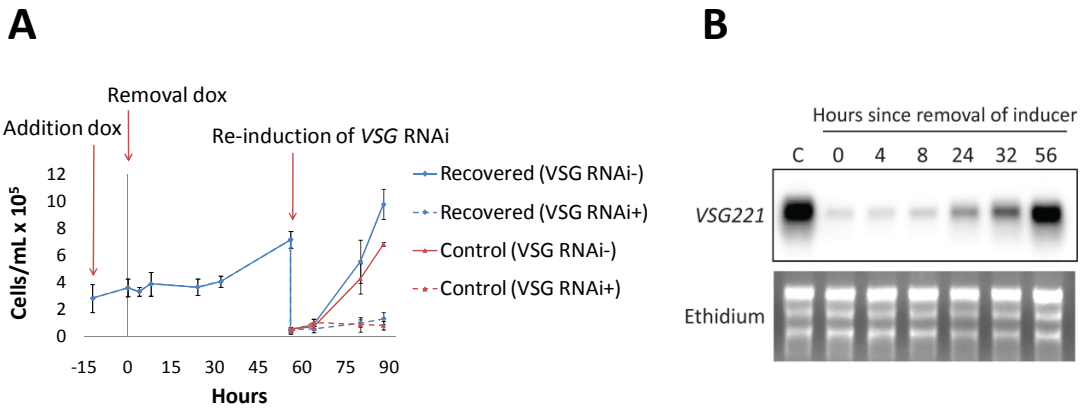


Figure 3.7: The *VSG221* RNAi-mediated growth arrest in 221VB1.1 *T. brucei* can be reversed after removal of doxycycline from the cell medium.

A. *VSG221* RNAi was induced in the 221VB1.1 *T. brucei* cell line (Addition dox) for 12 h, after which it was removed (Removal dox) from the medium and growth of the cells was monitored for the time specified in hours. After the cells have resumed their growth, *VSG221* RNAi was re-induced (Re-induction of *VSG* RNAi – blue dashed line) and compared with uninduced diluted recovered 221VB1.1 *T. brucei* cells (blue solid line). 221VB1.1 *T. brucei* where *VSG221* RNAi has never been induced is shown as a control (red lines). The average cell density from triplicate counts is shown in cells per mL x 10^5 and the error bars represent the standard deviation.

B. Total RNA was isolated from 221VB1.1 *T. brucei* cells following removal of doxycycline at the times specified in hours and from uninduced 221VB1.1 *T. brucei* (C) and analysed using a northern blot. The blot was probed for *VSG221* mRNA and the ethidium stain of the gel is shown below for loading comparison.

The growth of the recovered cells could be blocked again by re-induction of *VSG* RNAi (Figure 3.7A). This suggested that the cells where VSG synthesis was blocked were not irreversibly dying, but were merely quiescent. It was therefore possible that the *VSG* RNAi-triggered cell cycle arrest was an important check point for the parasites that prevented them from progressing through cell division in the absence of sufficient VSG synthesis and diluting their VSG surface coat and exposing invariant surface proteins to attack from the immune system.

3.2.5. The *VSG* RNAi-triggered growth arrest does not resemble a state of differentiation to procyclic form cells

In the bloodstream of an infected mammal a proportion of the *T. brucei* population undergoes differentiation to the stumpy form of the parasite. This stage, ingested in the blood meal of a tsetse fly, is predisposed to differentiate into procyclic form cells in the fly gut. Stumpy form cells are a non-proliferative stage that have stopped transcription of the active *VSG* Expression site, although they still express a VSG coat on their cell surface (Amiguet-Vercher et al. 2004). Therefore, the *VSG* RNAi-triggered growth inhibition in *T. brucei* could possibly be correlated with differentiation of the bloodstream form parasites into procyclic form cells.

Procyclic form *T. brucei* is adapted for life in the tsetse fly gut and does not express any VSG on the cell surface (K Vickerman 1985). Instead, the major surface protein in these cells is procyclin (Ziegelbauer et al. 1990; Matthews & Gull 1994; Acosta-Serrano et al. 1999). There are two major forms of procyclin, EP and GPEET and both can be co-expressed in cells *in vitro*, although *in vivo* these proteins have a developmentally regulated order of expression (Mowatt & C. E. Clayton 1987; Mowatt et al. 1989; Roditi et al. 1987; Vassella et al. 2000; Vassella et al. 2001; Acosta-serrano et al. 2001). We investigated if in cells where VSG synthesis has been blocked, there is evidence for the initiation of development into procyclic form cells. Therefore, the levels of both *EP* mRNA and protein were determined after the induction of *VSG* RNAi (Figure 3.8).

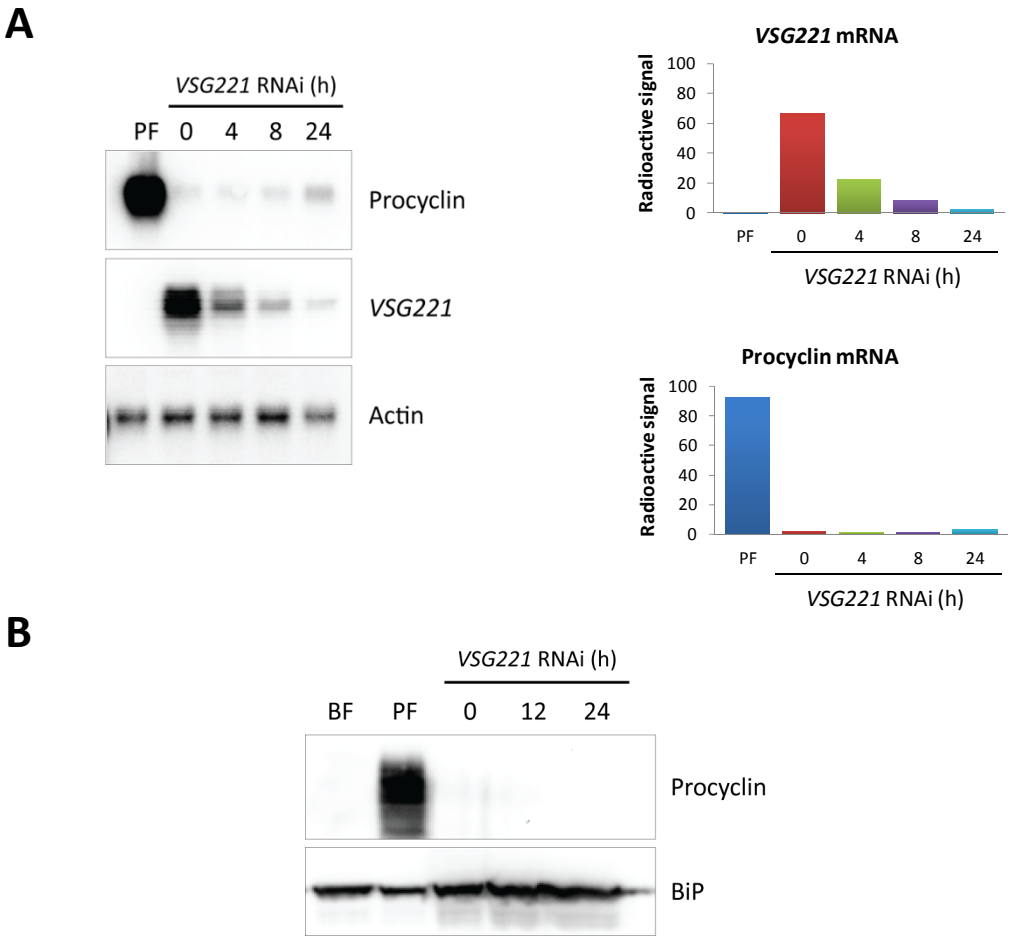


Figure 3.8: Procyclin transcript and protein levels are not significantly elevated after induction of *VSG221* RNAi in 221VB1.1 *T. brucei*.

A. Levels of procyclin and *VSG221* mRNA after the induction of *VSG221* RNAi for the times specified in hours were analysed on a northern blot and compared with RNA from procyclic form 29-13 *T. brucei* cells (PF). The blot was also probed for actin mRNA as a loading control. The levels of procyclin and *VSG221* mRNA were quantified. Radioactive signal was quantified using BioRad Quantity One software and expressed as arbitrary units of radioactivity.

B. Levels of procyclin protein after the induction of *VSG221* RNAi for the time specified in hours were analysed on a western blot and compared with lysates from bloodstream form cells expressing VSGVO2 (BF) and procyclic form 29-13 *T. brucei* cell line (PF). The blot was additionally probed for BiP as a loading control.

EP procyclin mRNA appeared to increase slightly (less than 2 fold) after 24 hours of induction of *VSG* RNAi, but these levels were very low compared with the amount of *EP* mRNA expressed by procyclic form cells (Figure 3.8A). In addition, no EP protein was detected after 24 hours of induction of *VSG* RNAi, which was expected since general protein synthesis had been blocked (Figure 3.8B). Therefore, there was no evidence that parasites stalled after induction of *VSG* RNAi were in fact undergoing differentiation into procyclic form cells.

3.3. Conclusions

The VSG coat is highly important for the survival of bloodstream form *T. brucei* and for its protection in the hostile environment of the mammalian bloodstream. Maintaining high levels of VSG is clearly an evolutionarily conserved

mechanism in these cells. Even in the absence of host immune pressure *in vitro*, it was not possible to generate trypanosomes, which lack their VSG coat.

The *VSG221* messenger RNA was rapidly degraded after induction of *VSG221* RNAi (Figure 3.1B). It has been proposed that the RNAi machinery is closely associated with the cellular translation apparatus and untranslated mRNAs are somewhat less accessible for RNAi-mediated degradation than the translated mRNAs (Shi et al. 2009). The *VSG* messenger RNA is one of the most highly translated mRNAs in trypanosomes owing to the large demand for VSG protein. This could explain why RNAi against *VSG* mRNA was so efficient, even though it was targeted against one of the most abundant transcripts in these cells.

Induction of *VSG* RNAi was observed to cause a growth arrest and pre-cytokinesis cell cycle block, indicating that levels of either *VSG* mRNA or protein are stringently monitored by the cells (Figure 3.1C, Figure 3.2 and Figure 3.3B). VSG synthesis appeared to be an essential check point that determined if the cell cycle can progress beyond cytokinesis (Figure 3.2). Even blocking synthesis of various signalling molecules and cyclins does not invariably arrest the cells at a particular point in the cell cycle. For example, RNAi of the anaphase promoting complex APC1, and the mitotic cyclin CYC6, both cause a block in cytokinesis, but replication of organelles is nevertheless observed (Kumar & C. C. Wang 2005; Hammarton et al. 2003). The ablation of synthesis of essential proteins, such as GPI8, which is responsible for the addition of GPI anchors to polypeptides and PFR2 (paraflagellar rod protein) also cause a failure in cytokinesis, accompanied by the repeated rounds of re-initiation of organelle replication (Ralston et al. 2006; Bastin et al. 2000; Lillico et al. 2003).

T. brucei is an early divergent eukaryotic unicellular organism and their cell biology and regulation of gene expression are significantly different from other model eukaryotes such as yeast. One of the most notable features of gene regulation in *T. brucei* is that there is very little transcriptional control. Almost all of the regulation of gene expression occurs at a post-transcriptional level, through RNA processing and stability and protein synthesis, modification and degradation. As observed, even under conditions of stress which lead to a global translation block to 1-2% of original levels after 24 hours of induction of *VSG* RNAi, the mRNA levels of all transcripts tested remained largely unchanged (Figure 3.3C and D).

After the induction of a VSG synthesis block, the levels of transcripts from the *VSG* Expression sites appeared to be have increased. This was observed for transcripts such as *eGFP* (present in the active ES) and *ESAG3*, *ESAG5* and *ESAG6/7* (present in both active and silent ESs), which were elevated after induction of *VSG* RNAi (Figure 3.3C and D). It was not possible to distinguish whether the increased levels of these transcripts was a result of upregulation of the active or the silent ESs or both or stabilisation of the mRNAs due to the global translation arrest. It is possible that the block in protein synthesis caused the depletion of proteins involved in mRNA degradation, resulting in increase of the transcripts. Alternatively, upregulation of ES transcription could point to the presence of potential compensatory mechanisms that could be operating in these cells that attempt to make up for the loss of *VSG* mRNA.

In addition, the observed 3-fold increase in the levels of *eGFP* mRNA after the induction of *VSG* RNAi may have been a consequence of increased stabilisation of this transcript. The 3' processing signal on the transgenic *eGFP* gene was a *VSG221* 3'UTR (Figure 3.3A). The *VSG* mRNA is highly abundant and relatively

stable presumably due to the properties of its 3'UTR (Berberof et al. 1995; Hotz et al. 1997). This transcript stability may be due to a protein factor binding to the *VSG* 3'UTR, which facilitates stability of the *VSG* transcript. After the induction of *VSG221* RNAi, the *VSG* transcript was rapidly degraded and putative *VSG* 3'UTR-binding proteins were possibly re-directed to the *VSG221* 3'UTR on the *eGFP* mRNA. This could cause its enhanced stability, resulting in increase of *eGFP* transcript (Figure 3.3C and D).

Another possibility was that the translation arrest was a consequence of a lethal phenotype, due to a stress response in the cells after induction of *VSG* RNAi. However, other lethal phenotypes tested did not generate similar drops in levels of translation. For example the induction of tubulin and *PFR2* RNAi is lethal in both cases, but does not cause such a dramatic block in translation (T. K. Smith et al. 2009).

Additionally, intracellular levels of various amino acids after induction of *VSG* RNAi were similar to wild-type amounts and thus, the block in translation was not caused by a lack of amino acid building blocks (T. K. Smith et al. 2009). Instead, the translation arrest appeared to be operating at the level of translation itself and polysome analysis showed that it was a consequence of inhibition of translation initiation (Figure 3.4). Investigation of a number of translation initiation factors, however, did not reveal any obvious changes that could explain the mechanism of the block in translation initiation (Figure 3.5). *T. brucei* appears to have multiple copies of genes encoding a number of translation initiation factors. The *eIF4A* gene has 15 copies in the *T. brucei* genome and there are four homologues of eIF4E, as opposed to the single copy in yeast (Aslett et al. 2010; Berriman et al. 2005; Freire et

al. 2010). This could indicate that *T. brucei* employs significantly different pathways for translational control and deviates from the conventional signalling cascades known in other eukaryotes.

The cells where *VSG* RNAi has been induced bear some superficial similarities to stumpy form parasites. Their growth is also arrested and the morphology of the cells is also shorter and broader compared with slender proliferative bloodstream form cells (Sheader et al. 2005). In addition, stumpy form cells also lack *VSG* transcript, because they have stopped transcription of their active ES. The stumpy form cell cycle arrest, however, is at the G0/G1 stage, rather than the precytokinesis stage observed after induction of *VSG* RNAi (Shapiro et al. 1984). In addition, there was no evidence for upregulation of procyclin mRNA and protein after blocking VSG synthesis, indicating that the observed phenotype was unlikely to be relevant for differentiation of the parasites (Figure 3.8).

The cells, which were stalled after blocking VSG synthesis remained viable in culture for days post induction of *VSG* RNAi (Figure 3.1C and Figure 3.4B) (T. K. Smith et al. 2009). This raised the possibility that the growth arrest was not a lethal phenotype, but rather a quiescent state. Indeed, it was possible to reverse the *VSG* RNAi-induced growth inhibition by removal of the inducer from the culture medium (Figure 3.7A). The parasites were observed to restore wild-type levels of *VSG* transcript and resume exponential growth (Figure 3.7B). Upon re-induction of *VSG* RNAi, the growth of the recovered cells was once again stalled, which showed that these were not mutants that had escaped the RNAi, but were, in fact, true revertants. This indicated that although the cells underwent a dramatic loss of the *VSG* transcript after induction of *VSG* RNAi, they were fully capable of returning to normal growth

once VSG synthesis was resumed. It is unlikely that trypanosomes *in vivo* experience anything close to a complete loss of their *VSG* mRNA. However, it is possible that there are natural fluctuations in *VSG* transcript levels. In response to this, the parasites could possibly be capable of adjusting their growth rates to ensure continuing synthesis of VSG protein and integrity of their important VSG coat. Thus, the *VSG* RNAi-triggered phenotype might be an extreme manifestation of a biologically relevant protective mechanism that prevents the dilution of the trypanosome surface VSG coat.

Chapter 4

Expression of high levels of a second *VSG* that is not recognised by the *VSG221* RNAi can rescue the cells from *VSG221* RNAi-induced growth arrest

4.1. Introduction

As discussed in Chapter 3, the induction of *VSG221* RNAi caused a rapid growth inhibition with a precise pre-cytokinesis cell cycle block and a global translation arrest (Sheader et al. 2005; T. K. Smith et al. 2009). However, we wanted to exclude the possibility that the *VSG221* RNAi-induced phenotype was a stress response caused by siRNA toxicity. The work presented in this chapter shows that expression of high levels of a second *VSG* from the active *VSG* ES, that is not targeted by the *VSG221* RNAi could rescue the parasites from *VSG221* RNAi-induced growth arrest. Integration of a construct containing the complementing *VSG* into genomic locations other than the active *VSG* Expression site did not result in high levels of VSG protein and failed to alleviate the *VSG221* RNAi-triggered growth inhibition.

4.2. Results

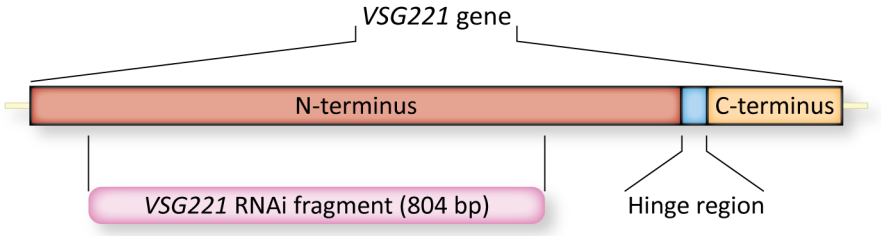
4.2.1. VSG117 and VSG221 sequence analysis

The remarkable sequence diversity of VSG proteins, together with the strong conservation at the tertiary level of protein structure, forms the basis for the success of antigenic variation as an immune evasion strategy for *T. brucei*. The highly divergent N-terminal domains of *VSGs* share only about 10% sequence homology and due to these differences between the *VSG* sequences, RNAi against one *VSG* is highly unlikely to recognise a different *VSG*.

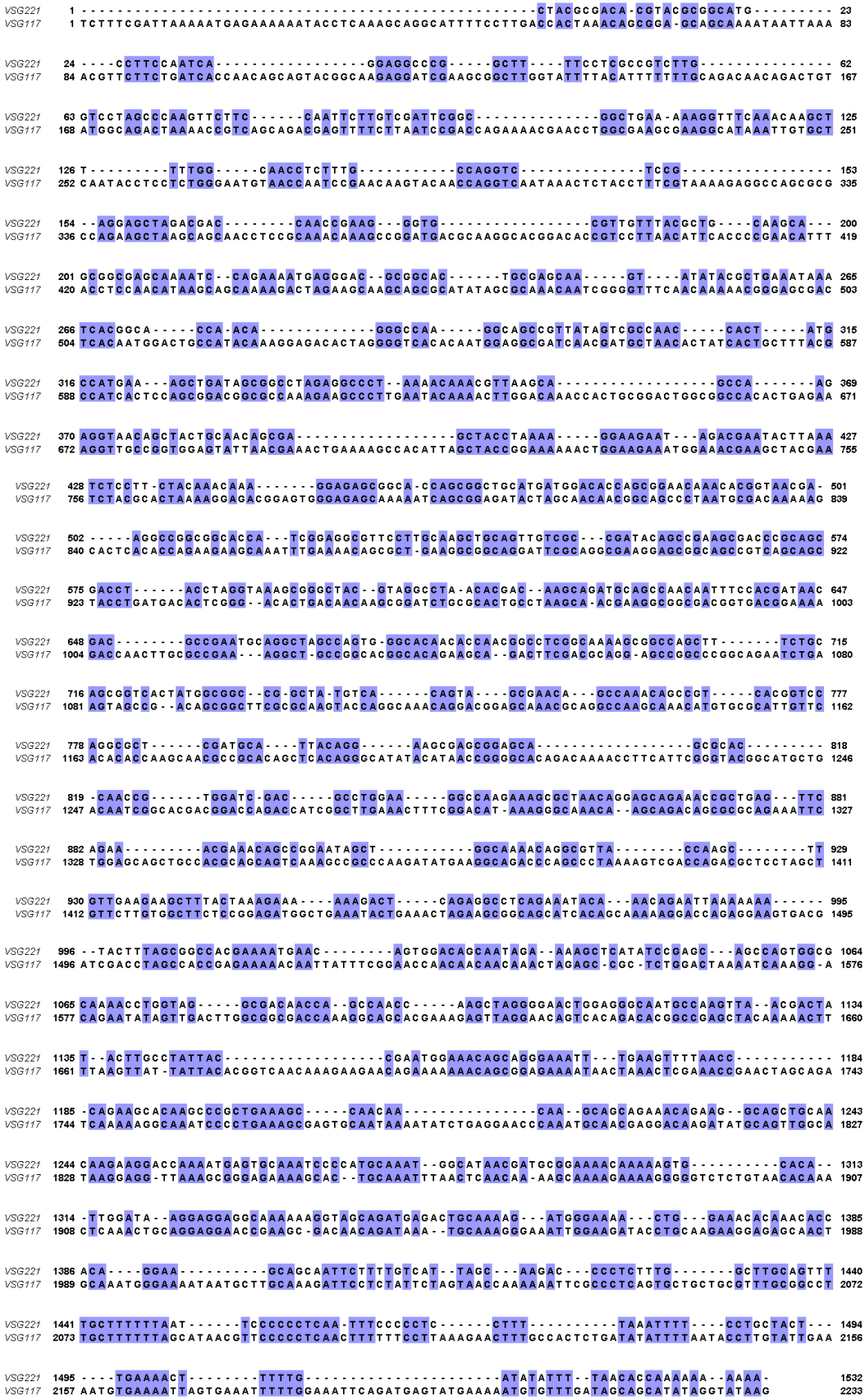
The *VSG221* RNAi fragment used to achieve specific *VSG221* transcript degradation was approximately 800 bp and targeted a region in the N-terminus of the

VSG221 mRNA (Figure 4.1A). VSG117 (also known as MITat 1.4) contains an A-type VSG N-terminal domain, based on the pattern of cysteine residues, but has a highly divergent sequence compared with VSG221 (Figure 4.1B). An alignment of the *VSG221* and *VSG117* gene sequences showed only 31% identity (Figure 4.1B). Effective RNAi requires 18-20 nt stretches of sequence identity. The *VSG221* and *VSG117* genes lack these areas of identity and, therefore, *VSG221* RNAi was not expected to recognize the *VSG117* transcript and cause its degradation (Figure 4.1B). This allowed investigation if induction of *VSG221* RNAi could be alleviated by the provision of a second, different *VSG*, namely *VSG117*. This was not recognized by the *VSG221* RNAi and would allow assessment whether the *VSG221* RNAi-induced growth arrest was a consequence of siRNA toxicity.

A



B



C

```
VSG221   1 MPSNQEARL------FLAVLVLAQVLPILVDSAAEKGFKQAFWQPLCQVSEELDDQPKGALFTLQAAASKIQK 67
VSG117   1 MDCHTKETLGVTQWRRSTMLTLSLLYAITPADGAKEALEYKTWTNHCGLAATLRKVAGGVLTKLKSHISYRKK 73

VSG221  68 MRDAALRASIYAEINHGTNRAKAAVIVANHYAMKADSGLEALKQTLSSQEVTATATASYLKGRIDEYLNLLLQ 140
VSG117  74 LEEMETKLRIYALKGDGVGEQKSAEILATTAALMRQKALTPEEANLKT-ALKAAGFAGEGAAAVSSYLMTLGT 145

VSG221 141 TKESGTSGCMMDTSGTNTVTKAGGTIGGVPCKLQLSPIQPKRPAATYLGKAGYVGLTRQADAANNFHDNDAEC 213
VSG117 146 LTTSGSAHCLSNEGGDGDGKDQLAPKG-CRHGTEADFDAGAGPAESEVADSGFAQVPGKQDGANAGQANMCAL 217

VSG221 214 R--LASGHNTNGLGKSGQLSAAVTMAAGYVTVANSQTAVTVQALDALQEASGAAHQPWIDAWKAKKALTGAET 284
VSG117 218 FTHQATPHSSQGIYITG-AQTKPSFGYGMLTIGTTDQTIGLKLSDIKGKQADSAQKFWSSCHAAVKAAQDMKA 289

VSG221 285 -AEFRNETAGIAGKTGVTKLVEEALLKKKDSEAS-------EIQTELKKYFSGHENEQWTAIEKLISEQPVAQ 349
VSG117 290 DPALKVDQTLLAVLVASPEMAEILKLEAAASQQKGPEEVTIDLATEKNNYFG-TNNNKLEPLWTKIKGQNIVD 361

VSG221 350 NLVGDNQPTKLGELEGNAKLTTILAYYRMETAGKFEVLTQKHKPAE---SQQQAAETEGSCNKK-DQNECKSP 418
VSG117 362 LAATKGSTKELGTVTDTAELQKLLSYYYTVNKEEQKKTAEKITKLETELADQKGKSPESECNKISEEPKCNED 434

VSG221 419 --CKWHNDAEN--KKCTLDKEEAKKVADETAKDGKTGNTNTTGS---------------------------- 458
VSG117 435 KICSWHKEVKAGEKHCKFNSTKAKEKGVSVTQTQTAGGTEATTDKCKGKLEDTCKKESNCKWENNACKDSSIL 507

VSG221 459 -SNSFVISKTPLWLAVLLF                                                       476
VSG117 508 VTKKFALTVVSAAFVALLF                                                       526
```

D

```
          .........10.........20.........30.........40.........50
VSG221    AAEKGFKQAF WQPLCQVSEE LDDQPKGALF TLQAAASKIQ KMRDAALRAS
VSG117    -AKEALEYKT WTNHCGLAAT LRKVAGGVLT KLKSHISYRK KLEEMETKLR

          .........60.........70.........80.........90.........100
VSG221    IYAEINHGTN RAKAAVIVAN HYAMKADSGL EALKQTLSSQ EVTATATASY
VSG117    IYALKGDGVG EQKSAEILAT TAALMRQKAL TPEEAN-LKT ALKAAGFAGE

          .........110.........120.........130.........140.........150
VSG221    LKGRIDEYLN LLLQTKESGT SGCMMDTSGT NTVTKAGGTI GGVPCKLQLS
VSG117    GAAAVSSYLM TLGTLTTSGS AHCLSNEGGD GDGKDQLAPK GC-RHGTEAD

          .........160.........170.........180.........190.........200
VSG221    PIQPKRPAAT YLGKAGYVGL TRQADAANNF HDNDAECRLA SGHNTNGL--
VSG117    FDAGAGPAES EVADSGFAQV PGKQDGAN-- AGQANMCALF THQATPHSSQ

          .........210.........220.........230.........240.........250
VSG221    -GKSGQLSAA VTMAAGYVTV ANSQTAVTVQ ALDALQEASG AAHQPWIDAW
VSG117    GIYITGAQTK PSFGYGMLTI GTTDQTIGLK LSDIKGKQAD SAQKFWSSCH

          .........260.........270.........280.........290.........300
VSG221    KAKKALTGAE TAEF----RN ETAGIAGKTG VTKLVEEALL KKK---DSEA
VSG117    AAVKAAQDMK ADPALKVDQT LLAVLVASPE MAEILKLEAA ASQQKGPEEV

          .........310.........320.........330.........340.........350
VSG221    SEIQTELKKY FSGHENEQWT AIEKLISEQP VAQNLVGDNQ PTKLGELEGN
VSG117    TIDLATEKNN YFGTNNNKLE PLWTKIKGQN IVDLAATKGS TKELGTVTDT

          .........360.........370.........380.........390.........400
VSG221    AKLTTILAYY RMETAGKFEV LTQKH---KP AESQQQAAET EGSCNKK-DQ
VSG117    AELQKLLSYY YTVNKEEQKK TAEKITKLET ELADQKGKSP ESECNKISEE

          .........410.........420.........430.........440.........450
VSG221    NEC--KSPCK WHNDAE--NK KCTLDKEEAK KVADETAKDG KTGNTNTTGS
VSG117    PKCNEDKICS WHKEVKAGEK HCKFNSTKAK EKGVSVTQTQ TAGGTEATTD

          .........460.........470.....
VSG221    S---------- ---------- -----
VSG117    KCKGKLEDTC KKESNCKWEN NACKD
```

HELIX (H) STRAND (E)

Figure 4.1: *VSG221* RNAi is not expected to cause degradation of *VSG117* transcript due to the significant sequence diversity between these genes.

A. The *VSG221* RNAi fragment (pink box) comprises a region in the N-terminal domain of *VSG221*.

B. The *VSG221* and *VSG117* genes were aligned using ClustalW2. The conserved residues are highlighted in blue.

C. VSG221 and VSG117 amino acid sequences were aligned using ClustalW2. The conserved residues are highlighted in blue.

D. Alignment of VSG221 and VSG117 polypeptides based on secondary structure predictions. Secondary structure prediction was performed using DSSP and PSIPRED (Kabsch & Sander 1983; D. T. Jones 1999). The predicted helical (red) and strand (blue) regions are indicated on the alignment and the legend is shown below.

4.2.2. The *VSG221* 3'UTR contains conserved sequence elements and plays an important role in ensuring high levels of expression of the transgenic VSG117 gene

In order to express high levels of VSG117, the construct, containing *VSG117* was targeted into the active *VSG221* ES, flanked by a *VSG221* 3'UTR and tubulin 5'UTR signal sequences (Figure 4.2). It has previously been shown that the *VSG* 3'UTR confers high levels of life cycle stage-specific expression of transcripts in bloodstream form *T. brucei* (Berberof et al. 1995).

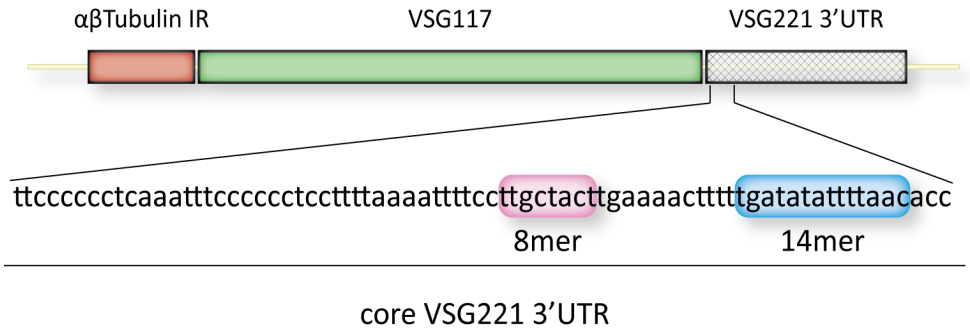


Figure 4.2: The *VSG221* 3'UTR is important for high levels of *VSG* mRNA expression. A 600 bp region downstream of the *VSG221* gene was used to provide the 3'UTR of the *VSG117* gene targeted into the active *VSG221* ES. The core *VSG221* 3'UTR is 75 bp and contains the highly conserved 8mer (magenta box) and 14mer (blue box) sequence elements. The αβ-tubulin intergenic (IR) region was used to provide the 5' trans-splice acceptor site upstream of the *VSG117* gene. The schematic is drawn to scale.

A 600 bp region downstream of the wild-type *VSG221* gene was used as the 3'UTR for the *VSG117* gene, with the core 75 bp long *VSG221* 3'UTR within this fragment (Figure 4.2). This short core *VSG221* 3'UTR has two highly conserved sequence elements, known as the 8mer and the 14mer sequences, that are thought to be important for the high stability observed for the *VSG* transcripts in bloodstream form *T. brucei* (Figure 4.2) (Berberof et al. 1995; Borst & G. A. M. Cross 1982; Ehlers et al. 1987).

4.2.3. Expression of *VSG117* from the active *VSG221* Expression site

A *T. brucei* cell line expressing *VSG221* (221VB1.1) and also containing a construct allowing the ability to perform *VSG221* RNAi was genetically modified to

express *VSG117* from immediately downstream of the promoter of the active *VSG221* Expression site (221VP117) (Figure 4.3).

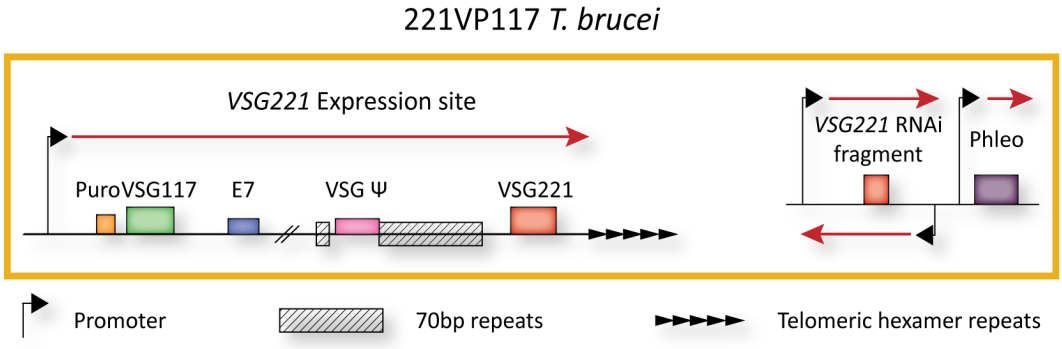


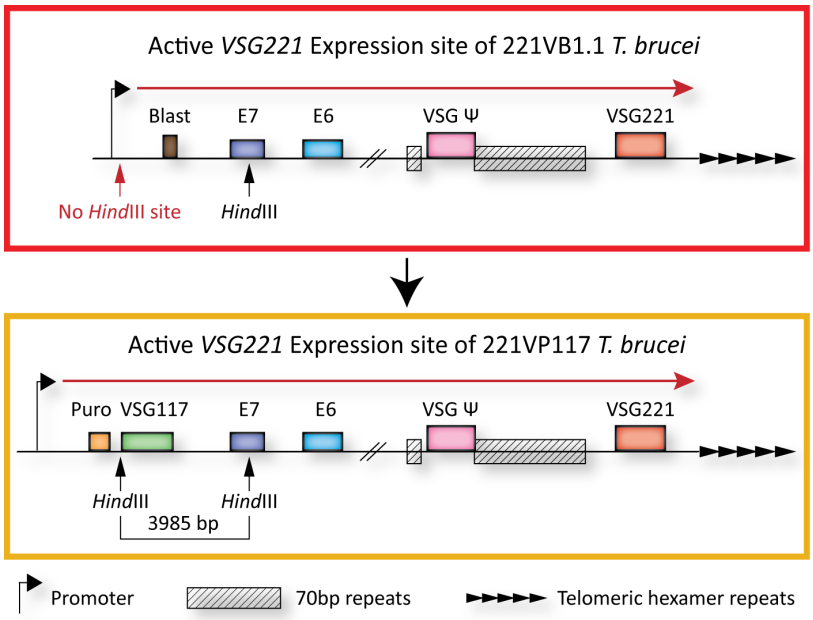
Figure 4.3: A construct containing the *VSG117* gene and the puromucin resistance gene (Puro) have been inserted immediately downstream of the promoter of the active *VSG221* Expression site of 221VB1.1 *T. brucei*.

The correct integration of the construct containing the *VSG117* gene immediately downstream of the active *VSG221* ES promoter was confirmed by Southern blot analysis (Figure 4.4). A *Hind*III digestion of genomic DNA from 221VP117 clones was performed. Hybridisation of the blot with a probe for *VSG117* yielded the expected 3985 bp fragment, due to the presence of a *Hind*III recognition site in both the *ESAG7* and *VSG117* genes, as well as a large fragment that remained in the compression zone (Figure 4.4B). An equivalent digest of the genomic DNA from the parental 221VB1.1 *T. brucei* cell line generated only the large fragment (Figure 4.4B). This large fragment was due to the detection of the basic copy array *VSG117* gene present in the genome of both 221VB1.1 and 221VP117 *T. brucei* cell lines.

Re-probing the blot with a probe for *ESAG7* generated the same 3985 bp band in the 221VP117 *T. brucei* clones, indicating linkage of VSG117 with ESAG7

(Figure 4.4B). The blot probed for *ESAG7* gene also showed a number of other bands that were also present in the parental 221VB1.1 cell line (Figure 4.4B). This was due to the presence of *ESAG7* in all other known *VSG* Expression sites and the high sequence similarity between *ESAG6* and *ESAG7* genes. This analysis, verified the successful integration of the *VSG117* gene-containing construct immediately downstream of the promoter of the active *VSG221* ES.

A



B

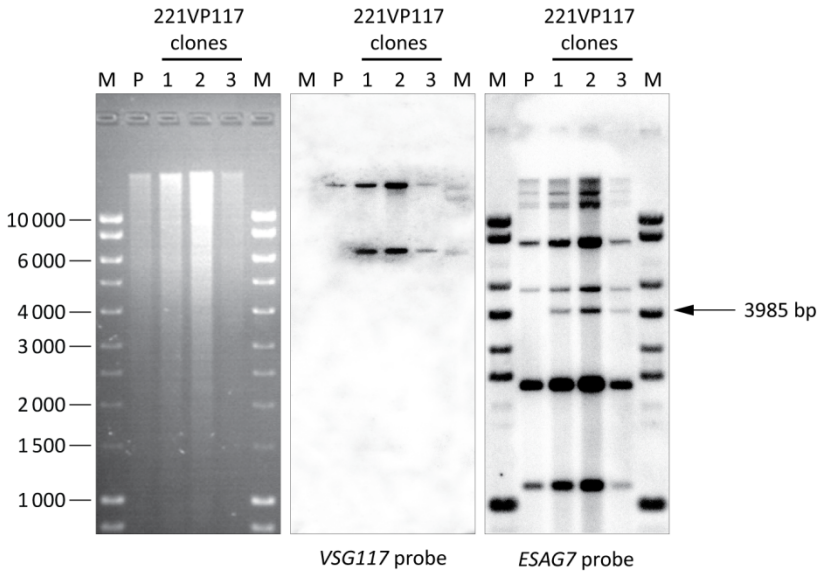


Figure 4.4: The integration of the construct containing the *VSG117* gene behind the promoter of the active *VSG221* Expression site of 221VP117 *T. brucei* as verified by Southern blot analysis.

A. Schematic showing the insertion of the construct containing the *VSG117* gene linked to the puromycin resistance gene (Puro) to generate the 221VP117 *T. brucei* cell line (yellow box). Correct integration of the construct would result in the acquisition of new *Hind*III and *Sac*I restriction enzyme recognition sites upstream of the *VSG117* gene that were not present in the parental 221VB1.1 *T. brucei* cell line (red box).

B. Southern blot analysis of *Hind*III digest of the parental 221VB1.1 *T. brucei* (P) and 221VP117 clones genomic DNA. The blot was probed for both the *ESAG7* gene and *VSG117* gene. The fragment of expected size confirming correct integration of the construct is indicated with a black arrow.

4.2.4. VSG221-VSG117 double-expressor *T. brucei* presents both VSGs on its cell surface

To assess whether the 221VP117 *T. brucei* cell line expressed both VSG221 and VSG117 on the cell surface, the VSG surface coat of the parasites was analysed by immunofluorescence. Although the two VSGs are very different in their amino acid sequence and size, they were both expressed simultaneously on the cell surface of 221VP117 *T. brucei* cells (Figure 4.5). In contrast, no VSG117 could be detected on the cell surface of the parental 2221VB1.1 *T. brucei* cell line (Figure 4.5).

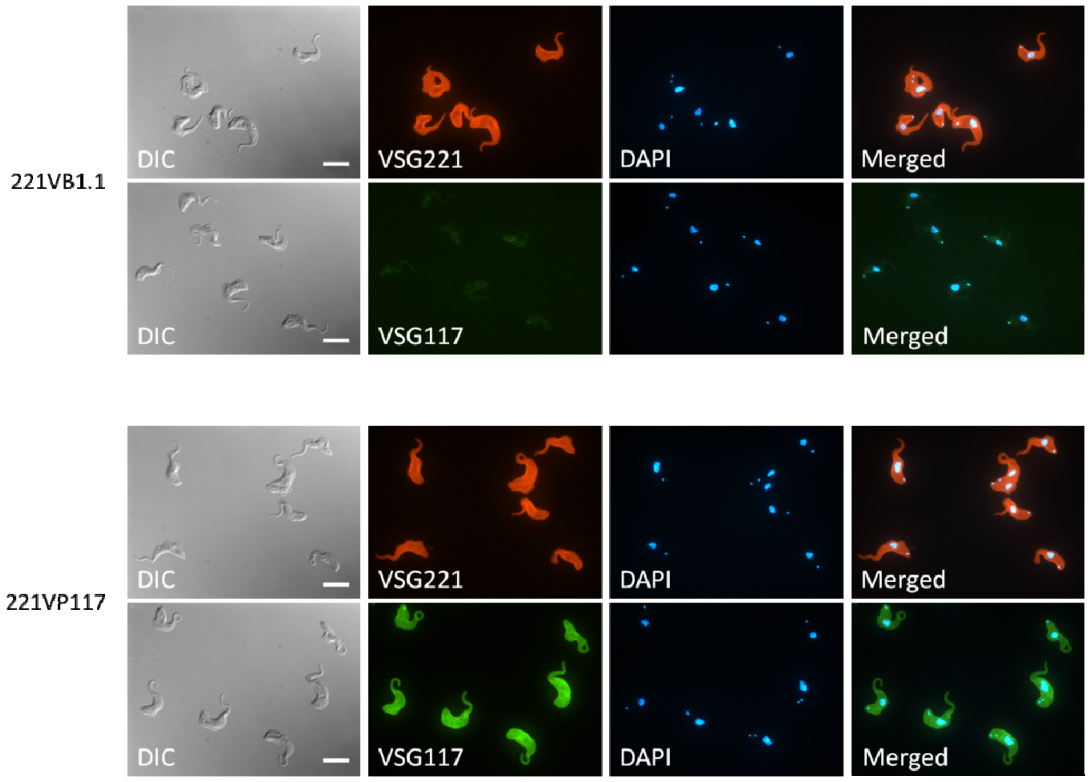


Figure 4.5: VSG221 and VSG117 are expressed simultaneously on the surface of 221VP117 *T. brucei*. The 221VP117 and 221VB1.1 *T. brucei* cells were probed with either anti-VSG221 (orange) or anti-VSG117 (green) antibodies and stained with DAPI (blue) for DNA content. The scale bar represents 10 µm.

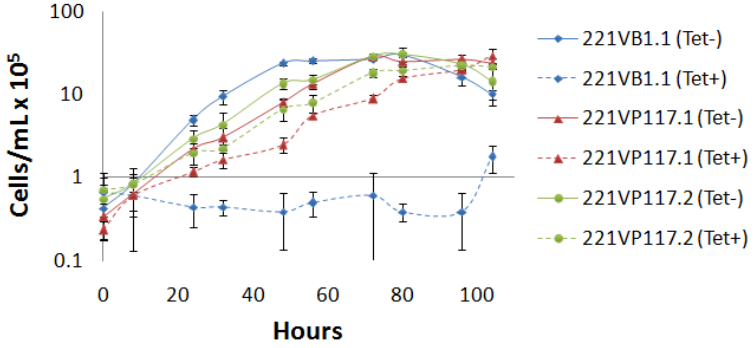
The molecular weight of the VSG221 protein is 46 kDa, whereas the VSG117 protein is 50 kDa. Both VSGs have A-type VSG N-terminal domains, as defined by their cysteine residues pattern. They are both predicted to have high secondary structure conservation, which presumably facilitates their simultaneous expression on the cell surface of the 221VP117 *T. brucei* cell line (Figure 4.1B and C and Figure 4.5).

4.2.5. High levels of expression of *VSG117* from the active *VSG221* ES of 221VP117 *T. brucei* can rescue the parasites from the *VSG221* RNAi-induced growth arrest

To investigate whether VSG117 can alleviate the *VSG221* RNAi-triggered growth inhibition, growth analysis was performed on the double-expressing 221VP117 cell line after induction of *VSG221* RNAi (Figure 4.6A). It was observed that 221VP117 *T. brucei* expressing both *VSG221* and *VSG117* did not stall after induction of *VSG221* RNAi (Figure 4.6A). In contrast, the growth of the parental 221VB1.1 *T. brucei* that expressed only VSG221 was inhibited after induction of *VSG221* RNAi.

Northern blot analysis of the 221VP117 *T. brucei* showed that *VSG221* mRNA rapidly disappeared within 6 hours after induction of *VSG221* RNAi, whereas *VSG117* transcript was not degraded and increased slightly in response to the degradation of the *VSG221* mRNA (Figure 4.6B). Additionally, the ability of VSG117 to compensate for the loss of VSG221 was also observed at the protein level (Figure 4.6C). After induction of *VSG221* RNAi in 221VP117 *T. brucei*, VSG221 protein was observed to gradually disappear over a period of several days, whereas the levels of VSG117 protein increased, presumably to compensate for the decreasing amounts of VSG221 protein (Figure 4.6C).

A



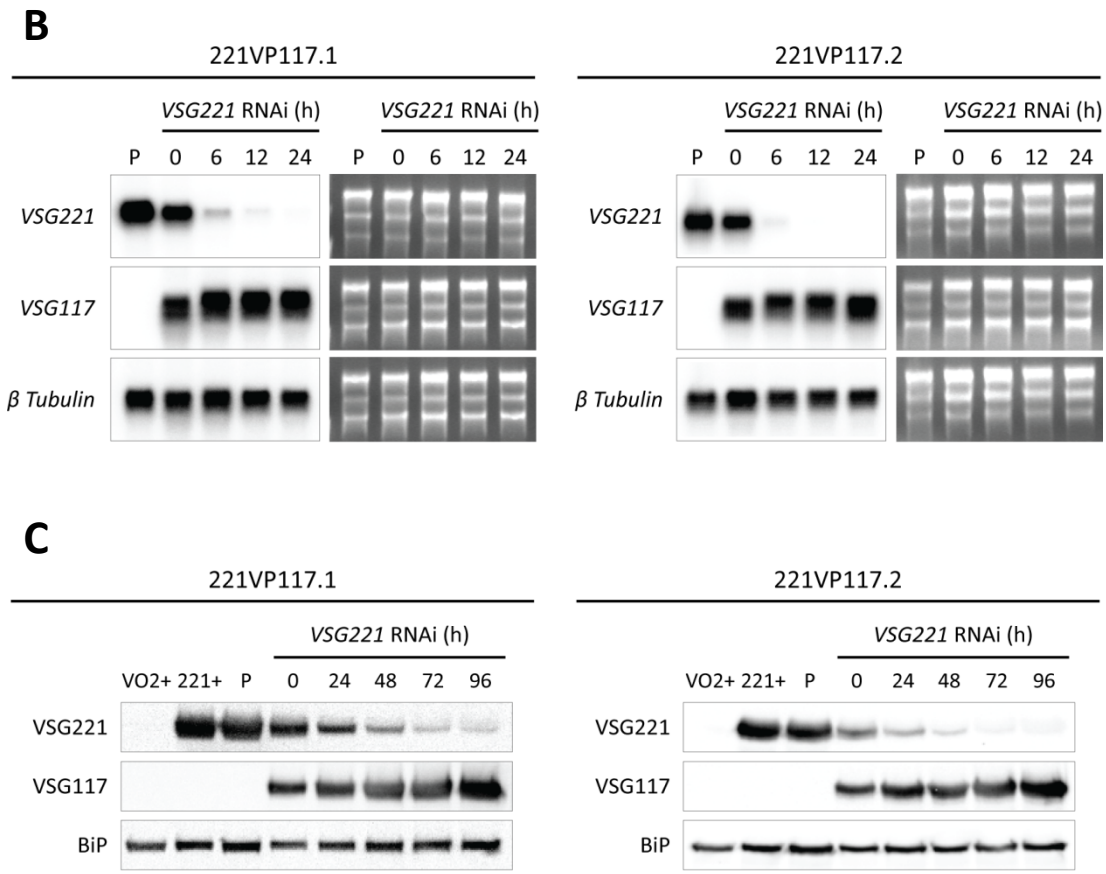


Figure 4.6: The cell cycle arrest caused by *VSG221* RNAi can be alleviated in the 221VP117 *T. brucei* cell line expressing a second *VSG* (*VSG117*).

A. The growth of the 221VP117.1 and 221VP117.2 *T. brucei* clones was compared with that of the parental 221VB1.1 *T. brucei* cell line. Uninduced cells (Tet-) were compared with cells where *VSG221* RNAi was induced (Tet+) for the time specified in hours. The average cell density from triplicate counts is represented in cells per mL x 10^5 and the standard deviation is shown as error bars.

B. Northern blot analysis comparing *VSG221* and *VSG117* transcript levels from 221VP117 *T. brucei* cells (expressing *VSG117* and *VSG221*; clones 1 and 2) and the Parental (P) 221VB1.1 *T. brucei* cell line. *VSG221* RNAi was induced in the *VSG* double-expressor cells for the time specified in hours (h).

C. Western blot analysis of cells expressing both VSG117 and VSG221 (clones 1 and 2) after induction of *VSG221* RNAi for the time specified in hours (h). Levels of VSG221 and VSG117

protein were compared with those present in cells expressing only VSG221 (221+) and the parental cell line (P). A cell line expressing only VSG VO2 (VO2+) was used as a negative control. The blots were additionally probed for BiP as a loading control.

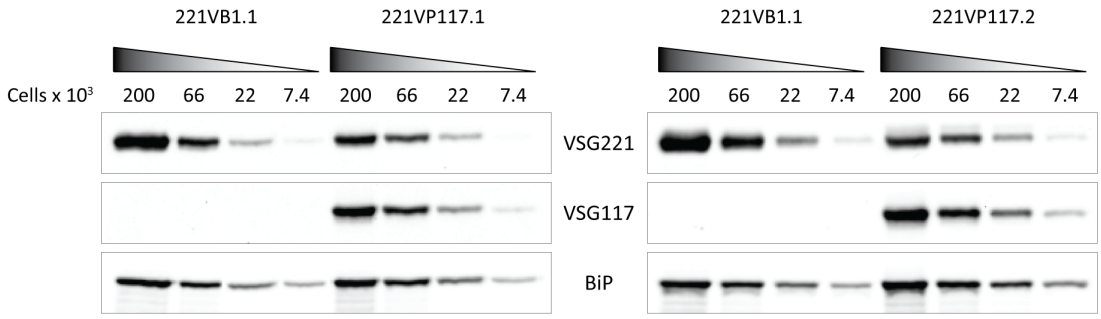
It appeared that VSG117 was able to compensate for the loss of VSG221 in the VSG221-VSG117 double-expressing *T. brucei* and prevent the block in cell growth. The ability of *VSG117* to rescue the stalled phenotype generated by blocking VSG synthesis demonstrates that the observed growth arrest was not triggered by siRNA toxicity. Induction of *VSG221* RNAi in the 221VP117 *T. brucei* cell line caused the degradation of the *VSG221* transcript, resulting in large amounts of siRNA. However, but the growth of these parasites despite the large quantity of siRNAs was not inhibited (Figure 4.6A and B).

4.2.6. 221VP117 *T. brucei* expressing both VSG221 and VSG117 from the active *VSG221* ES have the same volume as the parental 221VB1.1 *T. brucei*

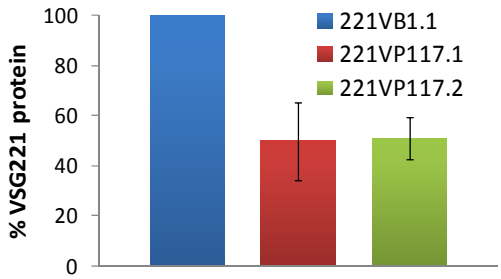
Western blot analysis of the VSG221-VSG117 double-expressor 221VP117 *T. brucei* cell line showed that these cells appeared to produce lower levels of VSG221 protein compared with the parental 221VB1.1 cell line expressing only VSG221 (Figure 4.6C – 0 h of *VSG221* RNAi). The rest of the VSG protein pool in the 221VP117 *T. brucei* cell line was composed of VSG117. This suggested that *T. brucei* may have a limit on the maximal amount of VSG protein that they can express. The presence of two *VSG* transcripts appears to have resulted in approximately equal levels of the two proteins in uniduced cells.

Quantification of the levels of expression of VSG221 and VSG117 protein in the 221VP117 *T. brucei* cell line showed that VSG117 and VSG221 protein were both produced at approximately equal levels (Figure 4.7A). The amount of VSG221 protein synthesized by the VSG221 double-expressor *T. brucei* was less than in the parental cell line, amounting to about 50% of the total VSG221 protein expressed by the parental 221VB1.1 *T. brucei* cell line (Figure 4.7A and B). The levels of VSG221 protein expressed by the 221VP117. 1 and 221VP117.2 clones were determined to be 49% and 51%, respectively (Figure 4.7A and B). These levels were estimated as a fraction of the levels present in the parental 221VB1.1 *T. brucei*, which were arbitrarily set to 100% VSG221 (Figure 4.7A and B). The rest of the total intracellular VSG pool in 221VP117 *T. brucei* appeared to be comprised of VSG117 (about 50% of total VSG protein), resulting in an approximately 1:1 ratio of the two proteins in the cells.

A



B



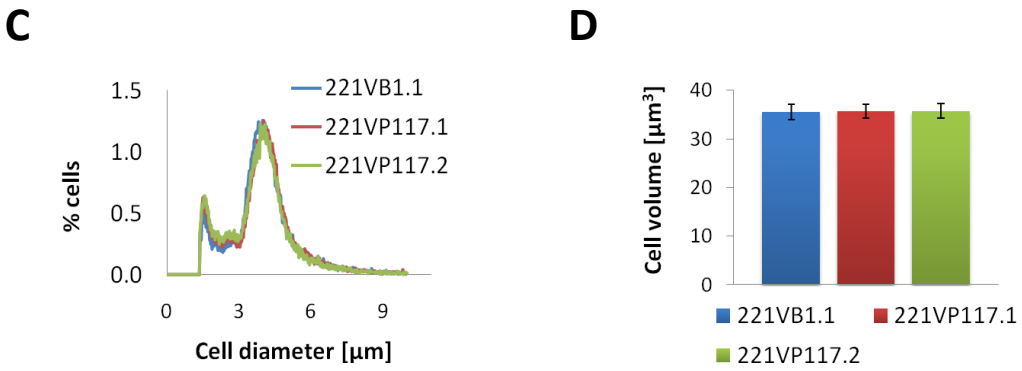


Figure 4.7: The 221VP117 *T. brucei* cell line expressing both VSG221 and VSG117 at approximately equal levels does not differ in cell size to 221VB1.1 *T. brucei* expressing only VSG221.

A. Western blot analysis of dilution series of the protein samples was performed to estimate the levels of VSG117 and VSG221 protein in VSG117-VSG221 double-expressor *T. brucei* (221VP117.1 and 221VP117.2 clones) compared with the parental *T. brucei* cell line expressing only VSG221 (221VB1.1). The blots were additionally probed for BiP as a loading control.

B. Quantification of VSG221 protein expressed by the 221VP117.1 and 221VP117.2 *T. brucei* clones as a percentage of total VSG221 produced by the parental cell line 221VB1.1 cell line. The quantification was performed using BioRad Quantity One software and the average values obtained from three independent experiments are shown with standard deviation indicated with error bars.

C. The estimated diameter of VSG221-VSG117 double-expressor *T. brucei* (221VP117.1 and 221VP117.2 clones) was compared with the parental 221VB1.1 *T. brucei* expressing only VSG221 using a CASY® Cell Counter.

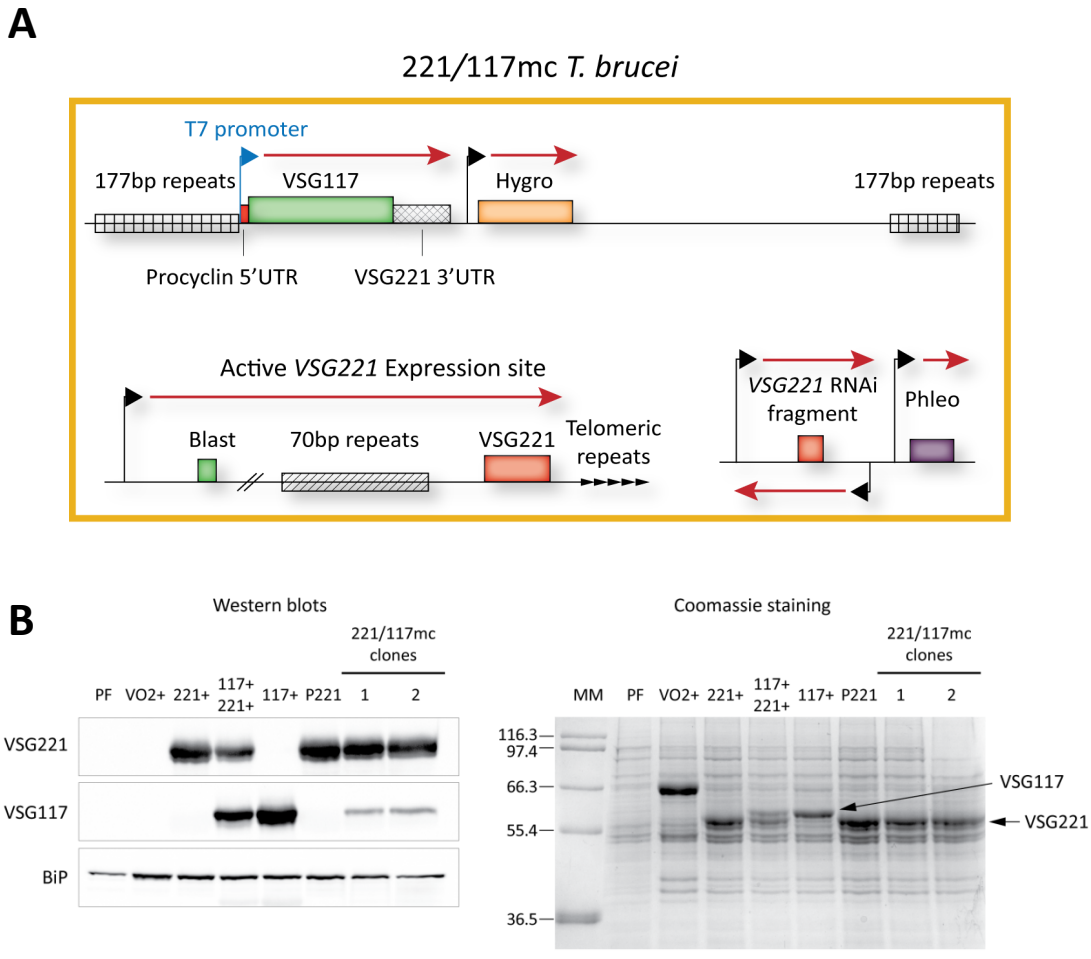
D. The calculated cell volume of the VSG221-VSG117 double-expressor (221VP117.1 and 221VP117.2 clones) and the parental VSG221 single-expressor (221VB1.1) was determined using the estimated diameter of pseudo-spheres as shown in (**C**). The average values from five independent experiments are presented with standard deviation as error bars.

It has been previously suggested that *T. brucei* expressing two different VSGs on its cell surface may have a larger cell volume compared with parasites that express only one VSG variant (L. M. Figueiredo et al. 2008). However, we found that the volume of the VSG221-VSG117 double-expressor 221VP117 cell line was very similar to the volume of the parental 221VB1.1 *T. brucei* that expressed only VSG221 (Figure 4.7C and D). The calculated cell volumes of both 221VP117.1 and 221VP117.2 clones were estimated at 35.7 μm^3, which was not significantly different to the cell volume of the parental 221VB1.1 cell line (35.5 μm^3) (Figure 4.7D). Thus, expression of two different VSGs did not appear to result in an increase in trypanosome cell size.

4.2.7. The *VSG117* gene targeted into the minichromosomal 177 bp repeats or the αβ-tubulin array is not expressed at sufficiently high levels to alleviate the *VSG221* RNAi-induced growth arrest

As already shown, high levels of VSG117 expression could be achieved by integration of a construct containing a transgenic *VSG117* into the active *VSG221* ES (Figure 4.3 and Figure 4.6). In order to determine whether the *VSG221* RNAi-triggered growth arrest could be alleviated by expressing VSG117 from a genomic location other than the active *VSG* Expression site, a construct containing a *VSG117* gene was targeted into the minichromosomal 177 bp or the αβ-tubulin array in a cell line that was capable of performing inducible *VSG221* RNAi (P221) (Figure 4.8 and Figure 4.9). Induction of *VSG221* RNAi in the P221 *T. brucei* caused a rapid growth arrest, comparable to that observed in the 221VB1.1 *T. brucei* (results not shown).

The 177 bp repeats comprise the bulk of the transcriptionally silent minichromosomes, and are arranged as palindromic repeats (Wickstead et al. 2004). These chromosomes contain part of the genomic reservoir of silent *VSG* genes. The *VSG* genes in the minichromosomes are located at the telomeres, as is also the case with the *VSG* Expression sites. There are, however, no promoters in the minichromosomes and *VSGs* that are located there are therefore not expressed. A construct containing the *VSG117* gene was targeted into the 177 bp repeats using hygromycin drug selection, with the *VSG* under the control of an exogenous T7 polymerase promoter, to achieve high levels of transcription (Figure 4.8A). The *VSG221* 3'UTR was again used downstream of the *VSG117* coding sequence to ensure high levels of stability of the *VSG117* transcript (Figure 4.8A).



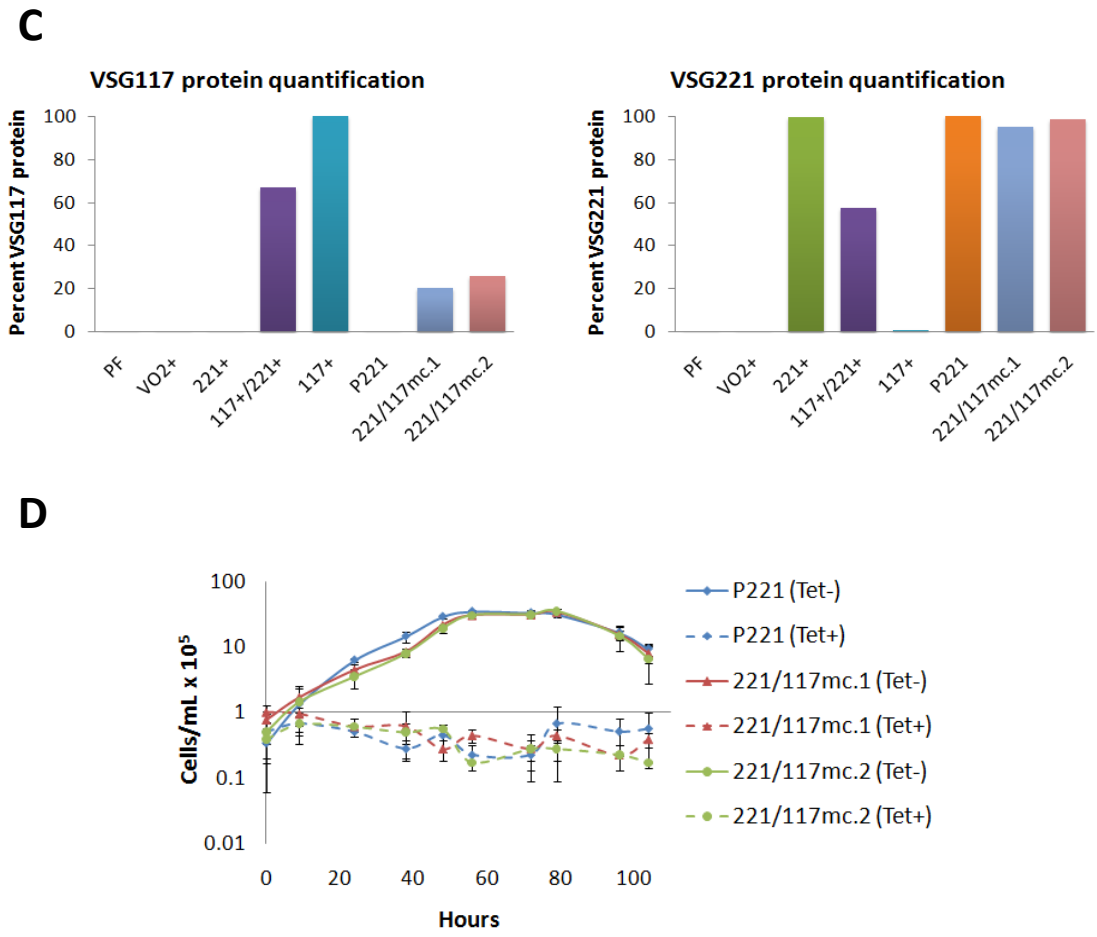


Figure 4.8: Expression of *VSG117* from a location within the 177 bp repeats is too low to achieve complementation of the *VSG221* RNAi-induced growth arrest.

A. A construct containing a *VSG117* gene was targeted into the transcriptionally silent 177 bp repeats under hygromycin (Hygro) drug resistance. The expression of *VSG117* was directed by a strong T7 polymerase promoter and the stability of the transcript was facilitated by the presence of the *VSG221* 3'UTR. Blasticidin (Blast) drug selection was used to select for activation of the *VSG221* ES. A construct containing the *VSG221* RNAi fragment was integrated into the cells using phleomycin (Phleo) drug selection.

B. Western blot analysis of cells expressing VSG117 from a construct integrated in the 177 bp repeats (221/117mc.1 and 221/117mc.2). Levels of VSG117 and VSG221 protein were compared with those present in cells expressing only VSG221 (221+), both VSG221 and VSG117 (221+/117+), only VSG117 (117+) and the parental cell line (P221 – a VSG221-only expressor). A cell line

expressing VSG VO2 (VO2+) and the procyclic 29-13 *T. brucei* cell line (PF) were used as negative controls. The blot was additionally probed for BiP as a loading control.

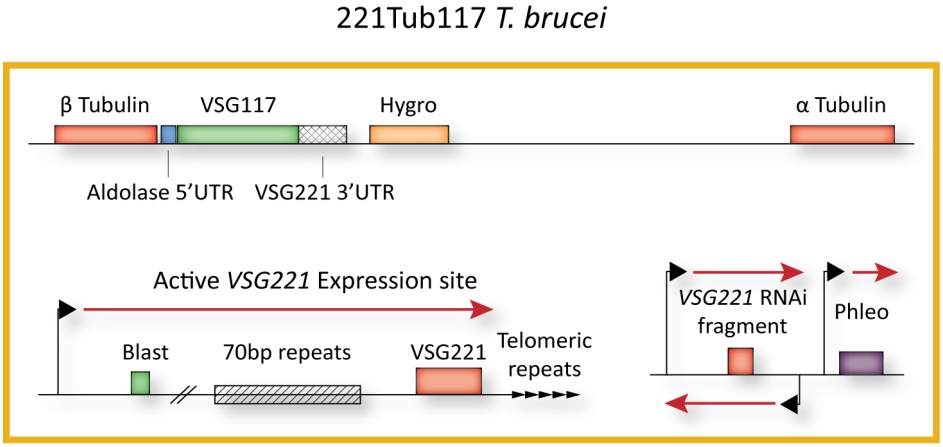
C. Quantification of VSG221 and VSG117 protein levels was performed using BioRad Image Lab software. The amounts of the two proteins are expressed as percentages of total VSG.

D. The growth of 221/117mc *T. brucei* (clones 1 and 2) was compared with the parental P221 *T. brucei* cell line after induction of *VSG221* RNAi. Uninduced cells (Tet-) were compared with cells where *VSG221* RNAi had been induced (Tet+) with 1μg/mL tetracycline for the time specified in hours. The average cell density from triplicate counts is represented in cells per mL x 10^5 and the standard deviation is shown as error bars.

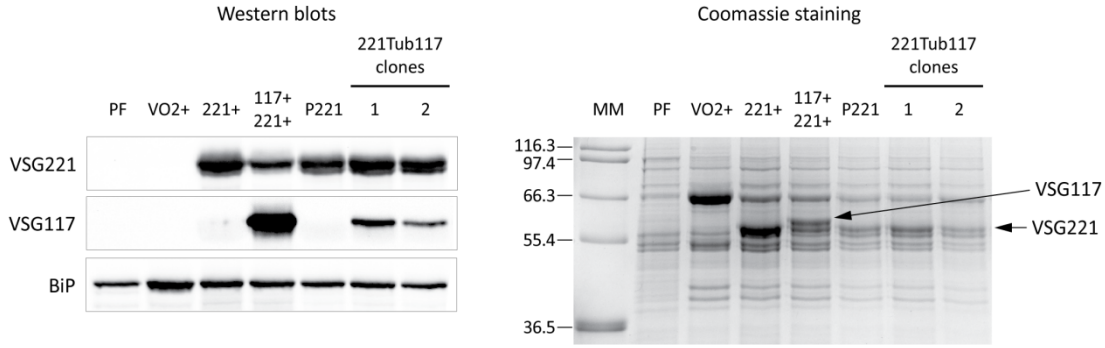
The western blot analysis of the levels of VSG117 protein expressed from a construct integrated in the 177 bp repeats showed that the amounts of VSG117 protein expressed were very low, and comprised only about 20-25% of the total VSG117 protein produced by a VSG117 single-expressor (221/117mc compared with 117+ in Figure 4.8B and C). It was, therefore, not surprising that upon induction of *VSG221* RNAi, the low levels of VSG117 protein failed to compensate for the block of VSG221 synthesis. The 221/117mc *T. brucei* were stalled, similar to the parental P221 *T. brucei* cell line that expressed only *VSG221* (Figure 4.8D). Comparable results were obtained for the cell line expressing VSG117 from a construct integrated in the αβ-tubulin array (Figure 4.9).

Unlike the transcriptionally silent 177 bp repeats, the αβ-tubulin array, composed of repeating units of α- and β- tubulin genes, is transcribed in *T. brucei*. The construct containing a *VSG117* gene, flanked by the aldolase 5'UTR and the *VSG221* 3'UTR, was targeted into the αβ-tubulin array intergenic region under the selection of hygromycin drug resistance (Figure 4.9A).

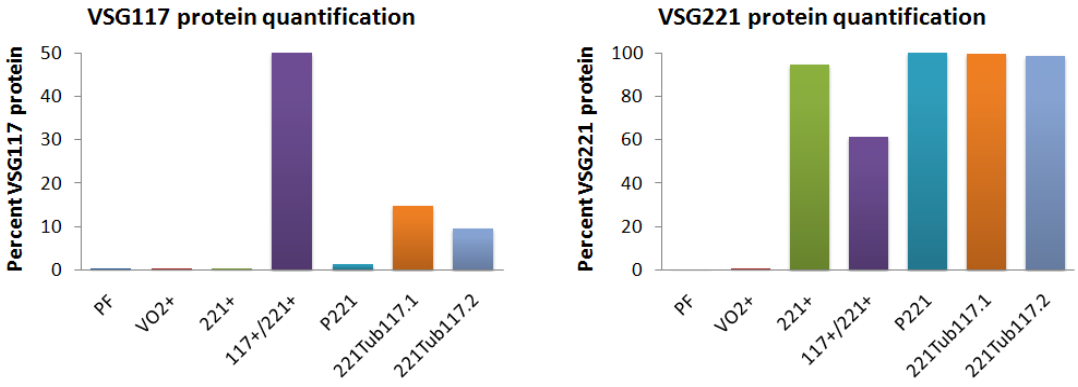
A


221Tub117 T. brucei
β Tubulin
VSG117
Hygro
α Tubulin
Aldolase 5'UTR
VSG221 3'UTR
Active VSG221 Expression site
Blast
70bp repeats
VSG221
Telomeric repeats
VSG221 RNAi fragment
Phleo

B


Western blots
221Tub117 clones
PF
VO2+
221+
117+ 221+
P221
1
2
VSG221
VSG117
BiP
Coomassie staining
MM
116.3
97.4
66.3
55.4
36.5
VSG117
VSG221

C


VSG117 protein quantification
Percent VSG117 protein
50
40
30
20
10
0
PF
VO2+
221+
117+/221+
P221
221Tub117.1
221Tub117.2
VSG221 protein quantification
Percent VSG221 protein
100
80
60
40
20
0

D

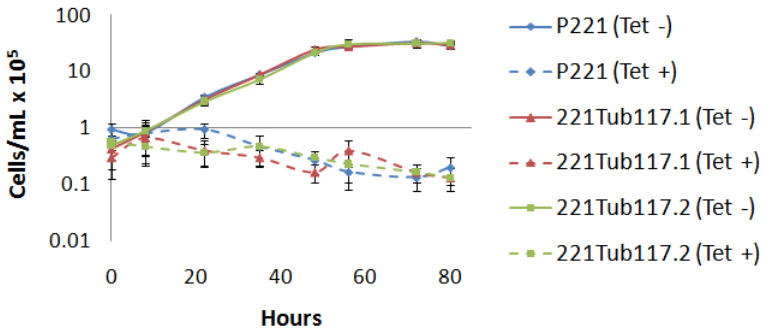


Figure 4.9: Expression of *VSG117* from the αβ-tubulin array was too low to achieve complementation of the *VSG221* RNAi-induced growth arrest.

A. A construct containing a *VSG117* gene was targeted into the transcriptionally active αβ-tubulin array under hygromycin (Hygro) drug resistance. The *VSG117* gene was flanked by aldolase 5' and *VSG221* 3'UTRs. Blasticidin (Blast) drug selection was used to select for activation of the *VSG221* ES. A construct containing the *VSG221* RNAi fragment was integrated into the cells using phleomycin (Phleo) drug selection.

B. Western blot analysis of cells expressing VSG117 from a construct integrated in the αβ-tubulin array (221Tub117.1 and 221Tub117.2). Levels of VSG117 and VSG221 protein were compared with those present in cells expressing only VSG221 (221+), both VSG221 and VSG117 (221+/117+) and the parental cell line (P – a VSG221-only expressor). A cell line expressing VSG VO2 (VO2+) and procyclic 29-13 *T. brucei* cell line (PF) were used as a negative control. The blots were additionally probed for BiP as a loading control.

C. Quantification of VSG221 and VSG117 protein levels was performed using BioRad Image Lab software. The levels of the two proteins are expressed as percentages of total VSG.

D. The growth of the 221Tub117 *T. brucei* (clones 1 and 2) was compared with the parental P221 *T. brucei* cell line after induction of *VSG221* RNAi. Uninduced cells (Tet-) were compared with cells where *VSG221* RNAi had been induced (Tet+) with 1μg/mL tetracycline for the time specified in

hours. The average cell density from triplicate counts is represented in cells per mL x 10^5 and the standard deviation is shown as error bars.

The quantification of the amounts of VSG117 protein expressed from the αβ-tubulin locus as observed from the western blot analysis showed that these cells were producing only about 10-15% of the total VSG117 protein compared with the VSG117-VSG221 double-expressor (221Tub117.1 and 221Tub117.2 compared with 117+/221+ in Figure 4.9B and C). The amount of VSG117 protein synthesised by the VSG117-VSG221 double-expressor (117+/221+) was arbitrarily set at 50%, with the rest of the VSG protein in these cells made up of VSG221. The 221Tub117 *T. brucei* appeared to rely on the expression of VSG221 for growth, as western analysis estimated that levels of VSG221 protein in these cells were about 98-99% of the levels synthesised by the parental cell line P221 *T. brucei*, which expressed only VSG221 (Figure 4.9B and C). The amount of VSG117 protein expressed in the 221Tub117 *T. brucei* cell line was lower than levels obtained from a construct integrated in the 177 bp repeats. These levels of VSG117 were also insufficient to rescue the 221Tub117 *T. brucei* cells from the *VSG221* RNAi-induced growth arrest, and the parasites stalled after blocking VSG synthesis, similar to the parental P221 *T. brucei* (Figure 4.9D).

4.3. Conclusions

The VSG surface coat of *Trypanosoma brucei* provides the parasite with a dynamic layer of physical protection from the host immune system. Although the immune system is absent in *in vitro* culturing conditions, *T. brucei* can nonetheless

maintain an intact VSG coat, and blocking VSG synthesis caused a rapid growth arrest and block in the cell cycle (Figure 3.1C and Figure 3.2). As *VSG* mRNA is one of the most abundant transcripts in *T. brucei*, its degradation through induction of *VSG* RNAi resulted in the generation of large quantities of siRNA. Therefore the *VSG* RNAi-triggered phenotype may have been a stress response due to siRNA toxicity. To eliminate this possibility, we attempted to alleviate the growth arrest after induction of *VSG221* RNAi by expressing a second *VSG*, *VSG117*, from the active *VSG221* ES.

VSG protein comprises about 10% of total cellular protein in *T. brucei* and is synthesized at exceptionally high levels. The active *VSG* gene, located in the polycistronic *VSG* Expression site transcription unit, is transcribed at a high rate by RNA polymerase I (Günzl et al. 2003). The ES occupies a specialized site outside of the nucleolus, known as the Expression site body (ESB) (Navarro & Gull 2001). The high processivity of the RNA polymerase I, combined with the location of the ESB, where the transcription and RNA processing machinery necessary for the production of the *VSG* transcript is thought to be specifically recruited, ensure the production of large amounts of *VSG* mRNA. Therefore, to achieve high levels of VSG expression, a construct containing *VSG117* was integrated into the active *VSG221* Expression site (Figure 4.1). In addition, the transgenic *VSG117* was inserted into the cells flanked by the *VSG221* 3'UTR (Figure 4.2) (Berberof et al. 1995; E. Pays, Coquelet, et al. 1989; Davies et al. 1997). Although, it is not clear how the *VSG* 3'UTR facilitates high levels of transcript stability, it has been observed that there is about 700 fold difference between the levels of *VSG* and *ESAG1* mRNA – two transcripts that originate from the same polycistronic transcription unit (Figure 1.10) (Cully et al. 1985). Thus, post-transcriptional regulation clearly is an important factor that

determines the stability of the *VSG* transcript to ensure high levels of VSG protein and the *VSG* 3'UTR is one of the primary features allowing this transcript stabilisation.

Wild-type *VSG* genes are normally located at telomeres in the *VSG* Expression sites. The generation of VSG double-expressor *T. brucei* has previously been reported (Muñoz-Jordán et al. 1996). However, here the authors reported integration of a construct containing the second *VSG* immediately upstream of the wild-type telomeric *VSG*. These authors showed that the simultaneous expression of two VSGs from the same ES was not detrimental to the growth of the parasites *in vivo* or *in vitro* (Muñoz-Jordán et al. 1996). In contrast, in the experimental system used in this study, the transgenic *VSG117* gene was inserted immediately downstream of the promoter of the active *VSG221* ES (Figure 4.3). This unusual location of the *VSG117* gene did not appear to impact on its expression and the VSG221-VSG117 double-expressor (221VP117) was shown to produce high levels of *VSG117* mRNA (Figure 4.6B).

Due to the significant sequence diversity observed between the N-terminal domains of different *VSG* genes, the *VSG221* RNAi fragment directed against the N-terminus of *VSG221* was predicted not to cause the degradation of *VSG117* mRNA (Figure 4.1 and Figure 4.6B) (Carrington et al. 1991; O. C. Hutchinson et al. 2003). Growth analysis of the 221VP117 *T. brucei* cell line after induction of *VSG221* RNAi confirmed the ability of *VSG117* to rescue the parasites from growth inhibition after blocking VSG221 synthesis (Figure 4.6A) (T. K. Smith et al. 2009). Induction of *VSG221* RNAi in VSG221-VSG117 double expressing *T. brucei* resulted in the accumulation of high levels of *VSG* siRNAs, but the growth of these cells was not stalled. This eliminated the concern that the *VSG221* RNAi-triggered growth arrest

was simply a toxicity response and indicated that it was a direct consequence of blocking VSG synthesis (T. K. Smith et al. 2009).

As expected, induction of *VSG221* RNAi resulted in the rapid disappearance of the *VSG221* mRNA but did not cause degradation of the *VSG117* transcript (Figure 4.6B). In contrast, a slight increase in the *VSG117* mRNA was observed after 6 hours of induction of *VSG221* RNAi. This might have been a consequence of the stabilization of the remaining *VSG* transcript, *VSG117* mRNA. As the *VSG221* mRNA had been ablated, possibly RNA binding proteins functioning as stabilization factors might have been released from the *VSG221* 3'UTR on the *VSG221* mRNA. These could have stabilised the *VSG117* transcript in a manner similar to that discussed previously for the *eGFP* mRNA (Chapter 3.6). Alternatively, it was also possible that the sudden reduction in the total *VSG* mRNA pool caused an increased rate of transcription of the active ES in order to compensate for the loss of *VSG221* transcript.

VSG protein is extremely stable with a half-life of approximately 36 hours (Bülow et al. 1989; Seyfang et al. 1990). Therefore, it was not surprising that the rapid degradation of the *VSG221* mRNA after the induction of *VSG221* RNAi did not manifest in an equally rapid disappearance of the VSG221 protein (Figure 4.6C). Instead, the VSG221 protein levels appeared to decrease gradually over a period of several days, presumably due to the dilution effect of the continuously dividing cells, and this loss of the VSG221 protein was compensated for by the gradual increase in the VSG117 protein (Figure 4.6C) (T. K. Smith et al. 2009).

Western blot analysis of the VSG221-VSG117 double expressing *T. brucei* (221VP117) showed that these cells produced lower levels of VSG221 protein compared with the parental VSG221 single-expressor *T. brucei* (221VB1.1) (Figure

4.7A and B). Quantification of the levels of VSG221 protein in the 221VP117 double-expressor *T. brucei* showed these to be approximately 50% of the total wild-type VSG221 protein levels in 221VB1.1 *T. brucei* (Figure 4.7A and B). The rest of the VSG protein pool in the VSG221-VSG117 double-expressors was composed of VSG117 protein, which appeared to be expressed as approximately 50% of total cellular VSG. This suggested that the parasite has a limited capacity for the production of VSG protein, and presented with two *VSG* transcripts, the translation machinery selected them at random for protein synthesis, resulting in a roughly 1:1 ratio of the two VSG proteins. In addition, the VSG double-expressor cells were found to have a similar cell volume to the parental VSG221-only expressor (Figure 4.7C and D). It is possible that an intrinsic restriction on the size of the parasites limits the expression levels of VSG protein, which caused each of the two VSGs to be expressed at half the wild-type levels. Alternatively, the metabolic capacity of the cells for VSG protein production could prevent an increase in cell size in order to avoid dilution of the surface VSG coat. These results suggest that the expression of VSG protein is saturated in the parasites, in contrast to data presented in other studies (Y.-N. Wang et al. 2010).

Although VSG proteins are extremely diverse in their amino acid sequence, their overall tertiary structure is thought to be highly conserved. Both VSG221 and VSG117 contain the A-type VSG N-terminal domain, and the two proteins are predicted to have a high level of secondary structure conservation (Figure 4.1C and D) (G. A. M. Cross 1975; Carrington et al. 1991; Chattopadhyay et al. 2005; N. G. Jones et al. 2008). The evolutionary importance of this overall preservation of protein folds could be due to the need for the VSG surface coat to remain protective as the parasite switches to a new VSG variant. Therefore, it was not surprising that

the VSG221-VSG117 double expressing *T. brucei* were found to display both VSGs on its cell surface, even though the two proteins differed in size and amino acid sequence (Figure 4.5).

Production of insufficient quantities of the complementing VSG117 was not capable of rescuing the parasite from the *VSG221* RNAi-induced growth arrest (Figure 4.8 and Figure 4.9). It appeared that the cells are highly sensitive to their VSG protein levels. Although approximately 9-14% or 20-25% of wild-type VSG levels were produced from constructs integrated into either the αβ-tubulin array or the 177 bp repeats, respectively, these low levels of expression were not sufficient to complement the growth inhibition observed after the induction of *VSG221* RNAi (Figure 4.8 and Figure 4.9). As the transgenic *VSG117* in both of these locations was flanked with the *VSG221* 3'UTR, its position outside of the active *VSG221* Expression site could have been a factor in its lower levels of expression. It is possible that both the RNA polymerase II promoter driving tubulin transcription and the T7 promoter are less strong than a fully active ES promoter. Thus, the localization of the *VSG* in the active *VSG* Expression site, as well as transcript UTRs are both important for the high expression levels necessary for successful complementation of the *VSG221* RNAi-triggered phenotype in 221VP117 *T. brucei* (Figure 4.2 and Figure 4.3).

Although the functionality of *VSG117* expressed immediately downstream of the promoter of the active *VSG221* Expression site was confirmed through its ability to rescue the cells from the growth arrest after the induction of *VSG221* RNAi, its unusual location in the ES posed interesting questions. First of all, was the VSG117 coat expressed from this location fully protective in immunocompetent mice? Secondly, is a parasite expressing the VSG from promoter-adjacent position able to

undergo antigenic variation? To address these questions, a deletion of the telomeric *VSG221* gene from the active *VSG221* ES of VSG221-VSG117 double expressing *T. brucei* was attempted.

Chapter 5

VSG expressed from a non-telomeric location can form a protective surface coat

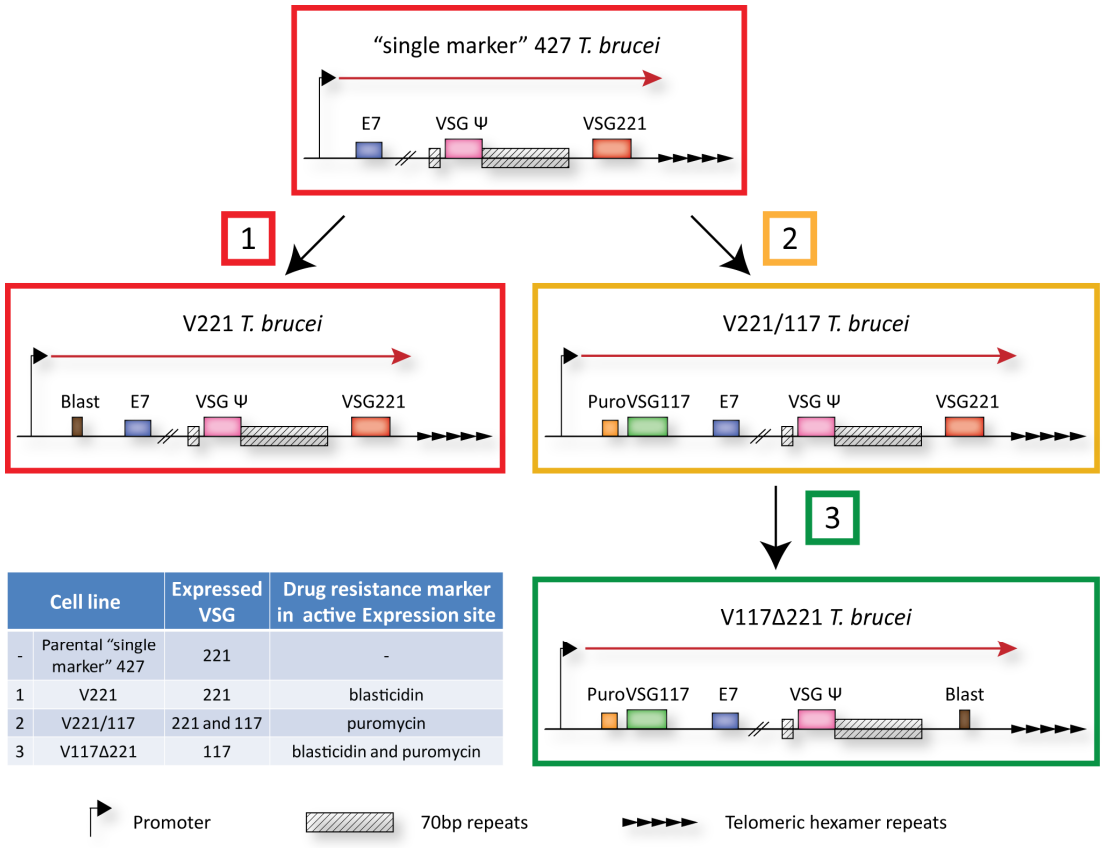
5.1. Introduction

The Bloodstream *VSG* Expression sites (BESs) are polycistronic transcription units of about 50 kbp in length and have a highly conserved organisation with the *VSG* gene invariably located at the telomeric end of the BES (Hertz-Fowler et al. 2008; Berriman et al. 2002; Kooter et al. 1987; E. Pays, Tebabi, et al. 1989). The *VSG* gene is preceded by a variable number of Expression site associated genes (*ESAGs*), most with unknown function (Figure 1.9) (E. Pays et al. 2001; Paindavoine et al. 1992; Salmon et al. 1997; Hoek et al. 2000; Hoek et al. 2002; Gottesdiener 1994; Redpath et al. 2000; M. J. L. Ligtenberg et al. 1994). In addition to the *ESAGs* and *VSG* genes, the BESs are also defined by a number of characteristic repeat regions. Long stretches of 50 bp repeats are located immediately upstream of the promoter region of the BES (Figure 1.10) (Zomerdijk et al. 1990; Berriman et al. 2002; Sheader et al. 2003). In addition, imperfect TAA-rich repeats, known as 70 bp repeats, occur upstream of most *VSG* genes, both in the active and silent Expression sites, as well as in other genomic locations (Figure 1.9) (A. Y. C. Liu et al. 1983; Campbell et al. 1984). It is unclear why the *VSG* is invariably located at the BES telomere, although this location may facilitate homologous recombination (Yang et al. 2009; Bernards et al. 1983; Van der Ploeg, A. Y. C. Liu, et al. 1984; Horn & Barry 2005). The current chapter investigates the importance of the telomeric localisation of the *VSG* gene for high expression levels necessary for full functionality and protectiveness of the VSG surface coat.

5.2. Results

5.2.1. Expression of *VSG117* from the active *VSG221* Expression site allows for the deletion of the telomeric *VSG221*

As was previously shown, it was possible to alleviate the *VSG221* RNAi-induced phenotype by providing the cells with a second different *VSG* that was not recognised by the *VSG221* RNAi machinery (Chapter 4.2.3 and 4.2.5) (T. K. Smith et al. 2009). Thus, it was predicted that it should be possible to delete the *VSG221* gene from the active *VSG221* Expression site of the VSG221-VSG117 double-expressor *T. brucei* (Figure 5.1).



	Cell line	Expressed VSG	Drug resistance marker in active Expression site
-	Parental "single marker" 427	221	-
1	V221	221	blasticidin
2	V221/117	221 and 117	puromycin
3	V117Δ221	117	blasticidin and puromycin

Figure 5.1: Deletion of the telomeric *VSG221* gene from the active *VSG221* Expression site. The active *VSG221* Expression site parental "single marker" 427 *T. brucei* was genetically modified by (1)

either inserting a blasticidin resistance gene (Blast) (V221 *T. brucei*), or (2) a *VSG117* gene using puromycin selection (Puro) (V221/117 *T. brucei*) immediately downstream of the ES promoter. (3) The telomere-proximal *VSG221* was subsequently replaced with a blasticidin drug resistance marker (Blast) (V117Δ221 *T. brucei*). The table summarises the *VSG* genes expressed by each of the constructed cell lines, as well as the drug resistance genes present in the active Expression site.

For this study three different cell lines were constructed using the parental "single marker" 427 *T. brucei* cell line (Figure 5.1) (Wirtz et al. 1999). A VSG221-only expressor was constructed by integrating a construct with a blasticidin resistance gene immediately downstream of the promoter of the active *VSG221* Expression site (step 1 in Figure 5.1). The presence of the blasticidin gene allowed for selection for activation of the *VSG221* ES. A VSG221-VSG117 double-expressor cell line, V221/117 *T. brucei*, was generated by integrating a construct containing the *VSG117* gene using puromycin drug selection immediately downstream of the promoter of the active *VSG221* Expression site. This was performed in an analogous fashion to the integration of *VSG117* into the active *VSG221* Expression site of the 221VB1.1 *T. brucei* cell line (Chapter 4.2.3, Figure 4.3 and step 2 in Figure 5.1). This cell line was maintained in the presence of puromycin which allowed for selection of cells expressing both *VSG221* and *VSG117* from the same active *VSG* ES. The V117Δ221 *T. brucei* cell line was generated from the V221/117 cell line by replacing the telomere-proximal *VSG221* gene with a construct containing a blasticidin drug resistance marker (step 3 in Figure 5.1). The V117Δ221cell line was cultured in the presence of both puromycin and blasticidin, which enabled selection for cells that were expressing *VSG117* from immediately downstream of the promoter of the active *VSG221* Expression site and had deleted their telomeric

VSG221 gene. The three cell lines were then assessed for surface VSG expression, VSG coat protectiveness and the ability to switch to a new VSG.

5.2.1.1. Construction of the V221 *T. brucei* cell line

The *VSG221* single-expressor cell line, V221, was transfected with a construct which resulted in a blasticidin resistance gene (henceforth referred to as *Blast*) integrating immediately downstream of the promoter of the active *VSG221* Expression site (Figure 5.2A). The successful integration of the *Blast* gene into the active *VSG221* Expression site of V221 *T. brucei* clones was established using PCR linking the *Blast* gene with the *ESAG7* gene, which generated the expected 2463 bp fragment (Figure 5.2B). The parental "single marker" 427 *T. brucei* genomic DNA, which did not have the *Blast* gene, did not yield any product, as expected (Figure 5.2B).

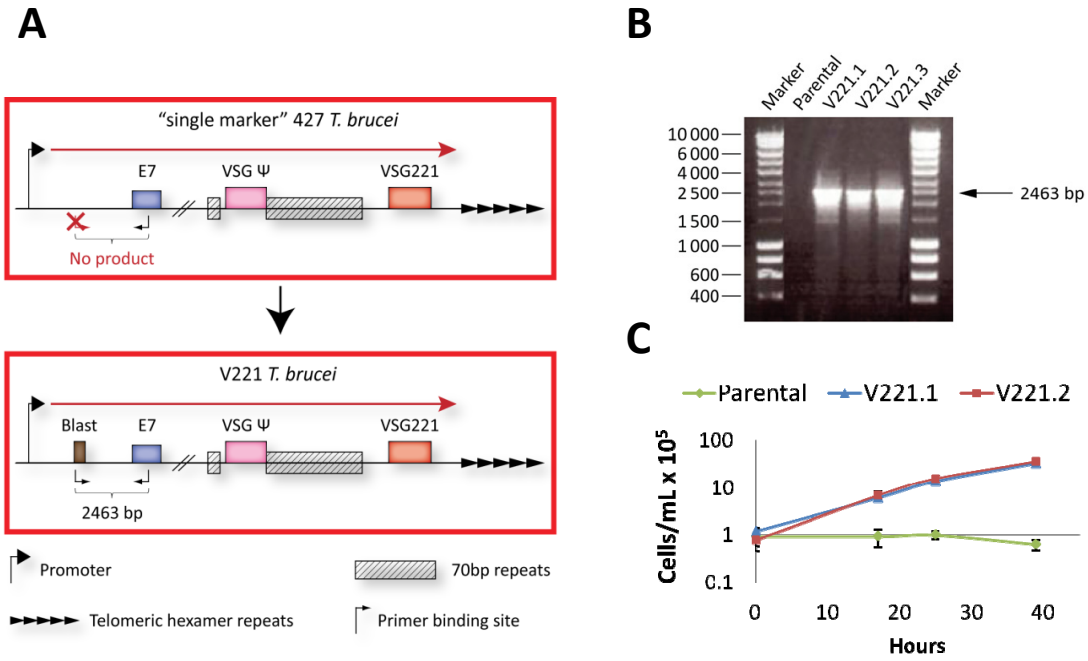


Figure 5.2: Integration of a construct containing a blasticidin drug resistance gene into the active *VSG221* Expression site of the "single marker" 427 *T. brucei* to generate the V221 cell line.

A. The schematic shows the 2463 bp fragment expected to be generated from PCR linking the *Blast* gene and the *ESAG7* gene when using genomic DNA of V221 *T. brucei* as a template. No product is expected to be obtained from the parental "single marker" 427 *T. brucei*.

B. The *Blast* gene was linked to the downstream *ESAG7* gene using PCR in V221.1 and V221.2 *T. brucei* clones. The same PCR did not yield a product using parental "single marker" 427 *T. brucei* (Parental) genomic DNA as a template.

C. Growth of the V221.1 and V221.2 clones *T. brucei* in the presence of blasticidin drug was compared with the parental "single marker" 427 cell line (Parental) for the time specified in hours. The average cell density from triplicate counts is represented in cells per mL x 10^5 and the standard deviation is shown as error bars.

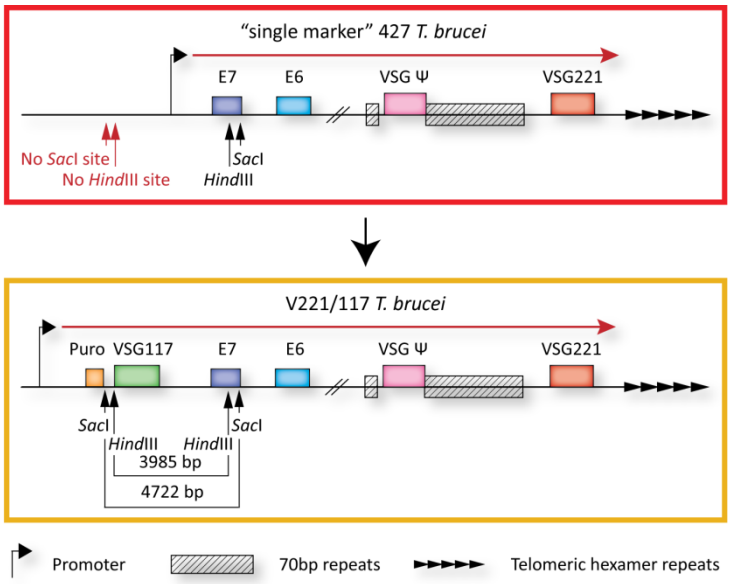
Blasticidin was inhibitory to the growth of the parental "single marker" 427 cell line, because it lacked the *Blast* gene (Figure 5.2C). V221 *T. brucei* clones, however, grew in the presence of blasticidin, which suggested that these parasites have correctly integrated the *Blast* gene in the active *VSG221* ES (Figure 5.2C). The V221.1 clone was selected as a control VSG221 single-expressor cell line, necessary for experiments attempting deletion of *VSG221* from its wild-type telomeric location.

5.2.1.2. Construction of the V221/117 *T. brucei* cell line

The V221/117 cell line was generated by targeting a construct containing *VSG117* immediately downstream of the promoter of the active *VSG221* ES of a

"single marker" 427 *T. brucei* (Figure 5.3A). To verify the correct integration of the construct, V221/117 *T. brucei* cell line was analysed by Southern blotting (Figure 5.3). Digests were performed using either *Hind*III or *Sac*I restriction enzymes. The Southern blot analysis using *Hind*III digest was equivalent to that previously described for 221VP117 *T. brucei* and resulted in the expected 3985 bp fragment in the V221/117 cell line (Figure 5.3 and Chapter 4.2.3, Figure 4.4) The *Sac*I digest of the V221/117 clones genomic DNA resulted in the expected 4722 bp fragment, which was not present in the parental "single marker" 427 cell line (Figure 5.3C). The Southern blot analysis therefore confirmed the correct integration of the construct containing *VSG117* immediately downstream of the promoter of the active *VSG221* ES.

A



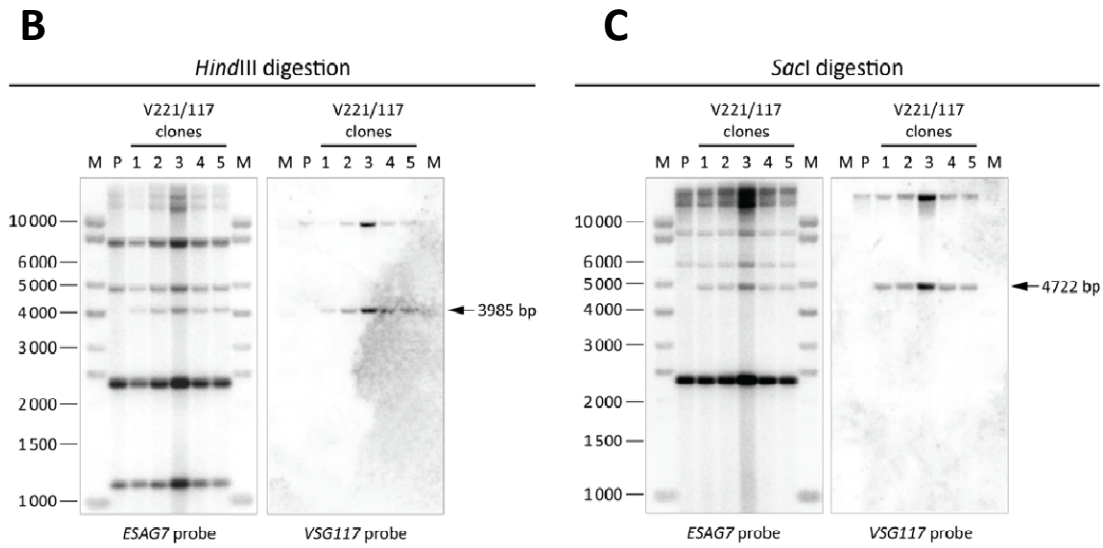


Figure 5.3: Integration of a construct containing the *VSG117* gene into the active *VSG221* Expression site of the "single marker" 427 *T. brucei* to generate the V221/117 cell line.

A. A *VSG117* gene linked to a puromycin resistance gene (Puro) was inserted immediately downstream of the promoter of the active *VSG221* Expression site. The schematic also shows the Southern blot analysis strategy to verify the insertion of the *VSG117* gene. The *T. brucei* V221/117 clones (1-5) have acquired new *Hind*III and *Sac*I restriction enzyme recognition sites upstream of the integrated *VSG117* gene that were not present in the parental "single marker" *T. brucei* (P) cell line.

B. Southern blot analysis of *Hind*III digest of the genomic DNA from V221/117 clones (1-5) and the parental "single marker" 427 *T. brucei* (P) cell lines. The blot was hybridised with probes for *ESAG7* and *VSG117* to show linkage for these sequences. The expected 3985 bp fragment in the V221/117 *T. brucei* clones is indicated.

C. Southern blot analysis of *Sac*I digest of the V221/117 clones (1-5) and the parental "single marker" 427 *T. brucei* (P) cell lines genomic DNA. The blot was probed for the *ESAG7* and *VSG117* gene to show linkage. The expected 4722 bp fragment in the V221/117 *T. brucei* clones is indicated.

The growth rate of the V221/117 *T. brucei* clones was found to be very similar to that of the parental "single marker" 427 cell line (Figure 5.4A). This indicated that the expression of two VSGs from the active *VSG* ES was not detrimental to the growth of the parasites *in vitro*. Western blot analysis of the V221/117 cell line revealed that both clones expressed both VSG221 and VSG117 in similar ratios, as was previously observed for the 221VP117 *T. brucei* (Figure 5.4B and Figure 4.7A). Thus, the V221/117.1 clone was selected as a parental cell line for the subsequent deletion of the *VSG221* gene from its telomere-proximal position in the active *VSG221* Expression site. This cell line is henceforth referred to as V221/117 *T. brucei*.

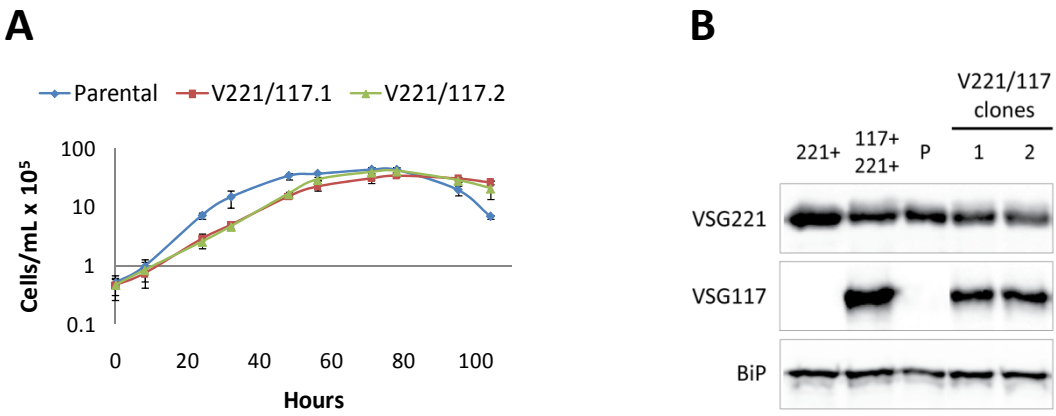


Figure 5.4: Expression of both *VSG221* and *VSG117* from the same active *VSG* Expression site is not detrimental to the growth of the V221/117 *T. brucei* cell line.

A. The growth of the V221/117.1 and V221/117.2 *T. brucei* clones was compared with the parental "single marker" 427 *T. brucei* cell line for the duration of time specified in hours. The average cell density from triplicate counts is represented in cells per mL x 10^5 and the standard deviation is shown as error bars.

B. Western blot analysis of V221/117.1 and V221/117.2 *T. brucei* clones. Levels of VSG117 and VSG221 protein were compared with levels present in cells expressing only VSG221 (221+), both

VSG221 and VSG117 (221+/117+), and in the parental 90-13 "single marker" 427 *T. brucei* cell line (P). The blots were additionally probed for BiP as a loading control.

5.2.1.3. Construction of the V117Δ221 *T. brucei* cell line

The V117Δ221 cell line was generated from the V221/177.1 *T. brucei* cell line by transfection with a construct containing a *Blast* gene, that replaced the telomeric *VSG221* from the active *VSG* Expression site (Figure 5.5A). The *Blast* gene in the construct was flanked by the *VSG221* RNA processing sequences (trans-splice site and polyadenylation sequences) that also functioned as targeting fragments for the construct. Southern blot analysis of the V117Δ221 *T. brucei* cell line was performed in order to confirm the replacement of the *VSG221* gene with the *Blast* gene (Figure 5.5). Digests were performed with *Sal*I/*Pvu*I or *Spe*I/*Pvu*I restriction enzymes. The V117Δ221 *T. brucei* clones have acquired a *Pvu*I site in the integrated *Blast* gene (Figure 5.5A). The *Sal*I site is located downstream of the *ESAG1* gene. A *Sal*I/*Pvu*I digestion of the V117Δ221 clones genomic DNA yielded the expected 5666 bp fragment, which was not observed in the parental V221/117 *T. brucei* cell line (Figure 5.5B). The *Spe*I restriction enzyme site is located within the *ESAG11* pseudogene in the active *VSG221* Expression site (Figure 5.5A). A double digest of the genomic DNA from the V117Δ221 clones using *Spe*I and *Pvu*I restriction enzymes generated the expected fragment of 9333 bp, which was not found in the parental V221/117 cell line (Figure 5.5C). Both blots were probed for the *Blast* gene and the *VSG* pseudogene confirming linkage of these sequences, and the successful deletion of the *VSG221* gene.

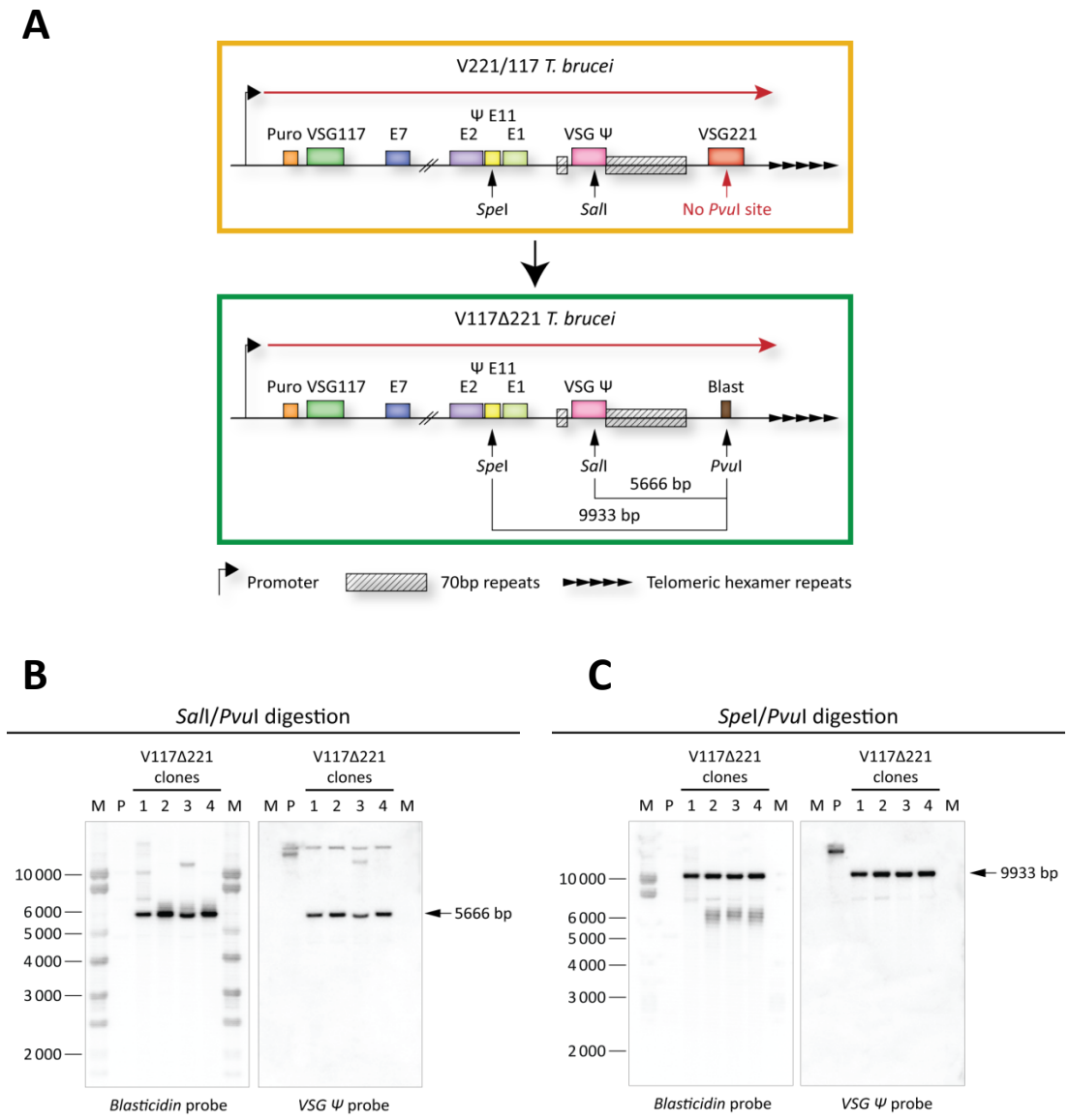


Figure 5.5: The *VSG221* gene can be deleted from the active *VSG* Expression site of *VSG221-VSG117* double-expressor *T. brucei.*

A. In the V117Δ221 cell line a blasticidin resistance gene (Blast) was inserted in place of the *VSG221* gene in the active *VSG221* ES. The schematic shows the Southern blot mapping strategy to verify the replacement of the *VSG221* gene with the *Blast* gene. The V117Δ221 *T. brucei* clones (1-4) have acquired a *Pvu*I restriction enzyme site in the *Blas*t gene that was not present in the parental *T. brucei* V221/117 cell line.

B. Southern blot analysis of *Sal*I/*Pvu*I digest of genomic DNA from the V117Δ221 clones (1-4) and V221/117 *T. brucei* cell lines. The blot was probed for both the *Blast* and *VSGψ* genes to show linkage of these sequences. The expected 5666 bp fragment in the V117/Δ221 clones is indicated.

C. Southern blot analysis of *Spe*I/*Pvu*I digest of genomic DNA from the V117Δ221 clones (1-4) and V221/117 *T. brucei* cell lines. The blot was probed for both the *Blast* and *VSGψ* genes to demonstrate linkage. The expected 9933 bp fragment in the V117Δ221 clones is indicated.

5.2.2. The active *VSG* does not need to be expressed from a telomeric location for *T. brucei* growth *in vitro*

To show that V221Δ221 *T. brucei* were fully dependent on the expression of VSG117 for growth and did not synthesise any VSG221, the cells were analysed using a western blot (Figure 5.6A). No VSG117 protein was detected in the control V221 cell line, which expressed only VSG221 (Figure 5.6A). The parental double-expressor V221/117 *T. brucei* expressed both VSG221 and VSG117 at approximately equal levels (Figure 5.4B and Figure 5.6A). The V117/Δ221 clones, however, expressed only VSG117 protein and no detectable VSG221 was observed (Figure 5.6A). The levels of VSG117 protein in the V117Δ221 clones were higher than those in the double-expressing V221/117 cell line. This suggested that the cells were completely reliant on *VSG117* expression for growth.

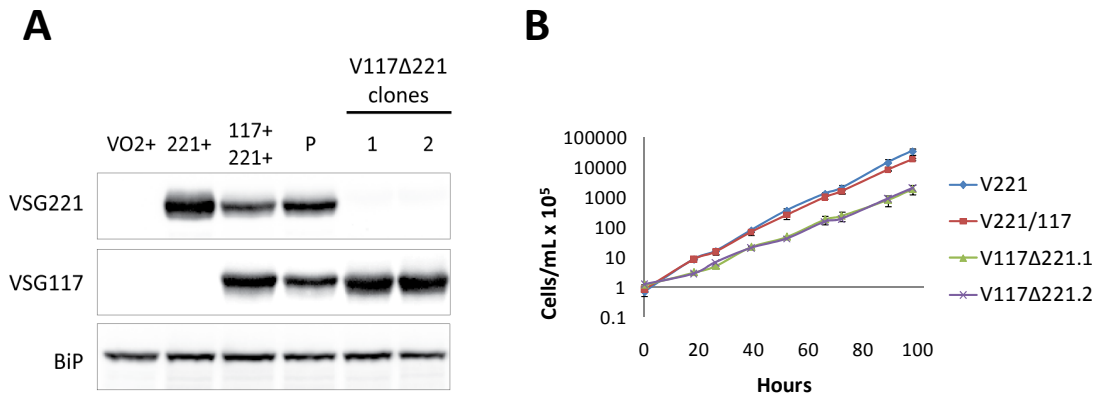


Figure 5.6: V117Δ221 *T. brucei* expresses high levels of VSG117 protein that enable them to grow *in vitro*.

A. Western blot analysis of the V117Δ221.1 and V117Δ.2 *T. brucei* clones. Levels of VSG117 and VSG221 protein were compared with levels present in cells expressing only VSGVO2 (VO2+), VSG221 (221+) and both VSG221 and VSG117 (117+/221+). The blots were additionally probed for BiP as a loading control.

B. Cumulative growth curve of V221, V221/117 and V117Δ221 (clones 1 and 2) *T. brucei*. The cells were diluted to $1x10^5$ cells/mL each time they reached $1x10^6$ cells/mL. The cumulative cell numbers were extrapolated from the dilution factor. The average cell density from triplicate counts is represented in cells per mL x 10^5 and the standard deviation is shown as error bars.

The growth of the V221, V221/117 and V117Δ221 cell lines was monitored and it was observed that the V221/117 cell line divided at a slower rate (doubling time of 6.24 h) than V221 *T. brucei* (6.18 h) (Figure 5.6B). Both of the V117Δ221 clones grew at a similar rate, but had a higher generation time of 9.62 h (Figure 5.6B). Therefore, it was concluded that parasites relying on expression of the *VSG* from a promoter proximal position in the active *VSG* ES were able to grow *in vitro*.

5.2.3. *VSG* expressed from a non-canonical location within the *VSG* Expression site is presented on the cell surface

The VSG coat of the parasites was analysed by surface immunofluorescence to determine whether the slight reduction in the growth rate of V117Δ221 *T. brucei* compared with the V221 and V221/117 cell lines was due to reduced expression of VSG117 protein on the cell surface (Figure 5.7).

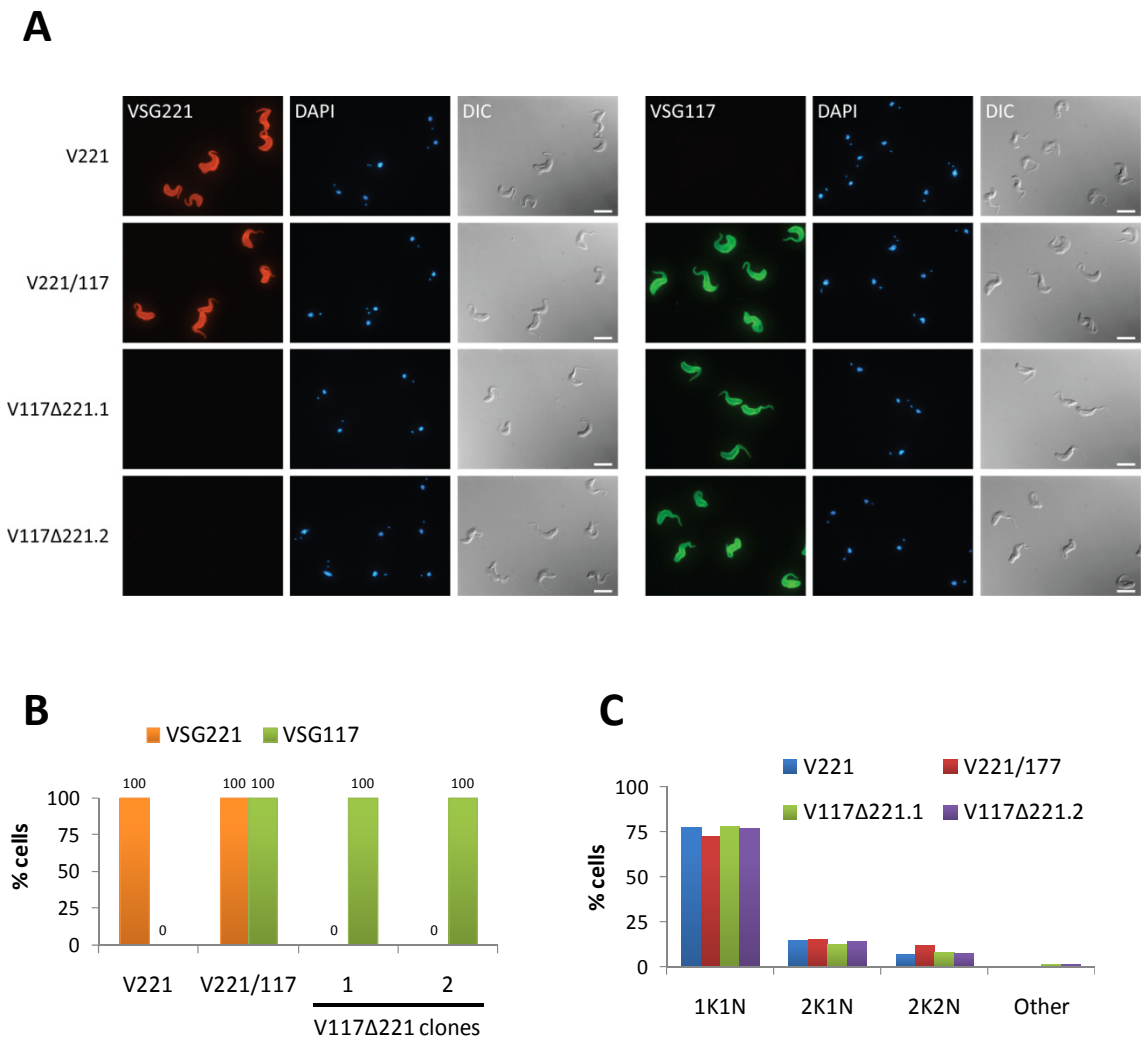


Figure 5.7: VSG expressed from immediately downstream of the promoter in the active *VSG221* Expression site is presented on the cell surface.

A. Microscopy analysis of surface immunofluorescence of V221, V221/117 and V117Δ221 (clones 1 and 2) *T. brucei* cell lines. The parasites were probed with either anti-VSG221 (orange) or anti-VSG117 (green) monoclonal antibody. The cells were stained with DAPI (blue) for DNA content and the scale bar in the DIC image represents 10 μm.

B. Quantification of surface anti-VSG221 (orange) and anti-VSG117 (green) immunofluorescence of V221, V221/117 and V117Δ221 (clones 1 and 2) *T. brucei* cell lines. For each cell population counted n>300.

C. Cell cycle analysis of the V221, V221/117 and V117Δ221 (clones 1 and 2) *T. brucei* cell lines. For each cell line counted n>300.

The V221 *T. brucei* cell line did not express any VSG117 on the cell surface, whereas the V221/117 cells were both VSG221 and VSG117 positive (Figure 5.7A). The simultaneous surface presentation of both VSG221 and VSG117 on the surface of the V221/117 *T. brucei* cell line once again confirmed that the two different VSG proteins can pack efficiently on the cell surface forming a heterogeneous VSG coat. The V117Δ221 parasites showed normal surface distribution of VSG117 protein, whereas there was no VSG221 detected on the surface of these cells (Figure 5.7A). Quantification of the immunofluorescence results showed that all three cell lines, V221, V221/117 and V117Δ221, were homogeneous for surface VSG expression (Figure 5.7B).

Cell cycle analysis as determined through the quantification of distribution of cells with different DNA content was performed (Figure 5.7C). The V117Δ221 *T. brucei* cell line was observed to have a normal distribution of cells within the population, with no increase in multinucleated or multikinetoplastid cells or cells with either 2K1N or 2K2N DNA content (Figure 5.7D). Thus, the slight reduction in

the growth rate of the V117Δ221 cell line, compared to the V221 and V221/117 *T. brucei* lines was not accompanied by abnormalities in cell morphology.

5.2.4. *VSG* expressed from a promoter-adjacent location in the active *VSG* Expression site can form a fully protective surface coat

The survival of bloodstream form *T. brucei* in the infected host completely depends on the protectiveness of the VSG coat. This not only shields invariant surface proteins from recognition by the immune system, but is also rapidly recycled and cleared intracellularly of bound host molecules, including antibodies (Barry 1979; O'Beirne et al. 1998; Balber et al. 1979; McLintock et al. 1993). Therefore, it was important to determine if the VSG117 coat expressed from a gene located immediately downstream of the promoter in the active *VSG* ES was as protective as a coat generated from a telomere-proximal *VSG*. To answer this question *in vitro* experiments were performed that allowed us to test the integrity of the VSG117 coat in the presence of an active complement system (Figure 5.8).

The complement system is part of the innate immune system and can be activated according to three different pathways: the lectin pathway, the classical pathway and the alternative pathway. The lectin pathway is activated by carbohydrates that are recognised as foreign by the host organism, such as the bacterial surface glycocalyx (Fujita 2002). The classical pathway is normally initiated by host immunoglobulin bound to a target antigen, although it can also be triggered in an antibody-independent manner by viruses and Gram negative bacteria (S. K. A. Law & Reid 1995). The alternative pathway is spontaneously activated on biological surfaces, such as foreign membranes of invading parasites (Pangburn &

Müller-Eberhard 1984). A wild-type VSG coat has been shown to protect the bloodstream form parasites from non-specific lysis by the complement system that is activated via the alternative pathway (Ferrante & Allison 1983). In contrast, procyclic form *T. brucei* expresses several million procyclin molecules on their cell surface, which do not protect these cells from complement-mediated lysis (Ferrante & Allison 1983).

Complement activation takes place in four main steps: initiation of complement activation by an appropriate trigger, C3 convertase activation and amplification, C5 convertase activation, and assembly of the membrane attack complex (MAC) (S. K. A. Law & Reid 1995). Cleavage of complement C3 is an important step in all three pathways of complement activation, as it leads to the formation of the cleaved form C3a, which is an anaphylactic and antimicrobial peptide, and the opsonin C3b that can be deposited on nearby surfaces (Zipfel & Skerka 2009). Once deposited on foreign surfaces, C3b can interact with C3b receptors present on the surface of immune effector cells, such as macrophages, and mediate the destruction of the invading pathogen (Zipfel & Skerka 2009). The host can regulate complement activation and one such regulator is Complement Receptor 1 (CR1, also known as CD35). This is a multifunctional polymorphic glycoprotein which is normally expressed on the plasma membrane of various immune system effector cells, such as macrophages and B-lymphocytes (Khera & Das 2009). A soluble form of CR1 is also found in plasma, as it is released at very low concentrations from leukocytes by cleavage of the membrane-bound form of CR1 (Danielsson et al. 1994). CR1 has been found to regulate the complement activation cascade in several ways, e. g. in binding to C3b and C4b and enhancing the decay of

the C3 and C5 convertases from both the classical and the alternative pathways (Iida & Nussenzweig 1981; Weisman et al. 1990).

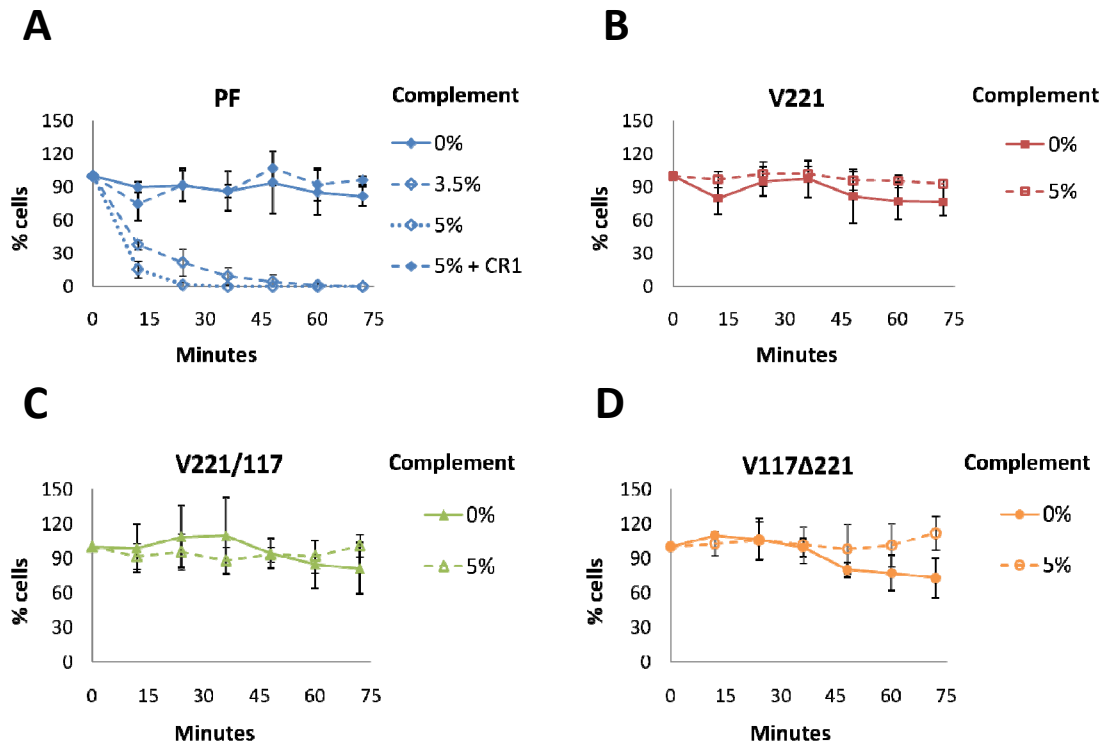


Figure 5.8: VSG117 coat expressed from a promoter-proximal location in the active *VSG* Expression site is fully protective against complement-mediated lysis *in vitro*.

The procyclic form (PF) 29-13 *T. brucei* cell line **(A)** was incubated in complement buffer only (0%), 3.5%, 5% guinea pig complement or 5% complement with the addition of CR1 inhibitor (5% + CR1). The bloodstream form V221 **(B)**, V221/117 **(C)** and V117/Δ221.1 **(D)** *T. brucei* cell lines were incubated in complement buffer only (0%) or 5% guinea pig complement (5%). The cells were counted every 12 minutes for the time specified in minutes. The average cell density from triplicate counts is represented in cells per mL x 10^5 and the standard deviation is shown as error bars.

Procyclic form *T. brucei* was incubated with 0%, 3.5% and 5% guinea pig complement. As a control, cells were also incubated in 5% complement with the addition of CR1 complement inhibitor (Figure 5.8A). Procyclic form cells were lysed

in the presence of 5% and 3.5% guinea pig complement with complete cell lysis within 30 and 60 minutes after the addition of complement, respectively (Figure 5.8A). Addition of the CR1 inhibitor to procyclic form cells incubated with 5% complement successfully inhibited complement-mediated lysis, and no cell death was observed (Figure 5.8A). Similarly, the bloodstream form V221, V221/117 and the V117Δ221.1 *T. brucei* cell lines were incubated with either 0% or 5% guinea pig complement (Figure 5.8B, C and D). As expected, the wild-type V221 cells were fully resistant to complement-mediated lysis. In addition, the VSG221-VSG117 heterogeneous coat of the V221/117 cells was also protective against lysis by complement, which was consistent with previously reported results (Muñoz-Jordán et al. 1996). The V117Δ221.1 cell line was also resistant to complement and no cell lysis was observed during the experiment (Figure 5.8D). Thus, the levels of expression of *VSG117* from the unusual promoter- adjacent location in the active *VSG* ES did not affect the protectiveness of the VSG117 coat against complement-mediated lysis.

5.2.5. The cells reliant on *VSG* expression from immediately downstream of the promoter of the active *VSG* Expression site can switch to a new *VSG*

T. brucei utilises several methods for switching its VSG coat. The most common mechanism involves homologous recombination, although it can also switch off the active *VSG* ES and activate a new one (Chapter 1.6). It was unclear if introducing additional sequences immediately downstream of the promoter of a *VSG* ES could interfere with ES regulation and disrupt the ability of the parasite to undergo antigenic variation. We, therefore, wanted to investigate if the deletion of

the active *VSG* from its wild-type telomeric location and expression of a second promoter-proximal *VSG* from the active *VSG* ES would interfere with the ability of the cells to switch to a new *VSG*.

To test this, the V221, V221/117 and V117Δ221 *T. brucei* cell lines were grown in the absence of drug selection pressure for four weeks (Figure 5.9). Protein samples were collected, and surface VSG immunofluorescence was performed once per week throughout the four week period of the experiment (Figure 5.9 and Figure 5.10). The protein samples were analysed using western blots, which were probed for VSG221, VSG117, VSGVO2 and VSG1.8 (Figure 5.9A). The V221 and the V221/117 cell lines continued expressing VSG221 throughout the four week period and the V221/117 cells also simultaneously expressed VSG117 throughout the course of the experiment (Figure 5.9A). This indicated that the V221 and the V221/117 cell lines did not frequently switch to a new VSG even after the removal of drug selection pressure. In contrast, the V117Δ221.1 and V117Δ221.2 clones switched away from VSG117 expression and expressed a new VSG (Figure 5.9A). It was unclear exactly which VSG the V117Δ221.1 clone had switched to, but the V117Δ221.2 clone formed a polyclonal population. Subpopulations of cells expressed different VSG variants, as was evident from the Coomassie-stained gel (Figure 5.9B). It was found that some of the V117Δ221.2 cells had switched to VSGVO2 and some had switched to VSG1.8 (Figure 5.9A).

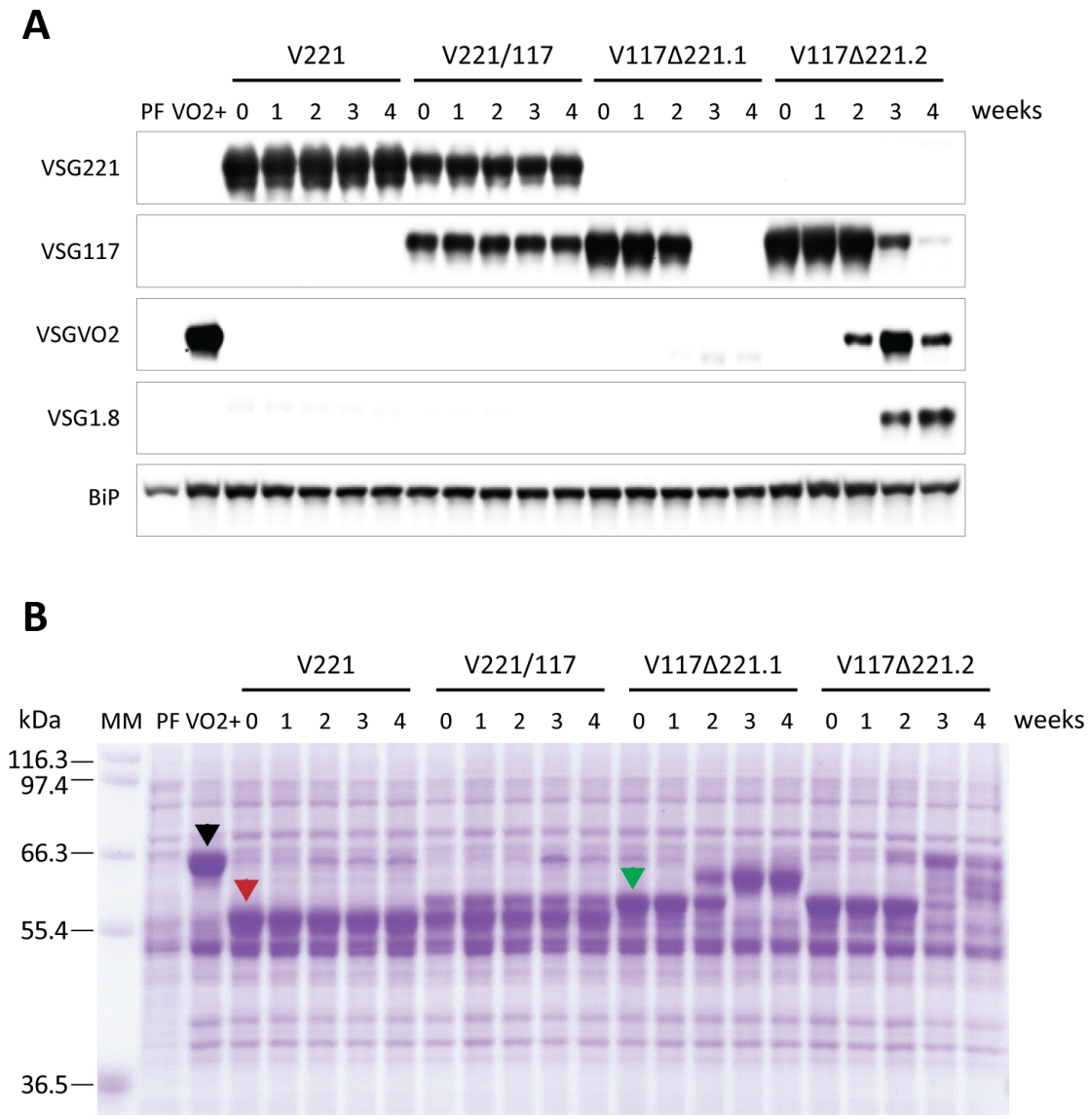


Figure 5.9: **Deletion of the telomeric *VSG221* does not impede the ability of the V117Δ221 *T. brucei* to switch to a new *VSG*.**

A. V221, V221/117 and V117Δ221.1 and V117Δ221.2 *T. brucei* cell lines were grown *in vitro* in the absence of drug selection pressure for 4 weeks. Protein lysates were collected from each cell line once per week and analysed by western blotting. Protein lysates from procyclic form 29-13 *T. brucei* (PF) and bloodstream form *T. brucei* cell line expressing VSG VO2 (VO2+) were used for comparison. The western blot was probed for VSG221, VSG117, VSGVO2, VSG1.8 and BiP as a loading control.

B. Coomassie-stained SDS-PAGE gel of protein lysates collected once per week from V221, V221/117 and V117Δ221.1 and V117Δ221.2 *T. brucei* cell lines where the cells were grown for 4 weeks in the absence of drug selection. Protein lysates from procyclic form 29-13 *T. brucei* (PF) and a bloodstream form *T. brucei* cell line expressing VSG VO2 (VO2+) were used for comparison. Bands corresponding to VSG VO2 (black arrowhead), VSG 221 (red arrowhead) and VSG117 (green arrowhead) are indicated.

These results were also confirmed by microscopic analysis of surface VSG immunofluorescence, where the V221/117 cells showed VSG117 surface expression during the entire four week period, whereas the V221 cells remained negative for VSG117 for the duration of the experiment (Figure 5.10A). Both V221 and V221/117 cell lines continued to express VSG221 on their cell surface throughout the experiment (Figure 5.10A). As expected, the V117Δ221.1 and V117Δ221.2 *T. brucei* clones switching to a new VSG showed a reduction in cells expressing VSG117 on their cell surface (Figure 5.10A andC). Quantification of the immunfluorescence results indicated that only 17% of the V117Δ221.1 cells expressed VSG117 on their surface by the second week after removal of drug selection. In contrast, the V117Δ221.2 clone population was 94% positive for surface VSG117 (Figure 5.10B and C). However, by the fourth week, only 21% of the V117Δ221.2 cell population was still expressing VSG117. Therefore, we concluded that the expression of the *VSG117* from a non-canonical promoter-proximal location in the active Expression site did not interfere with the process of VSG ES switching.

A

Weeks
V221
V221/117
V117Δ221.1
V117Δ221.2
0
1
2
3
4
DIC
VSG221 + DAPI

B

Weeks
V221
V221/117
V117Δ221.1
V117Δ221.2
0
1
2
3
4
DIC
VSG117 + DAPI

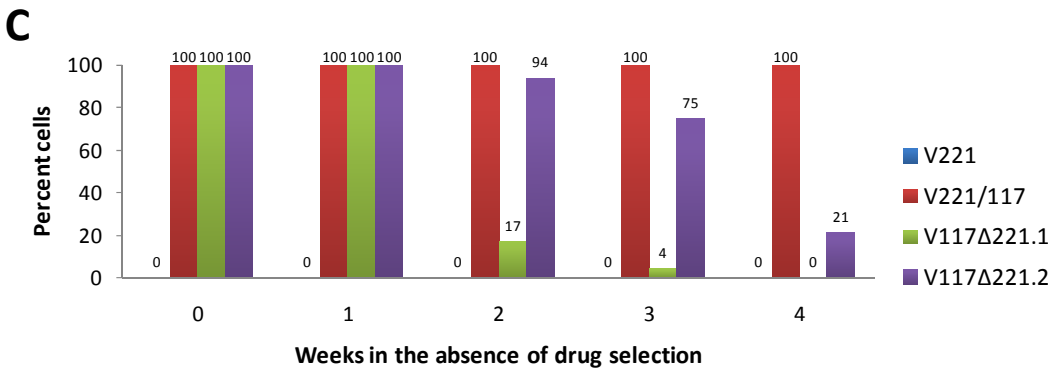


Figure 5.10: **Surface VSG immunofluorescence shows that deletion of the telomeric *VSG221* does not damage the ability of V117Δ221 *T. brucei* to switch to a new VSG.**

VSG221 (orange) **(A)** and VSG117 (green) **(B)** surface immunofluorescence of V221, V221/117 and V117Δ221.1 and V117Δ221.2 *T. brucei* cell lines grown in the absence of drug selection pressure for 4 weeks. Immunofluorescence was performed on each cell line once per week throughout the course of the experiment. The cells were stained with DAPI (blue) for DNA content. The scale bar represents 10μm. **(C)** Quantification of VSG117 immunofluorescence results in V221, V221/117 and V117/Δ221.1 and V117/Δ221.2 *T. brucei* after the cells were grown for four weeks in the absence of drug selection pressure. For each cell population counted n>300.

In addition, the protectiveness of the VSG117 coat on V117Δ221 cells was assessed *in vivo* by inoculating these cells into immunocompetent mice. This work was performed in the laboratory of Prof Philippe Büscher at the Department of Parasitology, Institute of Tropical Medicine, Antwerp, Belgium. The V221, V221/117 and V117Δ221 cells were injected into OF-1 outbred mice, and infection was monitored through cell counting and surface VSG immunofluorescence. It was observed that all cell lines were successful at establishing parasitemia in mice. The rates at which the different cell lines established parasitemia were reflected by their different growth rates (Figure 5.6B). The V221 *T. brucei*, which had the shortest

generation time, was the first to become apparent in the bloodstream of infected mice, followed by the V221/117 *T. brucei*. The V117Δ221 *T. brucei*, as the slowest growing cell line, was also the slowest to multiply in mice and subsequently, the mice infected with this cell line survived the longest. It was also observed that if the mice survived the first peak of parasitemia, then irrespective of which cell line they were infected with, the cells in the second peak switched to a new *VSG*. Thus all three cell lines were capable of dividing in mice, as well as switching to a new *VSG*.

The ability to generate a cell line completely reliant on the expression of *VSG117* from immediately downstream of the promoter of the active ES after deletion of the telomeric *VSG221* gene allowed us to investigate the reproducibility of the *VSG* RNAi-triggered phenotype. To investigate this further, a construct containing a *VSG117* RNAi fragment was targeted into the 177 bp repeats of a VSG221-VSG117 double-expresser *T. brucei* (Figure A2.1, Figure A2.2 and Figure A2.3). The telomeric *VSG221* gene was subsequently replaced with a blasticidin drug resistance gene to generate a cell line (BΔ221/117RNAi *T. brucei*) fully reliant on the expression of a promoter-adjacent *VSG117* (Figure A2.4). Induction of *VSG117* RNAi was caused a growth arrest in the BΔ221/117RNAi cell line, similar to that observed after induction of *VSG221* RNAi in 221VB1.1 and 221VG1.1 *T. brucei* (Figure A2.5, Figure 3.1C and Figure 3.3B). Therefore, it was concluded that the *VSG* RNAi-triggered growth arrest was reproducible using other *VSG* variants, and was not restricted to *VSG221*.

5.3. Conclusions

In this chapter the importance of the position of the *VSG* gene in the Expression site for functional levels of VSG expression, as well as the ability of the trypanosome to form a fully protective VSG coat was investigated. The high levels of expression of a second VSG, *VSG117*, from immediately downstream of the promoter of the active *VSG221* Expression site enabled the deletion of the telomeric *VSG221* gene, leaving the cells completely reliant on *VSG117* for growth (Figure 5.3 and Figure 5.5).

Although it had previously been determined that expression of high levels of a second *VSG*, *VSG117*, from the active *VSG221* Expression site can alleviate the *VSG221* RNAi-triggered growth arrest, the full functionality of the VSG117 coat had not been rigorously assessed (Figure 4.6A). The Bloodstream Expression Sites (BESs) have a highly conserved organisation, with the *VSG* gene located at the 3' end of the polycistronic transcription unit, just upstream of the telomere repeats (Hertz-Fowler et al. 2008). It is thought that the telomeric position of the *VSG* gene is important for recombinogenicity and the presence of the flanking 70 bp repeat region upstream plays an important role in VSG switching through gene conversions (Yang et al. 2009; Bernards et al. 1983; Van der Ploeg, A. Y. C. Liu, et al. 1984; Horn & Barry 2005).

The integration of *VSG117* immediately downstream of the promoter of the active *VSG221* Expression site of the "single marker" 427 *T. brucei* and the subsequent deletion of the telomeric *VSG221* was confirmed by Southern blot analysis (Figure 5.3 and Figure 5.5). The V221/117 *T. brucei* cell line was shown to

stably express two VSGs, VSG221 and VSG117, from the same active Expression site, as previously shown using the 221VP117 *T. brucei* cell line (Figure 4.4, Figure 4.5, Figure 4.6C, and Figure 5.4B). The levels of VSG221 protein, expressed by the V221/117 *T. brucei* cell line were found to be lower, compared with the parental "single marker" 427 *T. brucei* cell line, which expressed only VSG221 (Figure 5.4B). In contrast, the V117Δ221 cells expressed VSG117 protein at higher levels compared with the parental V221/117 *T. brucei* cell line, which suggested that the V117Δ221 cells were completely reliant on VSG117 for growth (Figure 5.6A).

V117Δ221 *T. brucei* had a longer generation time (9.63 h) compared with the V221 (6.18 h) or V221/117 (6.24 h) cells (Figure 5.6B). This could have been a consequence of slightly suboptimal expression of *VSG117*. This may have been due to the 5' RNA trans-splice site on the *VSG117* gene, for which the tubulin 5'UTR had been used (Figure 4.2). As previously discussed, high levels of *VSG* mRNA expression are enabled not only by the highly efficient transcription of the active Expression site, but also by the specialised 5' and 3' RNA processing sequences, which are thought to be responsible for the 700 fold difference between the levels of *VSG* and *ESAG1* mRNAs – transcripts that originate from the same polycistronic transcription unit (Cully et al. 1985; Berberof et al. 1995). Thus, it is possible that the presence of the *VSG221* 3'UTR on the exogenous *VSG117* gene ensured sufficiently high levels of *VSG117* transcript that allowed the successful deletion of *VSG221* from the active *VSG221* Expression site. However, possibly the tubulin 5'UTR was not optimal and contributed to the longer generation time of the V117Δ221 *T. brucei* cell line due to reduced stability of the *VSG117* mRNA, which increased the time

necessary to synthesize enough VSG117 protein to allow cell division to occur (Figure 5.6B).

VSG117 protein was detected on the cell surface of both V221/117 and V117Δ221 *T. brucei* cell lines (Figure 5.7). As previously observed for the 221VP117 *T. brucei* cell line, VSG117 was expressed on the surface of V221/117 cells together with VSG221 (Figure 4.5 and Figure 5.7). Although the growth rate of the V117Δ221 *T. brucei* cells was reduced compared with the parental V221/117 cell line, expression of VSG117 from the non-canonical promoter-adjacent location in the active ES did not result in any abnormal cell morphology in the V117Δ221 *T. brucei* cell population (Figure 5.7C). Thus, it was concluded that the expression of VSG117 from this different location in the active Expression site was not detrimental to parasite proliferation.

The functionality of the VSG117 coat was more stringently tested by incubating the parasites in the presence of guinea pig complement (Figure 5.8). All of the tested bloodstream form cell lines, V221, V221/117 and V117Δ221 *T. brucei* were resistant to complement-mediated lysis (Figure 5.8B, C and D). This indicated that the VSG117 coat of V117Δ221 *T. brucei* cells conferred protection to the lytic effect of complement. The heterogeneous VSG surface coat of V221/117 *T. brucei* cells also rendered the cells resistant to the alternative pathway of complement system, and is consistent with the previously reported ability of VSG double-expresser *T. brucei* to proliferate in immunocompetent mice (Figure 5.8C) (Muñoz-Jordán et al. 1996). This observation confirmed that the expression of a mixed VSG coat, which may mimic a wild-type switching event from one VSG variant to

another, does not render the parasites susceptible to lysis by the alternative pathway of the complement system (Dubois et al. 2005).

To test the ability of V117Δ221 *T. brucei* to switch to a new VSG, the cells were grown for four weeks in the absence of drug selection pressure (Figure 5.9 and Figure 5.10). It was observed that the V117Δ221 clones started switching to a new VSG within two weeks of removal of drug selection pressure (Figure 5.9 and Figure 5.10). This revealed that even though the conserved architecture of the active ES had been modified, this did not interfere with the ability of the parasites to switch to a new VSG. Although the precise switching mechanisms were not thoroughly investigated, western blot analysis revealed that at least some of the VSG switch events were *in situ* switches, as the activated *VSGs* were present in previously silent ESs (Figure 5.9). This indicated that the proximity of the *VSG117* gene to the ES promoter did not interfere with the ability of the cells to switch to a new VSG ES.

Although the V221 and V221/117 *T. brucei* cell lines did not appear to switch during this experiment, this could have been due to the experimental set up where the cells were passaged in bulk during the period of four weeks in the absence of drug selection pressure. Both V221 and V221/117 cells had a shorter generation time (6.18 h and 6.24 h, respectively), compared to V117Δ221 (9.63 h) (Figure 5.6B). Since all cell lines were grown in drug-free HMI-9 and passaged into fresh medium whenever necessary, the most rapidly dividing cells in each culture were selected for during each passaging event. Thus, the V117Δ221 cells, which had a reduced growth rate, may have switched to VSGs with more optimal processing signals. This could have allowed them to divide at an increased rate and these more rapidly dividing cells eventually took over the culture. In contrast, the growth rates of both V221 and

V221/117 *T. brucei* cell lines were significantly higher, and occurring switching events may not have conferred significant advantage over the original VSG221-expressing cells.

All three cell lines, V221, V221/117 and V117Δ221 *T. brucei* were shown to be able to switch to a new VSG when grown in mice. The VSG117 coat was fully functional *in vivo*, as well as *in vitro*, and both V221/117 and V117Δ221 *T. brucei* were capable of establishing an infection. Therefore, it was concluded that the promoter-proximal position of the *VSG* gene in the ES did not affect expression levels in a way, which impeded the full functionality and protectiveness of the VSG coat.

Chapter 6

The cell cycle arrest mediated by blocking VSG synthesis is not a direct consequence of decreased *VSG* transcript levels

6.1. Introduction

It was unclear which signaling mechanisms were operating to generate the *VSG* RNAi-induced growth arrest and precise pre-cytokinesis cell cycle block. Work presented in this chapter focuses on the elucidation of the molecular mechanisms used by *T. brucei* to monitor VSG transcript and protein levels.

6.2. Results

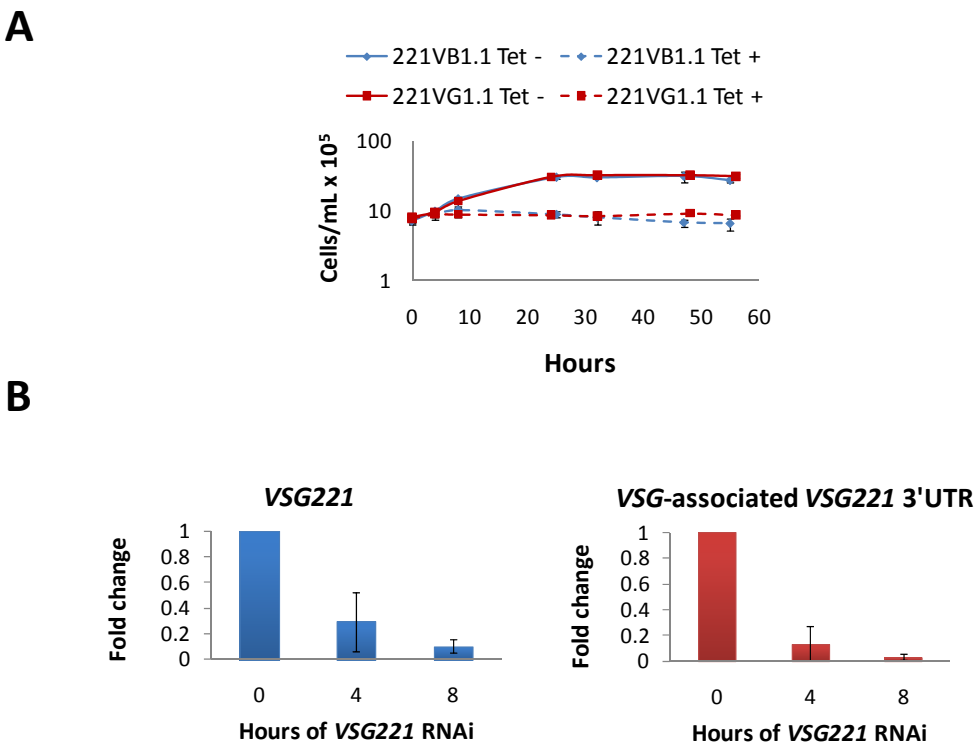
6.2.1. The *VSG221* 3'UTR does not appear to be an integral element of the VSG "sensing" machinery

VSGs are highly diverse in their sequence, therefore, it is unlikely that the cell measures its VSG protein pool using a conserved motif within the VSG protein itself. Although the *VSG* mRNA also shows little sequence conservation, the *VSG* 3'UTR contains two highly conserved sequence motifs, known as the 8mer and the 14mer (Figure 4.2) (Berberof et al. 1995; Cully et al. 1985). These two motifs are believed to be important for the life cycle specific expression and stability of the *VSG* mRNA (Cully et al. 1985; Berberof et al. 1995). The Engstler laboratory has hypothesized that the "counting" of the *VSG* transcript occurs at the level of the "sensing" the *VSG* mRNA through the conserved 3'UTR motifs. In this case, the *VSG* RNAi-triggered growth arrest could possibly be alleviated by providing the parasites with high levels of *VSG* 3'UTR.

To investigate this possibility, *VSG221* RNAi was induced in two different cell lines – 221VB1.1 and 221VG1.1 *T. brucei*. An important difference between the 221VB1.1 and the 221VG1.1 *T. brucei* cell lines is that the 221VG1.1 cells express

high levels of *eGFP* bearing a *VSG221* 3'UTR from the active *VSG221* Expression site (Chapter 3.2.1, Figure 3.1A and Chapter 3.2.2.1, Figure 3.3A). If the *VSG* 3'UTR was important for "sensing", the presence of high levels of expression of a second *VSG* 3'UTR could provide a compensatory effect.

The growth of 221VB1.1 and VG1.1 *T. brucei* after induction of *VSG221* RNAi was monitored, and total RNA was isolated from the parasites (Figure 6.1A). The levels of *VSG221* transcript, as well as the levels of *VSG221* 3'UTR sequence associated with the *VSG221* mRNA were assessed by quantitative PCR in both 221VB1.1 and 221VG1.1 *T. brucei* cell lines after the induction of *VSG*221 RNAi (Figure 6.1B and C). The levels of *eGFP* mRNA and of the *eGFP*-associated *VSG221* 3'UTR were also determined in the 221VG1.1 *T. brucei* (Figure 6.1C).



C

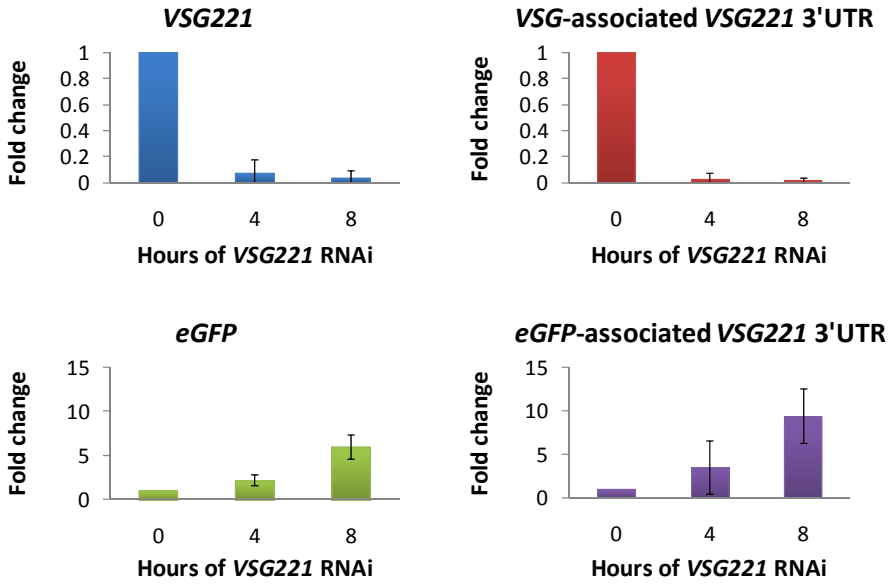


Figure 6.1: High levels of expression of *VSG221* 3'UTR in 221VG1.1 *T. brucei* do not alleviate the *VSG221* RNAi-induced growth arrest.

A. Growth analysis of 221VB1.1 and 221VG1.1 *T. brucei* after induction of *VSG221* RNAi for the time specified in hours. The induced cells (Tet +) were compared to cells where no *VSG221* RNAi has been induced (Tet -). The average cell density from triplicate counts is represented in cells per mL x 10^5 and the standard deviation is shown as error bars.

B. Quantification of levels of *VSG221* (blue) and *VSG221*-associated *VSG221* 3'UTR (red) by quantitative PCR after the induction of *VSG221* RNAi for the time specified in hours in 221VB1.1 *T. brucei*.

C. Quantification of levels of *VSG221* (blue), *VSG221*-associated *VSG221* 3'UTR (red), *eGFP* (green) and eGFP-associated *VSG221* 3'UTR (purple) by quantitative PCR after induction of *VSG221* RNAi for the time specified in hours in 221VG1.1 *T. brucei*.

For all graphs in **(B)** and **(C)** the average values obtained from three independent biological replicates are shown with standard deviation represented as error bars.

The induction of *VSG221* RNAi for 8 hours in 221VB1.1 and 221VG1.1 *T. brucei* caused a rapid decrease in the levels of *VSG221* transcript of 10-fold and 25-fold, respectively (panel 1 in Figure 6.1A and B). The levels of *eGFP* transcript increased 6-fold after induction of *VSG221* RNAi for 8 hours in 221VG1.1 *T. brucei*, which was consistent with previously observed results (panel 3 in Figure 6.1C and Chapter 3.2.2.1, Figure 3.3C and D).

As expected, the levels of *VSG221* 3'UTR on the *VSG221* mRNA decreased after 8 hours of induction of *VSG221* RNAi in both 221VB1.1 and 221VG1.1 *T. brucei* to 3% and 1.7% original levels, respectively (panel 2 in Figure 6.1B and C). In 221VG1.1 *T. brucei* cells, however, in addition to being present on the *VSG221* mRNA, the *VSG221* 3'UTR was also present on the *eGFP* transcript. Therefore, in the 221VG1.1 cell line, the *eGFP VSG221* 3'UTR levels increased up to 9-fold after 8 hours of induction of *VSG221* RNAi (panel 4 in Figure 6.1C). Therefore, although high levels of *VSG221* 3'UTR were present in 221VG1.1 *T. brucei* cell line after the induction of *VSG221* RNAi, the growth of the parasites was inhibited (Figure 6.1A). This suggested that the cells did not trigger a cell cycle arrest through sensing levels of *VSG* 3'UTR. However, it was still unclear whether other sequences on the *VSG* transcript could alternatively be sensed by the parasites and lead to a growth inhibition.

6.2.2. The cell cycle arrest induced by *VSG221* RNAi is due to absence of VSG221 protein, rather than *VSG* transcript

To determine whether the absence of *VSG* mRNA was being sensed by the parasites, we attempted to block VSG protein synthesis without ablating the *VSG*

transcript. Cells were treated with anti-*VSG* morpholino oligonucleotides. Morpholino oligonucleotides have been used to knock down gene expression, modify splicing or inhibit miRNA maturation and activity (Eisen & J. C. Smith 2008; Moulton & Yan 2008; Du & Gatti 2010; Moulton & Jiang 2009). Morpholino oligos are short chains of about 25 morpholino subunits, where each subunit contains a morpholine ring in place of a ribose or deoxyribose sugar ring, characteristic of RNA or DNA oligos, respectively (Moulton & Yan 2008). Morpholinos bind to their RNA target through Watson-Crick base pairing, but do not cause their degradation through the RNAi pathway, unlike the binding of ordinary RNA oligos (Summerton 1999; Samanta et al. 2009). Instead the morpholino oligos act via a steric blocking mechanism and prevent the initiation of translation (Samanta et al. 2009). Morpholinos are typically designed to bind specifically over the *AUG* start codon of the target mRNA and are highly stable in cells (Summerton 1999; Eisen & J. C. Smith 2008). Thus, treatment of *T. brucei* with anti-*VSG* morpholino oligonucleotides was expected to cause a block in VSG synthesis, but no degradation of the *VSG* mRNA.

6.2.2.1. Blocking VSG synthesis by treating the cells with anti-VSG morpholino oligonucleotides causes a growth arrest

An anti-*VSG221* morpholino 25 bp oligonucleotide was designed to specifically target the AUG start codon of the *VSG221* mRNA (Table 6.1). In addition, as a control, a 25 bp oligonucleotide directed against *VSG221*, but with 5 mismatched residues was also designed (Table 6.1). An anti-α-tubulin morpholino oligonucleotide was designed as a positive control for treatment of the cells with

morpholino oligos (Table 6.1) (Shi et al. 2009). Blocking α-tubulin synthesis is lethal for trypanosomes and causes the so-called "FAT" phenotype, where the parasites become almost spherical and with an increased DNA content (Shi et al. 2000). A mismatched anti-α-tubulin morpholino oligo was also designed, incorporating 5 mismatches, which would prevent it from binding to the α-tubulin mRNA (Table 6.1).

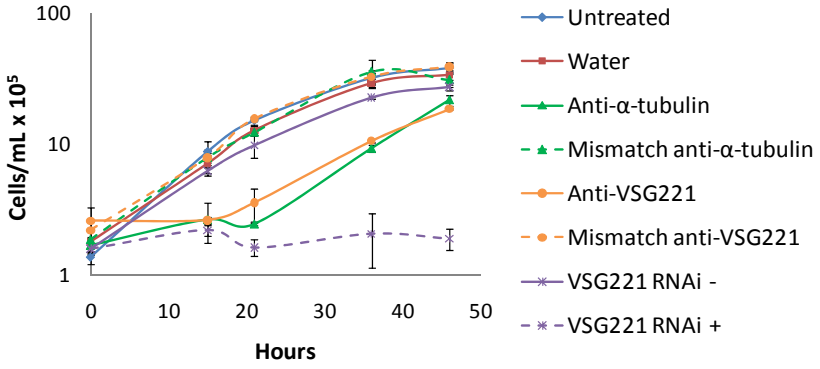
Table 6.1: Sequences of the designed anti-*VSG221* and anti-α-tubulin 25 bp morpholino oligonucleotides. The precise position of the binding sites on the target mRNAs for the anti-*VSG221* and anti-α-tubulin morpholinos are indicated with the AUG complementary sequence shown in red and underlined. The mismatching nucleotides in the mismatch anti-*VSG221* and the mismatch anti-α-tubulin morpholino oligos are indicated in green and underlined.

Morpholino ID	Sequence	Target position on mRNA
Anti-*VSG221*	5' – GCCGGGCCTCCTGATTGGAAGGCAT – 3'	1-25
Mismatch anti-*VSG221*	5' – GCCCGGCATCCTCATTGCAAGGGAT – 3'	-
Anti-α-tubulin	5' – TGTGGATGCAGATAGCCTCACGCAT – 3'	1-25
Mismatch anti-α-tubulin	5' – TGTGCATGCACATACCCTGACGGAT – 3'	-

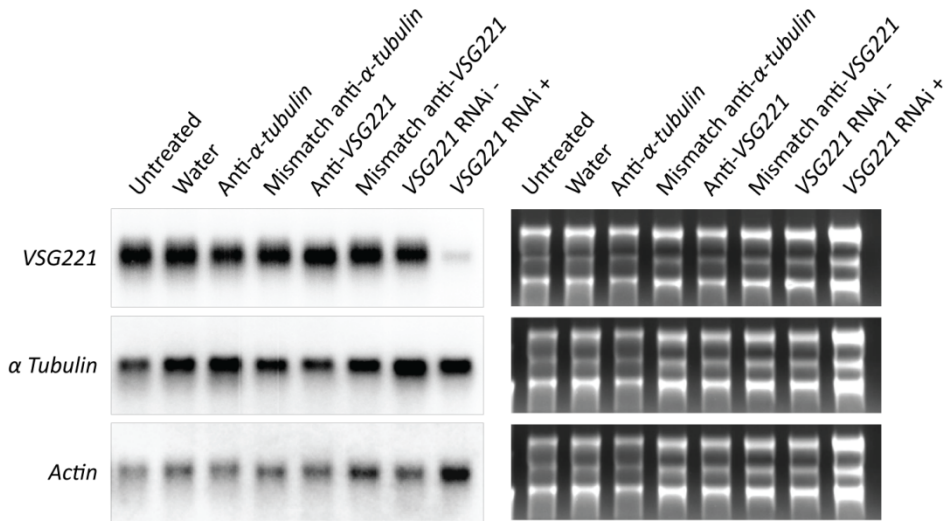
A VSG221-expressing *T. brucei* HNI (221+) was transfected with anti-*VSG221* morpholino oligos (Rudenko et al. 1998). *VSG* transcript is one of the most abundant transcripts in *T. brucei*, therefore anti-*VSG221* morpholino oligos were used at high concentrations of 12.8 μM (Figure 6.2). As a control for possible toxic effects of the high levels of anti-*VSG221* morpholino oligos, HNI (221+) *T. brucei* was also transfected with mismatching anti-*VSG221* morpholino oligos at the same concentration. As a positive control HNI (221+) *T. brucei* was treated with 3.2 μM

anti-α-tubulin morpholinos. In addition, the parasites were treated with 3.2 μM mismatched anti-α-tubulin morpholinos as a control for potential toxicity effects of treating the cells with morpholino oligos. Untransfected cells, as well as cells transfected with sterile water were also used as negative controls (Figure 6.2). Additionally, for comparison *VSG221* RNAi was induced in 221VB1.1 *T. brucei* and compared with the treatment with anti-*VSG221* morpholino oligos.

A



B



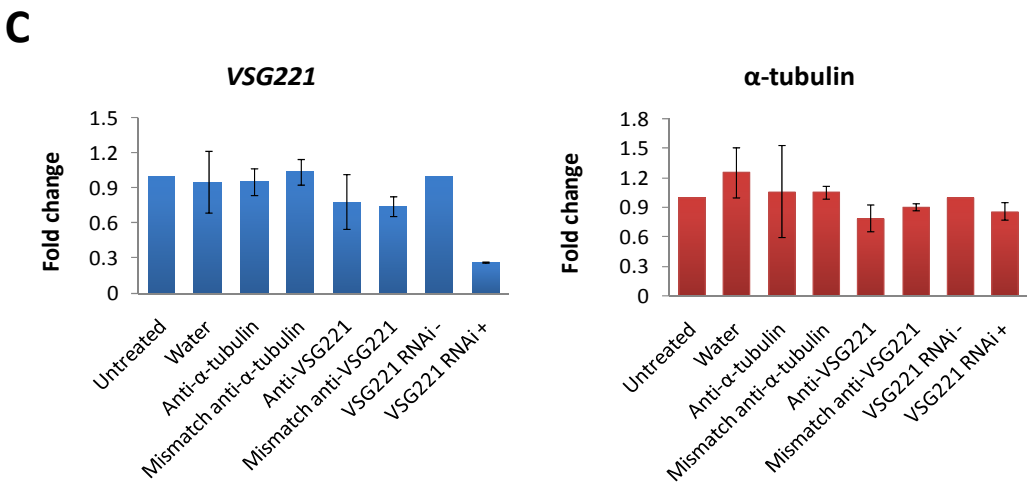


Figure 6.2: A growth arrest is triggered in HNI (221+) *T. brucei* treated with anti-*VSG221* morpholino oligos in the absence of *VSG221* mRNA degradation.

A. The growth of HNI (221+) *T. brucei* treated with anti-*VSG221* morpholino oligos was monitored and compared with cells treated with mismatched anti-*VSG221* morpholinos, untreated cells (Untreated) and cells transfected with sterile water (Water). In addition, cells were treated with anti-α-tubulin morpholinos and mismatched anti-α-tubulin morpholinos. Cells where *VSG221* RNAi was not induced (*VSG221* RNAi -) or induced (*VSG221* RNAi +), were used as a comparison. The cell numbers were determined at the times specified in hours post transfection or induction of *VSG221* RNAi. The average cell density from triplicate counts is represented in cells per mL x 10^5 and the standard deviation is shown as error bars.

B. Northern blot analysis of total RNA isolated 16 hours after treatment of HNI (221+) *T. brucei* with anti-*VSG221* morpholino oligos or mismatched anti-*VSG221* morpholinos. Untreated cells (Untreated) and cells transfected with sterile water (Water) were used as negative controls. Total RNA from cells treated with anti-α-tubulin morpholinos or mismatched anti-α-tubulin morpholinos, as well as uninduced 221VB1.1 *T. brucei* (*VSG221* RNAi -) or induced for *VSG221* RNAi (*VSG221* RNAi +), were used as additional controls. Blots were probed for *VSG221*, α-tubulin and actin transcripts. Ethidium staining of the gels is shown as a loading reference.

C. Levels of *VSG221* and α-tubulin transcripts were determined by quantitative PCR after treatment of the cells as described in **(B)**. The average values obtained from two independent biological

replicates are shown, with standard deviation from 6 independent PCR reactions represented as error bars.

Growth analysis of the cells treated with anti-*VSG221* morpholino oligos showed that cells stalled for 24 hours after transfection, whereas cells treated with mismatched anti-*VSG221* morpholino oligos continued to divide normally (Figure 6.2A). Similar results were obtained for cells treated with anti-α-tubulin morpholino oligos, where the growth of the treated cells was inhibited for up to 24 hours after transfection (Figure 6.2A). There was no observed toxic effect for the cells treated with morpholinos in general, as the mismatched anti-*VSG221* or anti-α-tubulin morpholinos did not cause a growth arrest (Figure 6.2A).

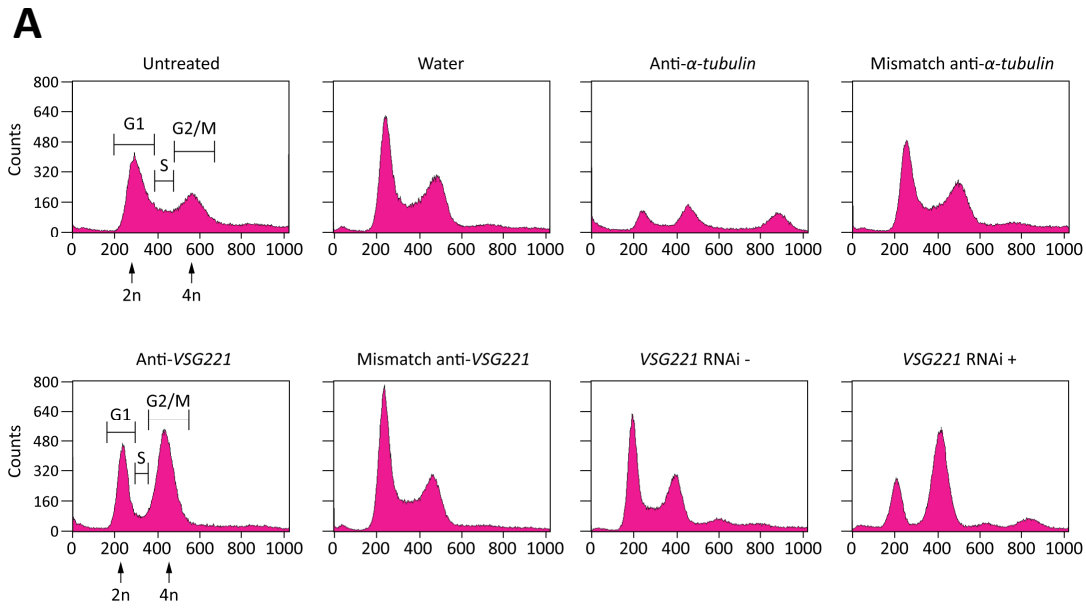
Northern blot and quantitative PCR analysis showed that levels of *VSG221* transcript remained unchanged in cells treated with anti-*VSG221* morpholino oligos, but were radically reduced in cells where *VSG221* RNAi had been induced (Figure 6.2B and C). The level of *VSG221* mRNA in cells treated with anti-*VSG221* morpholinos was similar to that detected in the control cell populations (i.e., No transfection, H_2O and mismatched anti-*VSG221* morpholinos) (Figure 6.2B and C). The level of α-tubulin transcript also did not decrease in cells treated with anti-α-tubulin morpholino oligos (Figure 6.2B and C). The levels of actin mRNA also remained constant, as had previously been observed after the induction of *VSG221* RNAi (Figure 3.3C and D and Figure 6.2B).

Therefore, treatment of HNI (221+) *T. brucei* with anti-*VSG221* morpholino oligos caused a growth inhibition similar to that observed after induction of *VSG221* RNAi, without degradation of the *VSG221* mRNA (Figure 6.2).

6.2.2.2. Treatment of cells with anti-*VSG* morpholino oligonucleotides caused an increase in cells with double DNA content

The DNA content of HNI (221+) *T. brucei* treated with anti-*VSG221* morpholino oligos was determined by propidium iodide flow cytometry and compared with cells where *VSG221* RNAi had been induced (Figure 6.3) (Deitch et al. 1982). The same control cell populations were used as previously described (Chapter 6.3.1).

The flow cytometry profile after propidium iodide staining of the trypanosomal DNA shows two peaks, where the first peak corresponds to cells with 2n DNA content and the second peak represents cells with 4n DNA content (Figure 6.3A, No transfection HNI (221+) *T. brucei*). Additionally, the propidium iodide profile also shows cells with DNA content greater than 4n, which corresponds to polyploid cells. These cells that appear as a third peak on the flow cytometry profile will have undergone several rounds of DNA synthesis without accomplishing cytokinesis, resulting in their increased DNA content (Figure 6.3A, profile of cells treated with anti-α-tubulin morpholino oligos).



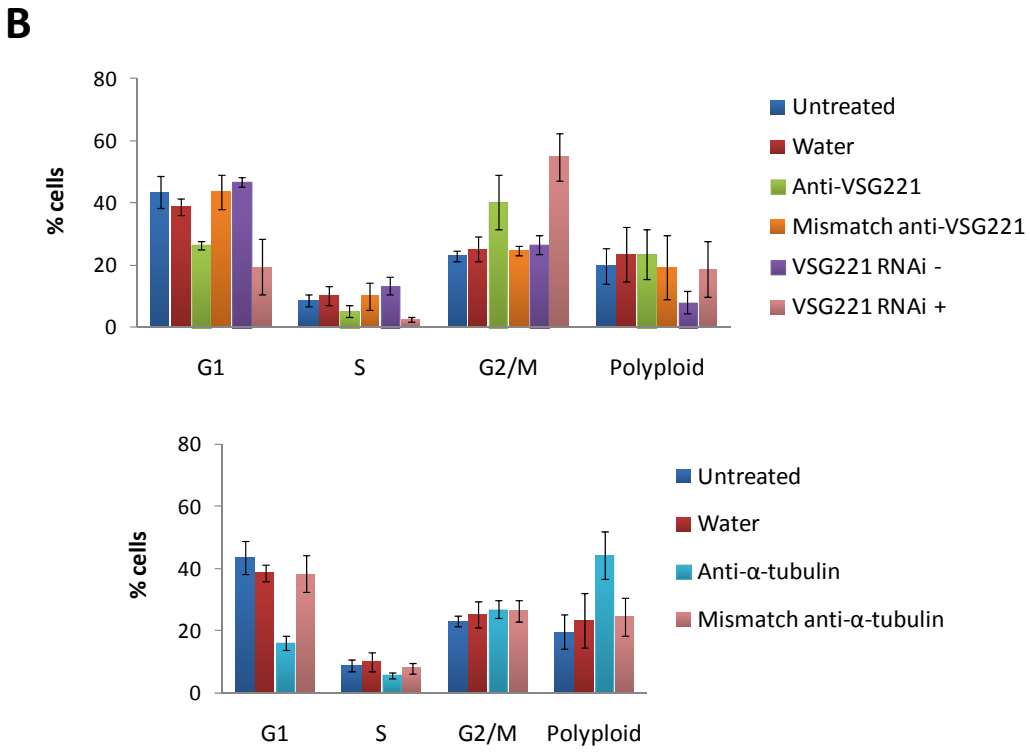


Figure 6.3: Treatment of HNI (221+) *T. brucei* with anti-*VSG221* morpholino oligos causes an accumulation of cells with double DNA content, similar to 221VB1.1 *T. brucei* after induction of *VSG221* RNAi.

A. DNA content monitored using propidium iodide flow cytometry. HNI (221+) *T. brucei*, treated with anti-*VSG221* morpholino oligos, was compared to cells transfected with mismatched anti-*VSG221* morpholinos, untreated cells (Untreated), cells transfected with sterile water (Water), or 221VB1.1 *T. brucei* in the absence (*VSG221* RNAi -) or presence (*VSG221* RNAi +) of *VSG221* RNAi. Cells treated with anti-α-tubulin morpholinos and mismatched anti-α-tubulin morpholinos were used as an additional control. Analysis was performed 16 hours post treatment. The scale shown on the leftmost graph is identical for all panels. The gates used to determine percentages of different cell populations are shown, with cells in G1, S and G2/M-stages of the cell cycle indicated.

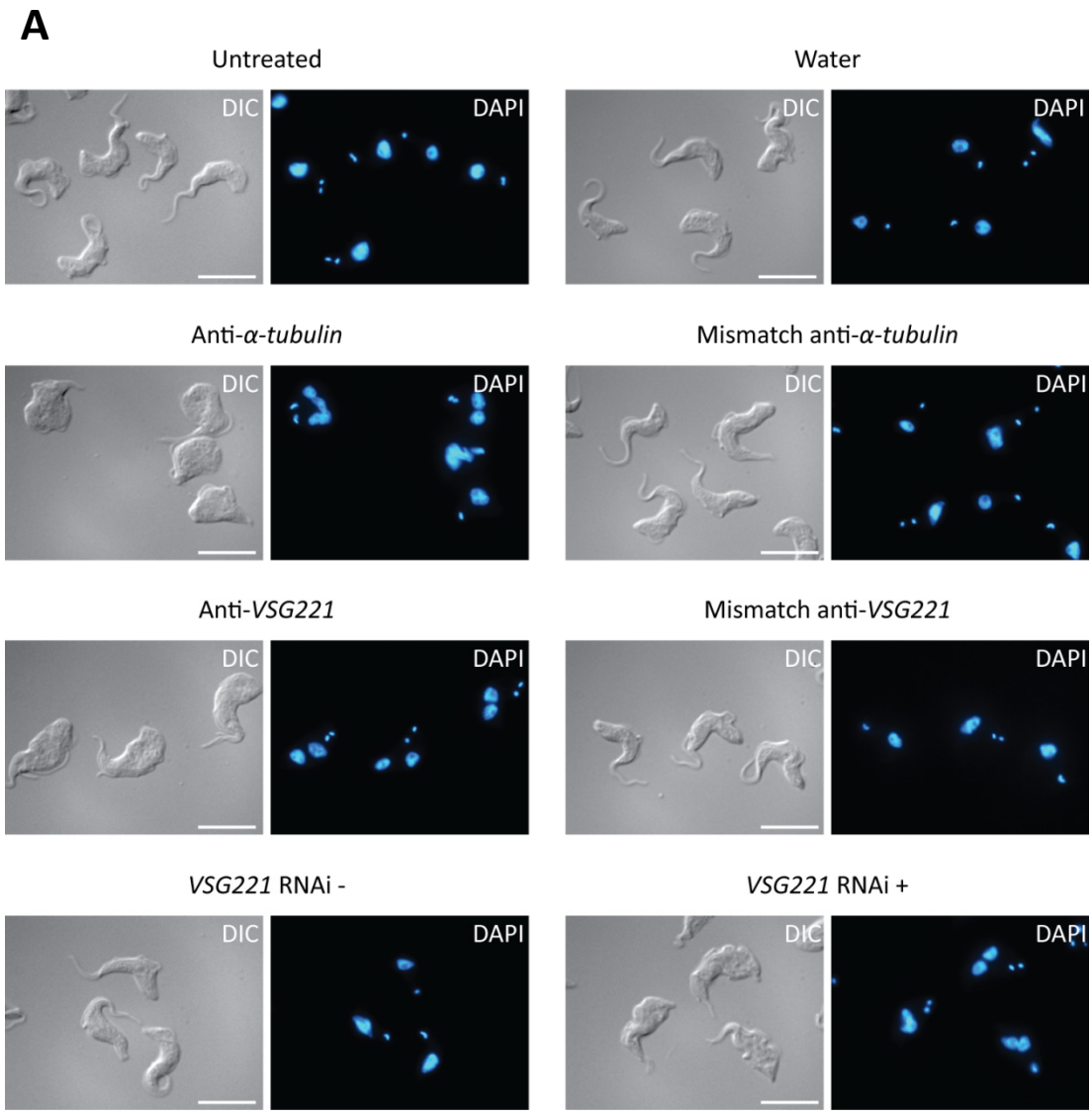
B. Quantification of propidium iodide flow cytometry analysis. The gates used are shown in **(A)**. The top panel shows the different cell populations after treatment of HNI (221+) *T. brucei* with anti-*VSG221* morpholino oligos, compared with 221VB1.1 *T. brucei* in the absence (*VSG221* RNAi -) or

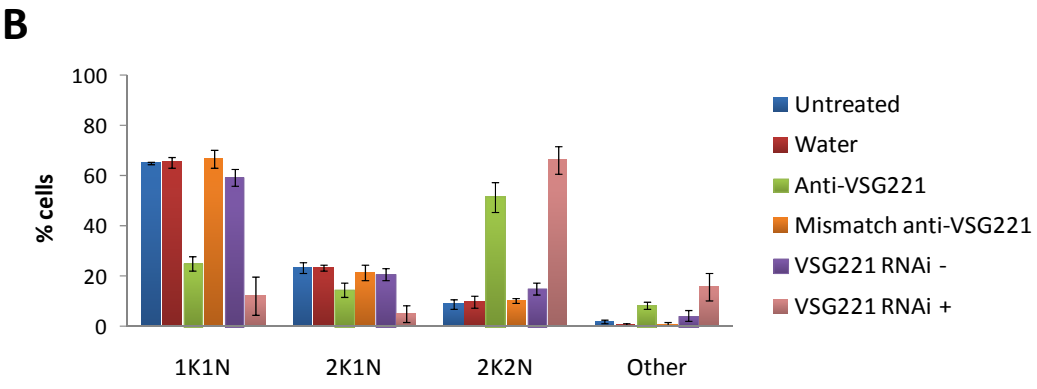
presence (*VSG221* RNAi +) of *VSG221* RNAi. In addition, parasites were treated with mismatched anti-*VSG221* morpholinos, untransfected (Untreated) or transfected with sterile water (Water). Cells transfected with anti-α-tubulin morpholinos and mismatched anti-α-tubulin morpholinos, untransfected (Untreated) or cells transfected with sterile water (Water) are shown in the lower panel. The values shown are the mean of three different experiments with the standard deviation indicated with error bars.

The flow cytometry profile of cells treated with anti-*VSG221* morpholinos was highly similar to the one generated after induction of *VSG221* RNAi (Figure 6.3A and B). The propidium iodide staining of the cells treated with anti-*VSG221* morpholinos showed a decrease in the G1 peak and an increase in the G2/M peak, with 40% of the total cell population in G2/M-stage (compared with normal levels of approximately 20%). This is similar to what is observed in cells where *VSG221* RNAi has been induced (55% of the entire cell population in G2/M-stage) (Figure 6.3A and B). In cells treated with anti-α-tubulin morpholino oligos, a prominent third peak, as well as an increase in the second peak was observed. This indicated that a large proportion of these cells had either doubled or further increased their DNA content (27% of cells in G/M-phase and 45% of cells polyploid) (Figure 6.3A and B). Cells treated with either mismatched anti-*VSG221* morpholinos or mismatched anti-α-tubulin morpholinos appeared to have wild-type propidium iodide flow cytometry profiles (Figure 6.3A and B). Therefore, the growth arrest observed after induction of *VSG221* RNAi and treatment with anti-*VSG221* morpholino oligos both coincided with a similar cell cycle arrest at the G2/M stage (Figure 6.2A and Figure 6.3).

6.2.2.3. Cells transfected with anti-*VSG* morpholino oligonucleotides were arrested precytokinesis and were morphologically similar to cells where *VSG* RNAi has been induced

It had previously been observed that the cell cycle arrest triggered by the induction of *VSG* RNAi is highly distinct morphologically, with the two kinetoplasts and nuclei appearing unusually close together (Figure 3.2A). Microscopic analysis of HNI (221+) *T. brucei* treated with anti-*VSG221* morpholino oligos revealed that the cells were highly similar morphologically to the 221VB1.1 *T. brucei* where *VSG221* RNAi has been induced (Figure 6.4A). In both cell populations, an increase in 2K2N cells was observed, together with a close association of the two kinetoplasts and nuclei, which is highly characteristic for the *VSG* RNAi-triggered phenotype (Figure 6.4A and B) (Sheader et al. 2005). In the HNI (221+) *T. brucei* cell line, transfected with anti-*VSG221* morpholinos, the increase in 2K2N cells was up to 51% of the total cell population. In the 221VB1.1 cells where *VSG221* RNAi had been induced, the 2K2N cells represented 66% of the entire cell population (Figure 6.4B). Cells treated with anti-α-tubulin morpholino oligos showed a dramatic increase in multinucleated cells to 67% of the total cell population (Figure 6.4B). These stalled cells were spherical and had an increased number of kinetoplasts and nuclei, which was consistent with reported results (Figure 6.4A) (Shi et al. 2000). In contrast, the parasites treated with mismatched anti-*VSG221* or mismatched anti-α-tubulin morpholinos did not produce phenotypes different to wild-type cells, where the 2K2N and multinucleated cells made up approximately 10% or 2% of the cell population (Figure 6.4A and B).


A
Untreated
DIC
DAPI
Water
DIC
DAPI
Anti-α-tubulin
DIC
DAPI
Mismatch anti-α-tubulin
DIC
DAPI
Anti-VSG221
DIC
DAPI
Mismatch anti-VSG221
DIC
DAPI
VSG221 RNAi -
DIC
DAPI
VSG221 RNAi +
DIC
DAPI


B
100
80
60
40
20
0
% cells
1K1N
2K1N
2K2N
Other
Untreated
Water
Anti-VSG221
Mismatch anti-VSG221
VSG221 RNAi -
VSG221 RNAi +

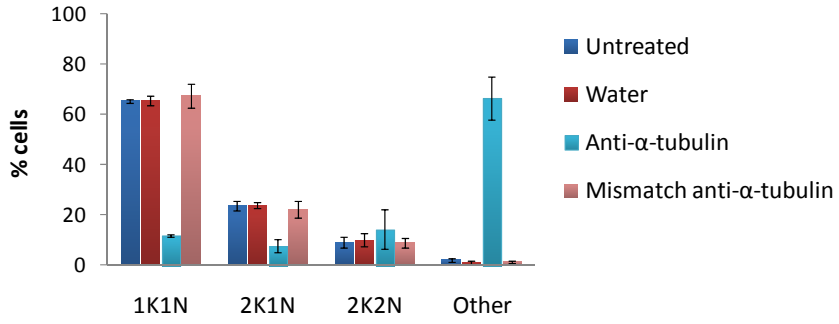


Figure 6.4: HNI (221+) *T. brucei* treated with anti-*VSG221* morpholino oligos show an increase in 2N2K cells, and are morphologically similar to 221VB1.1 *T. brucei* after induction of *VSG221* RNAi.

A. Microscopic analysis showing HNI (221+) *T. brucei* transfected with anti-*VSG221* morpholino oligos compared to 221VB1.1 *T. brucei* in the absence (*VSG221* RNAi -) or presence (*VSG221* RNAi +) of *VSG221* RNAi. Cells treated with mismatched anti-*VSG221* morpholinos, untreated cells (Untreated) or cells transfected with sterile water (Water) were used as controls. Cells were also treated with anti-α-tubulin morpholinos or mismatched anti-α-tubulin morpholinos. Analysis was performed 16 hours post treatment. The parasites were stained with DAPI (blue) for DNA content. The scale bar represents 10 μm.

B. The top panel shows quantification of the different cell populations after treatment of HNI (221+) *T. brucei* with anti-*VSG221* morpholino oligos or induction of *VSG221* RNAi in 221VB1.1 *T. brucei* (*VSG221* RNAi +), with controls as detailed in **(A)**. The lower panel shows quantification of cells transfected with anti-α-tubulin morpholinos or mismatched anti-α-tubulin morpholinos aor the control cell populations as in **(A)**. The average values from three independent experiments are shown with standard deviation represented as error bars. For each cell population counted n>300.

Phenotypic analysis of *T. brucei* after blocking VSG synthesis by treatment with anti-*VSG* morpholino oligos suggested that the parasites did not trigger cell cycle arrest through sensing levels of *VSG* transcript. Levels of VSG protein itself or some aspect of VSG protein synthesis or post-translational modification may have

been monitored. These modifications include protein folding in the endoplasmic reticulum, attachment to the GPI anchor, attachment of polysaccharides, transportation to and deposition on the cell surface, or recycling through the endosomes.

6.2.3. No significant decrease in VSG221 protein levels was observed after induction of *VSG221* RNAi in 221VB1.1 and VG1.1 *T. brucei*

We attempted to determine if induction of *VSG* RNAi resulted in a decrease in VSG protein, which could activate the signaling pathway leading to the *VSG* RNAi-triggered phenotype. As VSG protein is extremely abundant, its accurate quantification was problematic due to saturation of signal, and chemiluminescence-based protein detection on standard western blots was not suitable. Therefore, VSG protein quantification was performed using the LI-COR's Odyssey® Infrared Imaging System (Y. V. Wang et al. 2007; Kuo et al. 2010; Schmid & Bohn 2010; Pei et al. 2010). IRDye fluorescent dyes have absorption and narrow emission wavelengths in the near-infrared spectrum, between 680 and 800 nm. Secondary antibodies used in Odyssey western blotting are directly coupled to a IRDyes, allowing for a more accurate quantification of protein levels over a wider range of concentrations.

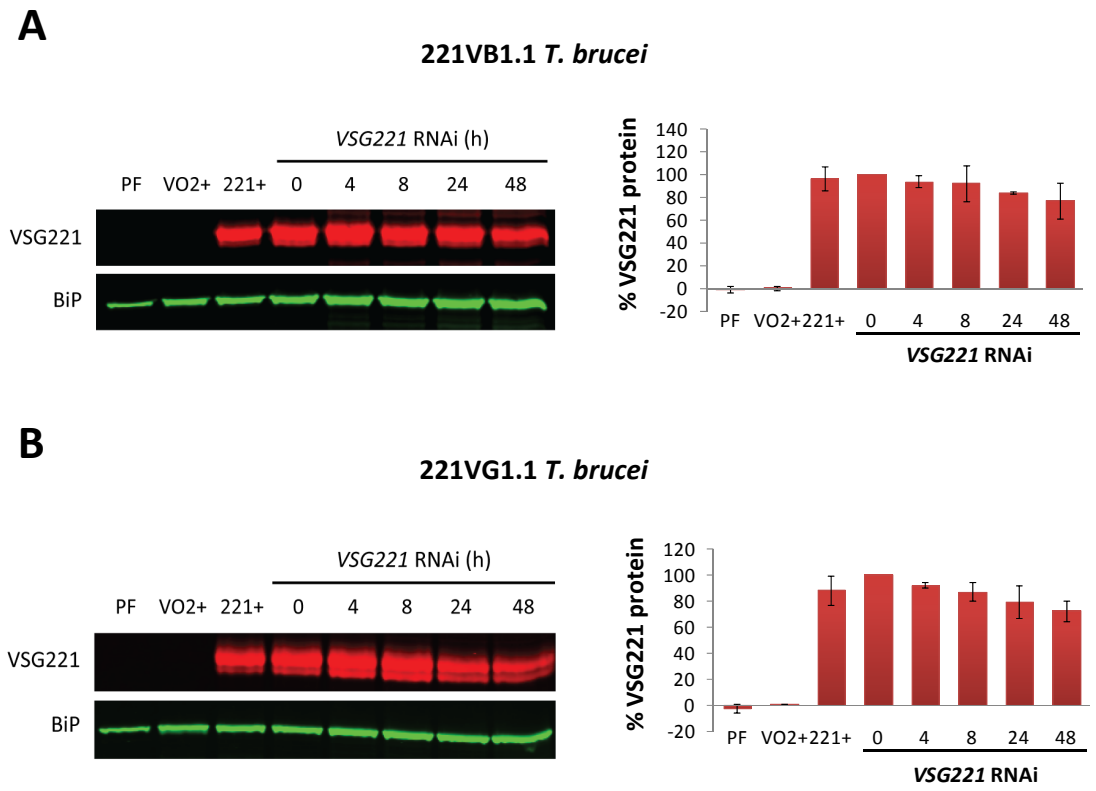


Figure 6.5: Induction of *VSG221* RNAi does not cause significant changes in VSG221 protein levels in 221VB1.1 and 221VG1.1 *T. brucei*.

Infrared western blot analysis of levels of VSG221 protein (red) in 221VB1.1 **(A)** or 221VG1.1 **(B)** *T. brucei* after induction of *VSG221* RNAi for the time specified in hours (h). Cells expressing VSG221 (221+), VSGVO2 (VO2+) and procyclic 29-13 *T. brucei* cell line (PF) were used as controls. Blots were additionally probed for BiP (green) as a loading control. Levels of VSG221 protein were quantified using the LI-COR Odyssey IR imaging system. The mean values obtained from three independent experiments and normalised to the loading control BiP are shown with standard deviation represented as error bars.

The infrared western blot analysis of 221VB1.1 and 221VG1.1 *T. brucei* revealed that there was no significant change in the levels of VSG221 protein after induction of *VSG221* RNAi for up to 48 hours (Figure 6.5). Since the half-life of VSG protein is 36 hours, it was expected that blocking VSG synthesis would result

in a decrease in VSG221 protein to 63% original levels after 24 hours, and to 40% of original levels after 48 hours of induction of *VSG221* RNAi. However, the levels of VSG221 protein in 221VB1.1 *T. brucei* after 24 and 48 hours of induction of *VSG221* RNAi were 82% and 77%, respectively (Figure 6.5A). The levels of VSG221 protein in VG1.1 *T. brucei* after 24 and 48 hours of induction of *VSG221* RNAi were 79% and 72%, respectively. This minor decrease in VSG221 protein levels could have been due to the increased fragility of the stalled cells, resulting in shedding of surface VSG.

6.2.4. No detectable change in the levels of ISG65 and ISG75 protein is observed after induction of *VSG221* RNAi

A number of *T. brucei* proteins presented on the cell surface display structural similarity to VSGs. These include the ESAG6 and ESAG7 heterodimer that forms the transferrin receptor, as well as the invariant surface glycoproteins (ISGs) 65 and 75 (Carrington & Boothroyd 1996; Ziegelbauer et al. 1992; Ziegelbauer & Overath 1992). Unlike most other surface proteins, ISG65 and ISG75 are not confined to the flagellar pocket, but instead are distributed among the VSG homodimers on the pellicular cell surface (D. G. Jackson et al. 1993). The VSG fold of the ISGs may be important for the efficient packing of these proteins between the VSG molecules on the parasite cell surface.

We investigated whether the parasites upregulated the expression of ISG65 and ISG75 proteins after induction of *VSG* RNAi, as a possible attempt to compensate for the loss of VSG synthesis. The levels of both ISG65 and ISG75

proteins were determined by infrared western blotting after induction of *VSG221* RNAi in 221VB1.1 *T. brucei* (Figure 6.6).

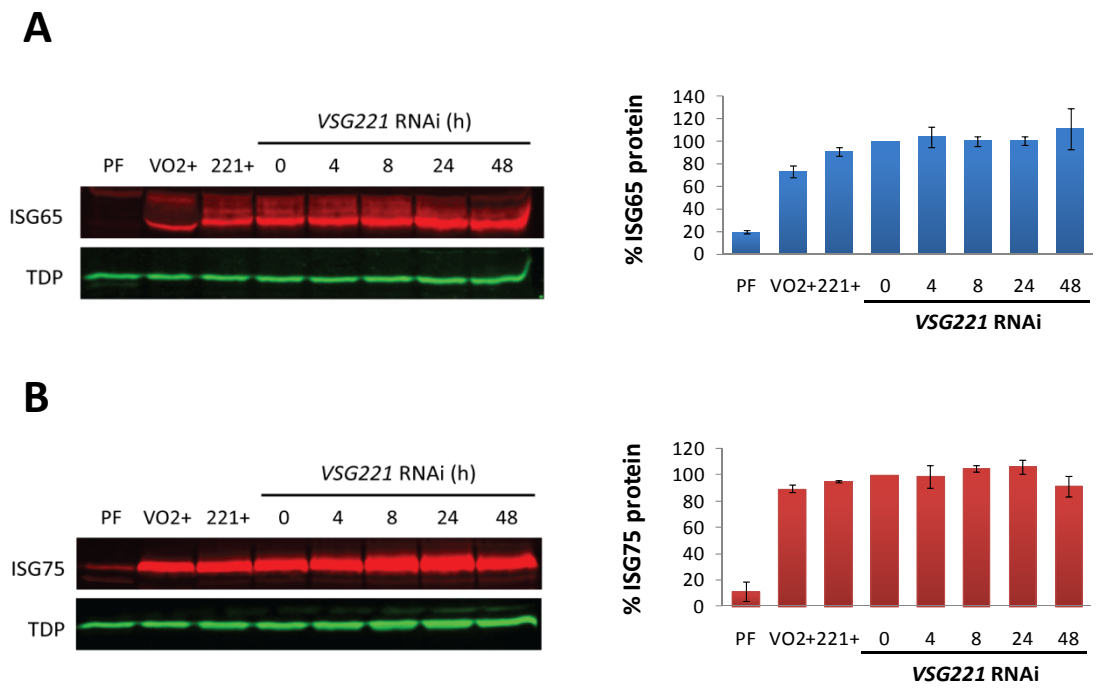


Figure 6.6: Induction of *VSG221* RNAi in 221VB1.1 *T. brucei* did not result in detectable changes in the ISG65 and ISG75 protein levels.

Infrared western blot analysis of levels of ISG65 **(A)** or ISG75 **(B)** protein in 221VB1.1 *T. brucei* after induction of *VSG221* RNAi for the time specified in hours (h). Cells expressing VSG221 (221+), VSGVO2 (VO2+) and procyclic 29-13 *T. brucei* cell line (PF) were used as controls. Blots were additionally probed for TDP (green) as a loading control. Levels of ISG65 (blue) **(A)** and ISG75 (red) **(B)** proteins were quantified using the LI-COR Odyssey IR imaging system. The mean values obtained from three independent experiments and normalised to loading control BiP are shown with standard deviation represented as error bars.

Infrared western blot analysis of ISG65 and ISG75 revealed no detectable change in the levels of these two proteins after the induction of *VSG221* RNAi (Figure 6.6). The levels of ISG65 and ISG75 proteins were determined to be 111%

(± 19%) and 91% (± 8%) at 48 hours post induction, respectively (Figure 6.6). Although ISG65 and ISG75 bear structural similarities to VSGs, there was no evidence that these two proteins could compensate for potential fluctuations in the levels of VSG protein.

6.3. Conclusions

The pre-cytokinesis cell cycle arrest observed after induction of *VSG* RNAi is one of the few precise cell cycle check points identified in *T. brucei*. Cell cycle progression in *T. brucei* is different to that in other model eukaryotes. For example, in *T. brucei* organelle replication does not appear to be linked to cytokinesis and multiple rounds of nuclear and kinetoplast replication can take place without accompanying cell division (Chapter 1.4) (Kumar & C. C. Wang 2005; Hammarton et al. 2003; Helms et al. 2006; Rothberg et al. 2006; B. S. Hall et al. 2006; LaCount et al. 2002; Ploubidou et al. 1999). Although drastic reduction in protein translation has been observed at the level of translation initiation after induction of *VSG* RNAi, no gross differences in the levels of the most abundant 1500 trypanosome proteins could be detected after the 2D-DIGE proteome analysis (Chapter 3.2.2) (T. K. Smith et al. 2009). Therefore, the precise signaling pathways operating behind the *VSG* RNAi-triggered cell cycle check points still remain unclear.

Although *VSGs* have vastly different sequences, the *VSG* 3'UTRs contain two highly conserved motifs, the 8mer and the 14mer, which are important for the stability of the *VSG* transcript in bloodstream form *T. brucei* (Figure 4.2) (Berberof et al. 1995; Borst & G. A. M. Cross 1982; Cully et al. 1985). The high level of conservation of these two motifs suggests that there may be regulatory proteins

binding them, although none have been identified yet. The hypothesis of the Engstler laboratory that parasites monitor *VSG* levels through sensing the amount of intracellular *VSG* 3'UTR was tested by using the 221VG1.1 *T. brucei* cell line that expresses *eGFP* flanked by a *VSG221* 3'UTR from the active *VSG221* Expression site (Figure 3.3A). Induction of *VSG221* RNAi in these cells resulted in a rapid growth arrest, similar to that observed in the 221VB1.1 *T. brucei* cell line not containing an additional gene with a *VSG221* 3'UTR (Figure 3.1A and C, Figure 3.3A and B and Figure 6.1A). Moreover, the levels of *eGFP* and its associated *VSG221* 3'UTR were observed to increase 6-fold after the induction of *VSG221* RNAi in 221VG1.1 *T. brucei* (Figure 6.1C). This indicated that expression of high levels of *VSG221* 3'UTR could not alleviate the *VSG* RNAi-triggered growth inhibition. *T. brucei*, therefore, does not appear to monitor *VSG* levels via the *VSG* 3'UTR.

We attempted to determine whether *T. brucei* sensed either *VSG* mRNA, or some aspect of the VSG protein (e.g. synthesis, processing or progression through the secretory system). HNI (221+) *T. brucei* was treated with anti-*VSG221* morpholino oligonucleotides that blocked VSG protein synthesis, but did not cause degradation of the *VSG221* mRNA (Figure 6.2). The growth of the cells treated with anti-*VSG221* morpholino oligos was inhibited for up to 24 hours after transfection (Figure 6.2A). The cells where *VSG* RNAi had been induced were stalled up to 72 hours post induction. This relatively stable phenotype was due to the continuous effect of the inducible RNAi, because tetracycline was present throughout the experiment (Figure 6.2A). In contrast, although morpholinos are highly stable, it is possible that they gradually diffused out of the cells. Eventually an intracellular concentration was reached that was too low to cause a sufficient block in VSG

synthesis. Once the anti-*VSG* morpholino-treated cells were able to undergo a cell division, further dilution of the morpholino oligos could take place, allowing subsequent cell divisions (Figure 6.2A).

Propidium iodide flow cytometry showed that treatment with anti-*VSG221* morpholinos caused an increase in cells with doubled DNA content (G2/M), similar to in cells where *VSG* RNAi has been induced (Figure 6.3). Although the increase in the proportion of cells with 4n DNA content was greater after induction of *VSG* RNAi, this could be explained by the greater efficiency of the inducible RNAi. Since treatment with morpholino oligos required transfection of cells, it was possible that a proportion of the cells did not take up sufficient amounts of morpholinos to block VSG synthesis and cause the associated phenotype. Microscopic analysis of anti-VSG morpholino-treated cells showed an accumulation of cells with two nuclei and two kinetoplasts (2K2N) with the typical close proximity of the two nuclei and the two kinetoplasts, similar to in cells where *VSG* RNAi had been induced (Figure 6.4).

The similar phenotypes generated through either treatment with anti-*VSG* morpholino oligos or induction of *VSG* RNAi suggested that *T. brucei* does not sense the loss of the *VSG* mRNA itself, but some aspect of VSG protein or its synthesis. However, no significant changes in VSG221 protein levels could be detected after induction of *VSG221* RNAi in either 221VB1.1, or 221VG1.1 *T. brucei* (Figure 6.5). Although VSG protein normally has a half-life of 36 hours, this lack of decrease in the levels of this protein up to 24 hours after induction of *VSG221* RNAi suggested that the VSG half-life must have increased in these cells (Bülow et al. 1989; Seyfang et al. 1990). Terry Smith indeed has evidence that VSG has a half-life of 65±5 hours in the stalled parasites (unpublished results), although it is not clear what is causing this change to the VSG half-life. In addition, ISGs have significantly shorter half-life

than VSG, with over 65% of ISG65 degraded within 4 hours of synthesis (W.-L. Chung et al. 2004). Levels of ISG65 and ISG75 proteins, however, also remained constant up to 48 hours after induction of *VSG* RNAi, which suggested that other surface proteins also displayed increased stability (Figure 6.6).

The enhanced stability of the VSG and ISG proteins observed after the induction of *VSG* RNAi, as well as the previously reported rapid clearance of the induced cells from the bloodstream of infected mice, suggests that the turnover of the surface VSG coat may have been affected in these parasites (Figure 6.5 and Figure 6.6) (Sheader et al. 2005). Since the disruption of surface coat internalisation could have provided a potential sensing mechanism operating behind the *VSG* RNAi-triggered cell cycle arrest, the dynamics of the VSG surface coat endocytosis after induction of *VSG* RNAi was investigated.

Chapter 7

Clearance of VSG from the surface of *Trypanosoma brucei* is impeded after the induction of *VSG* RNAi

7.1. Introduction

T. brucei, in which *VSG221* RNAi has been induced are rapidly cleared from the bloodstream of infected mice (Sheader et al. 2005). However parasites persist *in vitro* for several days after induction of *VSG* RNAi (Figure 3.1C and Figure 3.3B). As quiescent stumpy form *T. brucei* can persist in the mammalian bloodstream, the *VSG221* RNAi-triggered growth arrest on its own was not likely to be responsible for the abrupt clearance of the parasites from the murine bloodstream. The following chapter investigates the dynamics of VSG221 surface coat recycling after induction of *VSG221* RNAi in an attempt to understand the mechanism behind the rapid cell death observed in the bloodstream of infected mice.

7.2. Results

7.2.1. Rates of VSG221 clearance from the cell surface are reduced after the induction of *VSG221* RNAi

Trypanosoma brucei has one of the most rapid endocytosis rates reported with cells able to recycle their entire surface VSG within 12.5 min (Engstler et al. 2004). As already discussed, this rapid turn-over of the VSG coat is an important protective mechanism, and the removal of antibodies from the VSG surface coat allows the parasites to survive low levels of anti-VSG antibody (Balber et al. 1979; Barry 1979; McLintock et al. 1993; O'Beirne et al. 1998).

The rapid clearance of the parasites from the bloodstream of infected mice after induction of *VSG221* RNAi suggests that the VSG221 coat in these cells has

been compromised (Sheader et al. 2005). Therefore, VSG221 endocytosis rates were investigated in cells after induction of *VSG221* RNAi.

VSG removal from the cell surface of *T. brucei* can be monitored using anti-VSG antibodies. The parasites were cooled to 4°C, at which temperature endocytosis stops. Anti-VSG antibodies were allowed to bind to the surface coat (Brickman et al. 1995). Cells were then incubated at 37°C and endocytosis of VSG-antibody complexes was allowed to occur (Figure 7.1). Parasites were then fixed, and the surface VSG-bound primary antibodies were detected with fluorescently-labeled secondary antibodies and assessed microscopically or using flow cytometry.

Internalisation of surface VSG221 was assessed after induction of *VSG221* RNAi or, as a control, *TDP 1* RNAi for either 8 or 12 hours and compared with uninduced cells (Figure 7.1). TDP 1 is an essential protein involved in transcriptional control in *T. brucei* and induction of *TDP 1* RNAi is lethal (M. Narayanan and G. Rudenko unpublished). It had previously been determined that induction of *VSG221* RNAi-triggered a global translation arrest to 1-2% of original levels within 24 hours (T. K. Smith et al. 2009). In these experiments, at 8 and 12 hours post induction, the levels of translation were at 60% and 30% of wild-type levels, respectively (T. K. Smith et al. 2009). As the pre-cytokinesis cell cycle arrest was already maximal 8 hours after induction of *VSG221* RNAi, this time point was used to investigate the effect of *VSG221* RNAi on VSG surface coat dynamics. The 90-13 TDP C1 *T. brucei* cell line capable of inducible *TDP 1* RNAi and expressing VSG221 on its cell surface was used as a control for a nonspecific effect caused by a lethal phenotype (Figure A3.1 and Figure 7.1B).

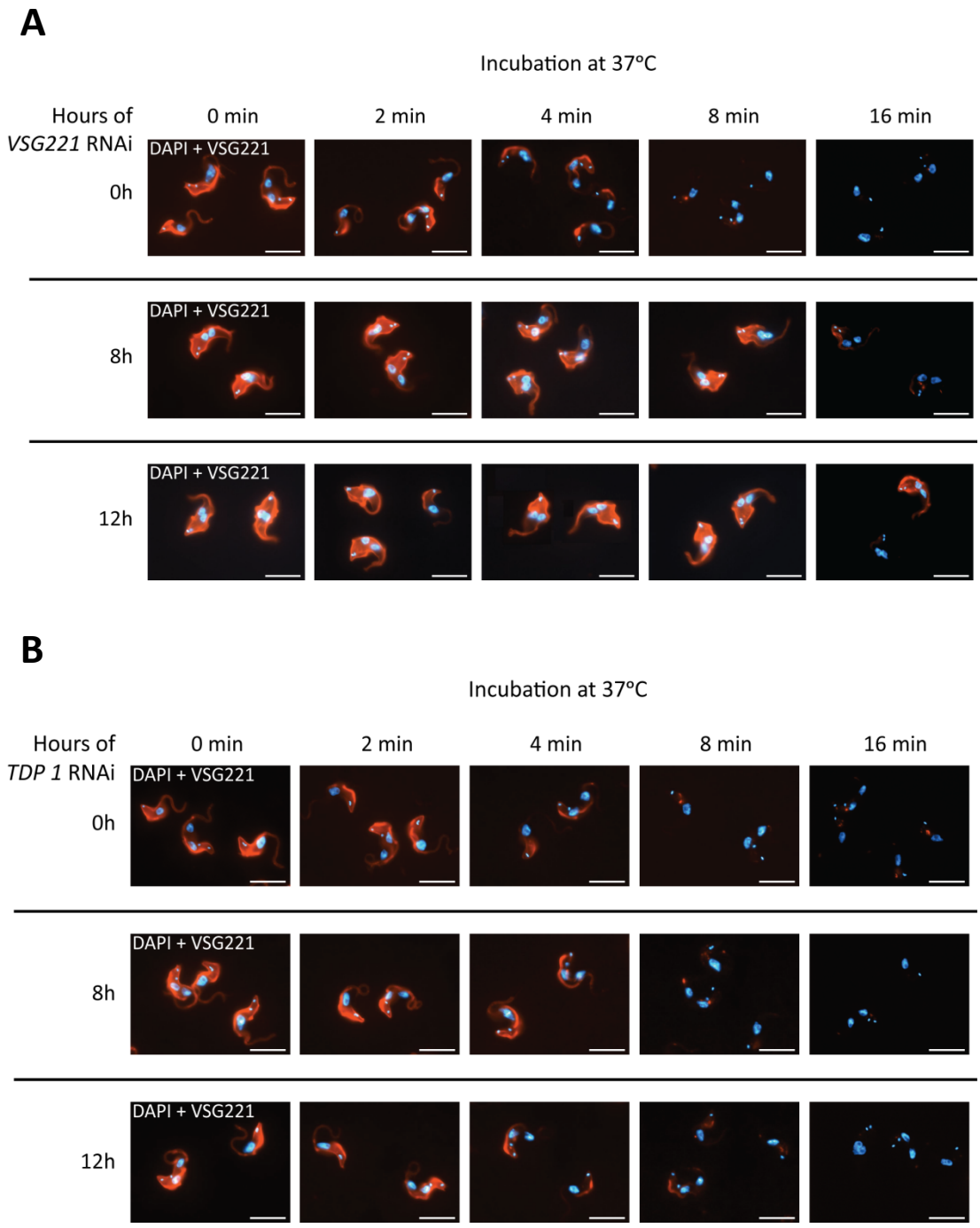


Figure 7.1: Surface VSG221 clearance is affected after the induction of *VSG221* RNAi but not after the induction of *TDP 1* RNAi.

Internalisation of surface VSG221 was monitored microscopically in 221VB1.1 **(A)** and 90-13 TDP C1 **(B)** *T. brucei* after the induction of *VSG221* and *TDP 1* RNAi, respectively, for 8 h or 12 h and compared with uninduced cells (0 h). Parasites were probed with anti-VSG221 (orange) antibody and

incubated at 37°C for the time specified in minutes to allow surface VSG221 internalisation. Cells were additionally stained with DAPI (blue) for DNA content. The scale bar represents 10 μm.

It was observed that the rate of VSG221 clearance from the cell surface after induction of *VSG221* RNAi was reduced compared to uninduced cells (Figure 7.1A). Cells where no *VSG221* RNAi had been induced rapidly internalised the labeled surface VSG221, so that almost no surface fluorescence could be detected after 8 minutes of incubation at 37°C (Figure 7.1A). However, cells where *VSG221* RNAi has been induced for 8 or 12 hours appeared to have a reduced rate of clearance of surface VSG221, with most of the cell body still fluorescent after 8 minutes of incubation at 37°C (Figure 7.1A).

The observed effect did not appear to be a consequence of a lethal phenotype, because induction of *TDP 1* RNAi for 8 or 12 hours did not result in reduced rates of surface VSG221 internalisation (Figure 7.1B). Cells where *TDP 1* RNAi had been induced for 8 or 12 hours endocytosed surface VSG221 at similar rates to uninduced parasites, with cells devoid of VSG221-antibody complexes within 8 minutes of incubation at 37°C (Figure 7.1B).

7.2.2. General endocytosis is not inhibited after the induction of *VSG221* RNAi

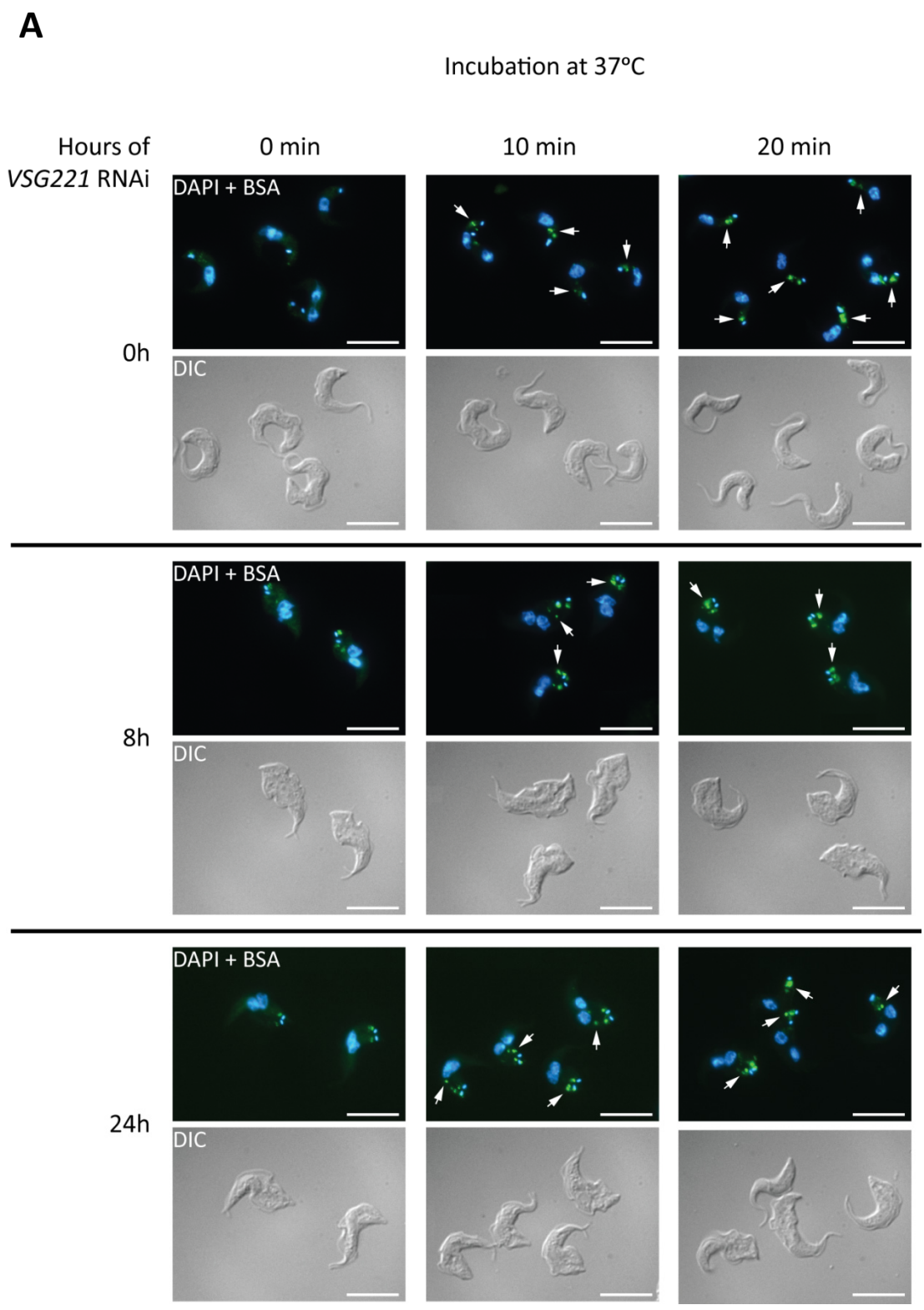
The block in VSG221 coat internalisation observed after the induction of *VSG221* RNAi could have been due to impaired endocytosis in the flagellar pocket, which is the site of all endocytosis in *Trypanosoma brucei* (Overath et al. 1997; Grünfelder et al. 2002; Gull 2003). It has been shown that all endocytosis in *Trypanosoma brucei*, including VSG221 surface coat clearance, occurs in a clathrin-

mediated manner (Allen et al. 2003; Grünfelder et al. 2003). Therefore, it was expected that if surface VSG221 clearance had been affected due to the inhibition of endocytosis in the flagellar pocket, then endocytosis of fluid phase markers, as well as receptor mediated endocytosis would be blocked. To investigate this possibility, the endocytosis rates of BSA and tomato lectin were monitored after induction of *VSG221* and *TDP 1* RNAi (Figure 7.2 and Figure 7.3).

7.2.2.1. Endocytosis of the fluid phase marker bovine serum albumin (BSA) is not impaired after induction of *VSG221* RNAi

Bovine serum albumin (BSA) is a commonly used marker for fluid phase endocytosis in *Trypanosoma brucei* (Coppens et al. 1987). As with VSG internalisation, the rate of endocytosis of BSA is very rapid at 37°C. Cells were initially incubated at 4°C, which allowed the accumulation of FITC-BSA in the flagellar pocket, but prevented endocytosis from taking place (Brickman et al. 1995). The parasites were subsequently incubated at 37°C to allow endocytosis of FITC-BSA to occur (Figure 7.2).

The endocytosis of FITC-BSA was investigated in 221VB1.1 *T. brucei* cells after induction of *VSG221* RNAi for 8 or 24 hours (Figure 7.2A). As previously described, the induction of *VSG221* RNAi for 24 hours causes a dramatic translation arrest to 1-2% of wild-type levels (Chapter 3.3) (T. K. Smith et al. 2009). If the block in protein synthesis was affecting endocytosis, this would be most apparent 24 hours after induction of *VSG221* RNAi. FITC-BSA endocytosis was also determined in 90-13 TDP C1 *T. brucei* after induction of *TDP 1* RNAi for 8 or 24 hours (Figure 7.2B).


A
Incubation at 37°C
Hours of
VSG221 RNAi
0 min
10 min
20 min
0h
8h
24h
DAPI + BSA
DIC

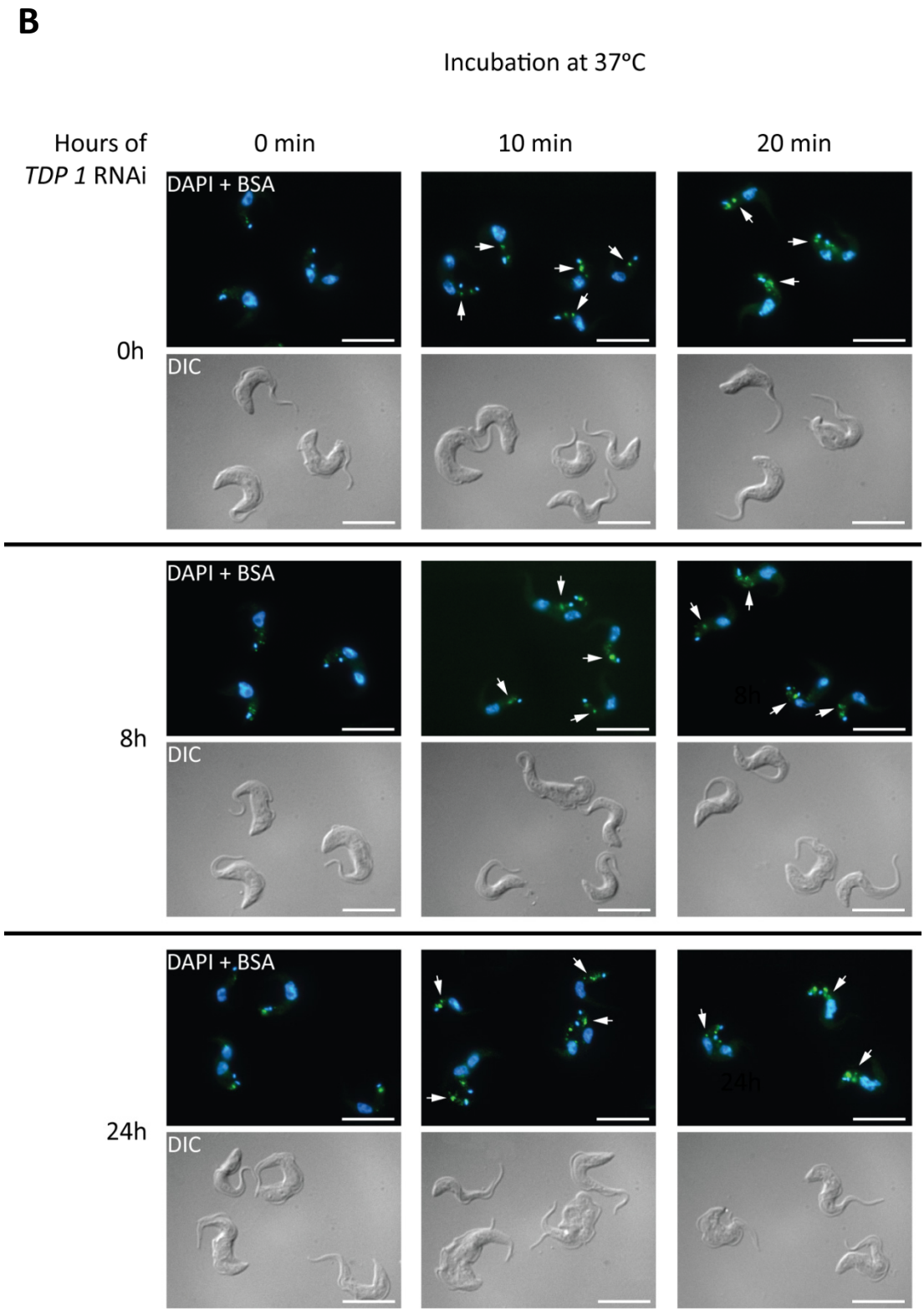


Figure 7.2: Endocytosis of the fluid phase marker FITC-BSA is not affected after the induction of *VSG221* or *TDP 1* RNAi.

FITC-BSA endocytosis was monitored microscopically in 221VB1.1 **(A)** and 90-13 TDP C1 **(B)** *T. brucei* after the induction of *VSG221* and *TDP 1* RNAi, respectively, for 8 h or 24 h and compared with uninduced cells (0 h). Parasites were initially pre-incubated with FITC-BSA (green) at 4°C, followed by incubation at 37°C to activate endocytosis for the time indicated in minutes. Cells were additionally stained with the DNA stain DAPI (blue). The scale bar represents 10 μm.

Fluid phase endocytosis of FITC-BSA was not affected 8 or 24 hours after induction of *VSG221* RNAi (Figure 7.2A). FITC-BSA was initially detected in the flagellar pocket after 0 min at 37°C (pre-incubation at 4°C only) and was further observed to gradually redistribute to the endocytic compartment after incubations for up to 20 min at 37°C (Figure 7.2A). This indicated that FITC-BSA was successfully internalised from two functional flagellar pockets in pre-cytokinesis stalled cells (2N2K). Fluid phase endocytosis was also not affected by the induction of *TDP 1* RNAi for 8 or 24 hours (Figure 7.2B). FITC-BSA signal was observed to relocate from the flagellar pocket to intracellular compartments within 5 min of incubation at 37°C in both uninduced cells, as well as in cells where *TDP 1* RNAi had been induced (Figure 7.2B).

7.2.2.2. Receptor-mediated endocytosis of tomato lectin is not affected by the induction of *VSG221* RNAi

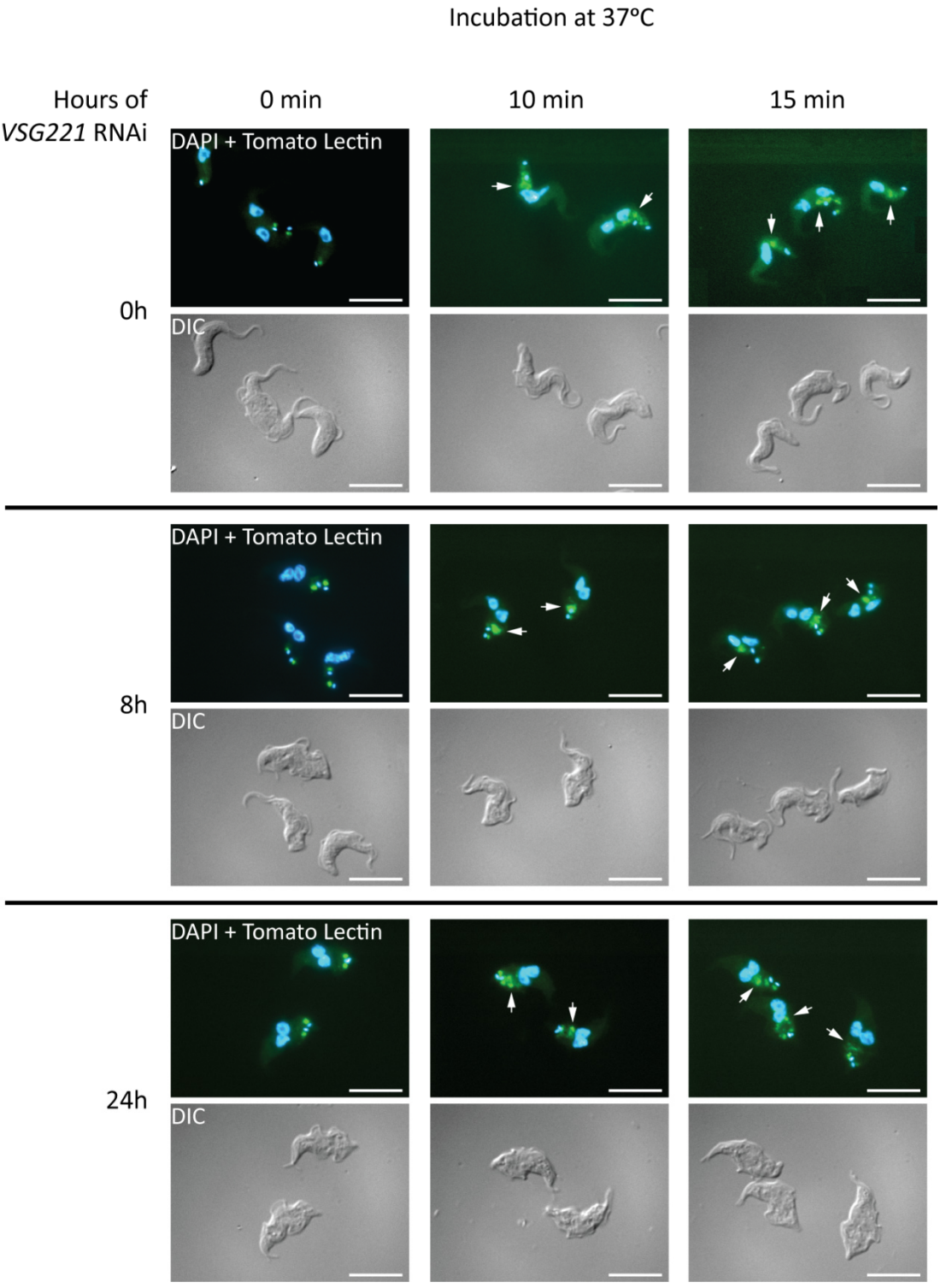
Receptor-mediated endocytosis in *Trypanosoma brucei* also occurs in a clathrin-dependent fashion (Chapter 1.9) (Allen et al. 2003). To investigate whether receptor-mediated internalisation had been impaired after induction of *VSG221* RNAi, the endocytosis of FITC-conjugated tomato lectin was monitored in parasites

where *VSG221* RNAi had been induced for 8 or 24 hours (Figure 7.3A) (Merkles & Cummings 1987). Tomato lectin only binds with high affinity if three or more linear repeats of poly-*N*-acetyllactosamine (pNAL) are present. In *Trypanosoma brucei* this posttranslational modification is restricted to proteins that are either in the flagellar pocket, or the endocytic pathway (Nolan et al. 1999).

Cells where *VSG221* RNAi had been induced for 8 or 24 hours were pre-incubated at 4°C with FITC-tomato lectin. The parasites were subsequently incubated at 37°C to allow FITC-tomato lectin endocytosis to take place (Figure 7.3A). In addition, the internalisation of FITC-tomato lectin was investigated after induction of *TDP 1* RNAi (Figure 7.3B).

Pre-incubation of parasites with FITC-tomato lectin resulted in localization of the fluorescent signal in the flagellar pockets, rather than the cell surface (Figure 7.3). This was consistent with the previously reported binding of tomato lectin to *N*-linked glycans containing three or more disaccharide repeats, found in the flagellar pocket (Nolan et al. 1999). VSG, as well as ISG proteins are *N*-glycosylated and are distributed evenly over the pellicular cell membrane of bloodstream form parasites (Mehlert et al. 1998; Mehlert et al. 2002). These VSG and ISG-attached *N*-linked oligosaccharides are branched, rather than linear, explaining why the FITC-tomato lectin signal is not uniformly distributed over the entire cell surface, but is restricted to the flagellar pocket (Figure 7.3).

A


Incubation at 37°C
Hours of
VSG221 RNAi
0 min
10 min
15 min
0h
8h
24h
DAPI + Tomato Lectin
DIC

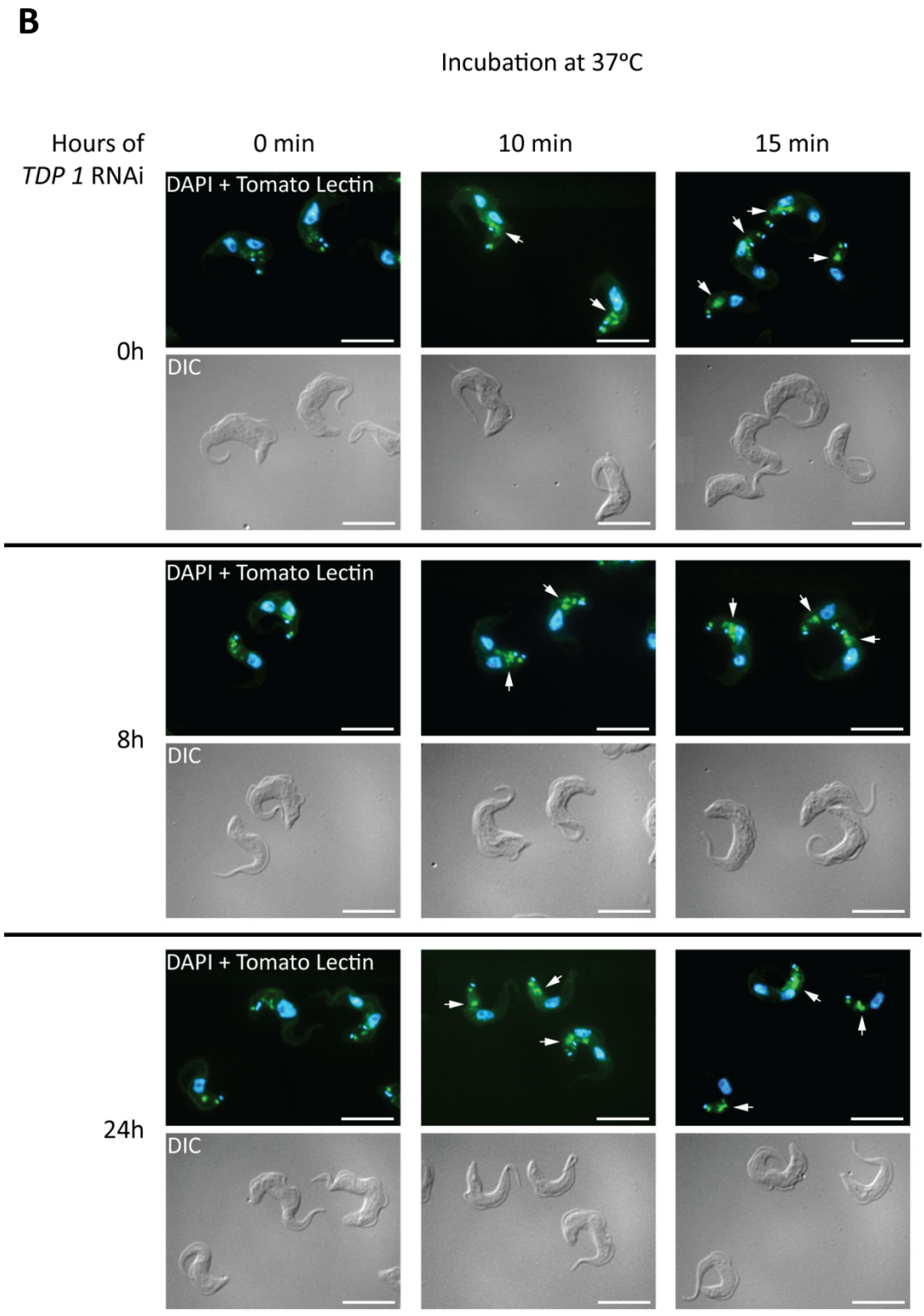


Figure 7.3: Receptor-mediated internalisation of FITC-tomato lectin is not impaired after the induction of *VSG221* or *TDP 1* RNAi.

FITC-tomato lectin endocytosis was monitored in 221VB1.1 **(A)** and 90-13 TDP C1 **(B)** *T. brucei* after the induction of *VSG221* and *TDP 1* RNAi, respectively, for 8 h or 24 h and compared with uninduced cells (0 h). Parasites were initially pre-incubated with FITC-tomato lectin (green) at 4°C, followed by incubation at 37°C for the time indicated in minutes. Cells were additionally stained with the DNA stain DAPI (blue). The scale bar represents 10 μm.

Similar to endocytosis of FITC-BSA, FITC-tomato lectin was also observed to gradually accumulate in the parasites after incubation at 37°C in both uninduced cells and cells where *VSG221* RNAi had been induced for up to 24 hours (Figure 7.3A). However, blocking TDP 1 synthesis by induction of *TDP 1* RNAi for 8 or 24 hours did not result in a reduction in receptor-mediated endocytosis of FITC-tomato lectin (Figure 7.3B). Therefore, clathrin-mediated endocytosis did not appear to be impaired after induction of *VSG221* RNAi, and was not the responsible for the reduced rates of internalisation of the VSG221 surface coat.

7.2.3. Endocytosis of surface VSG221 is impaired in pre-cytokinesis stalled cells, but not in other cell cycle stages after induction of *VSG221* RNAi

Endocytosis of VSG221 was observed to be particularly affected in cells that were stalled pre-cytokinesis (2K2N). However, clearance of surface VSG221 appeared to proceed at wild-type rates in 1K1N and 2K1N cells. To further investigate this, cells where *VSG221* RNAi had been induced were stained simultaneously for surface VSG221 using anti-VSG221 antibodies and for DNA content with propidium iodide (Figure 7.4). The parasites were analysed by flow cytometry, where surface VSG221 fluorescence was detected in the FL1 channel and the DNA content was simultaneously detected in the FL2 channel (Figure 7.4).

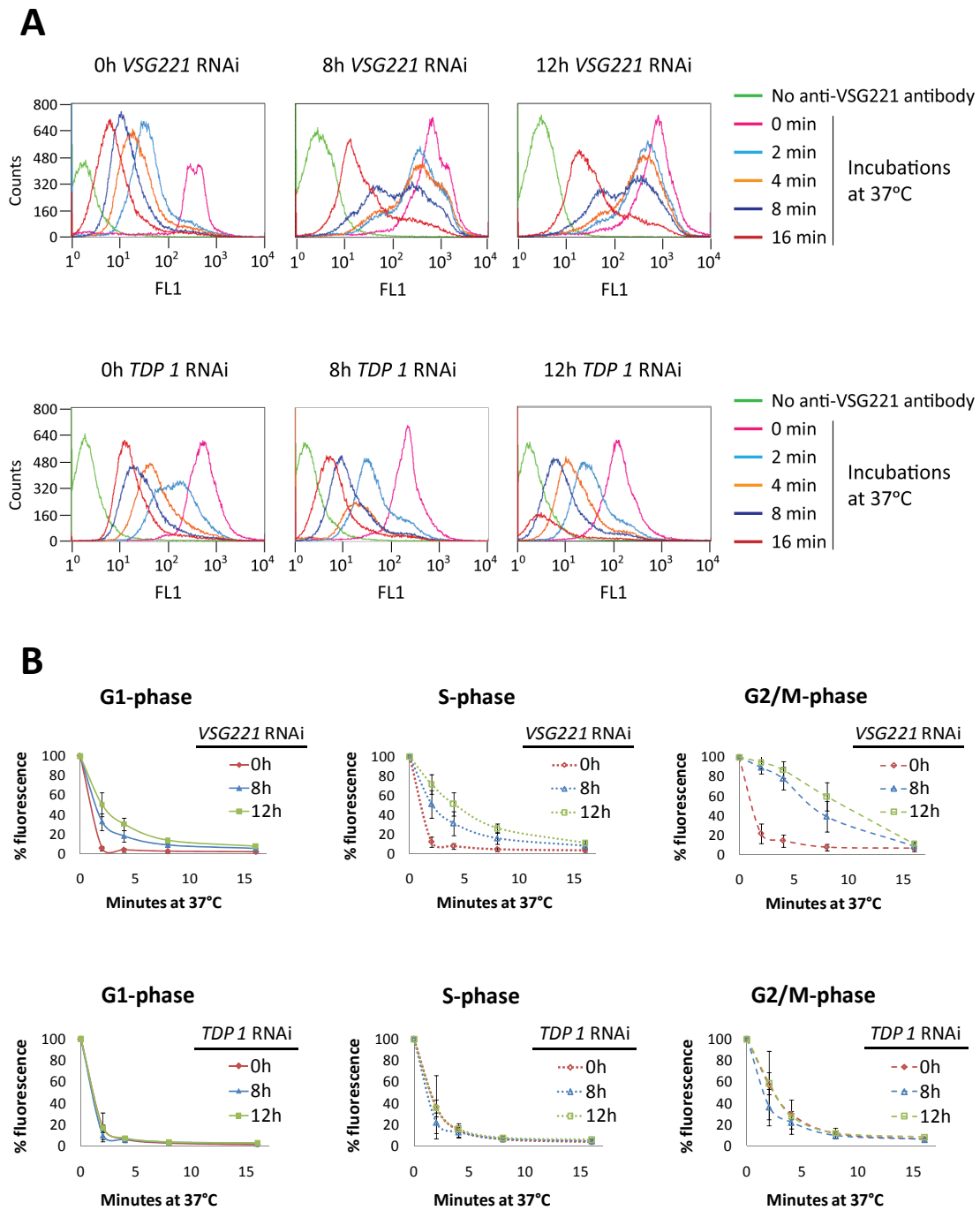


Figure 7.4: Rates of clearance of VSG221 from the surface of 221VB1.1 *T. brucei* in G2/M-phase are reduced after the induction of *VSG221* RNAi, but not after the induction of *TDP 1* RNAi.

A. Decrease in surface fluorescence in the total population of 221VB1.1 or 90-13 TDP C1 *T. brucei* stained for surface VSG221 after induction of *VSG221* or *TDP1* RNAi, respectively, for 8 h or 12 h

and compared with uninduced cells (0 h). Cells were incubated at 37°C for the time specified in minutes and remaining surface VSG221 fluorescence was determined by flow cytometry.

B. Internalisation of surface VSG221 after induction of *VSG221* or *TDP 1* RNAi in 221VB1.1 or 90-13 TDP C1 *T. brucei*, respectively, was determined after simultaneous staining for surface VSG221 and DNA content. Surface VSG221 endocytosis rates were quantified in G1-, S- and G2/M-phase cells. The average VSG221 surface fluorescence from three independent experiments is represented as percentage fluorescence change from fluorescence at 0 minutes at 37°C, and the standard deviation is shown as error bars.

Overlays of the disappearance of surface VSG221 fluorescence in 221VB1.1 *T. brucei* after the induction of *VSG221* RNAi showed the generation of two distinct populations, one of which appeared to clear its surface VSG221 coat at significantly slower rates (Figure 7.4A). Fluorescent scatter profiles revealed that the cells with reduced rates of surface VSG221 endocytosis were in the G2/M-stage of the cell cycle (Figure 7.4B). The induced cells in the G1-stage of the cell cycle internalised their VSG221 surface coat most rapidly, followed by cells in S-phase (Figure 7.4B). Although the rates of surface VSG221 endocytosis in G1- and S-phase cells where *VSG221* RNAi had been induced were higher than in G2/M-phase cells, they were still lower than in uninduced G1- and S-phase cells (Figure 7.4B). It was also observed that after 16 minutes of incubation at 37°C, all cell populations had internalised their surface VSG221 (Figure 7.4B). As a control, cells were induced for *TDP 1* RNAi (Figure 7.4).

The surface VSG221 coat of cells in G2/M-phase was cleared at similar rates after the induction of *TDP 1* RNAi, compared with the same cell cycle stage in uninduced cells (Figure 7.4B). However, as observed in the 221VB1.1 *T. brucei* cell

line, there were different rates of endocytosis of surface VSG on cells in different stages of the cell cycle. These were, however, the same after the induction of *TDP 1* RNAi (Figure 7.4). Therefore, the reduction in the rate of endocytosis of surface VSG221 in G2/M-phase cells after induction of *VSG221* RNAi in 221VB1.1 *T. brucei* was a specific effect of the *VSG221* RNAi-triggered phenotype and was not a consequence of the growth inhibition in these cells.

It was observed that cells in the G2/M-stage of the cell cycle internalised their surface VSG at slower rates compared with G1-stage cells in uniduced 221VB1.1 and 90-13 TDP C1 *T. brucei* (Figure 7.5).

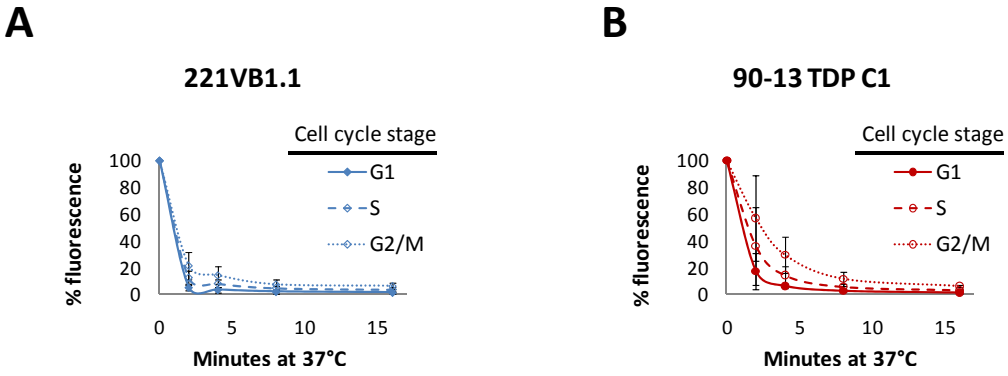


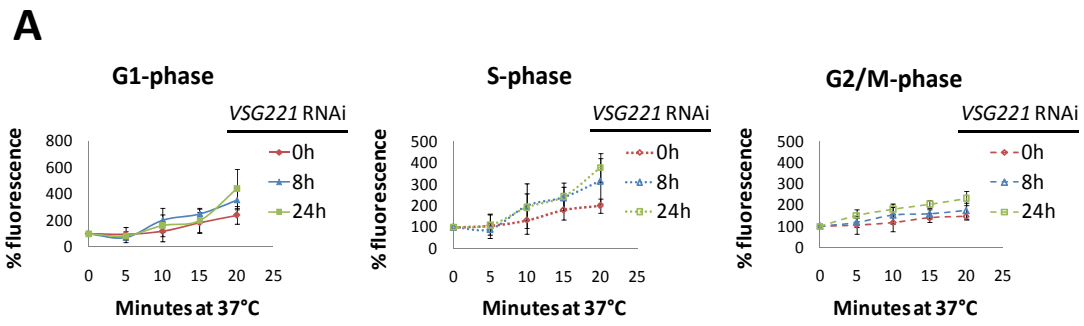
Figure 7.5: The rates of VSG221 internalisation from the surface of cells in the G2/M-stage of the cell cycle are lower compared with G1-stage cells of wild-type *T. brucei* cell population.

Internalisation of surface VSG221 in cells in different stages of the cell cycle of wild-type 221VB1.1 **(A)** and 90-13 TDP C1 **(B)** *T. brucei*. Cells have been stained simultaneously for surface VSG221 and DNA content with propidium iodide and analysed by flow cytometry. Surface VSG221 endocytosis rates were quantified in G1-, S- and G2/M-phase cells. The average VSG221 surface fluorescence from three independent experiments is represented as percentage fluorescence change from fluorescence at 0 minutes at 37°C and the standard deviation is shown as error bars.

Therefore, there appeared to be a naturally occurring difference in the rates of endocytosis of surface VSG in wild-type *T. brucei*, with pre-cytokinesis cells internalising VSG slower than G1- and S-stage parasites.

7.2.4. Rates of fluid phase endocytosis are not affected in cells stalled pre-cytokinesis after the induction of *VSG221* RNAi

Although fluid phase endocytosis was studied using microscopic analysis after induction of *VSG221* RNAi, this might not have been sufficiently sensitive to assess the precise rates of endocytosis in the different cell populations. As observed from the flow cytometry analysis of the internalisation rates of surface VSG221 in the different cell populations, the parasites stalled in the precytokinesis stage after induction of *VSG221* RNAi had reduced rates of surface VSG221 internalisation, compared with all other cell populations (Figure 7.4B). However, after extended incubation at 37°C, the G2/M-stage cells also achieved complete internalisation of their surface VSG221 (Figure 7.4B). Therefore, although endocytosis was occurring at the flagellar pocket in these cells, it may have been taking place at reduced rates. Endocytosis of FITC-BSA was therefore also investigated together with simultaneous staining for DNA in 221VB1.1 *T. brucei* where *VSG221* RNAi had been induced for 8 or 24 hours (Figure 7.6A).



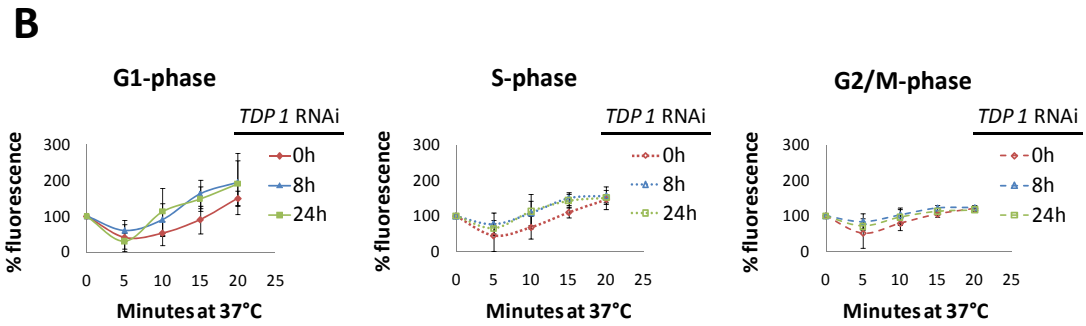


Figure 7.6: Rates of endocytosis of FITC-BSA in cells after induction of *VSG221* RNAi in 221VB1.1 *T. brucei* or *TDP 1* RNAi in 90-13 TDP C1 *T. brucei* are similar to those in uninduced cells.

Internalisation of FITC-BSA after induction of *VSG221* RNAi in 221VB1.1 *T. brucei* **(A)** and *TDP 1* RNAi in 90-13 TDP C1 *T. brucei* **(B)** for 8 h or 12 h compared with uninduced cells (0 h). Parasites were incubated at 37°C for the time specified in minutes to allow FITC-BSA endocytosis to occur, and were subsequently stained with propidium iodide for DNA content. The rates of FITC-BSA were monitored in G1-, S- and G2/M-phase cells by flow cytometry.

Analysis of endocytosis of FITC-BSA with simultaneous staining of the cells for DNA content revealed that cells in different stages of the cell cycle (G1-, S- and G2/M-phase) internalised FITC-BSA at similar rates after the induction of *VSG221* RNAi compared with uninduced cells (Figure 7.6A). No significant difference in the rates of fluid phase endocytosis could be detected in the cells in G2/M-phase in the induced and uninduced populations (Figure 7.6A).

Induction of *TDP 1* RNAi did not result in a significant difference in the rates of fluid phase endocytosis in the different populations (G1-, S- and G2/M-phase) (Figure 7.6B). Endocytosis at the flagellar pocket as assessed from the internalisation of FITC-BSA occurred at wild-type rates in all cell populations tested after induction of either *VSG221* or *TDP 1* RNAi (Figure 7.6). This suggested that the impaired

surface VSG221 clearance rates observed in pre-cytokinesis stalled (G2/M-stage) cells after induction of *VSG221* RNAi was not a consequence of impaired endocytic function of the flagellar pocket.

7.3. Conclusions

Cells where *VSG221* RNAi has been induced are rapidly cleared from the bloodstream of infected mice, while induction of *VSG221* RNAi *in vitro* does not cause immediate cell death (Figure 3.1C and Figure 3.3B) (Sheader et al. 2005). As quiescent trypanosomes are able to persist in immunocompetent mice, the rapid cell death observed after blocking VSG221 synthesis in the murine bloodstream might be a consequence of disruptions in VSG coat turn-over. Therefore, the dynamics of VSG221 surface coat internalisation after induction of *VSG221* RNAi were investigated.

Endocytosis of surface VSG was impaired after 8 and 12 hours of induction of *VSG221* RNAi (Figure 7.1A). In contrast, the induction of the lethal *TDP 1* RNAi in 90-13 TDP C1 *T. brucei* cells did not cause a reduction in the rates of surface VSG221 internalisation (Figure 7.1B). Thus, it was concluded that the reduced rate of clearance of surface VSG221 after induction of *VSG221* RNAi was not a direct consequence of growth inhibition in these cells. The impaired endocytosis of surface VSG221 could have been the cause of the rapid clearance of *T. brucei* where *VSG221* RNAi had been induced from the bloodstream of infected mice. This may have been due to insufficient removal of immune complexes from the cell surface of the parasites (Sheader et al. 2005).

Neither fluid phase endocytosis, nor receptor-mediated endocytosis were affected after 24 hours of induction of *VSG221* RNAi (Figure 7.2A and Figure 7.3A). Induction of *TDP 1* RNAi also did not result in a disruption of fluid phase or receptor-mediated endocytosis (Figure 7.2B and Figure 7.3B). Therefore, the reduced clearance rates of surface VSG221 protein after induction of *VSG221* RNAi were not caused by a general lack of endocytosis at the flagellar pocket.

It was observed that particularly cells stalled pre-cytokinesis after induction of *VSG221* RNAi internalised their surface VSG221 at a dramatically reduced rate compared with the uninduced G2/M-stage cells (Figure 7.4B, 3rd panel). This effect appeared to be specific to the *VSG221* RNAi-triggered phenotype, because G2/M-stage cells generated after induction of *TDP 1* RNAi endocytosed their surface VSG221 at similar rates to the uninduced G2/M-stage parasites (Figure 7.4B, 3rd panel). In addition, it was observed that induction of *VSG221* RNAi did not cause a decrease in rates of endocytosis in G2/M-stage stalled cells compared with G2/M-stage parasites that had not had *VSG221* RNAi induced (Figure 7.6A, 3rd panel). Rates of endocytosis in the different cell populations after induction of *TDP 1* RNAi were also comparable to rates in uninduced cells (Figure 7.6B, 3rd panel). It was, therefore, concluded that the reduced rates of surface VSG221 internalisation in G2/M-stage cells after induction of *VSG221* RNAi could not be explained by a general impairment of endocytosis at the flagellar pocket.

A possible explanation for the reduced rates of endocytosis of surface VSG221 in G2/M-stage cells after induction of *VSG221* RNAi could have been due to lack of VSG221 protein synthesis. Using electron microscopy gross expansion of the trans-Golgi cisternae that increased in a time-dependent manner had been observed after induction of *VSG* RNAi (E. Gluenz and G. Rudenko, unpublished). As

VSG is the major secreted protein in *T. brucei*, the lack of newly synthesised VSG could have resulted in a decrease in vesicles budding off the trans-Golgi to be deposited on the cell surface. This, in turn, could have caused the observed distortion of the Golgi apparatus.

The lack of VSG221 deposition on the cell surface could have affected the rates of VSG221 endocytosis. This effect may have been more pronounced in the stalled G2/M-stage cells due to their larger surface area. This would require more surface VSG221 protein, and therefore drain the limited intracellular VSG221 stores to a greater degree than in G1- or S-phase cells. However, rates of surface VSG uptake are the same as rates of endocytosis of fluid phase marker, which are representative of rates of membrane uptake (Engstler et al. 2004). Since cells in the G2/M-stage of the cell cycle after induction of *VSG* RNAi and uninduced cell were found to have similar rates of fluid phase endocytosis, the reduced uptake of surface VSG did not appear to be caused by an impaired endocytic machinery at the flagellar pocket (Figure 7.6A, 3rd panel).

Another possible explanation for the reduced rates of surface VSG221 clearance specifically in pre-cytokinesis stalled cells after induction of *VSG221* RNAi could have been due to reduced motility of these cells. It has previously been reported that the unidirectional movement of the parasite creates a hydrodynamic flow on its cell surface, and immune complexes bound to the VSG221 surface coat are driven towards the posteriorly located flagellar pocket due to these drag forces (Chapter 1.10) (Engstler et al. 2007; Rodriguez et al. 2009). The cells stalled pre-cytokinesis after induction of *VSG221* RNAi have a distinctly broader and shortened morphology, and this may have affected their motility (Sheader et al. 2005). In addition, the presence of two flagella could have contributed further to their reduced

directional motion. This could explain why the reduced rates of clearance of surface VSG221 were observed specifically in the G2/M-stage population, rather than in G1- or S-stage cells (Figure 7.4B).

This hypothesis was supported by the observation that even the pre-cytokinesis stalled cells where *VSG221* RNAi had been induced eventually cleared their surface VSG221, albeit at drastically reduced rates (Figure 7.1A and Figure 7.4B). After 16 minutes of incubation at 37°C, almost all stained surface VSG221 had been removed from the pellicular cell membrane of induced 221VB1.1 *T. brucei* (Figure 7.1A and Figure 7.4B). Since no immuno-stained surface VSG221 was observed to accumulate in the flagellar pocket of the parasites where *VSG221* RNAi had been induced, this confirmed the presence of a functional endocytosis machinery, and suggested that it was reduced movement of surface VSG221 protein towards the flagellar pocket that resulted in its decreased rates of internalisation (Figure 7.1A).

If reduced motility of the pre-cytokinesis stalled cells was the cause of the impaired surface VSG clearance rates, then in a wild-type cell population, G2/M-stage cells would also be slower to internalise their surface VSG coat. Indeed, this was the case and it was determined that endocytosis rates of surface VSG221 on G2/M cells were reduced compared with the G1-stage cells in wild-type 221VB1.1 and 90-13 TDP C1 *T. brucei* (Figure 7.5). This could have been a consequence of the change in morphology, as well as the presence of two flagella in the pre-cytokinesis cells, which might have affected their motility, and therefore the movement of the VSG on the cell surface in the direction of the flagellar pocket (Engstler et al. 2007).

The reduced rates of internalisation of surface VSG221 in the pre-cytokinesis stalled parasites after blocking VSG221 synthesis could provide an explanation for

the rapid clearance of these cells from the bloodstream of infected mice (Sheader et al. 2005). Possibly immune complexes were not cleared sufficiently quickly from the VSG coat of *T. brucei* where *VSG221* RNAi had been induced resulting in cell lysis by the alternative complement pathway or phagocytosis.

Chapter 8

Conclusions and future perspectives

8.1. Synthesis of Variant Surface Glycoprotein of *Trypanosoma brucei* as a cell cycle check point

Induction of *VSG221* RNAi revealed the presence of one of the few precise cell cycle check points discovered in *T. brucei*, as blocking VSG221 synthesis resulted in parasites that were stalled pre-cytokinesis (Chapter 3.2.1, Figure 3.1C and Figure 3.2) (Sheader et al. 2005). The *VSG221* RNAi-triggered growth arrest was accompanied by a global block in translation and evidence was shown suggesting that it was due to inhibition of translation initiation (Chapter 3.2.2, Figure 3.4) (T. K. Smith et al. 2009). As an early divergent eukaryote, *T. brucei* has different mechanisms for regulation of transcription and translation compared with other model eukaryotes. We did not detect any changes in a number of translation factors that are commonly involved in translation initiation that could explain the observed block in translation initiation (Chapter 3.2.3, Figure 3.5). However, other translation factors may have been involved. The investigation of the cause of the *VSG221* RNAi-induced translation arrest was limited by the available detection methods, such as available antibodies, known signaling cascades and the sensitivity of analyses.

In order to understand the signaling cascade that led to the precise cell cycle block, we attempted to identify whether the parasites sensed *VSG* mRNA or protein (Chapter 6). The Engstler laboratory has hypothesized that *T. brucei* senses the total level of *VSG* mRNA through the highly conserved *VSG* 3'UTR and that expression of high levels of *VSG* 3'UTR could alleviate the *VSG* RNA-triggered growth arrest. It was, however, observed that expression of high levels of *eGFP* with a *VSG221* 3'UTR from the active *VSG221* Expression site did not rescue the cells after blocking VSG221 synthesis (Chapter 3.2.2.1, Figure 3.3A and B and Chapter 6.2.1,

Figure 6.1A). Thus, we concluded that the observed cell cycle arrest was not triggered through the parasite sensing a drop in *VSG* transcript via the *VSG* 3'UTR.

To address whether *T. brucei* senses a drop in intracellular levels of *VSG* mRNA to cause a cell cycle arrest, the cells were treated with anti-*VSG221* morpholino oligonucleotides that specifically blocked the synthesis of VSG221 protein but did not cause the degradation of the *VSG221* transcript (Chapter 6.2.2, Figure 6.2). Treatment with anti-*VSG221* morpholino oligos inhibited the growth of the parasites and caused an accumulation in 2K2N cells, similar to that observed after induction of *VSG221* RNAi (Chapter 6.2.2.1, Figure 6.2A and Chapter 6.2.2.3, Figure 6.4). Although it was not possible to exclude that the morpholino-targeted *VSG221* mRNA was sequestered in the cells in a way that was interpreted by the parasites as a loss of *VSG221* transcript, this was considered unlikely. It therefore appeared that *T. brucei* senses a decrease in VSG protein synthesis rather than *VSG* transcript. It is therefore necessary to further study the synthesis and translocation of the VSG protein within the cell to identify what initiates the signaling cascade operating behind the *VSG* RNAi-induced cell cycle check point.

The abundance of VSG protein presents a formidable challenge to its investigation. Expression of high levels of mutant VSG protein that cannot pass the quality control of *T. brucei* is likely to be toxic to the cells, obscuring phenotypic interpretation. The Cross laboratory has reported a study of expression of mutant VSGs, where the introduction of mutations, such as the insertion of HA-tags and the deletion of conserved sequences drastically reduced the levels of expression of the mutant VSG (J. Wang et al. 2003). As was observed after the induction of *VSG221* RNAi in cells that expressed low levels of *VSG117* from a construct integrated in either the 177 bp repeats, or the αβ-tubulin array, that expression of insufficient

levels of VSG protein was detrimental to the growth of the parasites, (Chapter 4.2.7, Figure 4.8 and Figure 4.9). However, we showed that the expression of a second *VSG*, *VSG117*, from the active *VSG221* Expression site resulted in sufficiently high levels of VSG117 protein allowing the alleviation of the growth arrest generated by the induction of *VSG221* RNAi (Chapter 4.2.5, Figure 4.6). This in addition confirmed that the *VSG* RNAi-triggered phenotype was not a consequence of a toxic effect of high levels of siRNAs generated from the degradation of the highly abundant *VSG221* transcript.

VSG221-VSG117 double-expressor *T. brucei* presented both VSGs on the cell surface, which was consistent with previously reported results (Chapter 4.2.4, Figure 4.5) (Muñoz-Jordán et al. 1996). The Cross laboratory has reported that parasites expressing a heterogeneous VSG surface coat can proliferate in immunocompetent mice (Muñoz-Jordán et al. 1996). We also found that the mixed VSG coat of the VSG221-VSG117 double-expressor *T. brucei* rendered the cells fully resistant to complement-mediated lysis *in vitro* (Chapter 5.2.4, Figure 5.8C). In our experimental system, however, the second *VSG* was expressed from immediately downstream of the promoter of the active *VSG* Expression site, rather than the telomeric location reported by the Cross laboratory (Chapter 4.2.3, Figure 4.3). These results showed that the simultaneous expression of two VSGs from the same active *VSG* Expression site is not intrinsically detrimental to the growth of the parasites, although concurrent activation of two *VSG* Expression sites has been reported to be highly unstable in *T. brucei* (Chaves et al. 1999).

To further investigate the sensing mechanisms operating behind the *VSG* RNAi-induced phenotype, high levels of a protein containing a VSG three dimensional fold could be expressed from the active *VSG* Expression site. This may

help determine whether the growth inhibition observed after the induction of *VSG* RNAi could be alleviated by the expression of a protein with a VSG fold. Examples of proteins that have tertiary structures similar to VSG are ISG65 and ISG75, which did not show upregulated expression after the induction of *VSG221* RNAi (Chapter 6.2.4, Figure 6.6). Both ISG65 and ISG75 are anchored to the cell surface through a transmembrane domain, rather than a GPI anchor. Since over-expression of these two proteins could cause steric constraint on the pellicular membrane and be toxic to the parasites, the ISGs could be modified to include a GPI attachment signal to resemble VSGs and be expressed from the active *VSG* Expression site.

VSG protein synthesis might be the trigger for the activation of the pre-cytokinesis cell cycle check point. Therefore, it would be interesting to attempt selective degradation of the VSG protein after it has been synthesized. Since VSGs are secreted proteins, their synthesis is accompanied by simultaneous translocation into the endoplasmic reticulum. Recently reported methods of targeted protein degradation rely on the expression of a protein of interest fused to a destabilisation domain, or utilization of the ubiquitin-proteasome pathway. These methods have been successfully employed for cytosolic proteins (Banaszynski et al. 2006; Raina & Crews 2010). To investigate secreted proteins, it would be necessary to develop a new system to achieve targeted degradation of VSG. This could involve the expression of an inducible exogenous protease with a secretory signal, together with the simultaneous production of a mutant VSG with an incorporated recognition site for that particular protease.

8.2. The VSG surface coat

The highly conserved architecture of the bloodstream Expression sites in *T. brucei* raised the question of the importance of the telomeric location of the *VSG* gene for expression levels necessary to form a protective VSG surface coat. High levels of VSG117 protein were expressed from a construct integrated immediately downstream of the promoter of the active Expression site (Chapter 4.2.3, Figure 4.7, Chapter 4.2.6, Figure 4.3 and Chapter 5.2.1.2, Figure 5.3 and Figure 5.4). The functionality of the VSG117 surface coat was rigorously tested through the deletion of the telomeric *VSG221* from the active ES (Chapter 5.2.1.3, Figure 5.5A). The VSG117 surface coat rendered the parasites resistant to complement system-mediated lysis, and did not interfere with the ability of the parasites to switch to a new VSG (Chapter 5.2.4, Figure 5.8D and Chapter 5.2.5, Figure 5.9 and Figure 5.10). This suggested that the location of the *VSG* gene at the 3' end of the Expression site is not essential for levels of expression necessary for protectiveness. The invariably telomeric location of the active VSG is likely to be an important factor for its recombinogenicity. The presence of flanking repeat sequences at the telomeric VSG may be initiation sites for homologous recombination, allowing the parasites access to the extensive genomic reservoir of silent *VSGs* during antigenic variation (Shah et al. 1987).

T. brucei has very high rates of recycling of the VSG surface coat. This allows the trypanosome to survive in the presence of low levels of anti-VSG antibodies in the bloodstream of an infected host (Barry 1979; O'Beirne et al. 1998; Balber et al. 1979; McLintock et al. 1993). Induction of *VSG221* RNAi, however, results in rapid clearance of parasites from the bloodstream of infected mice (Sheader

et al. 2005). Our investigation of the dynamics of internalisation of the surface VSG221 coat after induction of *VSG221* RNAi revealed that VSG221 was cleared from the cell surface of induced cells at reduced rates compared with a wild-type population (Chapter 7.2.1, Figure 7.1A). The decreased rate of endocytosis of VSG221 after blocking VSG221 synthesis was not due to the inhibited growth of the parasites, because induction of *TDP 1* RNAi also caused a growth arrest, but did not affect the internalisation of surface VSG221 (Chapter 7.2.1, Figure 7.1B and Appendix II, Figure A2.1). General endocytosis occurred at wild-type rates after the induction of *VSG221* RNAi, which eliminated that as a possible cause for the impaired clearance of the VSG221 surface coat (Chapter 7.2.2, Figure 7.2A and Figure 7.3A).

The Engstler laboratory has shown that trypanosome motility creates a hydrodynamic pressure on the cell surface, which causes the rapid unidirectional movement of the VSG-antibody complexes towards the flagellar pocket (Chapter 1.10, Figure 1.14) (Engstler et al. 2007). Therefore, we hypothesized that the decreased motility of the parasites, in which *VSG* RNAi has been induced, could be responsible for the decreased internalisation of surface VSG. This was supported by the observation that the cells stalled at the pre-cytokinesis stage, which have a shortened and rounded morphology and two flagella, were particularly affected (Chapter 7.2.3, Figure 7.4). To test this hypothesis it would be necessary to perform motility studies on the parasites after induction of *VSG221* RNAi. The cells would have to be stained for DNA content with a non-toxic dye that would not affect viability and would allow discrimination between the G1-, S- and G2/M-phase cell populations. This would permit the determination of the rates of motility of the different cell populations in the induced cells. This would allow us to establish

whether there is a direct correlation between rates of motility and rates of surface VSG internalisation.

In addition, it is important to further investigate the precise mechanisms of cell lysis after induction of *VSG221* RNAi. Preliminary data from Dr V. Denninger in our laboratory suggest that the parasites are not susceptible to lysis via the alternative pathway of the complement system after blocking VSG221 synthesis. However, there appears to be increased deposition of C3 complement on the surface of induced cells, which correlates with reduced rates of surface VSG internalisation. This suggests that the VSG surface coat integrity is not compromised but rates of clearance of immune complexes from the cell surface may have been reduced, causing the eventual lysis of the parasites. To test this further, the induced cells can be incubated in the presence of macrophages, as well as specific anti-VSG221 antibodies. This would help elucidate the mechanisms of lysis in the bloodstream of infected mice after induction of *VSG221* RNAi.

8.3. *VSG* RNAi-induced phenotype – is this an extreme manifestation of a biologically relevant protective mechanism?

T. brucei appears to adjust its growth rates according to available intracellular levels of VSG protein. Although we achieved high levels of expression of *VSG117* from the active *VSG221* Expression site, the stability of the *VSG117* mRNA might have been suboptimal due to the use of αβ-tubulin 5'UTR, rather than *VSG* 5'UTR on the *VSG117* transcript (Figure 4.2). Possibly, there were slightly reduced levels of expression of VSG117 due to reduced stability of the *VSG117* mRNA. This could

have resulted in the decrease in growth rate observed in theV117Δ221 *T. brucei* cell line, compared with the VSG221 single-expressor and the VSG117-VSG221 double-expressor *T. brucei* (Figure 5.6B).

Induction of *VSG221* RNAi in *T. brucei* caused a growth inhibition, but cells survived *in vitro* for several days post induction (Chapter 3.2.1, Figure 3.1C and Figure 3.3B). Although blocking VSG synthesis triggered an arrest in global translation, uptake of amino acids, as well as general endocytosis continued in these cells (Chapter 3.2.2 and Chapter 7.2.2, Figure 7.2 and Figure 7.3) (T. K. Smith et al. 2009). This suggested that the stalled cells had entered a state of quiescence. This was supported by the fact that the *VSG221* RNAi-caused growth arrest was reversible. (Chapter 3.2.4, Figure 3.7). This indicated that the growth inhibition caused by blocking VSG synthesis was not a dead end lethal phenotype.

These results implied that there is a strong evolutionary selection pressure on *T. brucei* to maintain the integrity of its VSG surface coat and prevent its dilution. The cells might therefore be able to regulate their growth rates in response to rates of VSG protein synthesis. Therefore, *VSG* RNAi-induced inhibition of cell division may be an extreme manifestation of a biologically relevant mechanism, allowing the parasites to survive in the hostile environment of the host bloodstream despite minor fluctuations in the levels of VSG.

In conclusion, it was found that VSG synthesis is monitored as part of an important cell cycle check point in *T. brucei* and induction of *VSG* RNAi stalled the parasites at the pre-cytokinesis stage of the cell cycle. We showed that the *VSG* RNAi-triggered global translation arrest was due to a block in translation initiation. The *VSG221* RNAi-induced growth inhibition could be alleviated by expressing high levels of *VSG117* (that was not recognised by the *VSG221* RNAi) from the active

VSG221 Expression site. In addition, during this check point *T. brucei* appeared to sense the lack of VSG protein synthesis or processing rather than levels of *VSG* transcript after induction of *VSG* RNAi. We also showed that blocking VSG synthesis resulted in a decrease in the rates of endocytosis of surface VSG. This could provide an explanation for why trypanosomes are cleared so rapidly from the bloodstream of immunocompetent mice after the induction of *VSG* RNAi *in vivo*. It was determined that the telomeric location of the *VSG* gene within the conserved architecture of the *VSG* Expression site was not essential for high levels of expression necessary to form a protective VSG surface coat. Expression of high levels of a transgenic *VSG* from a promoter-adjacent position in the active *VSG* Expression site is an important step forward for studying the structure-function relationship of VSG proteins. This will also allow us to investigate further the signaling mechanisms operating behind the important *VSG* RNAi-induced cell cycle check point.

Chapter 9

References

Acosta-Serrano, A. et al., 2006. *Trypanosomes After the Genome* D. Barry et al., eds., Horizon Scientific Press.

Acosta-Serrano, A. et al., 1999. The procyclin repertoire of Trypanosoma brucei. Identification and structural characterization of the Glu-Pro-rich polypeptides. *The Journal of Biological Chemistry*, 274(42), p.29763–29771.

Acosta-serrano, A. et al., 2001. The surface coat of procyclic Trypanosoma brucei : Programmed expression and proteolytic cleavage of procyclin in the tsetse fly. *Proceedings of the National Academy of Sciences of the United States of America*, 98(4), pp.1513-1518.

Allen, C., Goulding, D. & Field, M.C., 2003. Clathrin-mediated endocytosis is essential in Trypanosoma brucei. *EMBO Journal*, 22(19), pp.4991-5002.

Amiguet-Vercher, A. et al., 2004. Loss of the mono-allelic control of the VSG expression sites during the development of Trypanosoma brucei in the bloodstream. *Molecular Microbiology*, 51(6), p.1577–1588.

Aslett, M. et al., 2010. TriTrypDB: a functional genomic resource for the Trypanosomatidae. *Nucleic acids research*, 38(Database issue), pp.D457-62.

Auffret, C.A. & Turner, M.J., 1981. Variant specific antigens of Trypanosoma brucei exist in solution as glycoprotein dimers. *The Biochemical journal*, 193(2), pp.647-50.

Balber, A.E. et al., 1979. Inactivation or elimination of potentially trypanolytic, complement-activating immune complexes by pathogenic trypanosomes. *Infection and immunity*, 24(3), p.617–627.

Baliga, B.S., Pronczvuk, A.W. & Munro, H.N., 1969. Mechanism in a Cell-free of Cycloheximide System Prepared Inhibition from Rat of Protein Liver. *Journal of Biological Chemistry*, 244(16), pp.4480-4489.

Banaszynski, L.A. et al., 2006. A rapid, reversible, and tunable method to regulate protein function in living cells using synthetic small molecules. *Cell*, 126(5), pp.995-1004.

Bangs, J.D. et al., 1992. Mass spectrometry of mRNA cap 4 from trypanosomatids reveals two novel nucleosides. *The Journal of Biological Chemistry*, 267(14), p.9805–9815.

Barrett, M.P. et al., 2003. The trypanosomiases. *Lancet*, 362(9394), pp.1469-80.

Barry, J.D., 1979. Capping of variable antigen on Trypanosoma brucei, and its immunological and biological significance. *Journal of Cell Science*, 37, p.287–302.

Barry, J.D. et al., 2005. What the genome sequence is revealing about trypanosome antigenic variation. *Biochemical Society transactions*, 33(Pt 5), pp.986-9.

Barry, J.D. & McCulloch, R., 2001. Antigenic variation in trypanosomes: enhanced phenotypic variation in a eukaryotic parasite. *Advances in parasitology*, 49, pp.1-70.

Bastin, P. et al., 2000. Flagellum ontogeny in trypanosomes studied via an inherited and regulated RNA interference system. *Journal of Cell Science*, 113(18), pp.3321-3328.

Benz, C. et al., 2010. Depletion of 14-3-3 proteins in bloodstream-form Trypanosoma brucei inhibits variant surface glycoprotein recycling. *International Journal for Parasitology*, 40(5), pp.629-34.

Berberof, M. et al., 1995. The 3'-terminal region of the mRNAs for VSG and procyclin can confer stage specificity to gene expression in Trypanosoma brucei. *The EMBO journal*, 14(12), pp.2925-34.

Bernards, A. et al., 1983. Growth of chromosome ends in multiplying trypanosomes. *Nature*, 303(5918), pp.592-597.

Bernards, A. et al., 1981. Activation of trypanosome surface glycoprotein genes involves a duplication-transposition leading to an altered 3' end. *Cell*, 27(3 Pt 2), pp.497-505.

Berriman, M. et al., 2002. The architecture of variant surface glycoprotein gene expression sites in Trypanosoma brucei. *Parasitology*, 122.

Berriman, M. et al., 2005. The Genome of the African Trypanosome Trypanosoma brucei. *Science*, 416, pp.416-22.

Bessat, M. & Ersfeld, K., 2009. Functional characterization of cohesin SMC3 and separase and their roles in the segregation of large and minichromosomes in Trypanosoma brucei. *Molecular Microbiology*, 71(6), pp.1371-1385.

Blum, M.L. et al., 1993. A structural motif in the variant surface glycoproteins of Trypanosoma brucei. *Nature*, 362, pp.603-609.

Borst, P., 2002. Antigenic variation and allelic exclusion. *Cell*, 109, pp.5-8.

Borst, P. & Cross, G.A.M., 1982. Molecular basis for trypanosome antigenic variation. *Cell*, 29(2), pp.291-303.

Brickman, M.J., Cook, J.M. & Balber, A.E., 1995. Low temperature reversibly inhibits transport from tubular endosomes to a perinuclear, acidic compartment in African trypanosomes. *Journal of cell science*, 108 (Pt 1, pp.3611-21.

Broadhead, R. et al., 2006. Flagellar motility is required for the viability of the bloodstream trypanosome. *Nature*, 440(7081), pp.224-7.

Brodersen, D.E. et al., 2000. The structural basis for the action of the antibiotics tetracycline, pactamycin, and hygromycin B on the 30S ribosomal subunit. *Medicine*, 103(7), pp.1143-1154.

Brun, R & Schönenberger, M., 1979. Cultivation and in vitro cloning or procyclic culture forms of Trypanosoma brucei in a semi-defined medium. Short communication. *Acta tropica*, 36(3), pp.289-92.

Brun, Reto et al., 2010. Human African trypanosomiasis. *The Lancet*, 375(9709), pp.148-159.

Bussler, H. et al., 1998. Determination of the disulfide bonds within a B domain variant surface glycoprotein from Trypanosoma congolense. *The Journal of biological chemistry*, 273(49), pp.32582-6.

Bülow, R., Nonnengässer, C. & Overath, P., 1989. Release of the variant glycoprotein during differentiation of bloodstream to procyclic forms of Trypanosoma brucei. *Molecular & Biochemical Parasitology*, 32(1), p.85–92.

Bülow, R., Overath, P. & Davoust, J., 1988. Rapid lateral diffusion of the variant surface glycoprotein in the coat of Trypanosoma brucei. *Biochemistry*, 27(7), p.2384–2388.

Callejas, S. et al., 2006. Hemizygous subtelomeres of an African trypanosome chromosome may account for over 75% of chromosome length. *Genome research*, 16(9), pp.1109-18.

Campbell, D.A., Van Bree, M.P. & Boothroyd, J.C., 1984. The 5'-limit of transposition and upstream barren region of a trypanosome VSG gene: tandem 76 base-pair repeats flanking (TAA)90. *Nucleic Acids Research*, 12(6), pp.2759-2774.

Campillo, N. & Carrington, M., 2003. The origin of the serum resistance associated (SRA) gene and a model of the structure of the SRA polypeptide from Trypanosoma brucei rhodesiense. *Molecular and Biochemical Parasitology*, 127(1), pp.79-84.

Carrington, M. & Boothroyd, J.C., 1996. Implications of conserved structural motifs in disparate trypanosome surface proteins. *Molecular and Biochemical Parasitology*, 81(2), pp.119-126.

Carrington, M. et al., 1991. Variant specific glycoprotein of Trypanosoma brucei consists of two domains each having an independently conserved pattern of cysteine residues. *Journal of cell science*, 221(3), pp.823-835.

Chattopadhyay, A. et al., 2005. Structure of the C-terminal domain from Trypanosoma brucei variant surface glycoprotein MITat1.2. *The Journal of biological chemistry*, 280(8), pp.7228-35.

Chaves, I. et al., 1999. Control of variant surface glycoprotein gene-expression sites in Trypanosoma brucei. *EMBO Journal*, 18(17), pp.4846-4855.

Chavrier, P. et al., 1990. Localization of low molecular weight GTP binding proteins to exocytic and endocytic compartments. *Cell*, 62(2), pp.317-329.

Chung, W.-L., Carrington, M. & Field, M.C., 2004. Cytoplasmic targeting signals in transmembrane invariant surface glycoproteins of trypanosomes. *The Journal of Biological Chemistry*, 279(52), p.54887–54895.

Clayton, C.E., 2002. Life without transcriptional control? From fly to man and back again. *The EMBO journal*, 21(8), pp.1881-1888.

Coppens, I. et al., 1987. Receptor mediated endocytosis in the Bloodstream form of Trypanosoma brucei. *Journal of Protozoology*, 34(4), pp.465-473.

Cross, G.A.M., 2002. Antigenic variation in African trypanosomes and malaria. *Molecular medical parasitology*, p.89–110.

Cross, G.A.M., 1996. Antigenic variation in trypanosomes: secrets surface slowly. *Bioessays*, 18(4), pp.283-91.

Cross, G.A.M., 1975. Identification, purification and properties of clone-specific glycoprotein antigens constituting the surface coat of Trypanosoma brucei. *Parasitology*, 71(3), pp.393-417.

Culjkovic, B., Topisirovic, I. & Borden, K.L.B., 2007. Controlling gene expression through RNA regulons: the role of the eukaryotic translation initiation factor eIF4E. *Cell Cycle*, 6(1), p.65–9.

Cully, D.F., Ip, H.S. & Cross, G.A.M., 1985. Coordinate transcription of variant surface glycoprotein genes and an expression site associated gene family in Trypanosoma brucei. *Cell*, 42(1), pp.173-82.

Danielsson, C. et al., 1994. Soluble complement receptor type 1 (CD35) is released from leukocytes by surface cleavage. *European Journal of Immunology*, 24(11), p.2725–2731.

Davies, K.P., Carruthers, V.B. & Cross, G.A.M., 1997. Manipulation of the vsg co-transposed region increases expression-site switching in Trypanosoma brucei. *Molecular and biochemical parasitology*, 86(2), pp.163-77.

Dean, S.D. & Matthews, K.R., 2007. Restless Gossamers : Antibody Clearance by Hydrodynamic Flow Forces Generated at the Surface of Motile Trypanosome Parasites. *Cell Host and Microbe*, 2(5), pp.279-281.

Deitch, A.D., Law, H. & deVere White, R., 1982. A stable propidium iodide staining procedure for flow cytometry. *The Journal of Histochemistry & Cytochemistry*, 30(9), pp.967-972.

Denny, P.W. et al., 2002. Leishmania RAB7: characterisation of terminal endocytic stages in an intracellular parasite. *Molecular & Biochemical Parasitology*, 123(2), p.105–113.

Dhalia, R. et al., 2006. The two eIF4A helicases in Trypanosoma brucei are functionally distinct. *Nucleic acids research*, 34(9), pp.2495-507.

Djikeng, A. et al., 2003. An siRNA ribonucleoprotein is found associated with polyribosomes in Trypanosoma brucei. *RNA*, 9(7), pp.802-808.

Du, L. & Gatti, R.A., 2010. Potential therapeutic applications of antisense morpholino oligonucleotides in modulation of splicing in primary immunodeficiency diseases. *Journal of immunological methods*, 365(1-2), pp.1-7.

Dubois, M.E., Demick, K.P. & Mansfield, J.M., 2005. Trypanosomes Expressing a Mosaic Variant Surface Glycoprotein Coat Escape Early Detection by the Immune System. *Infection and Immunity*, 73(5), pp.2690-2697.

Duggan, A.J. & Hutchinson, M.P., 1966. Sleeping sickness in Europeans: a review of 109 cases. *Journal of Tropical medicine and Hygiene*, 69(6), pp.124-31.

Ehlers, B., Czichos, J. & Overath, P., 1987. RNA turnover in Trypanosoma brucei. *Molecular and cellular biology*, 7(3), pp.1242-9.

Eisen, J.S. & Smith, J.C., 2008. Controlling morpholino experiments: don't stop making antisense. *Development*, 135(10), pp.1735-1743.

El-Sayed, N.M.A. et al., 2000. The African trypanosome genome. *International journal for parasitology*, 30(4), pp.329-45.

El-Sayed, N.M.A. et al., 2005. Comparative genomics of trypanosomatid parasitic protozoa. *Science*, 309(5733), p.404–409.

Engstler, M. & Boshart, M., 2004. Cold shock and regulation of surface protein trafficking convey sensitization to inducers of stage differentiation in Trypanosoma brucei. *Genes & Development*, 18(22), pp.2798-2811.

Engstler, M. et al., 2007. Hydrodynamic Flow-Mediated Protein Sorting on the Cell Surface of Trypanosomes. *Cell*, 131, pp.505-515.

Engstler, M. et al., 2004. Kinetics of endocytosis and recycling of the GPI- anchored variant surface glycoprotein in Trypanosoma brucei. *Journal of Cell Science*, 117(7), pp.1105-1115.

Engstler, M. et al., 2005. The membrane-bound histidine acid phosphataseTbMBAP1 is essential for endocytosis and membrane recycling in Trypanosoma brucei. *Journal of Cell Science*, 118(10), pp.2105-2118.

Erondu, N.E. & Donelson, J.E., 1992. Differential expression of two mRNAs from a single gene encoding an HMG1-like DNA binding protein of African trypanosomes. *Molecular & Biochemical Parasitology*, 51(1), pp.111-8.

Ersfeld, K. & Gull, K., 1997. Partitioning of Large and Minichromosomes in Trypanosoma brucei. *Science*, 276, pp.611-614.

Ersfeld, K., Melville, S.E. & Gull, K., 1999. Nuclear and genome organization of Trypanosoma brucei. *Parasitology today*, 15(2), pp.58-63.

Ferguson, M.A.J. et al., 1986. Biosynthesis of Trypanosoma brucei variant surface glycoproteins. N-glycosylation and addition of a phosphatidylinositol membrane anchor. *The Journal of biological chemistry*, 261(1), pp.356-62.

Fernandes, A.P., Nelson, K. & Beverley, S.M., 1993. Evolution of nuclear ribosomal RNAs in kinetoplastid protozoa: perspectives on the age and origins of parasitism. *Proceedings of the National Academy of Sciences of the United States of America*, 90(24), pp.11608-12.

Ferrante, A. & Allison, A.C., 1983. Alternative pathway activation of complement by African trypanosomes lacking a glycoprotein coat. *Parasite immunology*, 5(5), pp.491-8.

Field, M.C. & Carrington, M., 2009. The trypanosome flagellar pocket. *Nature Reviews Microbiology*, 7(11), pp.775-786.

Figueiredo, L.M. & Cross, G.A.M., 2009. Nucleosomes are depleted at the VSG expression site transcribed by RNA polymerase I in African trypanosomes. *Eukaryotic Cell*, 9(1), pp.148-54.

Figueiredo, L.M., Janzen, C.J. & Cross, G.A.M., 2008. A Histone Methyltransferase Modulates Antigenic Variation in African Trypanosomes. *PLoS Biology*, 6(7), p.e161.

Fire, A. et al., 1998. Potent and specific genetic interference by double-stranded RNA in Caenorhabditis elegans. *Nature*, 391(6669), pp.806-811.

Frearson, J.A. et al., 2010. N-myristoyltransferase inhibitors as new leads to treat sleeping sickness. *Nature*, 464(7289), pp.728-732.

Freire, E.R. et al., 2010. The four trypanosomatid eIF4E homologues fall into two separate groups, with distinct features in primary sequence and biological properties. *Molecular and biochemical parasitology*, 176(1), pp.25-36.

Freistadt, M.S., Cross, G.A.M. & Robertson, H.D., 1988. Discontinuously synthesized mRNA from Trypanosoma brucei contains the highly methylated 5′ cap structure, m7GpppA*A*C (2′-O) mU*A. *The Journal of Biological Chemistry*, 263(29), p.15071– 15075.

Fujita, T., 2002. Evolution of the lectin–complement pathway and its role in innate immunity. *Nature Reviews Immunology*, 2(5), p.346–353.

Furger, A. et al., 1997. Elements in the 3′ untranslated region of procyclin mRNA regulate expression in insect forms of Trypanosoma brucei by modulating RNA stability and translation. *Molecular and Cellular Biology*, 17(8), p.4372–4380.

Galanti, N. et al., 1998. Histone genes in trypanosomatids. *Parasitology today*, 14(2), pp.64-70.

Gear, J.H. & Miller, G.B., 1986. The clinical manifestations of Rhodesian trypanosomiasis: an account of cases contracted in the Okavango swamps of Botswana. *The American journal of tropical medicine and hygiene*, 35(6), pp.1146-52.

Gebauer, F. & Hentze, M.W., 2004. Molecular mechanisms of translational control. *Nature Reviews Molecular and Cellular Biology*, 5(10), p.827–835.

Goodfellow, I.G. & Roberts, L.O., 2008. Eukaryotic initiation factor 4E. *International Journal of Biochemical and Cellular Biology*, 40(12), p.2675–80.

Gottesdiener, K.M., 1994. A new VSG expression site-associated gene (ESAG) in the promoter region of Trypanosoma brucei encodes a protein with 10 potential transmembrane domains. *Molecular & Biochemical Parasitology*, 63(1), p.143–151.

Gottesdiener, K.M. et al., 1990. Chromosome organization of the protozoan Trypanosoma brucei. *Molecular and cellular biology*, 10(11), pp.6079-83.

Grünfelder, C.G. et al., 2002. Accumulation of a GPI-anchored protein at the cell surface requires sorting at multiple intracellular levels. *Traffic*, 3(8), p.547–559.

Grünfelder, C.G. et al., 2003. Endocytosis of a Glycosylphosphatidylinositol-anchored Protein via Clathrin-coated Vesicles , Sorting by Default in Endosomes , and Exocytosis via RAB11-positive Carriers □. *Molecular Biology of the Cell*, 14(5), pp.2029 -2040.

Gull, K., 2003. Host-parasite interactions and trypanosome morphogenesis: a flagellar pocketful of goodies. *Current opinion in microbiology*, 6(4), p.365–370.

Günzl, A. et al., 2003. RNA Polymerase I Transcribes Procyclin Genes and Variant Surface Glycoprotein Gene Expression Sites in Trypanosoma brucei. *Eukaryotic cell*, 2(3), pp.542-551.

Hall, B.S. et al., 2006. TbVps34, the trypanosome orthologue of Vps34, is required for Golgi complex segregation. *The Journal of Biological Chemistry*, 281(37), pp.27600-12.

Hall, B.S. et al., 2005. Trypanosoma brucei : TbRAB4 regulates membrane recycling and expression of surface proteins in procyclic forms. *Experimental Parasitology*, 111, pp.160-171.

Hall, B.S. et al., 2004. Rab4 Is an Essential Regulator of Lysosomal Trafficking in Trypanosomes. *The Journal of biological chemistry*, 279(43), pp.45047-45056.

Hamilton, P.B. et al., 2004. Trypanosomes are monophyletic: evidence from genes for glyceraldehyde phosphate dehydrogenase and small subunit ribosomal RNA. *International journal for parasitology*, 34(12), pp.1393-404.

Hammarton, T.C. et al., 2003. Stage-specific differences in cell cycle control in Trypanosoma brucei revealed by RNA interference of a mitotic cyclin. *The Journal of biological chemistry*, 278(25), pp.22877-86.

Hammarton, T.C., Monnerat, S. & Mottram, J.C., 2007. Cytokinesis in trypanosomatids. *Current opinion in microbiology*, 10(6), pp.520-7.

Helms, M.J. et al., 2006. Bloodstream form Trypanosoma brucei depend upon multiple metacaspases associated with RAB11-positive endosomes. *Journal of cell science*, 119(Pt 6), pp.1105-17.

Hertz-Fowler, C. et al., 2008. Telomeric expression sites are highly conserved in Trypanosoma brucei. *PloS one*, 3(10), p.e3527.

Hirumi, H. & Hirumi, K., 1989. Continuous Cultivation of Trypanosoma brucei Blood Stream Forms in a Medium Containing a Low Concentration of Serum Protein without Feeder Cell Layers. *The Journal of Parasitology*, 75(6), pp.985-989.

Hoek, M., Engstler, M. & Cross, G.A.M., 2000. Expression-site-associated gene 8 (ESAG8) of Trypanosoma brucei is apparently essential and accumulates in the nucleolus. *Journal of Cell Science*, 113(22), p.3959–3968.

Hoek, M., Zanders, T. & Cross, G.A.M., 2002. Trypanosoma brucei expression-site-associated-gene-8 protein interacts with a Pumilio family protein. *Molecular & Biochemical Parasitology*, 120(2), p.269–283.

Horn, D. & Barry, J.D., 2005. The central roles of telomeres and subtelomeres in antigenic variation in African trypanosomes. *Chromosome Research*, 13, pp.525-533.

Hotz, H.-R. et al., 1997. Mechanisms of developmental regulation in Trypanosoma brucei: a polypyrimidine tract in the 3′-untranslated region of a surface protein

mRNA affects RNA abundance and translation. *Nucleic Acids Research*, 25(15), p.3017–3026.

Hughes, K. et al., 2007. A novel ISWI is involved in VSG expression site downregulation in African trypanosomes. *The EMBO journal*, 26(9), pp.2400-10.

Hutchinson, O.C. et al., 2003. VSG structure: similar N-terminal domains can form functional VSGs with different types of C-terminal domain. *Molecular and Biochemical Parasitology*, 130(2), pp.127-131.

Iida, K. & Nussenzweig, V., 1981. Complement receptor is an inhibitor of the complement cascade. *Journal of Experimental Medicine*, 153(5), p.1138–1150.

Jackson, D.G., Windle, H.J. & Voorheis, H.P., 1993. The identification, purification, and characterization of two invariant surface glycoproteins located beneath the surface coat barrier of bloodstream forms of Trypanosoma brucei. *The Journal of Biological Chemistry*, 268(11), p.8085–95.

Jelinek, T. et al., 2002. Cluster of African trypanosomiasis in travelers to Tanzanian national parks. *Emerging infectious diseases*, 8(6), pp.634-5.

Jones, D.T., 1999. Protein secondary structure prediction based on position-specific scoring matrices. *Journal of molecular biology*, 292(2), pp.195-202.

Jones, N.G. et al., 2008. Structure of a Glycosylphosphatidylinositol-anchored Domain from a Trypanosome Variant Surface Glycoprotein. *Journal of Biological Chemistry*, 283(6), pp.3584 -3593.

Kabiri, M. & Steverding, D., 2000. Studies on the recycling of transferrin receptor in Trypanosoma brucei using an inducible gene expression system. *European Journal of Biochemistry*, 267(11), p.3309–3314.

Kabsch, W. & Sander, C., 1983. Protein Secondary Structure: Pattern Recognition of Hydrogen-Bonded and Geometrical Features. *Biopolymers*, 22(12), pp.2577-2637.

Khera, R. & Das, N., 2009. Complement Receptor 1 : Disease associations and therapeutic implications. *Molecular Immunology*, 46, pp.761-772.

Kooter, J.M. et al., 1987. The anatomy and transcription of a telomeric expression site for variant-specific surface antigens in T. brucei. *Cell*, 51(2), pp.261-72.

Kramer, S. et al., 2008. Heat shock causes a decrease in polysomes and the appearance of stress granules in trypanosomes independently of eIF2(alpha) phosphorylation at Thr169. *Journal of cell science*, 121(Pt 18), pp.3002-14.

Kumar, P. & Wang, C.C., 2005. Depletion of anaphase-promoting complex or cyclosome (APC/C) subunit homolog APC1 or CDC27 of Trypanosoma brucei

arrests the procyclic form in metaphase but the bloodstream form in anaphase. *The Journal of biological chemistry*, 280(36), pp.31783-91.

Kuo, W.-L. et al., 2010. Efficacy of the multi-kinase inhibitor enzastaurin is dependent on cellular signaling context. *Molecular cancer therapeutics*, 9(10), pp.2814-24.

LaCount, D.J., Barrett, B. & Donelson, J.E., 2002. Trypanosoma brucei FLA1 is required for flagellum attachment and cytokinesis. *The Journal of Biological Chemistry*, 277(20), pp.17580-8.

Lambrecht, F.L., 2011. Palaeoecology of Tsetse Flies and Sleeping Sickness in Africa. *Proceedings of the National Academy of Sciences of the United States of America*, 124(5), pp.367-385.

Langreth, S.G. & Balber, A.E., 1975. Protein uptake and digestion in bloodstream and culture forms of Trypanosoma brucei. *The Journal of Protozoology*, 22(1), p.40–53.

Law, S.K.A. & Reid, K.B.M., 1995. *Complement* 2nd ed., Oxford University Press.

Lejon, V. et al., 1998. A semi-quantitative ELISA for detection of Trypanosoma brucei gambiense specific antibodies in serum and cerebrospinal fluid of sleeping sickness patients. *Acta tropica*, 69(2), pp.151-64.

Lejon, V. et al., 2003. Human African trypanosomiasis: quantitative and qualitative assessment of intrathecal immune response. *European journal of neurology*, 10(6), pp.711-9.

Li, Z. & Wang, C.C., 2003. A PHO80-like cyclin and a B-type cyclin control the cell cycle of the procyclic form of Trypanosoma brucei. *The Journal of biological chemistry*, 278(23), pp.20652-8.

Liang, X.-hai et al., 2003. trans and cis splicing in trypanosomatids: mechanism, factors, and regulation. *Eukaryotic Cell*, 2(5), p.830–40.

Ligtenberg, M.J.L. et al., 1994. Reconstitution of a surface transferrin binding complex in insect form Trypanosoma brucei. *The EMBO journal*, 13(11), pp.2565-73.

Lillico, S.G. et al., 2003. Essential roles for GPI-anchored proteins in African trypanosomes revealed using mutants deficient in GPI8. *Molecular Biology of the Cell*, 14(3), pp.1182-1194.

Liu, A.Y.C. et al., 1983. The transposition unit of variant surface glycoprotein gene 118 of Trypanosoma brucei. Presence of repeated elements at its border and absence of promoter-associated sequences. *Journal of Molecular Biology*, 167(1), pp.57-75.

Magnus, E., Vervoort, T. & Van Meirvenne, N., 1978. A card-agglutination test with stained trypanosomes (C.A.T.T.) for the serological diagnosis of T. b. gambiense trypanosomiasis. *Ann. Soc. Belg. Med. Trop.*, 58(3), pp.169-176.

Marcello, L. & Barry, J.D., 2007. Analysis of the VSG gene silent archive in Trypanosoma brucei reveals that mosaic gene expression is prominent in antigenic variation and is favored by archive substructure. *Genome Research*, 17(9), pp.1344-1352.

Marcello, L. et al., 2007. VSGdb: a database for trypanosome variant surface glycoproteins, a large and diverse family of coiled coil proteins. *BMC bioinformatics*, 8, p.143.

Masterson, W.J., Taylor, D. & Turner, M.J., 1988. Topologic analysis of the epitopes of a variant surface glycoprotein of Trypanosoma brucei. *The Journal of Immunology*, 140(9), pp.3194-3199.

Matthews, K.R., 2005. The developmental cell biology of Trypanosoma brucei. *Journal of Cell Science*, 118(Pt 2), pp.283-290.

Matthews, K.R., Ellis, J.R. & Paterou, A., 2004. Molecular regulation of the life cycle of African trypanosomes. *Trends in Parasitology*, 20(1), pp.40-47.

Matthews, K.R. & Gull, K., 1994. Evidence for an Interplay between Cell Cycle Progression and the Initiation of Differentiation between Life Cycle Forms of African Trypanosomes. *The Journal of Cell Biology*, 125(5), pp.1147-1156.

Matthyssens, G. et al., 1981. Two variant surface glycoproteins of Trypanosoma brucei have a conserved C-terminus. *Nature*, 293, pp.230-233.

McCulloch, R., 2004. Antigenic variation in African trypanosomes: monitoring progress. *Trends in parasitology*, 20(3), pp.117-21.

McCulloch, R. et al., 2004. Transformation of monomorphic and pleomorphic Trypanosoma brucei. *Methods in Molecular Biology*, 262(1), pp.53-86.

McKean, P.G., 2003. Coordination of cell cycle and cytokinesis in Trypanosoma brucei. *Current Opinion in Microbiology*, 6(6), pp.600-607.

McLintock, L.M.L., Turner, C.M.R. & Vickerman, Keith, 1993. Comparison of the effects of immune killing mechanisms on Trypanosoma brucei parasites of slender and stumpy morphology. *Parasite immunology*, 15(8), p.475–480.

Mehlert, A., Bond, C.S. & Ferguson, M.A.J., 2002. The glycoforms of a Trypanosoma brucei variant surface glycoprotein and molecular modeling of a glycosylated surface coat. *Glycobiology*, 12(10), pp.607-612.

Mehlert, A. et al., 1998. The glycosylation of the variant surface glycoproteins and procyclic acidic repetitive proteins of Trypanosoma brucei. *Molecular and biochemical parasitology*, 91(1), pp.145-52.

Melville, S.E., Gerrard, C.S. & Blackwell, J.M., 1999. Multiple causes of size variation in the diploid megabase chromosomes of African trypanosomes. *Chromosome Research*, 7(3), pp.191-203.

Melville, S.E. et al., 1998. The molecular karyotype of the megabase chromosomes of Trypanosoma brucei and the assignment of chromosome markers. *Molecular and biochemical parasitology*, 94(2), pp.155-73.

Melville, S.E. et al., 2000. The molecular karyotype of the megabase chromosomes of Trypanosoma brucei stock 427. *Molecular and biochemical parasitology*, 111(2), pp.261-73.

Merkles, R.K. & Cummings, R.D., 1987. Relationship of the Terminal Sequences to the Length of Chains in Asparagine-linked Oligosaccharides from the Mouse Lymphoma Cell Line BW5147. *The Journal of Biological Chemistry*, 262(17), pp.8179-89.

Miller, E.N., Allan, L.M. & Turner, M.J., 1984a. Mapping of antigenic determinants within peptides of a variant surface glycoprotein of Trypanosoma brucei. *Molecular & Biochemical Parasitology*, 13(3), pp.309-322.

Miller, E.N., Allan, L.M. & Turner, M.J., 1984b. Topological analysis of antigenic determinants on a variant surface glycoprotein of Trypanosoma brucei. *Molecular & Biochemical Parasitology*, 13(1), pp.67-81.

Moulton, J.D. & Jiang, S., 2009. Gene knockdowns in adult animals: PPMOs and vivo-morpholinos. *Molecules*, 14(3), pp.1304-23.

Moulton, J.D. & Yan, Y.-L., 2008. Using Morpholinos to control gene expression. *Current protocols in molecular biology*, Chapter 26(July), p.Unit 26.8.

Mowatt, M.R. & Clayton, C.E., 1987. Developmental Regulation of a Novel Repetitive Protein of Trypanosoma brucei. *Molecular and Cellular Biology*, 7(8), pp.2838-2844.

Mowatt, M.R., Wisdom, G.S. & Clayton, C.E., 1989. Variation of Tandem Repeats in the Developmentally Regulated Procyclic Acidic Repetitive Proteins of Trypanosoma brucei. *Molecular and Cellular Biology*, 9(3), pp.1332-1335.

Mussmann, R. et al., 2004. Factors affecting the level and localization of the transferrin receptor in Trypanosoma brucei. *Journal of Biological Chemistry*, 279(39), p.40690–40698.

Muñoz-Jordán, J.L., Davies, K.P. & Cross, G.A.M., 1996. Stable expression of mosaic coats of variant surface glycoproteins in Trypanosoma brucei. *Science*, 272(5269), pp.1795-7.

Navarro, M. & Gull, K., 2001. A pol I transcriptional body associated with VSG mono-allelic expression in Trypanosoma brucei. *Nature*, 414(6865), pp.759-63.

Ngo, H. et al., 1998. Double-stranded RNA induces mRNA degradation in Trypanosoma brucei. *Proceedings of the National Academy of Sciences of the United States of America*, 95(December), pp.14687-14692.

Nolan, D.P., Geuskens, M. & Pays, E., 1999. N-linked glycans containing linear poly-N-acetyllactosamine as sorting signals in endocytosis in Trypanosoma brucei. *Current biology*, 9(20), pp.1169-72.

Ogbadoyi, E.O. et al., 2000. Architecture of the Trypanosoma brucei nucleus during interphase and mitosis. *Cell*, 108(8), pp.501-513.

Overath, P. & Engstler, M., 2004. Endocytosis , membrane recycling and sorting of GPI-anchored proteins : Trypanosoma brucei as a model system. *Molecular Microbiology*, 53(3), pp.735-744.

Overath, P., Stierhof, Y.-D. & Wiese, M., 1997. Endocytosis and secretion in trypanosomatid parasites—tumultuous traffic in a pocket. *Trends in Cell Biology*, 7(1), p.27–33.

O'Beirne, C., Lowry, C.M. & Voorheis, H.P., 1998. Both IgM and IgG anti-VSG antibodies initiate a cycle of aggregation-disaggregation of bloodstream forms of Trypanosoma brucei without damage to the parasite. *Molecular & Biochemical Parasitology*, 91(1), p.165–193.

Paindavoine, P. et al., 1992. A gene from the variant surface glycoprotein expression site encodes one of several transmembrane adenylate cyclases located on the flagellum of Trypanosoma brucei. *Molecular and Cellular Biology*, 12(3), p.1218–25.

Pal, A. et al., 2003. Rab5 and Rab11 mediate transferrin and anti-variant surface glycoprotein antibody recycling in Trypanosoma brucei. *Biochemical Journal*, 374(2), p.443–51.

Pal, A. et al., 2002. Differential endocytic functions of Trypanosoma brucei Rab5 isoforms reveal a glycosylphosphatidylinositol-specific endosomal pathway. *The Journal of Biological Chemistry*, 277(11), p.9529.

Pangburn, M.K. & Müller-Eberhard, H.J., 1984. The alternative pathway of complement. *Springer Seminars in Immunopathology*, 7, p.163–192.

Pays, E. et al., 1989. Trypanosoma brucei: posttranscriptional control of the variable surface glycoprotein gene expression site. *Molecular and cellular biology*, 9(9), pp.4018-21.

Pays, E. et al., 1985. Trypanosoma brucei: the extent of conversion in antigen genes may be related to the DNA coding specificity. *Cell*, 42(3), pp.821-9.

Pays, E. et al., 2001. The VSG expression sites of Trypanosoma brucei: multipurpose tools for the adaptation of the parasite to mammalian hosts. *Molecular & Biochemical Parasitology*, 114, pp.1 - 16.

Pays, E. et al., 1989. The genes and transcripts of an antigen gene expression site from T. brucei. *Cell*, 57(5), pp.835-45.

Pays, E., Vanhamme, L. & Perez-Morga, D., 2004. Antigenic variation in Trypanosoma brucei : facts , challenges and mysteries. *Current Opinion in Microbiology*, 7, pp.369-374.

Pei, Y. et al., 2010. Quantitative evaluation of siRNA delivery in vivo. *RNA*, 16(12), pp.2553-2563.

Perry, K.L., Watkins, K.P. & Agabian, N., 1987. Trypanosome mRNAs have unusual "cap 4" structures acquired by addition of a spliced leader. *Proceedings of the National Academy of Sciences of the United States of America*, 84(23), p.8190–8194.

Ploubidou, A. et al., 1999. Evidence for novel cell cycle checkpoints in trypanosomes : kinetoplast segregation and cytokinesis in the absence of mitosis. *Cell*, 4650, pp.4641-4650.

Raina, K. & Crews, C.M., 2010. Chemical inducers of targeted protein degradation. *The Journal of biological chemistry*, 285(15), pp.11057-60.

Ralston, K.S. et al., 2006. Flagellar motility contributes to cytokinesis in Trypanosoma brucei and is modulated by an evolutionarily conserved dynein regulatory system. *Eukaryotic cell*, 5(4), pp.696-711.

Redpath, M.B. et al., 2000. ESAG11, a new VSG expression site-associated gene from Trypanosoma brucei. *Molecular & Biochemical Parasitology*, 111(1), pp.223-8.

Robinson, D.R. & Gull, K., 1991. Basal body movements as a mechanism for mitochondrial genome segregation in the trypanosome cell cycle. *Nature*, 352(6337), pp.731-3.

Roditi, I., Carrington, M. & Turner, M., 1987. Expression of a polypeptide containing a dipeptide repeat is confined to the insect stage of Trypanosoma brucei. *Nature*, 325(6101), pp.272-4.

Roditi, I. & Liniger, M., 2002. Dressed for success: the surface coats of insect-borne protozoan parasites. *Trends in microbiology*, 10(3), pp.128-34.

Roditi, I. et al., 1989. Procyclin gene expression and loss of the variant surface glycoprotein during differentiation of Trypanosoma brucei. *The Journal of cell biology*, 108(2), pp.737-46.

Rodriguez, J.A. et al., 2009. Propulsion of African trypanosomes is driven by bihelical waves with alternating chirality separated by kinks. *Proceedings of the National Academy of Sciences of the United States of America*, 106(46), pp.19322-7.

Ross, R. & Thomson, D., 1910. A case of sleeping sickness studied by precise enumerative methods: regular periodical increase of the parasites disclosed. *Proceedings of the Royal Society of London*, 82(557), pp.411-425.

Rothberg, K.G. et al., 2006. The RACK1 homologue from Trypanosoma brucei is required for the onset and progression of cytokinesis. *The Journal of biological chemistry*, 281(14), pp.9781-90.

Rout, M.P. & Field, M.C., 2001. Isolation and characterization of subnuclear compartments from Trypanosoma brucei. Identification of a major repetitive nuclear lamina component. *The Journal of Biological Chemistry*, 276(41), pp.38261-71.

Rudenko, G. et al., 1998. Selection for activation of a new variant surface glycoprotein gene expression site in Trypanosoma brucei can result in deletion of the old one. *Molecular and Biochemical Parasitology*, 95(1), pp.97 - 109.

Salmon, D. et al., 1997. Characterization of the ligand-binding site of the transferrin receptor in Trypanosoma brucei demonstrates a structural relationship with the N-terminal domain of the variant surface glycoprotein. *The EMBO journal*, 16(24), pp.7272-8.

Samanta, A. et al., 2009. Morpholino, piperidino, and pyrrolidino derivatives of pyrimidine nucleosides as inhibitors of ribonuclease A: synthesis, biochemical, and crystallographic evaluation. *Journal of medicinal chemistry*, 52(4), pp.932-42.

Sambrook, J. & Russell, D., 2001. *Molecular Cloning: A Laboratory Manual*,

Schmid, C.L. & Bohn, L.M., 2010. Serotonin, but not N-methyltryptamines, activates the serotonin 2A receptor via a ß-arrestin2/Src/Akt signaling complex in vivo. *The Journal of neuroscience*, 30(40), pp.13513-24.

Schwartz, K.J. & Bangs, J.D., 2007. Regulation of protein trafficking by glycosylphosphatidylinositol valence in African trypanosomes. *Journal of Eukaryotic Microbiology*, 54(1), p.22–24.

Schwartz, K.J. et al., 2005. GPI valence and the fate of secretory membrane proteins in African trypanosomes. *Journal of Cell Science*, 118, pp.5499-5511.

Schwede, A. et al., 2011. The VSG C-terminal domain is inaccessible to antibodies on live trypanosomes. *Molecular and biochemical parasitology*, 175(2), pp.201-4.

Seyfang, A., Mecke, D. & Duszenko, M., 1990. Degradation, recycling, and shedding of Trypanosoma brucei variant surface glycoprotein. *The Journal of Protozoology*, 37(6), pp.546-52.

Shah, J.S. et al., 1987. The 5' flanking sequence of a Trypanosoma brucei variable surface glycoprotein gene. *Molecular and biochemical parasitology*, 24(2), pp.163-74.

Shapiro, S.Z. et al., 1984. Analysis by flow cytometry of DNA synthesis during the life cycle of African trypanosomes. *Acta tropica*, 41(4), p.313–23.

Sheader, K. et al., 2003. Delineation of the regulated Variant Surface Glycoprotein gene expression site domain of Trypanosoma brucei ϑ. *Parasitology*, 128, pp.147-156.

Sheader, K., te Vruchte, D. & Rudenko, G., 2004. Bloodstream form-specific up-regulation of silent vsg expression sites and procyclin in Trypanosoma brucei after inhibition of DNA synthesis or DNA damage. *The Journal of biological chemistry*, 279(14), pp.13363-74.

Sheader, K. et al., 2005. Variant surface glycoprotein RNA interference triggers a precytokinesis cell cycle arrest in African trypanosomes. *Proceedings of the National Academy of Sciences of the United States of America*, 102(24), pp.8716-21.

Sherwin, T. & Gull, K., 1989. The cell dividion cycle of Trypanosoma brucei brucei: timing of event markers and cytoskeletal modulations. *Philosophical transactions of the Royal Society of London. Series B, Biological sciences*, 323(1218), pp.573-88.

Shi, H. et al., 2009. RNA interference in Trypanosoma brucei: role of the n-terminal RGG domain and the polyribosome association of argonaute. *The Journal of Biological Chemistry*, 284(52), pp.36511-20.

Shi, H. et al., 2000. Genetic interference in Trypanosoma brucei by heritable and inducible double-stranded RNA. *RNA*, 6(7), pp.1069-1076.

Siegel, T.N., Hekstra, D.R. & Cross, G.A.M., 2008. Analysis of the Trypanosoma brucei cell cycle by quantitative DAPI imaging. *Molecular & Biochemical Parasitology*, 160, pp.171-174.

Smith, T.K. et al., 2009. Blocking Variant Surface Glycoprotein Synthesis in Trypanosoma brucei Triggers a General Arrest in Translation Initiation. *PloS one*, 4(10), p.e7532.

Sonenberg, N., 2008. eIF4E, the mRNA cap-binding protein: from basic discovery to translational research. *Biochemical and Cellular Biology*, 86(2), p.178–83.

Stanne, T.M. & Rudenko, G., 2010. Active VSG expression sites in Trypanosoma brucei are depleted of nucleosomes. *Eukaryotic cell*, 9(1), pp.136-47.

Steverding, D. et al., 1994. ESAG 6 and 7 products of Trypanosoma brucei form a transferrin binding complex. *European Journal of Cell Biology*, 64(1), p.78–87.

Steverding, D. et al., 1995. Transferrin-binding complex is the receptor for transferrin uptake in Trypanosoma brucei. *The Journal of Cell Biology*, 131(5), p.1173–1182.

Stich, A., Abel, P.M. & Krishna, S., 2002. Human African trypanosomiasis. *BMJ*, 325(7357), pp.203-206.

Summerton, J., 1999. Morpholino antisense oligomers: the case for an RNase H-independent structural type. *Biochimica et Biophysica Acta*, 1489(1), pp.141-58.

Thilo, L., 1985. Quantification of endocytosis-derived membrane traffic. *Biochimica at Biophysica Acta*, 822(2), p.243–266.

Triggs, V.P. & Bangs, J.D., 2003. Glycosylphosphatidylinositol-Dependent Protein Trafficking in Bloodstream Stage Trypanosoma brucei. *Society*, 2(1), pp.76-83.

Tyler, K.M., Matthews, K.R. & Gull, K., 2001. Anisomorphic cell division by African trypanosomes. *Protist*, 152(4), p.367–378.

Ullu, E., Matthews, K.R. & Tschudi, C., 1993. Temporal order of RNA processing reactions in trypanosomes: rapid trans splicing precedes polyadenylation of newly synthesized tubulin transcripts. *Molecular and Cellular biology*, 13(1), pp.720-725.

Van der Ploeg, L.H. et al., 1984. Chromosome rearrangements in Trypanosoma brucei. *Cell*, 39(1), pp.213-221.

Van der Ploeg, L.H., Liu, A.Y.C. & Borst, P., 1984. Structure of the growing telomeres of trypanosomes. *Cell*, 36(2), pp.459-468.

Van der Ploeg, L.H. et al., 1984. Antigenic variation in Trypanosoma brucei analyzed by electrophoretic separation of chromosome-sized DNA molecules. *Cell*, 37(1), pp.77-84.

Vassella, E. et al., 2000. A major surface glycoprotein of trypanosoma brucei is expressed transiently during development and can be regulated post-

transcriptionally by glycerol or hypoxia. *Genes & Development*, 14(5), p.615–626.

Vassella, E. et al., 2001. Multiple procyclin isoforms are expressed differentially during the development of insect forms of Trypanosoma brucei. *Journal of Molecular Biology*, 312(4), p.597–607.

Vickerman, K, 1985. Developmental cycles and biology of pathogenic trypanosomes. *British medical bulletin*, 41(2), pp.105-14.

von der Haar, T. et al., 2004. The mRNA cap-binding protein eIF4E in post-transcriptional gene expression. *Nature Structural & Molecular Biology*, 11(6), p.503–11.

Walrad, P. et al., 2009. Differential Trypanosome Surface Coat Regulation by a CCCH Protein That Co-Associates with procyclin mRNA. *PLoS Pathogens*, 5(2), p.e1000317.

Wang, J., Böhme, U. & Cross, G.A.M., 2003. Structural features affecting variant surface glycoprotein expression in Trypanosoma brucei. *Molecular and Biochemical Parasitology*, 128(2), pp.135-145.

Wang, Q.-ping, Kawahara, T. & Horn, D., 2010. Histone deacetylases play distinct roles in telomeric VSG expression site silencing in African trypanosomes. *Molecular Microbiology*, 77(July), pp.1237-1245.

Wang, Y.-N., Wang, M. & Field, M.C., 2010. Trypanosoma brucei: trypanosome-specific endoplasmic reticulum proteins involved in variant surface glycoprotein expression. *Experimental parasitology*, 125(3), pp.208-21.

Wang, Y.V. et al., 2007. Quantitative analyses reveal the importance of regulated Hdmx degradation for p53 activation. *Proceedings of the National Academy of Sciences of the United States of America*, 104(30), pp.12365-70.

Weisman, H.F. et al., 1990. Recombinant soluble CR1 suppressed complement activation, inflammation, and necrosis associated with reperfusion of ischemic myocardium. *Trans. Assoc. Am. Physicians*, 103, p.64–72.

Wickstead, B., Ersfeld, K. & Gull, K., 2003. The frequency of gene targeting in Trypanosoma brucei is independent of target site copy number. *Nucleic Acids Research*, 31(14), pp.3993-4000.

Wickstead, B., Ersfeld, K. & Gull, K., 2004. The Small Chromosomes of Trypanosoma brucei Involved in Antigenic Variation Are Constructed Around Repetitive Palindromes. *Genome Research*, 14(6), pp.1014-24.

Wirtz, E. & Clayton, C.E., 1995. Inducible gene expression in trypanosomes mediated by a prokaryotic repressor. *Science*, 268(5214), pp.1179-83.

Wirtz, E. et al., 1999. A tightly regulated inducible expression system for conditional gene knock-outs and dominant-negative genetics in Trypanosoma brucei. *Molecular and Biochemical Parasitology*, 99, pp.89 - 101.

Woodruff, A.W. et al., 1973. Anaemia in African Trypanosomiasis and "Big Spleen Disease" in Uganda. *Transactions of the Royal Society of Tropical Medicine and Hygiene*, 67(3), pp.329-337.

Woodward, R. & Gull, K., 1990. Timing of nuclear and kinetoplast DNA replication and early morphological events in the cell cycle of Trypanosoma brucei. *Journal of cell science*, 95(Pt 1), pp.49-57.

World Health Organisation, 1998. Control and surveillance of African trypanosomiasis. *World Health Organization technical report series*, 881, pp.I-VI, 1-114.

World Health Organisation, 2008. Global plan to combat neglected tropical diseases 2008-2015. , pp.1-50.

Wright, A.-D.G. et al., 1999. Phylogenetic position of the kinetoplastids, Cryptobia bullocki, Cryptobia catostomi , and Cryptobia salmositica and monophyly of the genus Trypanosoma inferred from small subunit ribosomal RNA sequences. *Molecular & Biochemical Parasitology*, 99, pp.69 - 76.

Yang, X. et al., 2009. RAP1 Is Essential for Silencing Telomeric Variant Surface Glycoprotein Genes in Trypanosoma brucei. *Cell*, 137(1), pp.99-109.

Young, R. et al., 2008. Isolation and analysis of the genetic diversity of repertoires of VSG expression site containing telomeres from Trypanosoma brucei gambiense, T. b. brucei and T. equiperdum. *BMC genomics*, 9, p.385.

Ziegelbauer, K., Multhaup, G. & Overath, P., 1992. Molecular characterization of two invariant surface glycoproteins specific for the bloodstream stage of Trypanosoma brucei. *The Journal of Biological Chemistry*, 267(15), p.10797–803.

Ziegelbauer, K. & Overath, P., 1992. Identification of invariant surface glycoproteins in the bloodstream stage of Trypanosoma brucei. *Journal of Biological Chemistry*, 267(15), p.10791–6.

Ziegelbauer, K. et al., 1990. Synchronous differentiation of Trypanosoma brucei from bloodstream to procyclic forms in vitro. *European Journal of Biochemistry*, 192, pp.373-378.

Zipfel, P.F. & Skerka, C., 2009. Complement regulators and inhibitory proteins. *Nature reviews. Immunology*, 9(10), pp.729-40.

Zomerdijk, J.C.B.M. et al., 1990. The promoter for a variant surface glycoprotein gene expression site in Trypanosoma brucei. *EMBO Journal*, 9(9), pp.2791-801.

Appendix I

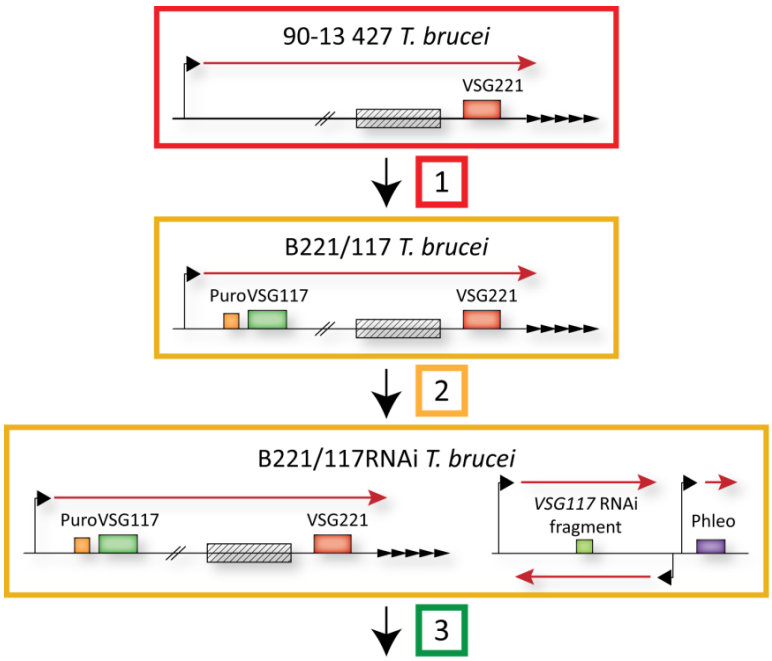
Induction of *VSG117* RNAi causes a growth arrest, similar to that observed after induction of *VSG221* RNAi

A2.1 Introduction

It was important to establish, if the *VSG* RNAi-triggered growth arrest could be reproduced using a different *VSG*, i.e. *VSG117*. The work presented in Appendix I focuses on the generation of a cell line capable of induction of *VSG117* RNAi and its effect on the growth of these cells.

A1.2 Results

To generate a VSG117-single expresser cell line capable of *VSG117* RNAi, 90-13 427 *T. brucei* was selected as the parental cell line. The genetic modifications performed are outlined in Figure A1.1, and the generated cell lines have been summarised in Table A1.1.



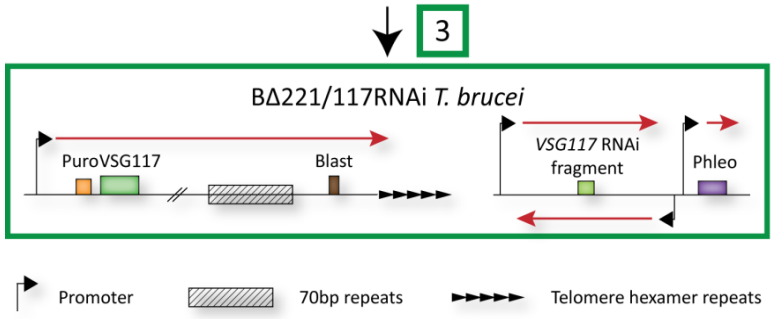


Figure A1.1: Construction of a VSG117-single expresser *T. brucei* line capable of inducible *VSG117* RNAi. The parental 90-13 427 *T. brucei* with an active *VSG221* Expression site was modified by inserting a construct containing *VSG117* gene using puromycin selection (Puro) (B221/117 *T. brucei*) immediately downstream of the ES promoter (**1**). (**2**) A construct containing a *VSG117* RNAi fragment was integrated into 177 bp repeats using phleomycin selection (Phleo) (B221/117RNAi *T. brucei*). (**3**) The telomeric *VSG221* was subsequently replaced with a blasticidin drug resistance gene (Blast) (BΔ221/117RNAi *T. brucei*).

Table A1.1: Cell lines generated in 90-13 427 *T. brucei* in order to obtain a VSG117-single expresser capable of inducible *VSG117* RNAi. The expressed VSGs, as well as the drug resistance gene and a construct containing a *VSG117* RNAi fragment are indicated for each cell line.

Cell line	Expressed VSG	Drug resistance marker in active Expression site	*VSG117* RNAi
Parental 90-13 427	221	-	NO
B221/117	221 and 117	puromycin	NO
B221/117RNAi	221 and 117	puromycin	YES
BΔ221/117RNAi	117	puromycin and blasticidin	YES

A1.2.1 Construction of the B221/117 *T. brucei* cell line

A construct containing a *VSG117* gene was integrated immediately downstream of the promoter of the active *VSG221* Expression site of 90-13 427 *T.*

brucei, generating the B221/117 *T. brucei* cell line (Figure A1.2 and Table A1.1). Expression of VSG117 was assessed by western blot analysis (Figure A1.2).

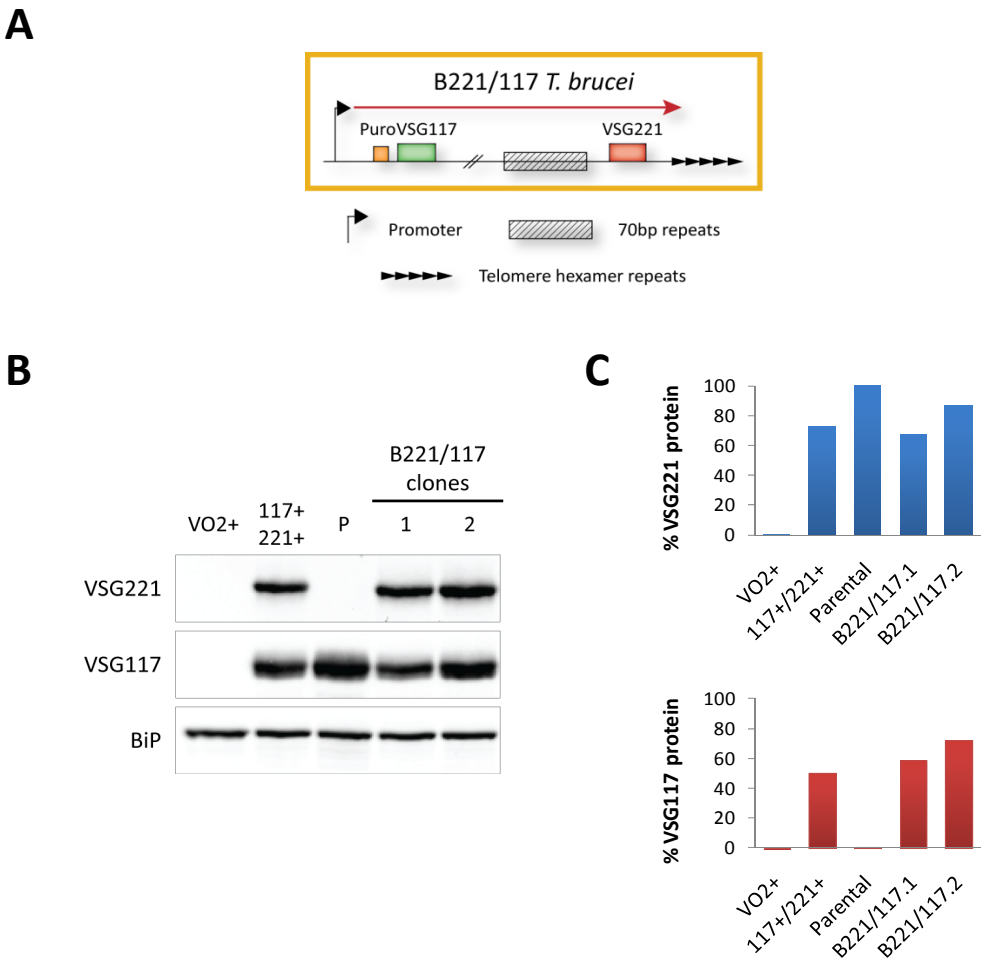


Figure A1.2: *VSG117* can be expressed at high levels from the active *VSG221* Expression site of 90-13 427 *T. brucei*.

A. The *VSG117* gene has been inserted using puromycin (Puro) selection immediately downstream of the promoter of the active *VSG221* Expression site of 90-13 427 *T. brucei*.

B. Western blot analysis of B221/117.1 and B221/117.2 *T. brucei* cells. Levels of VSG221 and VSG117 protein were compared with those present in cells expressing both VSG221 and VSG117 (117+/221+) and the parental 90-13 427 *T. brucei* cell line (P) expressing only VSG221. A cell line expressing only VSG VO2 (VO2+) was used as a negative control. The blots were probed for BiP as a loading control.

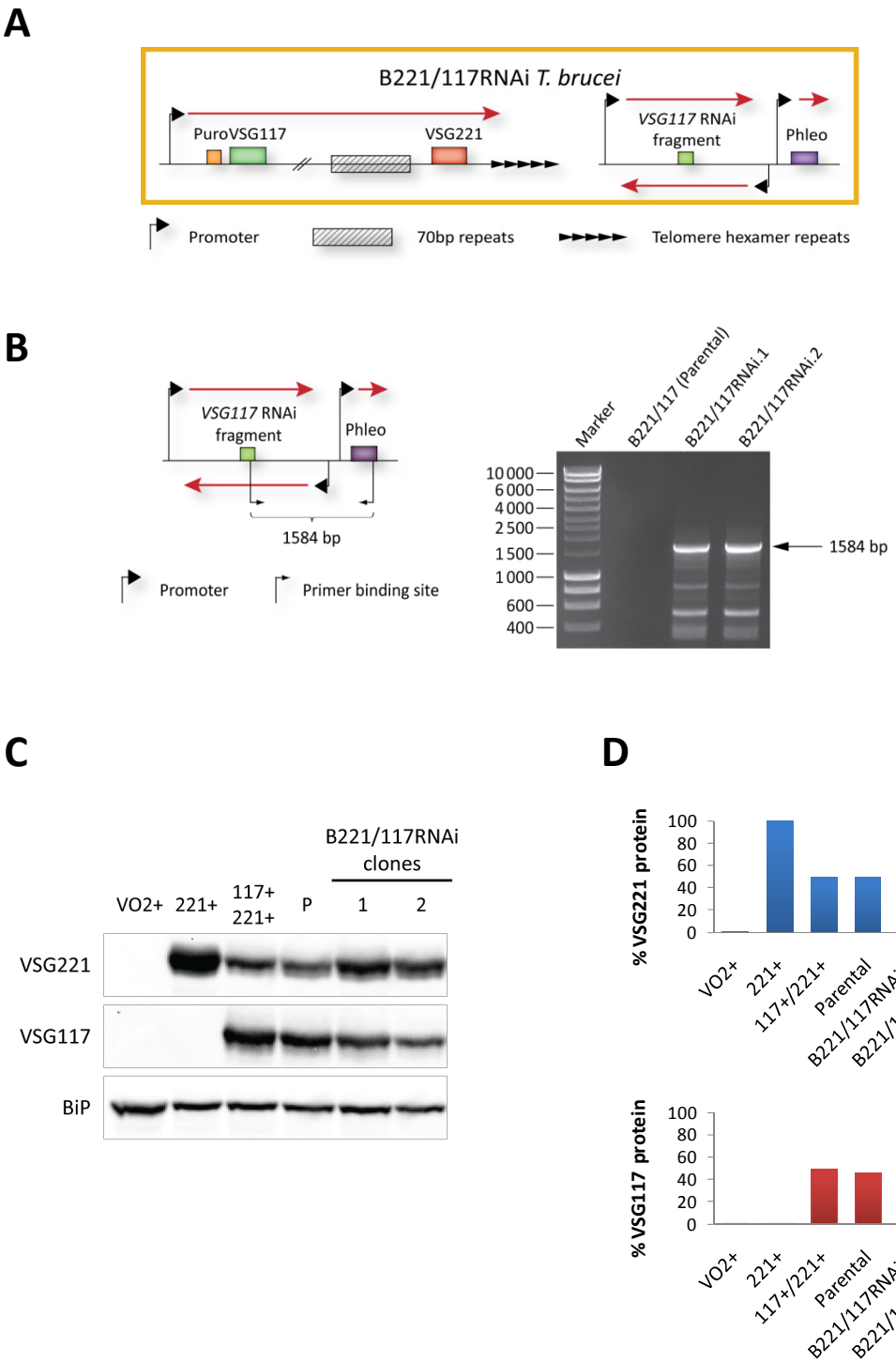
C. Quantification of VSG221 and VSG117 protein from the western blots was achieved using BioRad Quantity One software. Levels of VSG221 protein are represented as the percentage of total VSG221 expressed by the parental 90-13 427 *T. brucei* line (set at 100%). Levels of VSG117 protein are represented as the percentage of total VSG117 expressed by the VSG221-VSG117 double expresser *T. brucei* (117+/221+) (set at 50%).

The B221/117 *T. brucei* cells expressed high levels of VSG117 protein, comparable to the amount produced by the control VSG221-VSG117 double-expresser *T. brucei* cell line (117+/221+ in Figure A1.2C). The B221/117 *T. brucei* cells appeared to have reduced amounts of VSG221 protein, compared to the parental 90-13 427 *T. brucei*, which expressed only VSG221. B221/117.1 and B221/117.2 cells expressed 68% and 87% of VSG221 protein, respectively, calculated from the 100% expressed by the parental 90-13 427 *T. brucei* cell line. The levels of VSG117 protein in B221/117.1 and B221/117.2 clones were determined to be 59% and 72%, respectively, calculated from the amount synthesised by the VSG221-VSG117 double-expresser (VSG117+/VSG221+), which was set at 50% (Figure A1.2C). Therefore, high levels of VSG117 protein expression could be achieved from a gene integrated immediately downstream of the promoter of the active *VSG221* Expression site in the 90-13 427 *T. brucei* cell lines (Figure A1.2B).

A1.2.2 Construction of the B221/117RNAi *T. brucei* cell line

The B221/117 *T. brucei* cell line was transfected with a construct enabling to perform inducible *VSG117* RNAi (Figure A1.3 and Table A1.1). The *VSG117* RNAi construct was inserted into the 177 bp repeat region and integration was confirmed

using PCR linking the drug resistance gene (phleomycin) to the *VSG117* RNAi fragment, yielding the expected 1584 bp fragment (Figure A1.3B).



E

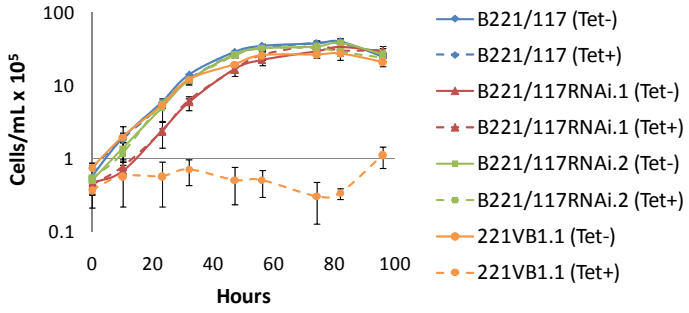


Figure A1.3: Constitutive transcription of the *VSG117* RNAi fragment reduces basal levels of *VSG117* transcript in B221/117RNAi *T. brucei*.

A. A construct containing the *VSG117* gene has been inserted immediately downstream of the promoter of the active *VSG221* Expression site of 90-13 427 *T. brucei* using puromycin selection (Puro) drug. A construct containing *VSG117* RNAi fragment has been integrated into the cells using phleomycin (Phleo) drug selection and *VSG117* RNAi was achieved through the bi-directional transcription of a *VSG117* fragment.

B. The *VSG117* RNAi fragment was linked to the downstream phleomycin drug resistance gene by PCR to confirm the presence of the construct in the genomic DNA of the B221/117RNAi *T. brucei* cell line. The expected 1584 bp band is indicated.

C. Western blot analysis of B221/117RNAi.1 and B221/117RNAi.2 *T. brucei* expressing both VSG117 and VSG221. Levels of VSG221 and VSG117 protein were compared with those present in cells expressing only VSG221 (221+), both VSG221 and VSG117 (117+/221+) and the parental B221/117 *T. brucei* cell line (P) that also expressed both VSG221 and VSG117. A cell line expressing only VSG VO2 (VO2+) was used as a negative control. The blots were probed for BiP as a loading control.

D. Quantification of VSG221 and VSG117 protein levels as determined by western blot analysis was achieved using BioRad Quantity One software. Levels of VSG221 protein are represented as the percentage of total VSG221 expressed by the VSG221 single expresser *T. brucei* (221+) (set at

100%). Levels of VSG117 protein are represented as the percentage of total VSG117 expressed by the VSG221-VSG117 double expresser *T. brucei* (117+/221+) (set at 50%).

E. Growth of the B221/117RNAi.1 and B221/117RNAi.2 *T. brucei* was compared to the parental B221/117 cell line. The 221VB1.1 cell line was used as a positive control. Uninduced cells (Tet-) were compared to cells where *VSG* RNAi had been induced (Tet+) for the time specified in hours. The average cell density from triplicate counts is represented in cells per mL x 10^5 and the standard deviation is shown as error bars.

B221/117RNAi.1 and B221/117RNAi.2 *T. brucei* expressed 32% and 27% of the VSG117 protein, respectively, compared with the 46% observed in the parental B221/117 *T. brucei* (Figure A1.3C and D). B221/117RNAi.1 and B221/117RNAi.2 *T. brucei*, however, expressed higher levels of VSG221 protein (65% and 70%, respectively), compared with the parental B221/117 *T. brucei* (50%) (Figure A1.3C and D). As expected, induction of *VSG117* RNAi in the B221/117RNAi *T. brucei* cell line did not result in growth inhibition (Figure A1.3E).

A1.2.3 Construction of the BΔ221/117RNAi *T. brucei* cell line

The B221/117RNAi.1 cell line was transfected with a construct replacing the telomeric *VSG221* with a blasticidin drug resistance marker (Blast), similar to the V117Δ221 *T. brucei* (Figure 5.5A and Figure A1.4 and Table A1.1).

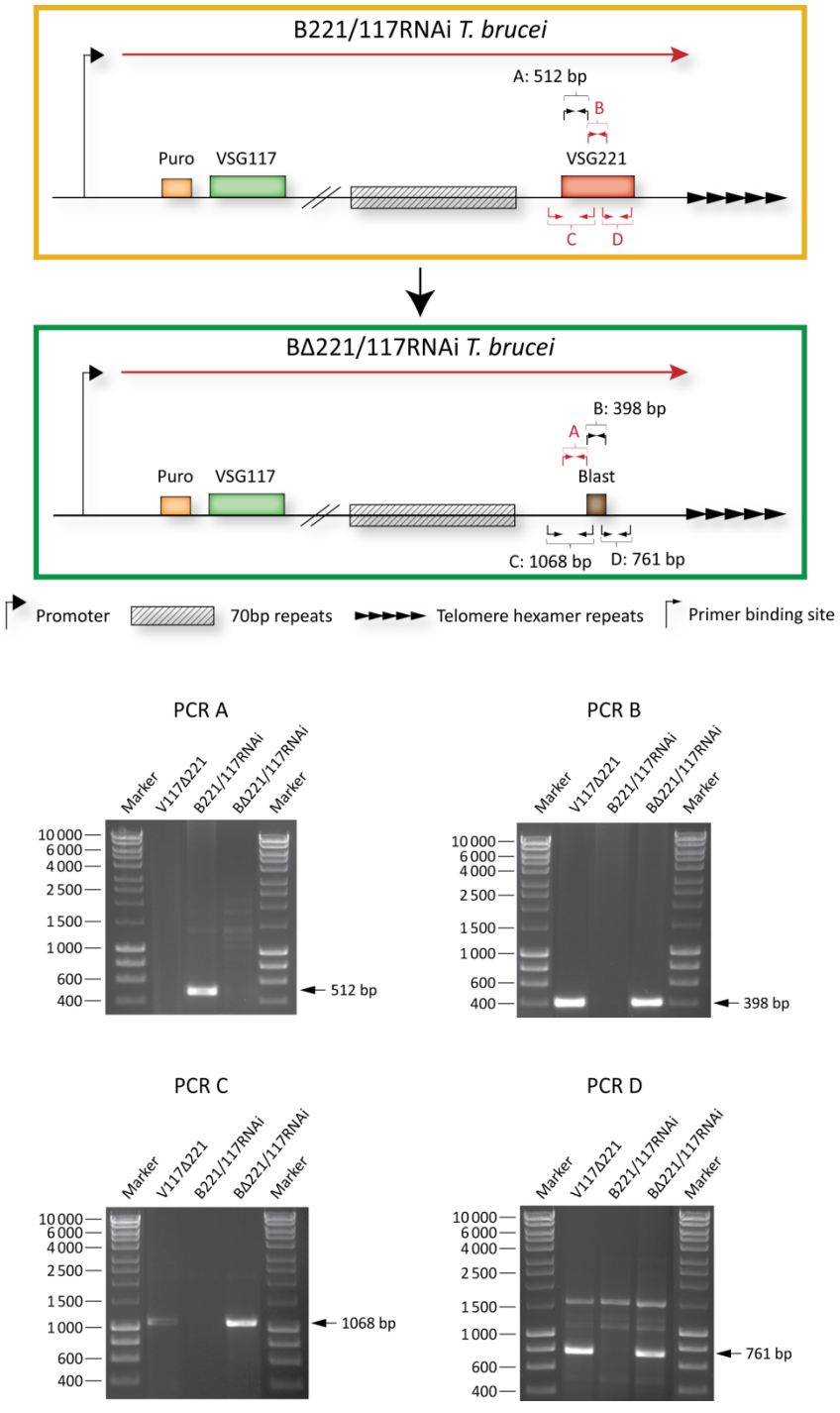


Figure A1.4: The *VSG221* gene can be deleted from the active *VSG221* Expression site in the B221/117RNAi *T. brucei* cell line. In the BΔ221/117RNAi cell line a blasticidin resistance gene (Blast) was inserted in place of the *VSG221* gene in the active *VSG221* Expression site already containing the *VSG117* gene. The deletion of the *VSG221* gene from the genomic DNA of BΔ221/117RNAi cell line (PCR **A**) and the insertion of the *Blast* gene (PCR **B**) were confirmed by PCR using internal primers for the two genes. The presence of the *Blast* gene in the genomic DNA of

the BΔ221/117RNAi cell line was confirmed by PCR by linking it to upstream (PCR **C**) and downstream (PCR **D**) sequences within the *VSG221* ES. The genomic DNA of V117Δ221and B221/117RNAi *T. brucei* were used as controls.

The deletion of the telomeric *VSG221* in the active *VSG221* Expression site of the B221/117RNAi cell line was confirmed by PCR (Figure A1.4). As *VSG221* is a single copy gene in the 90-13 427 *T. brucei* cell line, its absence from the BΔ221/117RNAi and V117Δ221 *T. brucei* genome could be confirmed by PCR (Figure A1.4, PCR A). The parental B221/117RNAi *T. brucei* cell line, however, did contain *VSG221*, and PCR amplification using internal primers in *VSG221* generated the expected 512 bp product (Figure A1.4, PCR A). Detection of the *Blast* gene in the genome of the BΔ221/117RNAi and V117Δ221 *T. brucei* cell lines was confirmed with internal primers that yielded the expected 398 bp product (Figure A1.4, PCR B). Linkage of the *Blast* gene to upstream and downstream sequences in the active ES of the BΔ221/117RNAi *T. brucei* cell line could be confirmed, as we could PCR amplify the expected 1068 bp and 761 bp products, respectively (Figure A1.4, PCR C and D). These products were also obtained when the V117Δ221 *T. brucei* cell line genomic DNA was used as a template (Figure 5.5 and Figure A1.4, PCR C and D).

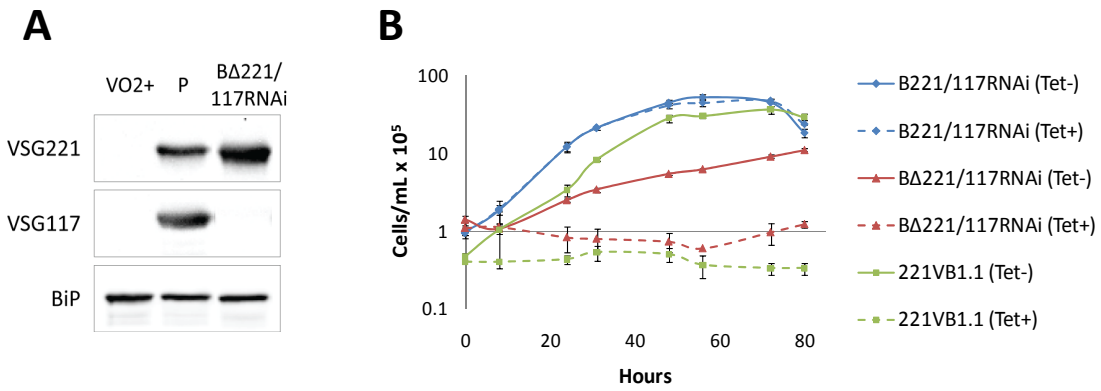


Figure A1.5: *VSG117* RNAi causes a growth arrest in the BΔ221/117RNAi *T. brucei* cell line.

A. Western blot analysis of the BΔ221/117RNAi *T. brucei* cell line. Levels of VSG221 and VSG117 protein were compared with those present in the parental B221/117RNAi *T. brucei* cell line (P) expressing both VSG221 and VSG117. A cell line expressing only VSG VO2 (VO2+) was used as a negative control. The blots were additionally probed for BiP as a loading control.

B. The growth of the BΔ221/117RNAi *T. brucei* was compared to the parental B221/117RNAi cell line. The 221VB1.1 cell line was used as a positive control. Uninduced cells (Tet-) were compared to cells where *VSG117* RNAi has been induced (Tet+) for the time specified in hours. The average cell density from triplicate counts is represented in cells per mL x 10^5 and the standard deviation is shown as error bars.

Western blot analysis showed that the BΔ221/117RNAi cell line expressed high levels of VSG117 protein, whereas no VSG221 protein could be detected (Figure A1.5A). The level of VSG117 protein was higher in the BΔ221/117RNAi *T. brucei* compared with the parental B221/117RNAi cell line. This suggested that in the BΔ221/117RNAi *T. brucei* the total cellular VSG was composed of VSG117. In contrast, in the parental B221/117RNAi cell line, the expression of two different

VSGs resulted in a relative reduction in the levels of the individual VSGs (Figure A1.3C and Figure A1.5A).

Induction of *VSG117* RNAi in the BΔ221/117RNAi cell line resulted in a growth inhibition, similar to the growth arrest triggered by *VSG221* RNAi in 221VB1.1 and 221VG1.1 *T. brucei* (Figure 3.1C, Figure 3.3B and Figure A1.5B). Therefore, the *VSG* RNAi-induced block in cell division was not specific to the *VSG221* RNAi.

A1.3 Conclusions

The growth arrest observed after the induction of *VSG221* RNAi was confirmed in three different cell lines, including the 221VB1.1, 221VG1.1 and P221 *T. brucei* cell lines (Figure 3.1C, Figure 3.3B and Figure A1.1B) (Sheader et al. 2005; T. K. Smith et al. 2009). The generation of a cell line that exclusively expressed *VSG117* allowed us to confirm the reproducibility of the *VSG* RNAi-induced growth arrest.

Previously, it was established that *VSG221* can be deleted from its telomeric location in the active ES, if the cells expressed high levels of a second *VSG* variant, *VSG117*, from immediately downstream of the ES promoter (Chapter 5.2.1.3, Figure 5.5). The growth rates of the cells, which expressed only the promoter-proximal *VSG117* in the active *VSG221* ES were reduced, compared with cells expressing either VSG221 (V221 *T. brucei*), or both VSG221 and VSG117 (V221/117 *T. brucei*) from the active *VSG221* ES (Figure 5.6B). These differences in the growth rates may have been a consequence of the presence of a sub-optimal tubulin 5' UTR

on the transgenic *VSG117* gene, which could have reduced the stability of the *VSG117* mRNA. In contrast, the *VSG221* transcript had the wild-type *VSG221* 5' and 3' processing sequences that have previously been reported to enhance the stability of the *VSG* mRNA (Berberof et al. 1995). The potential decreased stability of the *VSG117* mRNA could have impacted on levels of VSG expression, which affected the division rates of the V117Δ221 *T. brucei* cells, which relied solely on the expression of the promoter-proximal *VSG117* from the active ES (Figure 5.6).

The 90-13 427 *T. brucei* cell line was transfected with a construct containing the *VSG117* gene targeted immediately downstream of the promoter of the active *VSG221* ES to generate the B221/117 *T. brucei* cell line, similar to as had been done for the 221VP117 and V221/117 *T. brucei* cell lines (Figure 4.3, Figure 4.4, Figure 5.3, Figure A1.2 and Table A1.1). The VSG117 protein levels expressed by the VSG221-VSG117 double expresser B221/117 *T. brucei* were shown to be comparable to those found in the 221VP117 *T. brucei* cell line (117+/221+ in Figure A1.2B and C).

A *VSG117* RNAi construct was next transfected into B221/117 *T. brucei* (Figure A1.3A and Table A1.1). There appeared to be some leaky transcription of the *VSG117* RNAi fragment prior to induction of *VSG117* RNAi. This resulted in lower levels of VSG117 protein in the B221/117RNAi *T. brucei*, compared with the parental B221/117 cell line (Figure A1.3C and D). In addition, presumably as compensation for the reduced levels of VSG117 protein, the expression of VSG221 protein in the B221/117RNAi *T. brucei* was higher compared with the parental B221/117 cell line (Figure A1.3C and D).

The telomeric VSG221 was subsequently deleted from the active *VSG* ES of the B221/117RNAi *T. brucei*, as was confirmed by linking PCR (Figure A1.4).

Western blot analysis of the BΔ221/117RNAi cell line revealed that VSG221 protein could not be detected in these cells, whereas VSG117 protein was produced at high levels, which suggested that these cells relied solely on the expression of VSG117 for growth (Figure A1.5A).

The generation time of the BΔ221/117RNAi *T. brucei* cells (26.11 h) was reduced compared with either the parental B221/117RNAi *T. brucei* cell line (7.57 h) or V117Δ221 *T. brucei* (9.62 h) (another cell line where the *VSG221* gene had been deleted) (Figure 5.6B and Figure A1.5B). The growth rate of the parental B221/117RNAi cell line was not reduced by the presence of the construct containing the *VSG117* RNAi. These cells had a second VSG, VSG221 present in the active *VSG221* Expression site. Expression of this second VSG presumably helped complement the reduction in the levels of VSG117 protein, caused by the "leakiness" of the *VSG117* RNAi (Figure A1.3E). As previously discussed, the growth rates of the V117Δ221 *T. brucei* were reduced compared with cells expressing only VSG221 or both VSG221 and VSG117 (Chapter 5.2.2). In the BΔ221/117RNAi cell line the presence of leaky transcription of the *VSG117* RNAi fragment reduced the levels of the VSG117 protein, presumably resulting in a decrease in the growth rate of these cells (Figure A1.5B).

Induction of *VSG117* RNAi in BΔ221/117RNAi *T. brucei* caused an abrupt growth arrest, similar to as observed in the 221VB1.1 and 221VG1.1 cell lines after induction of *VSG221* RNAi (Figure 3.1C, Figure 3.3B and Figure A1.5B). This confirmed that the *VSG221* RNAi-triggered growth arrest was reproducible for RNAi directed against a different *VSG* variant, *VSG117* and was not specific to VSG221 (Figure A1.5B).

Appendix II

Controls for VSG endocytosis experiments

A2.1 TDP 1 is essential in *T. brucei*

TDP 1 is an HMG1-like DNA binding protein, which may be involved in transcription and/or DNA replication (Erondu & Donelson 1992). TDP 1 is essential in trypanosomes, and RNAi against it caused a rapid growth inhibition, even though no precise cell cycle block was observed after induction of *TDP 1* RNAi (Figure A2.1).

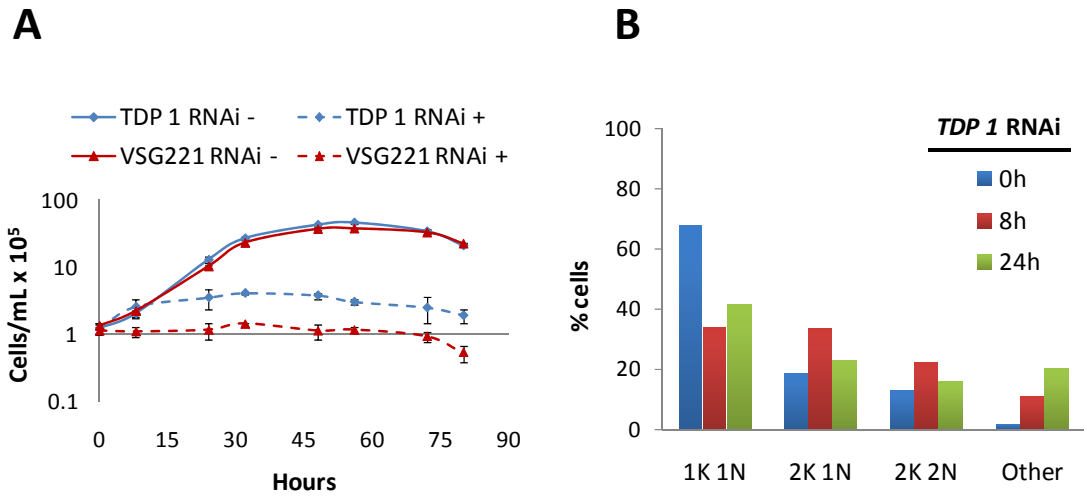


Figure A2.1: Induction of *TDP 1* RNAi results in a growth reduction in *Trypanosoma brucei* but does not cause a specific cell cycle arrest.

A. Growth analysis of 90-13 TDP C1 and 221VB1.1 *T. brucei* cells after induction of *TDP 1* or *VSG221* RNAi, respectively. Uninduced cells (Tet-) were compared to cells where *TDP1* RNAi or *VSG221* RNAi had been induced (Tet+) for the time specified in hours. The average cell density from triplicate counts is represented in cells per mL x 10^5 and the standard deviation is shown as error bars.

B. Cell cycle analysis of the different cell populations after induction of *TDP 1* RNAi in 90-13 TDP C1 *T. brucei* for the time specified in hours. For each cell population counted n>300.

Microscopic analysis of cells after induction of *TDP 1* RNAi for 8 or 24 hours showed that there was a progressive increase in multinucleated cells (Other), as

well as 2K1N and 2K2N cells (Figure A2.1B). The increase in 2N1K and 2N2K cells after induction of *TDP 1* RNAi did not appear to be due to a specific cell cycle effect, but appeared to be caused by cells undergoing multiple rounds of S-phase that eventually led to accumulation of multinucleated and multikinetoplast cells (Figure A2.1B).